APPENDIX A

PROGRAMMING

A.1 Introduction

A general computer program has been developed to obtain the analytical solution of the cracked stiffened panels. The computational algorithm has been developed based on the displacement potential function formulation. The computer code has been developed based on the C programming language.

The program named *file1.cpp* reads the input data from the input files *input.txt.* This file reads the modulus of elasticity, maximum intensity of the load and Poisson's ratio. The output file *inputtestt.txt* checks the validity of our input value. There are five output files such as *outputuresult.txt, outputvresult.txt, outputsigxxresult.txt, outputsigyyresult.txt and outputsigxyresult.txt.* Those files are used to write results of the displacment components and stress components after running the program. The cramer rule has been used to solve the four simultanous equation.

A.2 Description of the Program Variables

Notation	Definition
u[ ][ ]	Displacement in X-direction
v[ ] [ ]	Displacement in Y-direction
sigx[ ] [ ]	Stress in X- direction
sigy[ ] [ ]	Stress in Y- direction
sigxy[ ] [ ]	Shear stress in XY-plane
nsigx[ ] [ ]	Normalized axial stress
nsigy[ ] [ ]	Normalized lateral stress
nsigxy[ ] [ ]	Normalized shear stress
Pi	Constant (3.1416)

E	Modulus of Elasticity
Nu	Poisson's ration
L	Constant, $\alpha = (m\pi/a)$
O	Maximum intensity of the load
d1,d2,d3,d4	
f1,f2,f3,f4	Coefficient matrix of the four simultaneous
h1,h2,h3,h4	equations.
k1,k2,k3,k4	
ac[ ], bc[ ], a0, w	Constants of the curved fitted equation.
A	Width of the Panel
B	Length of the Panel
R	Aspect ratio (b/a)
c1	αx
c2	αy
c3	αb
i,j,k	Loop Variables
n1, n5	No. of nodes in *x*- and *y*-direction respectively.
M	Indicates the no. of terms in Fourier series.
U11,V11,X11,Y11,XY11	Displacement and Stress components at a particular point of the panel.

A3. Code of the Program.

```
/*Problem: Analysis of stiffened isotropic Panel with cracks length h/a = 0.2 a=1 fixed */

#include<stdio.h>
#include<math.h>

void main()
{
        double u[51][101],v[51][101],sigx[51][101],sigy[51][101],sigxy[51][101];
        double nsigx[51][101],nsigy[51][101],nsigxy[51][101];
        double pi,e,nu,L,o,d1,d2,d3,d4,f1,f2,f3,f4,h1,h2,h3,h4,k1,k2,k3,k4,z11;
        double a0 = -7.341e-005;
        double ac[3] = {-0.000117 ,-4.87e-005,-9.434e-006};
        double bc[3] = {-1.524e-005,-1.528e-005,-4.429e-006};
        double w = 10.47;
        double A1,A2,A3,A4,eq1,eq2,eq3,eq4,A11,B11,r,a,b,c1,c2,c3,Em,Im;
        double x1,u1,y1,xy1,v1,U11,V11,X11,Y11,XY11,sum;
        double m1,m2,m3,m4,det,ams,bms,cms,dms,aa,bb,cc;
        int n1,n5,m,i,j,k;

        FILE *input1, *inputtest, *outputu, *outputv, *outputsigxx, *outputsigyy,
        *outputsigxy,*outputtest;
        input1 = fopen("input.txt","r");
        inputtest = fopen("inputtestt.txt","w");
        outputu = fopen("outputuresult.txt","w");
        outputv = fopen("outputvresult.txt","w");
        outputsigxx = fopen("outputsigxxresult.txt","w");
        outputsigyy = fopen("outputsigyyresult.txt","w");
        outputsigxy = fopen("outputsigxyresult.txt","w");
        outputtest = fopen("outputtestt.txt","w");
```

```
fscanf(input1,"%lf %lf %lf",&e,&o,&nu);
fprintf(inputtest,"%18.3lf %18.3lf %18.3lf",e,o,nu);
n1 = 51;
n5 = 101;
pi = 3.141592654;
r = 1.0;
a = 1.0;
b = a * r;
bb = (-2*o*(1+nu)*(1+nu))/(e*(9-(3*nu)));
aa = -1.5*bb*(1-nu);

for (i = 0;i < n1;i++)
{       for(j = 0;j < n5;j++)
        {       A11 = (i/50.0);
                B11 = (j/100.0);
                U11 = 0.0;
                V11 = 0.0;
                X11 = 0.0;
                Y11 = 0.0;
                XY11 = 0.0;

                for(m = 1;m<=109;m++)
                {
                        c1 = m*pi*A11*r;
                        c2 = m*pi*B11;
                        c3 = m*pi*r;
                        L = (m*pi)/a;
                        z11 = ((-e)*L*L)/((1+nu)*(1+nu));
                        h1 = -L*L;
                        h2 = -L;
                        h3 = L*L;
```

```
h4 = -L;

k1 = z11*(1+nu)*L*exp(c3);
k2 = z11*((c3*(1+nu))+2)*exp(c3);
k3 = z11*(1+nu)*L*exp(-c3);
k4 = z11*((c3*(1+nu))-2)*exp(-c3);
d1 = (1+nu)*L;
d2 = (nu+3);
d3 = -(1+nu)*L;
d4 = (nu+3.0);
f1 = (1+nu)*L*exp(c3);
f2 = ((c3*(1+nu))+nu+3.0)*exp(c3);
f3 = -(1+nu)*L*exp(-c3);
f4 = -((c3*(1+nu))-nu-3.0)*exp(-c3);

Em = ((2*o)/(m*pi))*(1-cos(m*pi));

sum = ((2*a0)/(m*pi))*(cos((8*m*pi)/10)-cos(m*pi));
for(k = 0;k<3;k++)
{
sum = sum +(ac[k]*(((1/((m*pi)+((k+1)*w*a)))*cos(((m*pi)+((k+1)*w*a))*0.8))+
((1/((m*pi)-((k+1)*w*a)))*cos(((m*pi)-((k+1)*w*a))*0.8))\((1/((m*pi)+((k+1)
*w*a)))*cos((m*pi)+((k+1)*w*a)))-((1/((m*pi)-((k+1)*w*a)))*cos((m*pi)-((k+1)*
w*a)))))+(bc[k]*(-((1/((m*pi)+((k+1)*w*a)))*sin((m*pi)+((k+1)*w*a)))
+((1/((m*pi)-((k+1)*w*a)))*sin((m*pi)-((k+1)*w*a)))+((1/((m*pi)+((k+1)*w*a)))
*sin(((m*pi)+((k+1)*w*a))*0.8))-((1/((m*pi)-((k+1)*w*a)))*sin(((m*pi)-
((k+1)*w*a))*0.8))));
}
Im = sum;
m1= 0;
m2= 0;
m3 = Im;
```

```
m4 = Em;

det = (d1*((f2*((h3*k4)-(h4*k3)))-(f3*((h2*k4)-(h4*k2)))+(f4*((h2*k3)-(h3*k2)))))+(-d2*((f1*((h3*k4)-(h4*k3)))-(f3*((h1*k4)-(h4*k1)))+(f4*((h1*k3)-(h3*k1)))))+(d3*((f1*((h2*k4)-(h4*k2)))-(f2*((h1*k4)-(h4*k1)))+(f4*((h1*k2)-(h2*k1)))))+(-d4*((f1*((h2*k3)-(h3*k2)))-(f2*((h1*k3)-(h3*k1)))+(f3*((h1*k2)-(h2*k1)))));

ams = (m1*((f2*((h3*k4)-(h4*k3)))-(f3*((h2*k4)-(h4*k2)))+(f4*((h2*k3)-(h3*k2)))))+(-d2*((m2*((h3*k4)-(h4*k3)))-(f3*((m3*k4)-(h4*m4)))+(f4*((m3*k3)-(h3*m4)))))+(d3*((m2*((h2*k4)-(h4*k2)))-(f2*((m3*k4)-(h4*m4)))+(f4*((m3*k2)-(h2*m4)))))+(-d4*((m2*((h2*k3)-(h3*k2)))-(f2*((m3*k3)-(h3*m4)))+(f3*((m3*k2)-(h2*m4)))));
bms = (d1*((m2*((h3*k4)-(h4*k3)))-(f3*((m3*k4)-(h4*m4)))+(f4*((m3*k3)-(h3*m4)))))+(-m1*((f1*((h3*k4)-(h4*k3)))-(f3*((h1*k4)-(h4*k1)))+(f4*((h1*k3)-(h3*k1)))))+(d3*((f1*((m3*k4)-(h4*m4)))-(m2*((h1*k4)-(h4*k1)))+(f4*((h1*m4)-(m3*k1)))))+(-d4*((f1*((m3*k3)-(h3*m4)))-(m2*((h1*k3)-(h3*k1)))+(f3*((h1*m4)-(m3*k1)))));
cms = (d1*((f2*((m3*k4)-(h4*m4)))-(m2*((h2*k4)-(h4*k2)))+(f4*((h2*m4)-(m3*k2)))))+(-d2*((f1*((m3*k4)-(h4*m4)))-(m2*((h1*k4)-(h4*k1)))+(f4*((h1*m4)-(m3*k1)))))+(m1*((f1*((h2*k4)-(h4*k2)))-(f2*((h1*k4)-(h4*k1)))+(f4*((h1*k2)-(h2*k1)))))+(-d4*((f1*((h2*m4)-(m3*k2)))-(f2*((h1*m4)-(m3*k1)))+(m2*((h1*k2)-(h2*k1)))));
dms = (d1*((f2*((h3*m4)-(m3*k3)))-(f3*((h2*m4)-(m3*k2)))+(m2*((h2*k3)-(h3*k2)))))+(-d2*((f1*((h3*m4)-(m3*k3)))-(f3*((h1*m4)-(m3*k1)))+(m2*((h1*k3)-(h3*k1)))))+(d3*((f1*((h2*m4)-(m3*k2)))-(f2*((h1*m4)-(m3*k1)))+(m2*((h1*k2)-(h2*k1)))))+(-m1*((f1*((h2*k3)-(h3*k2)))-(f2*((h1*k3)-(h3*k1)))+(f3*((h1*k2)-(h2*k1)))));

A1 = ams/det;
A2 = bms/det;
A3 = cms/det;
```

```
                    A4 = dms/det;
                    eq1 = ((A1*k1)+(A2*k2)+(A3*k3)+(A4*k4));
                    eq2 = ((A1*f1)+(A2*f2)+(A3*f3)+(A4*f4));
                    eq3 = ((A1*h1)+(A2*h2)+(A3*h3)+(A4*h4));
                    eq4 = ((A1*d1)+(A2*d2)+(A3*d3)+(A4*d4));
        fprintf(outputtest,"%18.8e %18.8e %18.8e %18.8e\n",eq1,eq2,eq3,eq4);

u1 = ((A1*L*exp(c1))+(A2*(c1+1)*exp(c1))-(A3*L*exp(-c1))-(A4*(c1-1)*exp(-
c1)))*(-L)*sin(c2);

v1 = (((A1*(1+nu)*L*L*exp(c1))+(A2*(c1+(nu*c1)+4)*L*exp(c1)) +(A3*(1+nu) *
L * L*exp(-c1))+(A4*(c1+(nu*c1)-4)*L*exp(-c1)))*cos(c2))/(-(1+nu));

x1 = (z11)*((A1*(1+nu)*L*exp(c1))+(A2*(c1+(nu*c1)+2)*exp(c1))+(A3*(1+ nu)*
L*exp(-c1))+(A4*(c1+(nu*c1)-2)* exp(-c1)))*sin(c2);

y1 = (z11)*((A1*(-1-nu)*L*exp(c1))+(A2*(-c1*(1+nu)-2*nu-4)* exp(c1))+(A3*(-1-
nu)*L*exp(-c1))+(A4*(-c1*(1+nu)+2*nu+4)* exp(-c1)))*sin(c2);

xy1 = (z11)*((A1*(1+nu)*L*exp(c1))+(A2*(c1*(1+nu)+nu+3)*exp(c1))-(A3*(1+
nu) *L*exp(-c1))-(A4*(c1*(1+nu)-nu-3)* exp(-c1)))*cos(c2);/

                    U11 = U11 + u1;
                    V11 = V11 + v1;
                    X11 = X11 + x1;
                    Y11 = Y11 + y1;
                    XY11 = XY11 + xy1;
                }
                u[i][j] = U11/b;
                v[i][j] = V11/a;
                nsigx[i][j] = X11;
                nsigy[i][j] = Y11;
```

```
                nsigxy[i][j] = XY11;

                sigx[i][j] = nsigx[i][j]/abs(o);
                sigy[i][j] = nsigy[i][j]/abs(o);
                sigxy[i][j] = nsigxy[i][j]/abs(o);
        }
}
fprintf(outputu,"Displacement UU\n");
for (i = 0;i < n1;i++)
{
        for(j = 0;j < n5;j++)
        {
                fprintf(outputu,"%18.8e",u[i][j]);
        }
        fprintf(outputu,"\n");
}
fprintf(outputv,"Displacement VV\n");
for (i = 0;i < n1;i++)
{
        for(j = 0;j < n5;j++)
        {
                fprintf(outputv,"%18.8e",v[i][j]);
        }
        fprintf(outputv,"\n");
}
fprintf(outputsigxx,"Stress SigmaXX\n");
for (i = 0;i < n1;i++)
{
        for(j = 0;j < n5;j++)
        {
                fprintf(outputsigxx,"%18.8Lf",sigx[i][j]);
        }
```

```
            fprintf(outputsigxx,"\n");
        }
        fprintf(outputsigyy,"Stress SigmaYY\n");
        for (i = 0;i < n1;i++)
        {
            for(j = 0;j < n5;j++)
            {
                fprintf(outputsigyy,"%18.8Lf",sigy[i][j]);
            }
            fprintf(outputsigyy,"\n");
        }
        fprintf(outputsigxy,"Stress SigmaXY\n");
        for (i = 0;i < n1;i++)
        {
            for(j = 0;j < n5;j++)
            {
                fprintf(outputsigxy,"%18.8Lf",sigxy[i][j]);
            }
            fprintf(outputsigxy,"\n");
        }
        fclose(input1);
        fclose(inputtest);
        fclose(outputu);
        fclose(outputv);
        fclose(outputsigxx);
        fclose(outputsigyy);
        fclose(outputsigxy);
        fclose(outputtest);
}
```

STRESS ANALYSIS OF CRACKED STIFFENED PANELS UNDER FLEXURAL AND AXIAL LOADING

by

Hafijur Rahman

Roll No. 1009102028

Session: October 2009

MASTER OF SCIENCE IN MECHANICAL ENGINEERING
Department of Mechanical Engineering

Bangladesh University of Engineering and Technology
Dhaka-1000, Bangladesh

2013

The thesis entitled "**Stress Analysis of Cracked Stiffened Panels under Flexural and Axial Loading**", submitted by **Hafijur Rahman**, Roll no: 1009102028P, session October 2009 has been accepted as satisfactory in partial fulfillment of the requirement for the degree of MASTER OF SCIENCE IN MECHANICAL ENGINEERING on January 05, 2013.

BOARD OF EXAMINERS

Dr. S Reaz Ahmed Professor Department of Mechanical Engineering, BUET Dhaka, Bangladesh	Chairman
Dr. Muhammed Mahbubur Razzaque Professor Department of Mechanical Engineering, BUET Dhaka, Bangladesh	Member
Dr. Md. Abdus Salam Akhanda Professor Department of Mechanical Engineering, BUET Dhaka, Bangladesh	Member
Dr. Md. Ehsan Professor & Head Department of Mechanical Engineering, BUET Dhaka, Bangladesh	Member (Ex-officio)
Dr. Md. Fazli Ilahi Ex-Vice-Chancellor Islamic University of Technology Board Bazar, Gazipur Bangladesh	Member (External)

Acknowledgement

The author would like to express his gratitude to The Almighty God's continual mercy and help without which no work would have been possible to accomplish the goal. The author is pleased to acknowledge with gratefulness to his supervisor Dr. S Reaz Ahmed, Professor, Department of Mechanical Engineering, Bangladesh University of Engineering and Technology, for his guidance, constant support, intuitive suggestions and relentless encouragement, which he found very benevolent for the outcome of the research. The author would like to take the opportunity to thank the members of the examination committee, for their comments and constructive criticism. The author gratefully acknowledges the computing support provided by the Department of Mechanical Engineering.

CANDIDATE'S DECLARATION

It is hereby declared that no portion of the work contained in this thesis has been submitted elsewhere for any degree or diploma.

Author
Hafijur Rahman

Dedicated To

My Father and Mother

Table of Contents

List of Symbols

Notation	Definition
x,y	Rectangular co-ordinates
σ_{xx}, σ_{yy}	Normal stress components in *x*- and *y*-directions respectively
σ_{xy}	Shear stress component in the *xy* plane
u_x, u_y	Displacement components in *x*- and *y*-directions respectively
μ	Poisson's ratio
E	Modulus of elasticity
G	Modulus of rigidity
ψ	Displacement Potential Function
ϕ	Airy's Stress Function
b	Length of the panel
a	Width or height of the panel
E_1, E_2	Elastic modulus of the material in direction 1 & 2
E_x, E_y, E_z	Elastic Modulus in *x*-, *y*- and *z*-directions respectively
μ_{12}	Major Poisson's ratio
μ_{21}	Minor Poisson's ratio
G_{12}	In plane shear modulus in the plane 1-2 plane
G_{xy}	In plane shear modulus in the plane *x*-*y* plane
h	Depth of the crack
θ	Angle of fiber
σ_o	Maximum intensity of applied load

Abstract

This thesis deals with an efficient analytical scheme for the analysis of stress and displacement fields of boundary-value problems of plane elasticity with mixed boundary conditions and material discontinuity. More specifically, the mechanical behavior of a stiffened panel with an edge crack is analyzed under the influence of flexural and axial loadings, using a new analytical scheme.

Earlier mathematical models of elasticity were very deficient in handling the practical stress problems of solid mechanics. Analytical methods of solution have not gained that much popularity in the field of stress analysis, mainly because of the inability of dealing with mixed boundary conditions, irregular boundary shapes, and material discontinuity.

In this approach, the displacement components of plane elasticity are replaced by a single potential function and the two-dimensional elasticity problem is reduced to the solution of the potential function from a single partial differential equation of equilibrium, in which all the parameters of interest, namely stress, strain and displacements are expressed in terms of the same potential function. The solution of the differential equation is obtained in the form of infinite series, the coefficients of which are determined by satisfying the boundary conditions appropriately. The application of the method is then demonstrated through the analysis of the elastic field of a stiffened panel with an edge crack subjected to axial and flexural loadings. Some of the relevant issues of practical interest are also discussed in relation to the cracked stiffened panel. The analytical scheme is then extended to the case of composite materials, in which the effect of fiber orientation on the elastic filed of the cracked stiffened panel is investigated in details. It would be worth mentioning here that the analytical solutions of the present cracked stiffened panels even with isotropic materials are beyond the scope of the standard methods of the literature.

In an attempt to verify the reliability and accuracy of the analytical scheme developed, the present potential function solutions are compared with the

corresponding solution obtained by two standard computational methods. The three solutions are found to be in excellent agreement with each other for all the cases of stiffeners and loadings considered, which eventually establishes the soundness and appropriateness of the analytical scheme developed.

CHAPTER 1

INTRODUCTION

1.1Background

A crack is the most dangerous defect in structural components. The presence of a crack not only causes a local variation in the stiffness, but also affects the global mechanical behavior of the structure to a considerable extent. Among the cracks, the surface connected ones are most commonly encountered in practice as, most of the cases, critical stresses are found to occur at the surfaces of engineering structures. On the other hand, the use of stiffeners, especially in the construction of marine and aerospace structures is quite extensive. Stiffeners are usually attached along the boundaries of structural components mainly to increase the stiffness of the components, which, in turn, reduces the level of deformation as well as weight of the structure. As a result, the subject of analyzing the mechanical behavior of stiffened structures containing edge cracks has received widespread attention. In particular, reliable and accurate analysis of stresses in these structures is of great practical importance as far as the modern damage tolerant design philosophy is concerned.

Now-a-days, the theory of elasticity has found considerable application in the solution of engineering problems. There are many cases where elementary theory is inadequate to give accurate results. The elementary theory is insufficient to give the information regarding local stresses near the load and near the supports of beams as well as in regions of sharp variation of structure. This led to the emergence of a special trend of physics, i.e., the Theory of Elasticity to apply to elastic solids. The equations of theory of elasticity are a system of partial differential equations.

In cases where a rigorous solution can not be readily obtained, approximate method, such as, numerical methods have been developed. Numerical methods give approximate results instead of exact solution that can be obtained from analytical method. That is, analytical method is always preferable because results obtained by approximate method are not always reliable and acceptable for some applications where accuracy is important. These are sometimes expensive. Sometimes analytical method is not independently adequate to solve a practical problem and it needs some help from numerical methods.

Due to outstanding advantages of composite materials, they are being increasingly used as structural elements in various problems. The response of cracked composite panels to mechanical loadings largely depends on the fiber orientation. Therefore, the effect of fiber orientation on the distribution of stresses and displacements are required to be analyzed to ensure proper and safe application.

1.2 Literature Review

The analysis of mechanical behavior of structural components containing cracks drew the attention of researchers since late 1890s. The view of crack analysis from mechanics view point was stated by Love[1] in his authoritative work on Theory of Elasticity in the 1890s by "The conditions of rupture are but vaguely understood,…" At that time Coulomb and Mohr's theories were followed by many without considering the effects of flaws or cracks in materials. Most often structural failures were analyzed by metallurgists who knew little about the mechanics of the effects of flaws. In the early 1950s, there were studies of failure due to excessive deformations and various forms of instability but virtually nothing on crack. Love's statement was still the case.

Historically, some attempts were tried in the early 1900s but here only those connected to and leading directly to current methods will be mentioned. The first was that of Inglis [1] in 1913. He used elliptical-hyperbolic coordinates to solve the

elastic stress problem of an elliptical hole in a plate. Then he tried to degenerate the ellipse into a crack and his stress solution near the crack tip became unresolved.

Griffith [2] made use of the stress solution provided by Inglis for a plate under uniform tension with an elliptical hole which could be degenerated into a crack. However, neither Griffin nor his predecessors had the knowledge of stress fields near cracks which is now available. Sneddon [2] was the first to give stress-field expansions for crack tips for two individual examples.

As far as the earlier researches are concerned, the attempts of Williams [3] and Irwin [4-5] for finding analytical solutions for the stress and displacement fields near the crack tip are noticeable. In these analyses, an Airy stress function [6] has been suggested to derive a general governing equation for predicting the state of stress near the tip of a part-through crack in an infinite thin plate. Later Sedov[7] presented the general solution for an internal crack in an infinite plate using plane stress assumption. On the other hand, these solutions for stress distribution near the crack tip allowed the researchers to analyze the cracked structures from the stand-point of fracture mechanics. As a result, a number of successful attempts have been made to determine stress intensity factors based on the elastic stress distribution near the crack tip [8-10].

Even though several attempts have been made to obtain analytical solutions for the stress state in cracked bodies, closed form analytical solutions are only found for cracks in semi-infinite or infinitely large bodies under pure tension. It is worth mentioning that most of the solutions so obtained are only valid in the vicinity of the crack tip, which, in turn, identifies them to be inadequate for regions away from the crack tip. However, engineering structures in practice are of boundary value types and, usually encounter different types of physical conditions and shapes as well as cracks tend to occur in regions of high stress concentration. It is, therefore, important to take into account the effect of nearby boundaries appropriately. In fact, the necessity of finding stresses and displacements in cracked bodies in real cases

persuades the researchers to develop numerical and empirical methods. The most important and useful forms of such studies has been collected by Tada *et. al*. [11].

In cases where no analytical and numerical methods could be developed, solutions have been obtained by using experimental methods. Photoelastic methods, soap-film methods, application of strain gages, moiré fringe etc. are some of these experimental methods applied in the study of stress concentration at points of sharp variation of cross-sectional dimension and at sharp fillets of re-entrant corners. These results have considerably influenced the modern design of machine parts and helped in many cases to improve the construction by eliminating weak spots through which crack may switch on and hereby propagate.

The crack problem in finite bodies becomes more complex for the case of stiffened structures. As a result, serious attempts have hardly been made so far in the literature that can provide exact analytical solutions for the stresses in cracked stiffened structures with finite dimensions. Even successful attempts for analyzing edge cracks in semi-infinite stiffened structures are very few; the work of Shkarayev and Moyer can be cited as an example [12]. These analyses are mainly handled by approximate numerical techniques, as in most cases the available mathematical models are inadequate to provide exact analytical solutions to them. As a result, several numerical techniques, such as, matrix force method, finite element method, dual boundary element method, etc. have been found to apply extensively for the solution of crack problems in stiffened structures [13-15]. Ratwani and Wilham studied the influence of biaxial loading in stiffened panels using the FEM [14].

Composite materials have played a leading role over the past three decades in the advancement of different structures like aerospace, marine and automobile technology. Development of lighter, more efficient load carrying structures can be attributed to the inherent advantages that composite materials have over conventional metallic materials. However, behavior of these structures in the presence of various discontinuities, in particular, cracks could be very complicated. An accurate stress analysis for these structures can be performed using a detailed finite element method,

but this approach is not very efficient and convenient. Such an approach would not be very adequate to the cases where a large number of analyses are needed to study the effect of crack sizes, their location and also to study the design changes on the response. A simple global-local method was introduced by Haryadi et. al [27] for the analysis of simply supported composite panels with small cracks. This paper evaluated stresses and displacements around cracks in thin, composite plated under uniform transverse loading. S. Tang [28] introduced hybrid technique that is, coupling of finite element and boundary layer method to study the stress field of laminated composites.

Since the exact analytical solution of mixed boundary-value elastic problems with geometrical discontinuity is beyond the scope of existing mathematical models of elasticity, the use of a new analytical scheme is investigated here to analyze the elastic behavior of cracked stiffened panels of finite dimensions under different types of loading. Displacement potential formulation is used to solve these problems. The present modelling approach reduces the two dimensional problem to the solution of a single differential equations of equilibrium and also enables the mixed mode of the boundary conditions to be managed appropriately. It is worth mentioning that a number of researchers worked on the advancement of displacement potential approach to handle the beam and column like structures with different loading and supporting conditions. Ahmed et. al. have developed numerical solution of both ends fixed deep beams based on displacement potential formulation [18]. Ahmed et. al. [16] have carried out an investigation of stresses at the fixed end of deep cantilever beams. Akanda et. al. have carried out stress analysis of gear teeth using displacement potential function and finite differences [19]. The potential of the formulation has also been investigated by Ahmed et. al. [17] to design optimum shapes of tire-treads for avoiding lateral slippage between tires and roads. Recently, Ahmed et. al. [20] have proposed a general mathematical formulation for finite-difference solution of mixed-boundary-value problems of anisotropic materials. Further, Debnath et. al. have carried out analytical solution of short stiffened flat composite bars under axial loadings [21], and stiffened orthotropic composite panels under uniaxial tensile load [22]. All these solutions are mainly applicable for those

structures with no singularity; none of them is applicable to panel with crack present in them. As such the solution for edge-cracked stiffened panel is yet to be developed.

1.3 Objectives

The present study is on the displacement potential formulation in order to address the structural analysis of edge-cracked stiffened panel of orthotropic and isotropic materials having mixed boundary conditions which it is hoped will aid in the further understanding of the elastic-stress distribution due to presence of stationary crack. The main objectives of the present research work are summarized as follows:

(a) Mathematical modeling of a cracked stiffened panel considering it as a mixed-boundary-value stress problem of elasticity in terms of a single potential function of space variables

(b) Development of a suitable analytical scheme to obtain solutions for the elastic field of finite stiffened panels with an edge crack under flexural and axial loading

(c) Analysis of deformed shapes as well as the distributions of different stress components of interest in the perspective of both the axial and lateral directions of the panel

(d) Analysis of the corresponding elastic field caused by attaching axial and lateral stiffeners along the opposing longitudinal edges of a cracked panel

(e) Extension of the modeling scheme for the analysis of cracked stiffened panels of fiber reinforced composite materials

(f) Establishment of credibility of the analytical scheme for the analysis of cracked stiffened panels with finite dimensions by comparing with those of standard computational techniques

Results of the present analysis provide a reliable design guide for cracked stiffened panels with finite dimensions, which is expected to be of significant help for their improved and economic design. In addition, the present analytical solutions would be considered as a standard guide for checking reliability and accuracy of numerical and approximate solutions to be developed in future.

1.4 Study Procedure

In the present study, the elastic behavior of cracked stiffened panels of finite dimensions is investigated under flexural and axial loading through a new analytical scheme based on a single scalar potential [16-17]. In the potential function boundary modeling approach, the elastic problem is formulated in terms of a single scalar potential of space variables, defined in terms of the displacement components of plane elasticity, which has to satisfy a single fourth-order partial differential equation of equilibrium. Real boundary condition has been imitated in the form of Fourier series. Special cares are taken to model the physical conditions at different segments of the bounding surface of the panel in a reasonable and justifiable manner. The panel is assumed to be stiffened along the two opposing longitudinal edges, in which use of both the axial and lateral stiffeners is investigated separately. The edge crack of zero-degree notch angle is considered to be located at mid-length position of the panel. For checking the reliability as well as appropriateness of the present solution, numerical solutions of cracked stiffened panels are obtained by finite element method with the help of standard commercial software.

1.5 Importance of Present Study

The present study has the significance in regard to academic concept, design reference and manufacturing engineering. The study is going to present the application of a new concept, i.e., displacement potential approach for the analysis of stress and displacement in edge –cracked panels for both isotropic and orthotropic materials under mixed mode of boundary conditions. It is expected to find out some additional aspects to the theory of elasticity, which in turn may encourage

academicians and researchers to explore the concept further and eliminate the lack of suitable method for dealing with mixed boundary value problems of complex geometries. In this study a number of problems of edge-cracked stiffened panel problems are solved by using the present analytical scheme and results are presented in the form of graphs. The results may be used as a database and may be helpful to the designers working in the industries of aerospace, shipbuilding and automobile to verify the conventional numerical methods, where numerous composite structures are used and analyzed by numerical methods. The study of edge-cracked stiffened panel analysis on structural point of view is very pertinent for those machine parts where machine have to run with the presence of crack or structure remain safe without failure.

CHAPTER 2

THEORETICAL OUTLINE AND FORMULATION

2.1 Introduction

To determine the internal forces in a solid body, the theory of elasticity sets forth the solution of problem. Under the action of external forces the body deforms, the mutual position of molecules changes and so do the distance between them. The action of external forces that produce deformation gives rise to additional internal forces causing the stress of the body.

The requirement of the structural analysis is to investigate the state of stresses, strains and displacements at any point due to given body forces and given conditions at the boundary of the body. In most of the cases the requirement is to find the stress distribution in an elastic body. In some cases, it is also required to find the strain distribution of the body. The state of stress, strains and displacement are termed within the elastic limit. A complete description of the elastic field requires specification of forces acting on the elementary body and its surface orientation.

2.2 Equilibrium and Compatibility Conditions

Let us consider an infinitesimal cubic element from an elastic body with sides parallel to the coordinate axes. Six forces will act on the six different faces of the element to ensure the equilibrium of the element. The forces acting on each face may be resolved into two types i.e. one perpendicular to the plane of the face known as normal stress and the other parallel to the face known as shear stress as illustrated in Fig. 2.1.

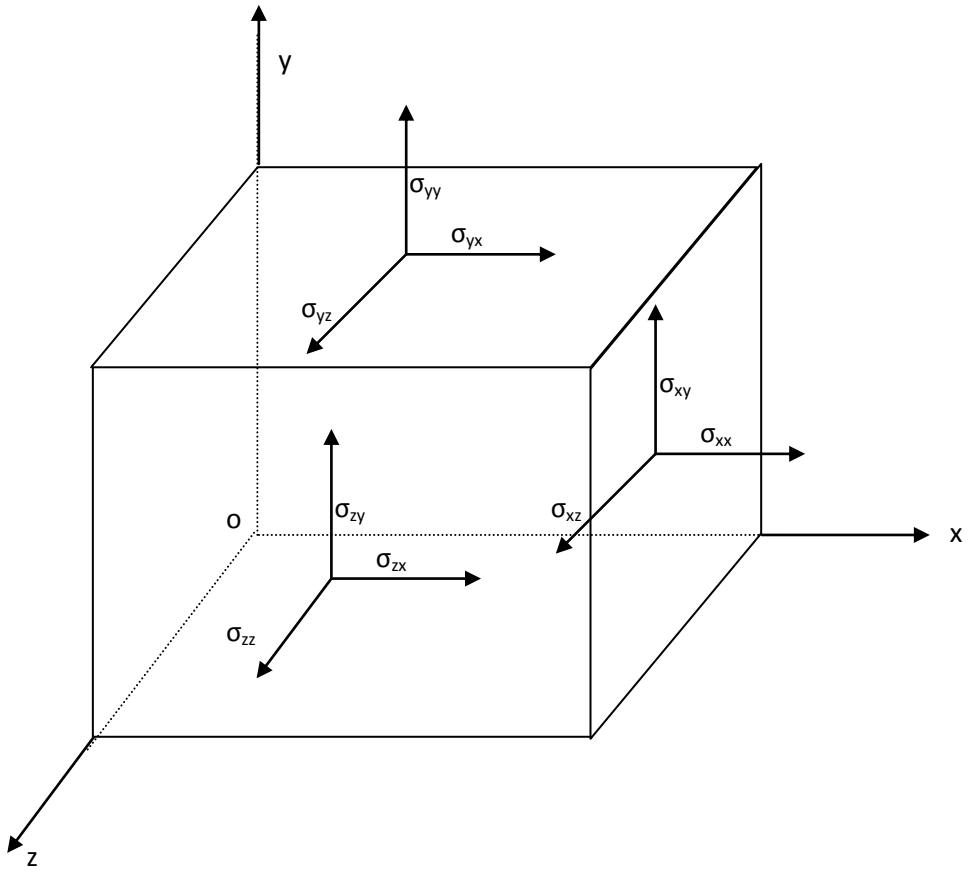

Fig. 2.1 Elementary Cubic Body.

It is necessary to determine nine stress components ($\sigma_{yy},\sigma_{zz},\sigma_{xy},\sigma_{yx},\sigma_{yz},\sigma_{zy},\sigma_{xz},\sigma_{zx}$ and σ_{xx}) and six strain components ($\varepsilon_{xx},\varepsilon_{yy},\varepsilon_{zz},\gamma_{xr},\gamma_{yz}$ and γ_{zx}) in order to provide complete information of an elastic field. Instead of strain components, sometimes the displacement components (u_x,u_y and u_z) are determined. It is worthy to mention that the components of strain and displacement can be determined from each other and each set provide the similar information. Therefore, either the components of strain or displacement are sufficient for a particular purpose.

By a simple consideration of the equilibrium of the element shown in fig. 2.1, it can be shown that $\sigma_{xy}=\sigma_{yx}$, $\sigma_{zx}=\sigma_{xz}$ and $\sigma_{yz}=\sigma_{zy}$ Thus, the nine components of stress are reduced to six σ_{xx}, σ_{yy}, σ_{zz}, σ_{xy}, σ_{yz} and σ_{zx} [23-24].

From the consideration of an infinitesimal cubic element surrounding a given point in a body, it is found that the static equilibrium of forces requires at this point is to satisfy the followings equations:

$$\left.\begin{aligned}
&\frac{\partial \sigma_{xx}}{\partial x}+\frac{\partial \sigma_{xy}}{\partial y}+\frac{\partial \sigma_{xz}}{\partial z}+F_x=0\\
&\frac{\partial \sigma_{yy}}{\partial y}+\frac{\partial \sigma_{xy}}{\partial x}+\frac{\partial \sigma_{yz}}{\partial z}+F_y=0\\
&\frac{\partial \sigma_{zz}}{\partial z}+\frac{\partial \sigma_{yz}}{\partial y}+\frac{\partial \sigma_{zx}}{\partial x}+F_z=0
\end{aligned}\right\} \qquad (2.1)$$

These equations are known as the equations of equilibrium, where F_x, F_y and F_z are the components of the body force in x, y and z directions respectively [24].

The above mentioned three equations of equilibrium are satisfied by the six stress components; but it is not practicable to obtain six stress components solving three equations. In this regard, following six relations are defining the three strain components in terms of the three displacement components through partial differentiation [24].

$$\begin{aligned}
&\varepsilon_{xx}=\frac{\partial u_x}{\partial x},\varepsilon_{yy}=\frac{\partial u_y}{\partial y},\varepsilon_{zz}=\frac{\partial u_z}{\partial z},\\
&\gamma_{xy}=\frac{\partial u_x}{\partial y}+\frac{\partial u_y}{\partial x},\gamma_{yz}=\frac{\partial u_y}{\partial z}+\frac{\partial u_z}{\partial y},\gamma_{zx}=\frac{\partial u_z}{\partial x}+\frac{\partial u_x}{\partial z}
\end{aligned} \qquad (2.2)$$

In addition, the six stress-strain relations are also there. Thus one can have altogether 15 unknowns and 15 equations. This system of equations is generally sufficient for the solution of an elasticity problem.

By differentiation and simple manipulation of Eq. (2.2), the following set of differential equations can be obtained.

$$\begin{aligned}
&\frac{\partial^2 \varepsilon_{xx}}{\partial y^2}+\frac{\partial^2 \varepsilon_{yy}}{\partial x^2}=\frac{\partial^2 \gamma_{xy}}{\partial x \partial y}; \quad 2\frac{\partial^2 \varepsilon_{xx}}{\partial y \partial z}=\frac{\partial}{\partial x}\left(-\frac{\partial \gamma_{yz}}{\partial x}+\frac{\partial \gamma_{xz}}{\partial y}+\frac{\partial \gamma_{xy}}{\partial z}\right)\\
&\frac{\partial^2 \varepsilon_{yy}}{\partial z^2}+\frac{\partial^2 \varepsilon_{zz}}{\partial y^2}=\frac{\partial^2 \gamma_{yz}}{\partial y \partial z}; \quad 2\frac{\partial^2 \varepsilon_{yy}}{\partial x \partial z}=\frac{\partial}{\partial y}\left(\frac{\partial \gamma_{yz}}{\partial x}-\frac{\partial \gamma_{xz}}{\partial y}+\frac{\partial \gamma_{xy}}{\partial z}\right)
\end{aligned} \qquad (2.3)$$

$$\frac{\partial^2 \varepsilon_{zz}}{\partial x^2}+\frac{\partial^2 \varepsilon_{xx}}{\partial z^2}=\frac{\partial^2 \gamma_{xz}}{\partial x \partial z}; \qquad 2\frac{\partial^2 \varepsilon_{zz}}{\partial x \partial y}=\frac{\partial}{\partial z}\left(\frac{\partial \gamma_{yz}}{\partial x}+\frac{\partial \gamma_{xz}}{\partial y}-\frac{\partial \gamma_{xy}}{\partial z}\right)$$

These differential relations are known as the conditions of compatibility. The solution of an elasticity problem must satisfy the equilibrium i.e. Eq (2.1) and the compatibility conditions i.e. Eq (2.3) along with the boundary conditions.

2.3 Hooke's Law

Hooke's law named after the 17th century British physicist Robert Hooke states that the relation between stress and strain is linear. The most general form of linear stress-strain relationship for anisotropic material is given by the following expression [25].

$$\begin{Bmatrix}\sigma_{xx}\\ \sigma_{yy}\\ \sigma_{zz}\\ \sigma_{yz}\\ \sigma_{zx}\\ \sigma_{xy}\\ \sigma_{yx}\\ \sigma_{xz}\\ \sigma_{zy}\end{Bmatrix}=\begin{bmatrix} c_{11} & c_{12} & c_{13} & c_{14} & c_{15} & c_{16} & c_{17} & c_{18} & c_{19}\\ c_{21} & c_{22} & c_{23} & c_{24} & c_{25} & c_{26} & c_{27} & c_{28} & c_{29}\\ c_{31} & c_{32} & c_{33} & c_{34} & c_{35} & c_{36} & c_{37} & c_{38} & c_{39}\\ c_{41} & c_{42} & c_{43} & c_{44} & c_{45} & c_{46} & c_{47} & c_{48} & c_{49}\\ c_{51} & c_{52} & c_{53} & c_{54} & c_{55} & c_{56} & c_{57} & c_{58} & c_{59}\\ c_{61} & c_{62} & c_{63} & c_{64} & c_{65} & c_{66} & c_{67} & c_{68} & c_{69}\\ c_{71} & c_{72} & c_{73} & c_{74} & c_{75} & c_{76} & c_{77} & c_{78} & c_{79}\\ c_{81} & c_{82} & c_{83} & c_{84} & c_{85} & c_{86} & c_{87} & c_{88} & c_{89}\\ c_{91} & c_{92} & c_{93} & c_{94} & c_{95} & c_{96} & c_{97} & c_{98} & c_{99}\end{bmatrix}\begin{Bmatrix}\varepsilon_{xx}\\ \varepsilon_{yy}\\ \varepsilon_{zz}\\ \gamma_{yz}\\ \gamma_{zx}\\ \gamma_{xy}\\ \gamma_{yx}\\ \gamma_{xz}\\ \gamma_{zy}\end{Bmatrix} \tag{2.4}$$

Where the 81 coefficients c_{11},……, c_{99} are called elastic coefficients or stiffness. For the equilibrium condition it is found that $\sigma_{ij}=\sigma_{ji}$ $\gamma_{ij}=\gamma_{ji}$. As such $\sigma_{xy}=\sigma_{yx}$, $\sigma_{zx}=\sigma_{xz}$, $\sigma_{yz}=\sigma_{zy}$, $\gamma_{xy}=\gamma_{yx}$, $\gamma_{zx}=\gamma_{zz}$ and $\gamma_{yz}=\gamma_{zy}$.
Therefore, the stress–strain relation becomes as follows

$$\begin{Bmatrix}\sigma_{xx}\\ \sigma_{yy}\\ \sigma_{zz}\\ \sigma_{yx}\\ \sigma_{zx}\\ \sigma_{xy}\end{Bmatrix}=\begin{bmatrix} c_{11} & c_{12} & c_{13} & c_{14} & c_{15} & c_{16}\\ c_{21} & c_{22} & c_{23} & c_{24} & c_{25} & c_{26}\\ c_{31} & c_{32} & c_{33} & c_{34} & c_{35} & c_{36}\\ c_{41} & c_{42} & c_{43} & c_{44} & c_{45} & c_{46}\\ c_{51} & c_{52} & c_{53} & c_{54} & c_{55} & c_{56}\\ c_{61} & c_{62} & c_{63} & c_{64} & c_{65} & c_{66}\end{bmatrix}\begin{Bmatrix}\varepsilon_{xx}\\ \varepsilon_{yy}\\ \varepsilon_{zz}\\ \gamma_{yz}\\ \gamma_{zx}\\ \gamma_{xy}\end{Bmatrix} \tag{2.5}$$

From the consideration of strain energy density, it can be shown that $c_{ij} = c_{ji}$ [22]. Therefore,

$c_{12} = c_{21}$, $c_{13} = c_{31}$, $c_{14} = c_{41}$, $c_{15} = c_{51}$, $c_{16} = c_{61}$

$c_{23} = c_{32}$, $c_{24} = c_{42}$, $c_{25} = c_{52}$, $c_{26} = c_{62}$, $c_{34} = c_{43}$

$c_{35} = c_{53}$, $c_{36} = c_{63}$, $c_{45} = c_{54}$, $c_{46} = c_{64}$, $c_{56} = c_{65}$

Thus, the 36 unknown coefficients of the stiffness matrix in Eq. (2.5) come down to 21 unknown and the stiffness matrix turns to a symmetric matrix as follows.

$$\left[C_{ij}\right] = \begin{bmatrix} c_{11} & c_{12} & c_{13} & c_{14} & c_{15} & c_{16} \\ c_{12} & c_{22} & c_{23} & c_{24} & c_{25} & c_{26} \\ c_{13} & c_{23} & c_{33} & c_{34} & c_{35} & c_{36} \\ c_{14} & c_{24} & c_{34} & c_{44} & c_{45} & c_{46} \\ c_{15} & c_{25} & c_{35} & c_{45} & c_{55} & c_{56} \\ c_{16} & c_{26} & c_{36} & c_{46} & c_{56} & c_{66} \end{bmatrix} \tag{2.6}$$

Materials having symmetry with respect to one plane is referred to as monoclinic materials. For such case of material, transformation of axis can be done and found that $c_{14} = c_{15} = c_{24} = c_{25} = c_{34} = c_{35} = c_{44} = c_{56} = 0$ and then the number of elastic coefficient becomes 13 only.

Thus, the stiffness matrix of Eq. (2.6) further reduces to

$$\left[C_{ij}\right] = \begin{bmatrix} c_{11} & c_{12} & c_{13} & 0 & 0 & c_{16} \\ c_{12} & c_{22} & c_{23} & 0 & 0 & c_{26} \\ c_{13} & c_{23} & c_{33} & 0 & 0 & c_{36} \\ 0 & 0 & 0 & c_{44} & c_{45} & 0 \\ 0 & 0 & 0 & c_{45} & c_{55} & 0 \\ c_{16} & c_{26} & c_{36} & 0 & 0 & 0 \end{bmatrix} \tag{2.7}$$

Now an orthotropic material has two orthogonal planes of symmetry, where material properties are independent of direction within each plane. Normally the reference system of coordinates is selected along the principal planes of material symmetry. Examples of an orthogonal material include a single lamina of continuous fibre composite arranged in a rectangular array, a wooden bar and rolled steel. For such

cases $c_{16} = c_{26} = c_{36} = c_{45} = 0$ and then this type of materials require 9 independent variables as elastic constants in their stiffness matrix as follows.

$$[C_{ij}](Orthotropic) = \begin{bmatrix} c_{11} & c_{12} & c_{13} & 0 & 0 & 0 \\ c_{12} & c_{22} & c_{23} & 0 & 0 & 0 \\ c_{13} & c_{23} & c_{33} & 0 & 0 & 0 \\ 0 & 0 & 0 & c_{44} & 0 & 0 \\ 0 & 0 & 0 & 0 & c_{55} & 0 \\ 0 & 0 & 0 & 0 & 0 & c_{66} \end{bmatrix} \tag{2.8}$$

Where

$$c_{11} = \frac{1-\mu_{yz}\mu_{zy}}{E_y E_z \nabla}; \quad c_{12} = \frac{\mu_{xy}+\mu_{zy}\mu_{xz}}{E_x E_z \nabla}$$

$$c_{13} = \frac{\mu_{xz}+\mu_{zy}\mu_{yz}}{E_x E_y \nabla}; \quad c_{22} = \frac{1-\mu_{xz}\mu_{zx}}{E_x E_z \nabla}$$

$$c_{23} = \frac{\mu_{yz}+\mu_{yx}\mu_{xz}}{E_x E_y \nabla}; \quad c_{33} = \frac{1-\mu_{xy}\mu_{yx}}{E_x E_y \nabla}$$

$$c_{44} = G_{yz}; c_{55} = G_{zx}; c_{66} = G_{xy}$$

$$\nabla = \frac{1-\mu_{xy}\mu_{yx}-\mu_{yz}\mu_{zy}-\mu_{zx}\mu_{xz}-2\mu_{yx}\mu_{zy}\mu_{xz}}{E_x E_y E_z}$$

The reciprocal relations are given by.

$$\frac{\mu_{ij}}{E_i} = \frac{\mu_{ji}}{E_j}; i, j = x, y, z$$

Most metallic alloys are considered isotropic material, where by definition the mechanical properties are independent of direction. In this case there are infinite planes of symmetry. Such materials have only two independent variables i.e. elastic constants in their stiffness matrix as

$$[C_{ij}](Isotropic)=\begin{bmatrix} c_{11} & c_{12} & c_{12} & 0 & 0 & 0 \\ c_{12} & c_{11} & c_{12} & 0 & 0 & 0 \\ c_{12} & c_{12} & c_{11} & 0 & 0 & 0 \\ 0 & 0 & 0 & \frac{c_{11}-c_{12}}{2} & 0 & 0 \\ 0 & 0 & 0 & 0 & \frac{c_{11}-c_{12}}{2} & 0 \\ 0 & 0 & 0 & 0 & 0 & \frac{c_{11}-c_{12}}{2} \end{bmatrix} \quad (2.9)$$

The constants are given by

$$c_{11}=\frac{E(1-\mu)}{(1-2\mu)(1+\mu)};\ c_{12}=\frac{\mu E}{(1-2\mu)(1+\mu)}\ ;\ \text{and}\quad \frac{c_{11}-c_{12}}{2}=\frac{E}{2(1+2\mu)(1-2\mu)}$$

The summarised form of independent elastic constants for general anisotropic, anisotropic with symmetric stress and strain components or with energy consideration, orthotropic and isotropic materials can be thus presented in Table 2.1 as follows.

Table 2.1 Number of Elastic Constants

Serial	Material	Condition	No of constant
1	Anisotropic	General form	81
2	Anisotropic	Equilibrium condition	36
3	Anisotropic	Strain energy consideration	21
4	Monoclinic	Symmetric to a plane	13
5	Orthotropic	Having mutually perpendicular planes of symmetry	09
6	Isotropic	Same elastic properties in all directions (having infinite perpendicular planes of symmetry)	02

2.4 Two-Dimensionalization of the Problem

Orthotropic and isotropic materials can be analyzed using two dimensions on the consideration of symmetry of planes, though the elastic analysis in general form is of three dimensional. For such simplification there are two options i.e. (i) plane strain condition and (ii) plane stress condition.

Plane strain is said to be a state of strain in which the strain normal to the x-y plane ε_{zz} and the shear strains $\gamma_{xz \text{ and }} \gamma_{yz}$ are assumed to be zero. The assumptions of the plane strain are realistic for long bodies (saying in the z direction) with constant cross-sectional area subjected to loads that act only in the x and/or y directions and do not vary in the z direction.

On the other hand Plane stress condition is considered to be a state of stress in which the normal stress σ_{zz} and the shear stresses σ_{xz} and σ_{yz} directed perpendicular to the plane are assumed to be zero (but not the strain). Generally, members that are thin (those with a small z dimension compared to the in-plane x and y dimensions) and whose loads act only in the x-y plane can be considered to be under plane stress. Thus, a state of plane stress exists in a thin object loaded in the plane of its largest dimensions. The non-zero stresses σ_{xx}, σ_{yy}, and σ_{xy} lie in the x-y plane and do not vary in the z direction.

The option (ii) i.e. the plane stress condition has been followed in the present study. Thus

$$\sigma_{zz} = 0;\ \sigma_{zx} = 0;\ \sigma_{yz} = 0 \tag{2.10}$$

At this condition, the equilibrium equation (2.1) having no body force reduces to

$$\frac{\partial \sigma_{xx}}{\partial x} + \frac{\partial \sigma_{xy}}{\partial y} = 0 \tag{2.11a}$$

$$\frac{\partial \sigma_{yy}}{\partial y} + \frac{\partial \sigma_{xy}}{\partial x} = 0 \tag{2.11b}$$

The stresses for a two dimensional element at plane stress condition are shown in Fig. 2.2.

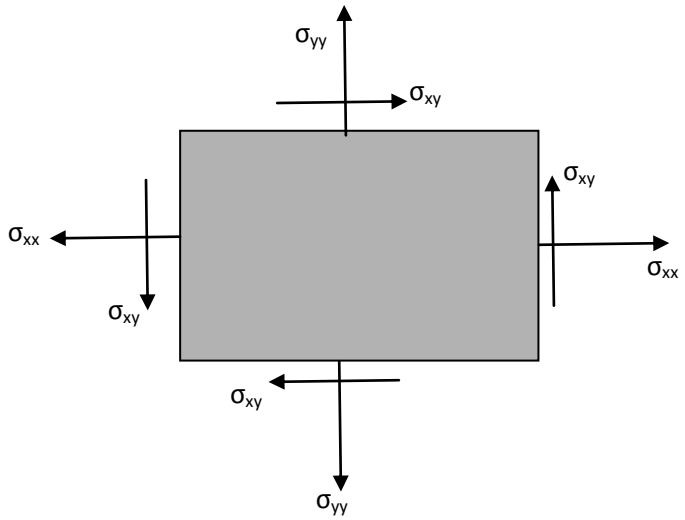

Fig. 2.2 Stress components on a plane

The two equilibrium equations (2.11) contain three unknown stress components. Thus, one more equation is required to obtain the solution of three unknowns. The third equation is the mathematical formulation of the condition for compatibility, which can be obtained from the strain displacement relations. For two dimensional cases, these relations are:

$$\varepsilon_{xx} = \frac{\partial u_x}{\partial x}, \quad \varepsilon_{yy} = \frac{\partial u_y}{\partial y}, \quad \gamma_{xy} = \frac{\partial u_x}{\partial y} + \frac{\partial u_y}{\partial x} \tag{2.12}$$

Differentiating the first equation of (2.12) twice with respective to *y,* the second twice with respect to *x* and the third once with respect to *x* and once with respect to *y,* the expression for condition of compatibility in term of strain then becomes as follows:

$$\frac{\partial^2 \varepsilon_{xx}}{\partial y^2} + \frac{\partial^2 \varepsilon_{yy}}{\partial x^2} = \frac{\partial^2 \gamma_{xy}}{\partial x \partial y} \tag{2.13}$$

But there is required one more equation in terms of stresses; which can be obtained using stiffness matrix in Eq. (2.13). For orthotropic material, while the stiffness matrix is given by Eq (2.8), the stress-strain relations in the case of plane stress can be reduced to:

$$\begin{bmatrix} \sigma_{xx} \\ \sigma_{yy} \\ \sigma_{xy} \end{bmatrix} = \begin{bmatrix} K_{11} & K_{12} & 0 \\ K_{12} & K_{22} & 0 \\ 0 & 0 & K_{66} \end{bmatrix} \begin{bmatrix} \varepsilon_{xx} \\ \varepsilon_{yy} \\ \gamma_{xy} \end{bmatrix} \tag{2.14}$$

It can be noted that the symbols of elastic constants (c) are replaced conveniently by the symbols *K*'s for the case of plane stress condition so that they can be identified easily, where

$$\left.\begin{aligned} K_{11} &= \frac{E_x}{1-\mu_{xy}\mu_{yx}}; \qquad K_{12} = \frac{\mu_{xy}E_y}{1-\mu_{xy}\mu_{yx}} = \frac{\mu_{yx}E_x}{1-\mu_{xy}\mu_{yx}} \\ K_{22} &= \frac{E_y}{1-\mu_{xy}\mu_{yx}}; \qquad K_{66} = G_{xy} \end{aligned}\right\} \tag{2.15}$$

From the elastic constant K_{12} of Eq. (2.15) the reciprocal relations can be reduced as:

$$\frac{\mu_{xy}}{E_x} = \frac{\mu_{yx}}{E_y} \tag{2.16}$$

Making use of Eqs. (2.13), (2.14), (2.15) and (2.16), the differential equation for compatibility condition in terms of stresses can be as follows:

$$\left(\frac{1}{E_x}\frac{\partial^2\sigma_{xx}}{\partial y^2} + \frac{1}{E_y}\frac{\partial^2\sigma_{yy}}{\partial x^2}\right) - \frac{\mu_{xy}}{E_x}\left(\frac{\partial^2\sigma_{yy}}{\partial y^2} + \frac{\partial^2\sigma_{xx}}{\partial x^2}\right) = \frac{1}{G_{xy}}\frac{\partial^2\sigma_{xy}}{\partial x\partial y} \tag{2.17}$$

Now Eq.(2.11) and (2.17) are to be solved to obtain elastic fields satisfying the boundary conditions.

2.5 Usual Method of Solution

The analytical solution of three simultaneous partial differential equations given by Eq (2.11) and (2.17) is fairly impossible as per existing mathematical methods. However, these equations may be solved numerically. The numerical solution procedure is even complicated and cumbersome for this type of equations. Moreover, it gives only approximate results. As such it continues to remain a challenging job for the researchers to obtain the solution of elastic fields analytically for a composite structural element under mixed mode boundary conditions using traditional

formulation. In this study, attention is paid to the theoretical enhancement of suitable and reliable formulation for the solution for elastic fields of orthotropic as well as isotropic composite panels under mixed mode of boundary conditions..

By assuming intermediate functions it is possible to reduce the number of unknowns. It is noticed that the number of partial differential equations (Eq. 2.11 and 2.17) and the unknown terms can be reduced to two when the stress components of these equations are replaced by displacement components. Using equations (2.12), (2.14) and (2.15) it is possible to get three expressions for three stresses in terms of two displacement components as follows:

$$\sigma_{xx} = \frac{\mathrm{E_x}}{1 - \mu_{xy}\mu_{yx}}\left[\frac{\partial u_x}{\partial x} + \mu_{yx}\frac{\partial u_y}{\partial y}\right] \tag{2.18a}$$

$$\sigma_{yy} = \frac{\mathrm{E_y}}{1 - \mu_{xy}\mu_{yx}}\left[\frac{\partial u_y}{\partial y} + \mu_{yx}\frac{\partial u_x}{\partial x}\right] \tag{2.18b}$$

$$\sigma_{xy} = \mathrm{G_{xy}}\left[\frac{\partial u_x}{\partial y} + \mu_{yx}\frac{\partial u_y}{\partial x}\right] \tag{2.18c}$$

Substituting Eq. (2.16) and (2.18) in to equilibrium equations (2.11) the following two elliptical partial differential equations are obtained.

$$\left(\frac{E_x^2}{E_x - \mu_{xy}^2 E_y}\right)\frac{\partial^2 u_x}{\partial x^2} + \left(\frac{\mu_{xy}E_xE_y}{E_x - \mu_{xy}^2 E_y} + G_{xy}\right)\frac{\partial^2 u_y}{\partial x \partial y} + G_{xy}\frac{\partial^2 u_x}{\partial y^2} = 0 \tag{2.19a}$$

$$\left(\frac{E_xE_y}{E_x - \mu_{xy}^2 E_y}\right)\frac{\partial^2 u_y}{\partial y^2} + \left(\frac{\mu_{xy}E_xE_y}{E_x - \mu_{xy}^2 E_y} + G_{xy}\right)\frac{\partial^2 u_x}{\partial x \partial y} + G_{xy}\frac{\partial^2 u_y}{\partial x^2} = 0 \tag{2.19b}$$

2.6 Stress Function Approach

Stress function is being used for long time in the analytical approach, since it was introduced by George Biddell Airy, a British astrologer and mathematician, in 1862. Airy's stress function *Φ(x,y)* is defined in terms of stresses as a function of *x* and *y* for which following conditions are met [23-24]:

$$\sigma_{xx} = \frac{\partial^2 \phi}{\partial y^2} \; ; \qquad \sigma_{yy} = \frac{\partial^2 \phi}{\partial x^2} \; ; \qquad \sigma_{xy} = -\frac{\partial^2 \phi}{\partial x \partial y} \tag{2.20}$$

Stress function satisfies the equilibrium equations and compatibility conditions. After applying the above relations of stresses in terms of *Φ(x,y)* in Eq. (2.17) following expression is obtained.

$$\left\{\frac{1}{E_x}\frac{\partial^2}{\partial y^2}\left(\frac{\partial^2 \phi}{\partial y^2}\right)+\frac{1}{E_y}\frac{\partial^2}{\partial x^2}\left(\frac{\partial^2 \phi}{\partial x^2}\right)\right\}-\frac{\mu_{xy}}{E_x}\left\{\frac{\partial^2}{\partial y^2}\left(\frac{\partial^2 \phi}{\partial x^2}\right)+\frac{\partial^2}{\partial x^2}\left(\frac{\partial^2 \phi}{\partial y^2}\right)\right\}=\frac{1}{G_{xy}}\frac{\partial^2}{\partial x \partial y}\left(-\frac{\partial^2 \phi}{\partial x \partial y}\right)$$

or, $$\frac{1}{E_y}\frac{\partial^4 \phi}{\partial x^4}+\left(\frac{1}{G_{xy}}-\frac{2\mu_{xy}}{E_x}\right)\frac{\partial^4 \phi}{\partial x^2 \partial y^2}+\frac{1}{E_x}\frac{\partial^4 \phi}{\partial y^4}=0 \tag{2.21}$$

This expression is the bi-harmonic partial differential equation for Airy's stress function. Now Eq. (2.21) is to be solved satisfying the boundary conditions to obtain stress components using Eq. (2.20) and then Hooke's law as well as strain displacement relations are used to obtain the displacement components.

For orthotropic case [Fig. 2.3] the young's moduli E_x and E_y may be replaced by E_1 and E_2 where they are used to denote the Young's modulus in the fibre direction and in perpendicular to the fibre direction respectively. Further G_{xy} is replaced by G_{12} to denote the shear modulus for on-axis orientation.

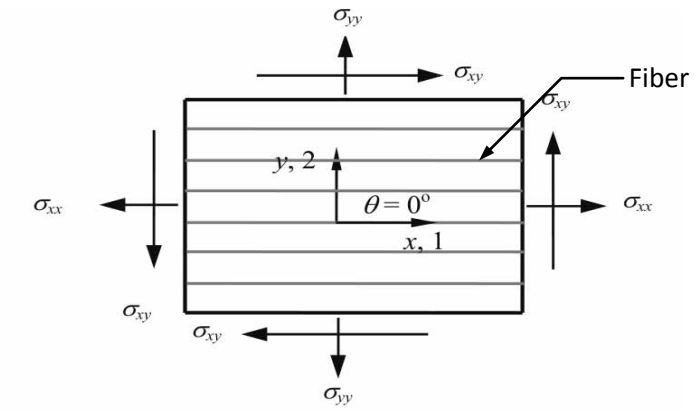

Fig. 2.3 Stress components on a composite plane

In such case the bi-harmonic governing differential equation orthotropic composites on the basis of stress function *Φ(x,y)* i.e. Eq. (2.21) becomes:

$$\frac{1}{E_2}\frac{\partial^4\phi}{\partial x^4}+\left(\frac{1}{G_{12}}-\frac{2\mu_{12}}{E_1}\right)\frac{\partial^4\phi}{\partial x^2\partial y^2}+\frac{1}{E_1}\frac{\partial^4\phi}{\partial y^4}=0 \tag{2.22}$$

For an isotropic elastic materials under the condition of plane stress $E_x = E_y = E$, $\mu_{xy}=\mu_{yx}=\mu$ and $G_{xy}=G=\frac{E}{2(1+\mu)}$. Substituting these relations in Eq. (2.21) the mathematical model for the isotropic condition is found as:

$$\frac{\partial^4\phi}{\partial x^4}+2\frac{\partial^4\phi}{\partial x^2\partial y^2}+\frac{\partial^4\phi}{\partial y^4}=0 \tag{2.23}$$

Eqs. (2.22) and (2.23) developed basing on Airy's stress function can handle elastic problems of orthotropic and isotropic materials, whose boundary conditions are in terms of stress or load only. Thus attention is obviously necessary towards the solution of the two elliptical partial differential equations for those problems where the boundary restrains are to be satisfied. Again it is not even easy task to obtain the values of displacement components by the solution of equations (2.19). Consequently, further simplification of the solution method is the necessity.

2.7 Displacement Potential Formulation

Since it is difficult to solve the equations (2.19), a single function $\psi(x,y)$ is taken into consideration [16] [22], which has to satisfy a single partial differential equation of equilibrium, somewhat similar in concept to that of Eq.(2.21). It is named as displacement potential function and defined as a function $\psi(x,y)$ of space variables *x* and *y,* where the displacement components are expressed as follows:

$$u_x=\alpha_1\frac{\partial^2\psi}{\partial x^2}+\alpha_2\frac{\partial^2\psi}{\partial x\partial y}+\alpha_3\frac{\partial^2\psi}{\partial y^2} \tag{2.24a}$$

$$u_y=\alpha_4\frac{\partial^2\psi}{\partial x^2}+\alpha_5\frac{\partial^2\psi}{\partial x\partial y}+\alpha_6\frac{\partial^2\psi}{\partial y^2} \tag{2.24b}$$

Here, $\alpha's$ are unknown material constants.

Using the expressions of Eq. (2.24) in Eq (2.19a) following equation is obtained.

$$\left(\frac{E_x^2}{E_x-\mu_{xy}^2E_y}\right)\frac{\partial^2}{\partial x^2}\left(\alpha_1\frac{\partial^2\psi}{\partial x^2}+\alpha_2\frac{\partial^2\psi}{\partial x\partial y}+\alpha_3\frac{\partial^2\psi}{\partial y^2}\right)+\left(\frac{\mu_{xy}E_xE_y}{E_x-\mu_{xy}^2E_y}+G_{xy}\right)$$
$$\frac{\partial^2}{\partial x\partial y}\left(\alpha_4\frac{\partial^2\psi}{\partial x^2}+\alpha_5\frac{\partial^2\psi}{\partial x\partial y}+\alpha_6\frac{\partial^2\psi}{\partial y^2}\right)+G_{xy}\frac{\partial^2}{\partial y^2}\left(\alpha_1\frac{\partial^2\psi}{\partial x^2}+\alpha_2\frac{\partial^2\psi}{\partial x\partial y}+\alpha_3\frac{\partial^2\psi}{\partial y^2}\right)=0$$

or,

$$\left(\frac{E_x^2}{E_x-\mu_{xy}^2E_y}\right)\left(\alpha_1\frac{\partial^4\psi}{\partial x^4}+\alpha_2\frac{\partial^4\psi}{\partial x^3\partial y}+\alpha_3\frac{\partial^4\psi}{\partial x^2\partial y^2}\right)+\left(\frac{\mu_{xy}E_xE_y}{E_x-\mu_{xy}^2E_y}+G_{xy}\right)$$
$$\left(\alpha_4\frac{\partial^4\psi}{\partial x^3\partial y}+\alpha_5\frac{\partial^4\psi}{\partial x^2\partial y^2}+\alpha_6\frac{\partial^4\psi}{\partial x\partial y^3}\right)+G_{xy}\left(\alpha_1\frac{\partial^4\psi}{\partial x^2\partial y^2}+\alpha_2\frac{\partial^4\psi}{\partial x\partial y^3}+\alpha_3\frac{\partial^4\psi}{\partial y^4}\right)=0$$

or,

$$\left(\frac{E_x^2}{E_x-\mu_{xy}^2E_y}\right)\alpha_1\frac{\partial^4\psi}{\partial x^4}+\left\{\left(\frac{E_x^2}{E_x-\mu_{xy}^2E_y}\right)\alpha_2+\left(\frac{\mu_{xy}E_xE_y}{E_x-\mu_{xy}^2E_y}+G_{xy}\right)\alpha_4\right\}\frac{\partial^4\psi}{\partial x^3\partial y}+$$
$$\left\{\left(\frac{E_x^2}{E_x-\mu_{xy}^2E_y}\right)\alpha_3+\left(\frac{\mu_{xy}E_xE_y}{E_x-\mu_{xy}^2E_y}+G_{xy}\right)\alpha_5+G_{xy}\alpha_1\right\}\frac{\partial^4\psi}{\partial x^2\partial y^2}+ \qquad (2.25)$$
$$\left\{\left(\frac{\mu_{xy}E_xE_y}{E_x-\mu_{xy}^2E_y}+G_{xy}\right)\alpha_6+G_{xy}\alpha_2\right\}\frac{\partial^4\psi}{\partial x\partial y^3}+G_{xy}\alpha_3\frac{\partial^4\psi}{\partial y^4}=0$$

The material constants α's are chosen in such a way that the equation (2.25) is automatically satisfied under all circumstances. This will happen when all of its coefficients are independently zero. In that situation,

$$\left(\frac{E_x^2}{E_x-\mu_{xy}^2E_y}\right)\alpha_1=0$$
$$\left(\frac{E_x^2}{E_x-\mu_{xy}^2E_y}\right)\alpha_2+\left(\frac{\mu_{xy}E_xE_y}{E_x-\mu_{xy}^2E_y}+G_{xy}\right)\alpha_4=0$$

$$\left(\frac{E_x^2}{E_x-\mu_{xy}^2E_y}\right)\alpha_3+\left(\frac{\mu_{xy}E_xE_y}{E_x-\mu_{xy}^2E_y}+G_{xy}\right)\alpha_5+G_{xy}\alpha_1=0$$

$$\left(\frac{\mu_{xy}E_xE_y}{E_x-\mu_{xy}^2E_y}+G_{xy}\right)\alpha_6+G_{xy}\alpha_2=0$$

$$G_{xy}\alpha_3=0$$

Therefore,

$$\left.\begin{aligned}&\alpha_1=\alpha_3=\alpha_5=0\\&\alpha_4=\frac{-E_x^2\alpha_2}{\left\{\mu_{xy}E_xE_y+G_{xy}\left(E_x-\mu_{xy}^2E_y\right)\right\}}\\&\alpha_6=\frac{-G_{xy}\left(E_x-\mu_{xy}^2E_y\right)\alpha_2}{\left\{\mu_{xy}E_xE_y+G_{xy}\left(E_x-\mu_{xy}^2E_y\right)\right\}}\end{aligned}\right\}\qquad(2.26)$$

Again from the second equation of (2.19) and Eq (2.24) it is found that

$$\left(\frac{E_xE_y}{E_x-\mu_{xy}^2E_y}\right)\frac{\partial^2}{\partial y^2}\left(\alpha_4\frac{\partial^2\psi}{\partial x^2}+\alpha_5\frac{\partial^2\psi}{\partial x\partial y}+\alpha_6\frac{\partial^2\psi}{\partial y^2}\right)+\left(\frac{\mu_{xy}E_xE_y}{E_x-\mu_{xy}^2E_y}+G_{xy}\right)$$
$$\frac{\partial^2}{\partial x\partial y}\left(\alpha_1\frac{\partial^2\psi}{\partial x^2}+\alpha_2\frac{\partial^2\psi}{\partial x\partial y}+\alpha_3\frac{\partial^2\psi}{\partial y^2}\right)+G_{xy}\frac{\partial^2}{\partial x^2}\left(\alpha_4\frac{\partial^2\psi}{\partial x^2}+\alpha_5\frac{\partial^2\psi}{\partial x\partial y}+\alpha_6\frac{\partial^2\psi}{\partial y^2}\right)=0$$

or, $$\left(\frac{E_xE_y}{E_x-\mu_{xy}^2E_y}\right)\left(\alpha_4\frac{\partial^4\psi}{\partial x^2\partial y^2}+\alpha_5\frac{\partial^4\psi}{\partial x\partial y^3}+\alpha_6\frac{\partial^4\psi}{\partial y^4}\right)+\left(\frac{\mu_{xy}E_xE_y}{E_x-\mu_{xy}^2E_y}+G_{xy}\right)$$
$$\left(\alpha_1\frac{\partial^4\psi}{\partial x^3\partial y}+\alpha_2\frac{\partial^4\psi}{\partial x^2\partial y^2}+\alpha_3\frac{\partial^4\psi}{\partial x\partial y^3}\right)+G_{xy}\left(\alpha_4\frac{\partial^4\psi}{\partial x^4}+\alpha_5\frac{\partial^4\psi}{\partial x^3\partial y}+\alpha_6\frac{\partial^4\psi}{\partial x^2\partial y^2}\right)=0$$

or, $$G_{xy}\alpha_4\frac{\partial^4\psi}{\partial x^4}+\left\{\left(\frac{\mu_{xy}E_xE_y}{E_x-\mu_{xy}^2E_y}+G_{xy}\right)\alpha_1+G_{xy}\alpha_5\right\}\frac{\partial^4\psi}{\partial x^3\partial y}+\left\{\left(\frac{E_xE_y}{E_x-\mu_{xy}^2E_y}\right)\alpha_4+\left(\frac{\mu_{xy}E_xE_y}{E_x-\mu_{xy}^2E_y}+G_{xy}\right)\alpha_2+G_{xy}\alpha_6\right\}$$
$$\frac{\partial^4\psi}{\partial x^2\partial y^2}+\left\{\left(\frac{E_xE_y}{E_x-\mu_{xy}^2E_y}\right)\alpha_5+\left(\frac{\mu_{xy}E_xE_y}{E_x-\mu_{xy}^2E_y}+G_{xy}\right)\alpha_3\right\}\frac{\partial^4\psi}{\partial x\partial y^3}+\left(\frac{E_xE_y}{E_x-\mu_{xy}^2E_y}\right)\alpha_6\frac{\partial^4\psi}{\partial y^4}=0\qquad(2.27)$$

Now using Eqs (2.26) and (2.27) it is found that

$$G_{xy}\alpha_4\frac{\partial^4\psi}{\partial x^4}+\left\{\left(\frac{E_xE_y}{E_x-\mu_{xy}^2E_y}\right)\alpha_4+\left(\frac{\mu_{xy}E_xE_y}{E_x-\mu_{xy}^2E_y}+G_{xy}\right)\alpha_2+G_{xy}\alpha_6\right\}\frac{\partial^4\psi}{\partial x^2\partial y^2}+\left(\frac{E_xE_y}{E_x-\mu_{xy}^2E_y}\right)\alpha_6\frac{\partial^4\psi}{\partial y^4}=0$$

or,

$$G_{xy}\alpha_4\left(E_x-\mu_{xy}^2E_y\right)\frac{\partial^4\psi}{\partial x^4}+\left[E_xE_y\alpha_4+\left\{\mu_{xy}E_xE_y+G_{xy}\left(E_x-\mu_{xy}^2E_y\right)\right\}\alpha_2+G_{xy}\left(E_x-\mu_{xy}^2E_y\right)\alpha_6\right]\frac{\partial^4\psi}{\partial x^2\partial y^2}+E_xE_y\alpha_6\frac{\partial^4\psi}{\partial y^4}=0$$

$$G_{xy}\left[\frac{-E_x^2\alpha_2}{\left\{\mu_{xy}E_xE_y+G_{xy}\left(E_x-\mu_{xy}^2E_y\right)\right\}}\right]\left(E_x-\mu_{xy}^2E_y\right)\frac{\partial^4\psi}{\partial x^4}+$$

or,

$$\left[E_xE_y\left\{\frac{-E_x^2\alpha_2}{\mu_{xy}E_xE_y+G_{xy}\left(E_x-\mu_{xy}^2E_y\right)}\right\}+\left\{\mu_{xy}E_xE_y+G_{xy}\left(E_x-\mu_{xy}^2E_y\right)\right\}\alpha_2+G_{xy}\left(E_x-\mu_{xy}^2E_y\right)\left\{\frac{-G_{xy}\left(E_x-\mu_{xy}^2E_y\right)\alpha_2}{\mu_{xy}E_xE_y+G_{xy}\left(E_x-\mu_{xy}^2E_y\right)}\right\}\right]$$

$$\frac{\partial^4\psi}{\partial x^2\partial y^2}+E_xE_y\left\{\frac{-G_{xy}\left(E_x-\mu_{xy}^2E_y\right)\alpha_2}{\mu_{xy}E_xE_y+G_{xy}\left(E_x-\mu_{xy}^2E_y\right)}\right\}\frac{\partial^4\psi}{\partial y^4}=0$$

For non-zero values of α_2,

$$-E_x^2G_{xy}\left(E_x-\mu_{xy}^2E_y\right)\frac{\partial^4\psi}{\partial x^4}+\left[-E_{x_x}^3E_y+\left\{\mu_{xy}E_xE_y+G_{xy}\left(E_x-\mu_{xy}^2E_y\right)\right\}^2-G_{xy}^2\left(E_x-\mu_{xy}^2E_y\right)^2\right]\frac{\partial^4\psi}{\partial x^2\partial y^2}-$$

$$E_xE_yG_{xy}\left(E_x-\mu_{xy}^2E_y\right)\frac{\partial^4\psi}{\partial y^4}=0$$

$$-E_x^2G_{xy}\left(E_x-\mu_{xy}^2E_y\right)\frac{\partial^4\psi}{\partial x^4}+\left[-E_x^2E_xE_y+\left\{\mu_{xy}E_xE_y+2G_{xy}\left(E_x-\mu_{xy}^2E_y\right)\right\}\mu_{xy}E_xE_y\right]\frac{\partial^4\psi}{\partial x^2\partial y^2}-$$

or,

$$E_xE_yG_{xy}\left(E_x-\mu_{xy}^2E_y\right)\frac{\partial^4\psi}{\partial y^4}=0$$

or,

$$E_xG_{xy}\frac{\partial^4\psi}{\partial x^4}+E_y\left(E_x-2\mu_{xy}G_{xy}\right)\frac{\partial^4\psi}{\partial x^2\partial y^2}+E_yG_{xy}\frac{\partial^4\psi}{\partial y^4}=0 \qquad (2.28)$$

The above fourth order differential equation (2.28) is only one governing equation for the solution of the displacement potential function ψ. Once the displacement potential function ψ is known, the components of displacement can be readily found from Eq. (2.24). Thereafter, using the stress displacement relations of Eq. (2.18) can be used for obtaining stress components.

Assuming the value of α_2 unity, and taking the values of α_1, α_3, α_4, α_5 and α_6 from Eq.(2.26), one can obtain the components of displacement and stress using Eqs. (2.24) and (2.18) respectively as follows:

$$u_x(x,y)=\frac{\partial^2\psi}{\partial x\partial y} \tag{2.29a}$$

$$u_y(x,y)=\left\{\frac{-1}{\mu_{xy}E_xE_y+G_{xy}\left(E_x-\mu_{xy}^2E_y\right)}\right\}\left[E_x^2\frac{\partial^2\psi}{\partial x^2}+G_{xy}\left(E_x-\mu_{xy}^2E_y\right)\frac{\partial^2\psi}{\partial y^2}\right] \tag{2.29b}$$

$$\sigma_{xx}(x,y)=\left\{\frac{-E_xG_{xy}}{\mu_{xy}E_xE_y+G_{xy}\left(E_x-\mu_{xy}^2E_y\right)}\right\}\left[E_x\frac{\partial^3\psi}{\partial x^2\partial y}-\mu_{xy}E_y\frac{\partial^2\psi}{\partial y^2}\right] \tag{2.29c}$$

$$\sigma_{yy}(x,y)=\left\{\frac{-E_xE_y}{\mu_{xy}E_xE_y+G_{xy}\left(E_x-\mu_{xy}^2E_y\right)}\right\}\left[\left(\mu_{xy}G_{xy}-E_x\right)\frac{\partial^3\psi}{\partial x^2\partial y}-G_{xy}\frac{\partial^3\psi}{\partial y^3}\right] \tag{2.29d}$$

$$\sigma_{xy}(x,y)=\left\{\frac{-E_xG_{xy}}{\mu_{xy}E_xE_y+G_{xy}\left(E_x-\mu_{xy}^2E_y\right)}\right\}\left[E_x\frac{\partial^3\psi}{\partial x^3}-\mu_{xy}E_y\frac{\partial^3\psi}{\partial x\partial y^2}\right] \tag{2.29e}$$

2.7.1 Displacement Potential Formulation for Orthotropic Materials

Case - A : θ = 0^o (Fibers are parallel to the direction of loading)

For orthotropic materials with fibre orientation $\theta = 0^o$ the young's moduli E_x and E_y would be replaced by E_1 and E_2. Further G_{xy} is replaced by G_{12} to denote the shear modulus for on-axis orientation. In such case the governing differential equation (2.28) for the solution of two dimensional orthotropic composite structures becomes:

$$E_1G_{12}\frac{\partial^4\psi}{\partial x^4}+E_2\left(E_1-2\mu_{12}G_{12}\right)\frac{\partial^4\psi}{\partial x^2\partial y^2}+E_2G_{12}\frac{\partial^4\psi}{\partial y^4}=0 \tag{2.30}$$

Then the components of displacement and stress are:

$$u_x(x,y)=\frac{\partial^2\psi}{\partial x\partial y} \tag{2.31a}$$

$$u_y(x,y) = -\frac{1}{Z_{11}}\left[E_1^2 \frac{\partial^2 \psi}{\partial x^2} + G_{12}\left(E_1 - \mu_{12}^2 E_2\right)\frac{\partial^2 \psi}{\partial y^2} \right] \tag{2.31b}$$

$$\sigma_{xx}(x,y) = -\frac{E_1 G_{12}}{Z_{11}}\left[E_1 \frac{\partial^3 \psi}{\partial x^2 \partial y} - \mu_{12} E_2 \frac{\partial^2 \psi}{\partial y^2} \right] \tag{2.31c}$$

$$\sigma_{yy}(x,y) = -\frac{E_1 E_2}{Z_{11}}\left[\left(\mu_{12} G_{12} - E_1\right)\frac{\partial^3 \psi}{\partial x^2 \partial y} - G_{12} \frac{\partial^3 \psi}{\partial y^3} \right] \tag{2.31d}$$

$$\sigma_{xy}(x,y) = -\frac{E_1 G_{12}}{Z_{11}}\left[E_1 \frac{\partial^3 \psi}{\partial x^3} - \mu_{12} E_2 \frac{\partial^3 \psi}{\partial x \partial y^2} \right] \tag{2.31e}$$

where $Z_{11} = \mu_{12} E_1 E_2 + G_{12}\left(E_1 - \mu_{12}^2 E_2\right)$

Case - B : θ = 90^o (Fibers are perpendicular to the direction of loading)

For orthotropic materials with fibre orientation $\theta = 90^o$ the young's moduli E_x and E_y would be replaced by E_2 and E_1. Further μ_{xy} and G_{xy} are replaced by μ_{21} and G_{12} (Since, $G_{12} = G_{21}$) to denote the poisons ratio and shear modulus for on-axis orientation. In such case the governing differential equation for the solution of two dimensional orthotropic composite structures becomes:

$$E_2 G_{12} \frac{\partial^4 \psi}{\partial x^4} + E_2\left(E_1 - 2\mu_{12} G_{12}\right)\frac{\partial^4 \psi}{\partial x^2 \partial y^2} + E_1 G_{12} \frac{\partial^4 \psi}{\partial y^4} = 0 \tag{2.32}$$

Then the components of displacement and stress are:

$$u_x(x,y) = \frac{\partial^2 \psi}{\partial x \partial y} \tag{2.33a}$$

$$u_y(x,y) = -\frac{1}{Z_{11}}\left[E_1 E_2 \frac{\partial^2 \psi}{\partial x^2} + G_{12}\left(E_1 - \mu_{12}^2 E_2\right)\frac{\partial^2 \psi}{\partial y^2} \right] \tag{2.33b}$$

$$\sigma_{xx}(x,y) = \frac{E_1 E_2 G_{12}}{Z_{11}}\left[\frac{\partial^3 \psi}{\partial x^2 \partial y} - \mu_{12} \frac{\partial^3 \psi}{\partial y^3} \right] \tag{2.33c}$$

$$\sigma_{yy}(x,y)=\frac{E_1}{Z_{11}}\left[E_2(\mu_{12}G_{12}-E_1)\frac{\partial^3\psi}{\partial x^2\partial y}-E_1G_{12}\frac{\partial^3\psi}{\partial y^3}\right] \tag{2.33d}$$

$$\sigma_{xy}(x,y)=-\frac{E_1E_2G_{12}}{Z_{11}}\left[\frac{\partial^3\psi}{\partial x^3}-\mu_{12}\frac{\partial^3\psi}{\partial x\partial y^2}\right] \tag{2.33e}$$

2.7.2 Displacement Potential Formulation for Isotropic Materials

For an isotropic elastic solid under the condition of plane stress $E_x = E_y = E$, $\mu_{xy}=\mu_{yx}=\mu$ and $G_{xy}=G=\frac{E}{2(1+\mu)}$. Then the values of α's of Eq. (2.24) are also obtained as follows:

$$\alpha_1=\alpha_3=\alpha_5=0;\ \ \alpha_2=1;\ \ \alpha_4=\frac{-2}{1+\mu};\qquad \alpha_6=\frac{1-\mu}{1+\mu} \tag{2.34}$$

Then the stress-displacement relations for the plane stress problems are obtained from the Hook's law as follows:

$$\sigma_{xx}=\frac{E}{1-\mu^2}\left[\frac{\partial u_x}{\partial x}+\mu\ \ \frac{\partial u_y}{\partial y}\right] \tag{2.35a}$$

$$\sigma_{yy}=\frac{E}{1-\mu^2}\left[\mu\frac{\partial u_x}{\partial x}+\ \ \frac{\partial u_y}{\partial y}\right] \tag{2.35b}$$

$$\sigma_{xy}=\frac{E}{2(1+\mu)}\left[\frac{\partial u_x}{\partial y}+\frac{\partial u_y}{\partial x}\right] \tag{2.35c}$$

When the displacement components in Eq. (2.19) are replaced by Eq. (2.24) having values of α as in Eq. (2.32), the single governing equation of equilibrium in partial differential form being satisfied by $\psi(x, y)$ is found for isotropic materials as follows:

$$\frac{\partial^4\psi}{\partial x^4}+2\frac{\partial^4\psi}{\partial x^2\partial y^2}+\frac{\partial^4\psi}{\partial y^4}=0 \tag{2.36}$$

From Eqs. (2.18), (2.33), and (2.34), the expressions of displacement and stress components in terms of function $\psi(x, y)$ are obtained as follows:

$$u_x(x,y)=\frac{\partial^2\psi}{\partial x\partial y} \tag{2.37a}$$

$$u_y(x,y)=-\frac{1}{1+\mu}\left[2\frac{\partial^2\psi}{\partial x^2}+(1-\mu)\frac{\partial^2\psi}{\partial y^2}\right] \tag{2.37b}$$

$$\sigma_{xx}(x,y)=-\frac{E}{(1+\mu)^2}\left[\frac{\partial^3\psi}{\partial x^2\partial y}-\mu\frac{\partial^2\psi}{\partial y^2}\right] \tag{2.37c}$$

$$\sigma_{yy}(x,y)=-\frac{E}{(1+\mu)^2}\left[(2+\mu)\frac{\partial^3\psi}{\partial x^2\partial y}+\frac{\partial^3\psi}{\partial y^3}\right] \tag{2.37d}$$

$$\sigma_{xy}(x,y)=-\frac{E}{(1+\mu)^2}\left[\frac{\partial^3\psi}{\partial x^3}-\mu\frac{\partial^3\psi}{\partial x\partial y^2}\right] \tag{2.37e}$$

2.8 Consideration of Boundary Conditions

In practical situation, along the edge or boundary of a structure, there are two parameters to be known, i.e. (i) displacements and (ii) loading or stress. Both the displacements and stresses are identified by their respective components as follows:

a. Normal displacement
b. Tangential displacement
c. Normal stress
d. Tangential stress

The solution of the governing equation requires specification of normal and tangential conditions. At any point on the boundary, two components out of four are known at a time. Thus there are six possible types of boundary conditions; which are,

i. Normal displacement and Tangential displacement
ii. Normal displacement and Normal stress
iii. Normal displacement and Tangential stress

iv. Tangential displacement and Normal stress
v. Tangential displacement and Tangential stress
vi. Normal stress and Tangential stress

While both the components are normal or tangential, the boundary conditions do not practically exist. As such boundary conditions of (ii) and (v) are no longer required to be considered and the remaining four boundary conditions would be considered for solving the physical problems of elastic body. If the shape of the boundary surface is rectangular, the structure may be oriented so that its edges are parallel to the co-ordinate axes. In that case, the normal and the tangential components of displacement and stress at the boundary are the corresponding coordinate components inside the structure. Out of the above mentioned four possible boundaries, only the number (vi) is suitable for Airy's stress function, whereas all four boundary conditions can be dealt with displacement potential function (ψ).

CHAPTER 3

CRACKED PANEL UNDER AXIAL STIFFENERS SUBJECTED TO AXIAL TENSION

The main focus of this chapter is to find the stress and displacement fields of a boundary value problem of elasticity using Potential function approach. In this chapter, a stiffened panel with an edge crack is considered for the analysis. The panel is stiffened by axial stiffeners at its opposing longitudinal edges and is loaded axially by uniform tension. The effect of crack length and the panel aspect ratio on the stress field are also discussed in this chapter.

3.1 Problem Articulation

A metallic stiffened panel with an edge crack emanating from the upper surface subjected to uniform tensile loading σ_o at both lateral ends is considered. The analytical model of the panel with a rectangular frame of reference *x-y* is shown in Fig. 4.2a. The geometrical properties of the panel are: length 2b, height *a* and crack length h. Since the structure is symmetric with reference to the y-axis, half of the panel may be considered for the analysis, as shown in Fig. 4.2b, i.e., the right half of the panel with the crack was analyzed due to symmetry. Since the thickness of such structures is very small compared to its other dimensions, the plane stress condition is adopted to model the problem for the determination of the corresponding displacement and stress fields. There will be no axial displacement along the ligament of the full panel due to the symmetry, but the crack surface is free from loading and restraints. No axial displacements will be allowed along the ligament (x=0) over the length $0 \leq y \leq (a-h)$, but the lateral displacements are free to assume any value.

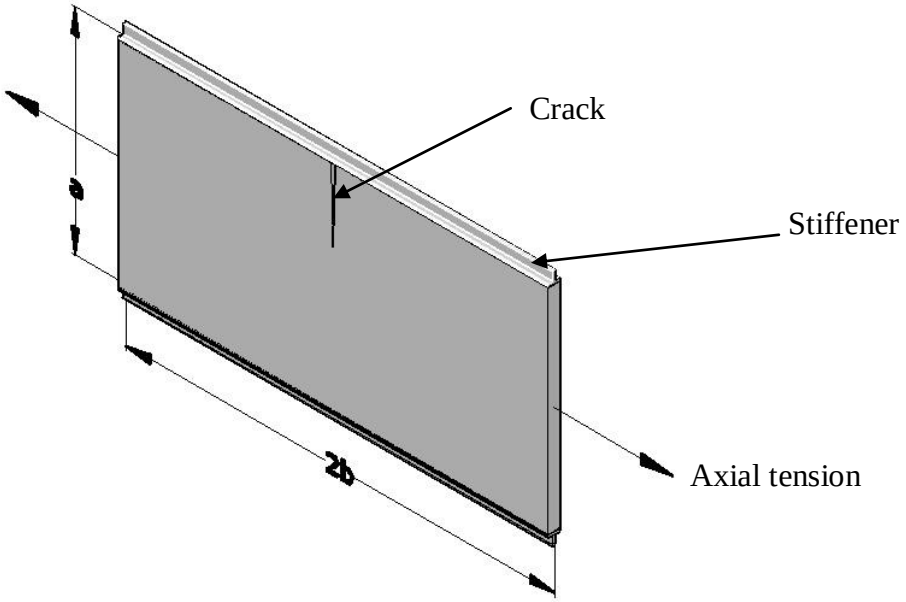

Fig 3.1: 3-D model of the full panel.

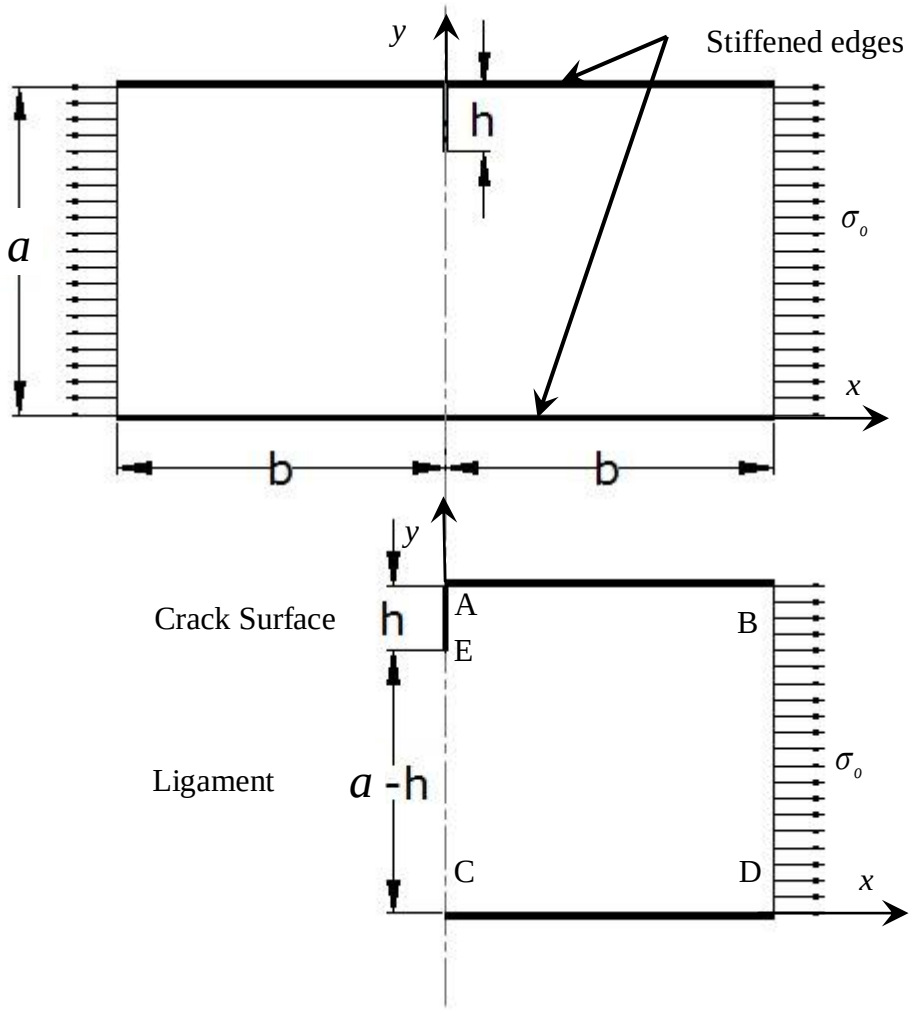

Fig 3.2: Geometry and loading of a stiffened cracked panel: (a) Full model of the panel (b) symmetric model of the panel.

3.2 Boundary Conditions

(i) Stiffened Edge, AB:

Since it is a longitudinal stiffener, there is no axial displacement and lateral stress. Thus,

$u_x(x,a) = 0$ and $\sigma_{yy}(x,a) = 0$ [$0 \le x \le b$]

(ii) Stiffened Edge, CD:

There is no axial displacement and lateral stress. Thus,

$u_x(x,0) = 0$ and $\sigma_{yy}(x,0) = 0$ [$0 \le x \le b$]

(iii) Ligament, EC:

Due to symmetry of the full model of the panel, axial displacement and shear stresses along this section are assumed to be zero.

$u_x(0,y) = 0$ [$0 \le y \le (a\text{-}h)$] and $\sigma_{xy}(0,y) = 0$ [$0 \le y \le (a\text{-}h)$]

Crack surface, AE:

Since the crack surface is free from loading and restraints, there will be no boundary constraints and shear stress.

$\sigma_{xy}(0,y) = 0$ and $\sigma_{xx}(0,y) = 0$ [$(a\text{-}h) \le y \le a$]

(iv) Loading Edge, BD:

The axial tension of the panel is realized by assigning a uniform value to the axial stress component. The boundary will also be free from shearing stress. Thus,

$\sigma_{xx}(b,y) = \sigma_o$ and $\sigma_{xy}(b,y) = 0$ [$0 \le y \le a$]

3.3 Solution Procedure

Displacement potential approach can easily be applied on to problems where the boundary condition at each ends remain the same. But, in this study, for the symmetric section of the panel containing crack two sets of boundary conditions are required, as shown in Fig 3.1. At the crack surface, shear stress and axial stress are zero, whereas at ligament section shear stress and axial displacement are zero. That

means, at the same surface there are two possible sets of boundary conditions available. To solve the problem using displacement potential approach, one set of boundary condition have to be chosen. In this study, shear stress and axial displacement have considered as boundary conditions at the left boundary of the model. Though shear stress is zero throughout the left boundary but at certain length axial displacement is zero and at the remaining length it is not zero. That's why this method needs the value of axial displacement at crack surface to solve it properly i.e. it has to depend on other numerical methods to get those data of axial displacement at crack surface. In such case, Finite Difference Method has been considered. FDM formulation has been used to get a set of value of axial displacement at the crack surface. That sets of data can't be directly used in displacement potential formulation. An equation, that will represent the trend of that set of data, can be used as boundary condition in Displacement Potential Formulation. In true sense, it may be semi-analytical method, the way we formulated the ψ-solution, depending on that we considered it as an analytical method. Besides that FDM scheme had been developed based on the displacement potential approach. To get such equation, one of the curve fitted method have to be followed. To make these computations easier, Curve Fitting Tool box in MATLAB has been used. Fourier series have been chosen as a type of fit. In this type of fit, value of correlation coefficient R^2 is almost equal to 1 which shows the strong strength of the relationship between the dependent variable i.e. axial displacement and the independent variable i.e. position on crack surface. After performing the curve fitted analysis, the following relation has been found:

$$u_x(0,y) = a_0 + \sum_{i=1}^{3} a_i \cos(i * w * y) + \sum_{i=1}^{3} b_i \sin(i * w * y) \qquad (3.1)$$

Where a_i and b_i are constants and i = 1~3. The value of these constants is readily obtained from Curve Fit Editor Dialogue box. This way the boundary condition has been set at the left end of model. Now, solution procedure of Displacement Potential Approach is discussed in the following paragraph.

The concept of structural analysis consists of four essential matters like any engineering system, such as, proper understanding of physical phenomena, derivation of governing equation, proper application of boundary conditions, and

development of routines for the solution and finally the interpretation of solutions. To solve the fourth order elliptical partial differential equation, attempt is made here, i.e., Eqs.(2.30 and 2.31) for orthotropic and Eq. (2.36) for isotropic materials through utilization of different trial functions for $\psi(x, y)$. Since the Airy's stress function of similar pattern has been solved using polynomials for quite long time, similar type of functions are considered here at first as trial solutions. It is observed that pure polynomials do not actually help much in this regard. Rather it is seen that various combinations of trigonometric and hyperbolic functions offer suitable choices for analytical functions. If these functions can be expressed as an infinite series, then construction of solutions of differential equations becomes more accurate. In the light of the ubiquitous problems which display aspects of periodic and a discontinuous nature, those infinite series known as Fourier series attain a place of special importance.

The Fourier series is probably the most commonly used of all the series for the solution of physical problems. It is a trigonometric series which can be used for the expansion of an arbitrary function. The usefulness of the Fourier series is due to the fact that certain functions which can not be expanded in power series form can still be represented by Fourier series. The reason for this is that the coefficients of the power series contain derivatives of the function; hence these derivatives must exist uniquely in order to obtain the power series expansion. Many functions which are not differentiable, including certain types of discontinuous function, can be expanded in Fourier series. Thus a much greater degree of generality is attained by taking the function as Fourier series.

Taking all this in mind trial and error operations are done to reach to the possible best displacement potential function to be assumed. In this assumption process, boundary conditions of the two ends should be satisfied automatically. Then the solution can be progressed further to make the boundary conditions of remaining two ends of the beam satisfied.

3.4 Mathematical Formulation

For the plane problems of isotropic material, the governing equilibrium equation based on the displacement potential function $\psi(x,y)$ is obtained from Eq. (2.36) as follows:

$$\frac{\partial^4\psi}{\partial x^4}+2\frac{\partial^4\psi}{\partial x^2\partial y^2}+\frac{\partial^4\psi}{\partial y^4}=0 \tag{3.2}$$

The expressions of displacement and stress components in terms of function $\psi(x, y)$ are also obtained from Eqs. (2.37) as follows:

$$u_x(x,y)=\frac{\partial^2\psi}{\partial x\partial y} \tag{3.3a}$$

$$u_y(x,y)=-\frac{1}{1+\mu}\left[2\frac{\partial^2\psi}{\partial x^2}+(1-\mu)\frac{\partial^2\psi}{\partial y^2}\right] \tag{3.3b}$$

$$\sigma_{xx}(x,y)=\frac{E}{(1+\mu)^2}\left[\frac{\partial^3\psi}{\partial x^2\partial y}-\mu\frac{\partial^3\psi}{\partial y^3}\right] \tag{3.3c}$$

$$\sigma_{yy}(x,y)=-\frac{E}{(1+\mu)^2}\left[(2+\mu)\frac{\partial^3\psi}{\partial x^2\partial y}+\frac{\partial^3\psi}{\partial y^3}\right]$$

(3.3d)

$$\sigma_{xy}(x,y)=-\frac{E}{(1+\mu)^2}\left[\frac{\partial^3\psi}{\partial x^3}-\mu\frac{\partial^3\psi}{\partial x\partial y^2}\right] \tag{3.3e}$$

In the present analytical approach, the potential function $\psi(x, y)$ is first assumed in a way so that the physical conditions of the two opposing stiffened edges are automatically satisfied. At the same time the solution has to satisfy the governing differential equation of equilibrium. Following a series of long trial and error processes, the solution of the governing equation (3.2), that is the potential function is thus approximated as follows:

$$\psi(x,\ y)=\sum_{m=1}^{\infty}X_m(x)\cos\alpha y \tag{3.4}$$

where, $X_m=f(x)$, $\alpha=(m\pi/a)$ and m = 1, 2, 3, …….. ∞.

Derivatives of equation (3.4) with respect to x and y are

$$\frac{\partial \psi}{\partial x} = \sum_{m=1}^{\infty} X'_m \cos \alpha y$$

$$\frac{\partial^2 \psi}{\partial x^2} = \sum_{m=1}^{\infty} X''_m \cos \alpha y$$

$$\frac{\partial^3 \psi}{\partial x^3} = \sum_{m=1}^{\infty} X'''_m \cos \alpha y$$

$$\frac{\partial^4 \psi}{\partial x^4} = \sum_{m=1}^{\infty} X''''_m \cos \alpha y$$

$$\frac{\partial^2 \psi}{\partial x \partial y} = -\sum_{m=1}^{\infty} X'_m \alpha \sin \alpha y$$

$$\frac{\partial^3 \psi}{\partial x \partial y^2} = -\sum_{m=1}^{\infty} X'_m \alpha^2 \cos \alpha y$$

$$\frac{\partial^3 \psi}{\partial x^2 \partial y} = -\sum_{m=1}^{\infty} X''_m \alpha \cos \alpha y$$

$$\frac{\partial^4 \psi}{\partial x^2 \partial y^2} = -\sum_{m=1}^{\infty} X''_m \alpha^2 \cos \alpha y$$

$$\frac{\partial \psi}{\partial y} = -\sum_{m=1}^{\infty} X_m \alpha \sin \alpha y$$

$$\frac{\partial^2 \psi}{\partial y^2} = -\sum_{m=1}^{\infty} X_m \alpha^2 \cos \alpha y$$

$$\frac{\partial^3 \psi}{\partial y^3} = \sum_{m=1}^{\infty} X_m \alpha^3 \sin \alpha y$$

$$\frac{\partial^4 \psi}{\partial y^4} = \sum_{m=1}^{\infty} X_m \alpha^4 \cos \alpha y$$

Substituting the expressions of above derivatives in Eq. (3.2) following equation is obtained.

$$\sum_{m=1}^{\infty} X''''_m \cos \alpha y - 2\sum_{m=1}^{\infty} X''_m \alpha^2 \cos \alpha y + \sum_{m=1}^{\infty} X_m \alpha^4 \cos \alpha y = 0$$

or, $$\sum_{m=1}^{\infty} \left[X''''_m - 2\alpha^2 X''_m + \alpha^4 X_m \right] \cos \alpha y = 0$$

or, $X_m^{////} - 2\alpha^2 X_m^{//} + \alpha^4 X_m = 0$ (3.5)

The solution of the above 4th order ordinary differential equation with constant coefficients [Eq. (3.5)] can normally be approximated as follows:

$$X_m = A_m e^{r_1 x} + B_m x e^{r_2 x} + C_m e^{r_3 x} + D_m x e^{r_4 x} \quad (3.6)$$

But the ordinary differential equation (3.5) has the complementary function of repeated roots. Thus $r_1 = r_2 = \alpha$ and $r_3 = r_4 = -\alpha$ and the general solution of Eq. (3.5) can be written as

$$X_m = (A_m + B_m x)e^{\alpha x} + (C_m + D_m x)e^{-\alpha x} \quad (3.7)$$

where A_m, B_m, C_m and D_m are arbitrary constants.

Differentiating equation (3.6) following expressions are found

$$X_m^{'} = (A_m\alpha + B_m\alpha x + B_m)e^{\alpha x} + (-C_m\alpha - D_m\alpha x + D_m)e^{-\alpha x}$$
$$X_m^{''} = (A_m\alpha^2 + B_m\alpha^2 x + 2B_m\alpha)e^{\alpha x} + (C_m\alpha^2 + D_m\alpha^2 x - 2D_m\alpha)e^{-\alpha x}$$
$$X_m^{'''} = (A_m\alpha^3 + B_m\alpha^3 x + 3B_m\alpha^3)e^{\alpha x} + (-C_m\alpha^3 - D_m\alpha^3 x + 3D_m\alpha^2)e^{-\alpha x}$$
$$X_m^{''''} = (A_m\alpha^4 + B_m\alpha^4 x + 4B_m\alpha^3)e^{\alpha x} + (C_m\alpha^4 + D_m\alpha^4 x - 4D_m\alpha^3)e^{-\alpha x}$$

Now substituting the derivatives of ψ and X_m in the expressions for displacement and stresses (3.3), following expressions are found.

$$u_x(x,y) = \frac{\partial^2\psi}{\partial x\partial y}$$

$$= -\sum_{m=1}^{\infty} X^{'}{}_m \alpha \sin\alpha y$$

$$= -\sum_{m=1}^{\infty}\left[(A_m\alpha + B_m\alpha x + B_m)e^{\alpha x} + (-C_m\alpha - D_m\alpha x + D_m)e^{-\alpha x}\right]\alpha \sin\alpha y$$

$$= -\sum_{m=1}^{\infty}\left[A_m\alpha e^{\alpha x} + B_m(\alpha x+1)e^{\alpha x} - C_m\alpha e^{-\alpha x} - D_m(\alpha x-1)e^{-\alpha x}\right]\alpha \sin\alpha y \quad (3.8a)$$

$$u_y(x,y) = -\frac{1}{(1+\mu)}\left[2\frac{\partial^2\psi}{\partial x^2} + (1-\mu)\frac{\partial^2\psi}{\partial y^2}\right]$$

$$= -\frac{1}{(1+\mu)}\left[2\left\{\sum_{m=1}^{\infty} X_m^{''}\cos\alpha y\right\} - (1-\mu)\left\{\sum_{m=1}^{\infty} X_m \alpha^2 \cos\alpha y\right\}\right]$$

$$= -\frac{1}{(1+\mu)}\begin{bmatrix} 2\sum_{m=1}^{\infty}\left\{\begin{matrix}\left(A_m\alpha^2 + B_m\alpha^2 x + 2B_m\alpha\right)e^{\alpha x} + \\ \left(C_m\alpha^2 + D_m\alpha^2 x - 2D_m\alpha\right)e^{-\alpha x}\end{matrix}\right\}\cos\alpha y - (1-\mu) \\ \sum_{m=1}^{\infty}\left\{\left(A_m + B_m x\right)e^{\alpha x} + \left(C_m + D_m x\right)e^{-\alpha x}\right\}\alpha^2\cos\alpha y \end{bmatrix}$$

$$= \frac{-1}{(1+\mu)}\left[\sum_{m=1}^{\infty}\begin{Bmatrix} A_m(1+\mu)\alpha^2 e^{\alpha x} + \\ B_m(\alpha x + \mu\alpha x + 4)\alpha e^{\alpha x} \\ + C_m(1+\mu)\alpha^2 e^{-\alpha x} + \\ D_m(\alpha x + \mu\alpha x - 4)\alpha e^{-\alpha x}\end{Bmatrix}\cos\alpha y\right] \tag{3.8b}$$

$$\sigma_{xx}(x,y) = \frac{E}{(1+\mu)^2}\left[\frac{\partial^3\psi}{\partial x^2\partial y} - \mu\frac{\partial^3\psi}{\partial y^3}\right]$$

$$= -\frac{E}{(1+\mu)^2}\left[\left\{\sum_{m=1}^{\infty} X_m^{''}\alpha\ \sin\alpha y\right\} + \mu\left\{\sum_{m=1}^{\infty} X_m\alpha^3\sin\alpha y\right\}\right]$$

$$= \frac{-E}{(1+\mu)^2}\begin{bmatrix}\sum_{m=1}^{\infty}\left\{\left(A_m\alpha^2 + B_m\alpha^2 x + 2B_m\alpha\right)e^{\alpha x} + \left(C_m\alpha^2 + D_m\alpha^2 x - 2D_m\alpha\right)e^{-\alpha x}\right\}\alpha^2\sin\alpha y \\ + \mu\sum_{m=1}^{\infty}\left\{\left(A_m + B_m x\right)e^{\alpha x} + \left(C_m + D_m x\right)e^{-\alpha x}\right\}\alpha^3\sin\alpha y\end{bmatrix}$$

$$= \frac{-E}{(1+\mu)^2}\left[\sum_{m=1}^{\infty}\begin{Bmatrix} A_m\alpha(1+\mu)e^{\alpha x} + B_m(\alpha x + \mu\alpha x + 2)e^{\alpha x} \\ + C_m\alpha(1+\mu)e^{-\alpha x} + D_m(\alpha x + \mu\alpha x - 2)e^{-\alpha x}\end{Bmatrix}\alpha^2\sin\alpha y\right] \tag{3.8c}$$

$$\sigma_{yy}(x,y) = \frac{-E}{(1+\mu)^2}\left[(2+\mu)\frac{\partial^3\psi}{\partial x^2\partial y} + \frac{\partial^3\psi}{\partial y^3}\right]$$

$$= \frac{-E}{(1+\mu)^2}\left[-(2+\mu)\left\{\sum_{m=1}^{\infty} X_m^{''}\alpha\ \sin\alpha y\right\} + \left\{\sum_{m=1}^{\infty} X_m\alpha^3\sin\alpha y\right\}\right]$$

$$= \frac{-E}{(1+\mu)^2}\left[\begin{array}{l} -(2+\mu)\sum_{m=1}^{\infty}\left\{\left(A_m\alpha^2 + B_m\alpha^2 x + 2B_m\alpha\right)e^{\alpha x} + \left(C_m\alpha^2 + D_m\alpha^2 x - 2D_m\alpha\right)e^{-\alpha x}\right\}\alpha \ \sin\alpha y \\ +\sum_{m=1}^{\infty}\left\{\left(A_m + B_m x\right)e^{\alpha x} + \left(C_m + D_m x\right)e^{-\alpha x}\right\}\alpha^3 \sin\alpha y \end{array}\right]$$

$$= \frac{-E}{(1+\mu)^2}\left[\sum_{m=1}^{\infty}\left\{\begin{array}{l} A_m\alpha(-1-\mu)e^{\alpha x} + B_m(-\alpha x - \mu\alpha x - 2\mu - 4)e^{\alpha x} + \\ C_m\alpha(-1-\mu)e^{-\alpha x} + D_m(-\alpha y - \mu\alpha x + 2\mu + 4)e^{-\alpha x} \end{array}\right\}\alpha^2 \sin\alpha y\right] \qquad (3.8d)$$

$$\sigma_{xy}(x,y) = \frac{-E}{(1+\mu)^2}\left[\frac{\partial^3\psi}{\partial x^3} - \mu\frac{\partial^3\psi}{\partial x\partial y^2}\right]$$

$$= \frac{-E}{(1+\mu)^2}\left[\sum_{m=1}^{\infty} X'''_m \cos\alpha y + \mu\left\{\sum_{m=1}^{\infty} X'_m\alpha^2 \cos\alpha y\right\}\right]$$

$$= \frac{-E}{(1+\mu)^2}[\sum_{m=1}^{\infty}\left\{\left(A_m\alpha^3 + B_m\alpha^3 x + 3B_m\alpha^2\right)e^{\alpha x} + \left(-C_m\alpha^3 - D_m\alpha^3 x + 3D_m\alpha^2\right)e^{-\alpha x}\right\}\cos\alpha y$$

$$+\mu\sum_{m=1}^{\infty}\left\{\left(A_m\alpha + B_m\alpha\, x + B_m\right)e^{\alpha x} + \left(-C_m\alpha - D_m\alpha\, x + D_m\right)e^{-\alpha x}\right\}\alpha^2 \cos\alpha y]$$

$$= \frac{-E}{(1+\mu)^2}\left[\sum_{m=1}^{\infty}\left\{\begin{array}{l} A_m(1+\mu)\alpha e^{\alpha x} + B_m(\alpha x + \mu\alpha x + \mu + 3)e^{\alpha x} \\ -C_m(1+\mu)\alpha e^{-\alpha x} - D_m(\alpha x + \mu\alpha x - \mu - 3)e^{-\alpha x} \end{array}\right\}\alpha^2 \cos\alpha y\right] \qquad (3.8e)$$

Now, the axial loading on the right edge of the panel can be taken as Fourier series in the following manner:

$$\sigma_{xx}(b,y) = \sigma^o_{xx} = \sum_{m=1}^{\infty} E_m \sin\alpha y \qquad (3.9)$$

To satisfy the boundary condition and loading distribution, Fourier sine series have been considered for the analysis.

$$E_m = \frac{2}{a}\int_0^a \sigma^o_{xx} \sin(\alpha y)dy$$

$$= \frac{2\sigma^o_{xx}}{a}\int_0^a \sin(\alpha y)dy$$

$$= \frac{2\sigma^0_{xx}}{\alpha a}[-\cos(\alpha y)]_0^a$$

$$= \frac{2\sigma^o_{xx}}{m\pi}[1-\cos(m\pi)], \text{ where m = 1, 2, 3, 4, 5 } \ldots\ldots\ldots\ldots\ldots\infty$$

Due to symmetry, the axial displacement at the left edge from 0 to (*a*-*h*) is zero. But at the crack surface, the distribution of the axial displacement can be expressed as the Fourier series in the following manner:

$$u_x(0,y) = a_0 + \sum_{i=1}^{3} a_i \cos(i*w*y) + \sum_{i=1}^{3} b_i \sin(i*w*y) = \sum_{m=1}^{\infty} I_m \sin(\alpha y) \tag{3.10}$$

The curve fitted equation as Fourier series up to 7th term have been considered. This is because of up to 7th term we always achieve R^2 value above 0.99. If we increase the term it will make the mathematical calculation more complicated.

Here

$$I_m = \frac{2}{a}\int_{a-h}^{a} (a_0 + \sum_{i=1}^{3} a_i \cos(i*w*y) + \sum_{i=1}^{3} b_i \sin(i*w*y))\sin(\alpha y)dy$$

After performing integration of the above equation, the result is obtained as below:

$$I_m = \left(\frac{2a_o}{m\pi}\left(\cos\left(\frac{(a-h)hm\pi}{a}\right) - \cos(m\pi)\right)\right) + \sum_{i=1}^{3} a_i \begin{pmatrix} \left(\frac{1}{m\pi + iwa}\cos\left(\left(\frac{a-h}{a}\right)(m\pi + iwa)\right)\right) + \\ \left(\frac{1}{m\pi - iwa}\cos\left(\left(\frac{a-h}{a}\right)(m\pi - iwa)\right)\right) - \\ \left(\frac{1}{m\pi + iwa}\cos(m\pi + iwa)\right) - \\ \left(\frac{1}{m\pi - iwa}\cos(m\pi - iwa)\right) \end{pmatrix}$$

$$+ \sum_{i=1}^{3} b_i \begin{pmatrix} -\left(\frac{1}{m\pi - iwa}\sin(m\pi + iwa)\right) + \\ \left(\frac{1}{m\pi - iwa}\sin(m\pi - iwa)\right) + \\ \left(\frac{1}{m\pi + iwa}\sin\left(\left(\frac{a-h}{a}\right)(m\pi + iwa)\right)\right) - \\ \left(\frac{1}{m\pi - iwa}\sin\left(\left(\frac{a-h}{a}\right)(m\pi - iwa)\right)\right) \end{pmatrix}$$

Using boundary condition $\sigma_{xy}(0,y)=0$ at the edge of $x=0$, it is found that

$$\frac{-E}{(1+\mu)^2}\left[\sum_{m=1}^{\infty}\{A_m(1+\mu)\alpha+B_m(\mu+3)-C_m(1+\mu)\alpha-D_m(-\mu-3)\}\alpha^2\cos\alpha y\right]=0$$
$$or,\left[A_m\alpha(1+\mu)+B_m(\mu+3)-C_m\alpha(1+\mu)+D_m(\mu+3)\right]=0 \tag{3.11}$$

Using boundary condition $\sigma_{xy}(b,y)=0$ at the edge of $x=b$, it is found that

$$\frac{-E}{(1+\mu)^2}\left[\sum_{m=1}^{\infty}\begin{Bmatrix}A_m\alpha(1+\mu)e^{\alpha b}+B_m(\alpha b+\mu\alpha b+\mu+3)e^{\alpha b}\\-C_m(1+\mu)\alpha e^{-\alpha b}-D_m(\alpha b+\mu\alpha b-\mu-3)e^{-\alpha b}\end{Bmatrix}\alpha^2\cos\alpha y\right]=0$$
$$or,\begin{bmatrix}A_m\alpha(1+\mu)e^{\alpha b}+B_m(\alpha b+\mu\alpha b+\mu+3)e^{\alpha b}\\-C_m\alpha(1+\mu)e^{-\alpha b}-D_m(\alpha b+\mu\alpha b-\mu-3)e^{-\alpha b}\end{bmatrix}=0 \tag{3.12}$$

Using boundary condition $u_x(0,y)=a_0+\sum_{i=1}^{3}a_i\cos(i*w*y)+\sum_{i=1}^{3}b_i\sin(i*w*y)$ at the edge of $x=0$, it is found that

$$-\sum_{m=1}^{\infty}[A_m\alpha+B_m-C_m\alpha+D_m]\alpha\sin\alpha y=\sum_{m=1}^{\infty}I_m\sin(\alpha y)$$
$$or,[A_m\alpha+B_m-C_m\alpha+D_m]\alpha=-I_m \tag{3.13}$$

Using boundary condition $\sigma_{xx}(b,y)=\sigma_{xx}^{o}$ at the edge of $x=b$, it is found

$$\frac{-E}{(1+\mu)^2}\left[\sum_{m=1}^{\infty}\begin{Bmatrix}A_m\alpha(1+\mu)e^{\alpha b}+B_m(\alpha b+\mu\alpha b+2)e^{\alpha b}\\+C_m\alpha(1+\mu)e^{-\alpha b}+D_m(\alpha b+\mu\alpha b-2)e^{-\alpha b}\end{Bmatrix}\alpha^2\sin\alpha y\right]=\sum_{m=1}^{\infty}E_m\sin\alpha y$$
$$or,\begin{bmatrix}A_m\alpha(1+\mu)e^{\alpha b}+B_m(\alpha b+\mu\alpha b+2)e^{\alpha b}\\+C_m\alpha(1+\mu)e^{-\alpha b}+D_m(\alpha b+\mu\alpha b-2)e^{-\alpha b}\end{bmatrix}=\frac{E_m(1+\mu)^2}{E\alpha^2} \tag{3.14}$$

The simultaneous equations (3.11), (3.12), (3.13) and (3.14) can be arranged in a simplified matrix form for the solution of unknown terms like A_m , B_m , C_m and D_m as follows:

$$\begin{bmatrix} DD_1 & DD_2 & DD_3 & DD_2 \\ FF_1 & FF_2 & FF_3 & FF_4 \\ HH_1 & HH_2 & HH_3 & HH_2 \\ KK_1 & KK_2 & KK_3 & KK_4 \end{bmatrix} \begin{bmatrix} A_m \\ B_m \\ C_m \\ D_m \end{bmatrix} = \begin{bmatrix} 0 \\ 0 \\ I_m \\ E_m \end{bmatrix} \tag{3.15}$$

Where

$$DD_1 = \alpha(1+\mu)$$

$$DD_2 = (\mu+3)$$

$$DD_3 = -\alpha(1+\mu)$$

$$FF_1 = \alpha(1+\mu)e^{\alpha b}$$

$$FF_2 = (\alpha b + \mu\alpha b + \mu + 3)e^{\alpha b}$$

$$FF_3 = -\alpha(1+\mu)e^{-\alpha b}$$

$$FF_4 = -(\alpha b + \mu\alpha b - \mu - 3)e^{-\alpha b}$$

$$HH_1 = -\alpha^2$$

$$HH_2 = -\alpha$$

$$HH_3 = \alpha^2$$

$$KK_1 = Z_{11}\alpha(1+\mu)e^{\alpha b}$$

$$KK_2 = Z_{11}(\alpha b + \mu\alpha b + 2)e^{\alpha b}$$

$$KK_3 = Z_{11}\alpha(1+\mu)e^{-\alpha b}$$

$$KK_4 = Z_{11}(\alpha b + \mu\alpha b - 2)e^{-\alpha b}$$

$$Z_{11} = \frac{-E\alpha^2}{(1+\mu)^2}$$

Solution of the above matrix Eq. (3.14) yields the unknown constants A_m , B_m , C_m and D_m . Once the value of the unknowns are determined, they are directly substituted in Eqs.[3.8(a)-3.8(e)] to obtain the explicit expressions for the different

parameters of interest, namely, the two displacement and the three stress components at various points. The corresponding code written in C programming language is given in Appendix-A.

3.5 Analysis of Elastic Field

The solutions of displacement and stress components using displacement potential approach are obtained for steel panel (Poisson ratio μ = 0.3 and Modulus of Elasticity E = 209 GPa), aspect ratio b/a = 1.0, crack length ratio h/a = 0.2 and the uniform loading parameter, σ_o = 40 N/mm. The results of the stress field is presented in a sequence of axial displacement (u_x), lateral displacement (u_y), bending stress (σ_{xx}), normal stress (σ_{yy}) and shearing stress (σ_{xy}). In order to make the results non-dimensional, the displacements are expressed as the ratio of actual displacement to the actual dimension of the bar, and the stresses are expressed as the ratio of the actual stress to the applied loading parameter. Finally the effects of panel aspect ratio and crack length ratio on the elastic fields are analyzed.

i. Displacement Field

In Fig. 3.3 the distribution of the normalized distribution component u_x/b at different sections of panel is illustrated. The distribution of this displacement component is parabolic except near the region of the crack edge. Due to symmetry no axial displacement happened at mid section along the ligament (at x=0) but at crack surface since the panel is free, axial displacement happens and it is almost parabolic. Below the region $x/b \leq 0.4$ it is not symmetric but bottom skewed because of the presence of the crack. As the axial load is applied on the right lateral edge, the displacement will be maximum at section x = 0.5, and it will gradually decrease as moving towards the left supporting edge. Zero value of u_x at the stiffened edges confirms the satisfaction of boundary condition of those ends.

Figure 3.4 presents the normalized displacement component u_y/a as a function of y/a at different sections of the panel. The displacement component varies almost

symmetrically from one stiffener to another with a zero value at y/a =0.5 for x/b ≥0.1. But at x/b = 0 due to presence of crack some fluctuation of displacement happens at y/a = 0.8 that's why the distribution is anti symmetric. It is observed that the displacement component u_y varies from a positive value at the lower stiffener to a negative value at the upper stiffener and the opposite happens at the other region.

Figure 3.5 shows the deformed shape of the panel under uniform loading at the left and right edges with the magnification of 2000 times of displacement. Since the panel is subjected to axial loading it must be obvious that it is elongated with the reduction of the width due to the effect of Poisson's ratio. This expectation is found to be true over the range $0 \leq x/b \leq 0.9$. But over the region $x/b \geq 0.9$, the panel is expanded in the y-direction, which is in contrast to our general intuition and may be attributed to the physical conditions of the stiffened under tension.

ii. Stress Field

Fig. 3.6 reveals the distribution of the normalized stress component σ_{xx}/σ_o is also found in good agreement with the physical characteristic of the stiffened panel. It is maximum at mid section x/b = 0.5. But due to presence of crack a sudden fluctuation of stress happens at the crack tip (x = 0 and y = 0.8a) of the panel. Crack tip concentrates stresses and strains that approaches singularity. According to linear elastic fracture mechanics, the stress near the crack tip merges to infinity. In reality, a sudden fluctuation of stress happen but it has some values not infinity. The fluctuation decays as moving from the crack tip. It is observed that the stress distribution is symmetric around the mid-longitudinal section y/a = 0.5 for the region x/b = 0.5. But for x/b <0.5 it is not symmetric. This is because of the effect of the crack. The stress at the stiffened edge is completely zero. As appears from the distribution, the present isotropic panel is always in tension in the x-direction as the distribution is everywhere positive throughout the panel. At crack surface the stress is nearly zero because it is free. But at crack tip the stress becomes almost 0.6 times of the applied load.

The distribution of the normalized stress σ_{yy}/σ_o at various sections of the panel is shown in Fig. 3.7. The lateral stress is zero at the two stiffened edges that satisfies our boundary condition. There is a sudden fluctuation of lateral stress at the crack tip due to stress concentration. The maximum value of the lateral stress at crack tip is almost 0.3 times of the applied load. The overall distribution of the stress component reveals that the major portion of the panel is under compression, as the stress component is negative for sections $0 \leq x/b \leq 0.50$.

Fig. 3.8 reveals the distribution of normalized shearing stress σ_{xy}/σ_o at various section of the panel. It is observed that there is very little effect of the crack on shear stress throughout the whole panel. The shearing stress at the left boundary is found to be zero which verifies the physical boundary conditions of the problem. The shearing stress varies from a positive value at y =0 to a negative value at y =1.0 with zero value at the mid-longitudinal section y/a = 0.5 of the panel. It is noted here that unlike the other stress components, shearing stress has a maximum magnitude on the stiffened boundaries.

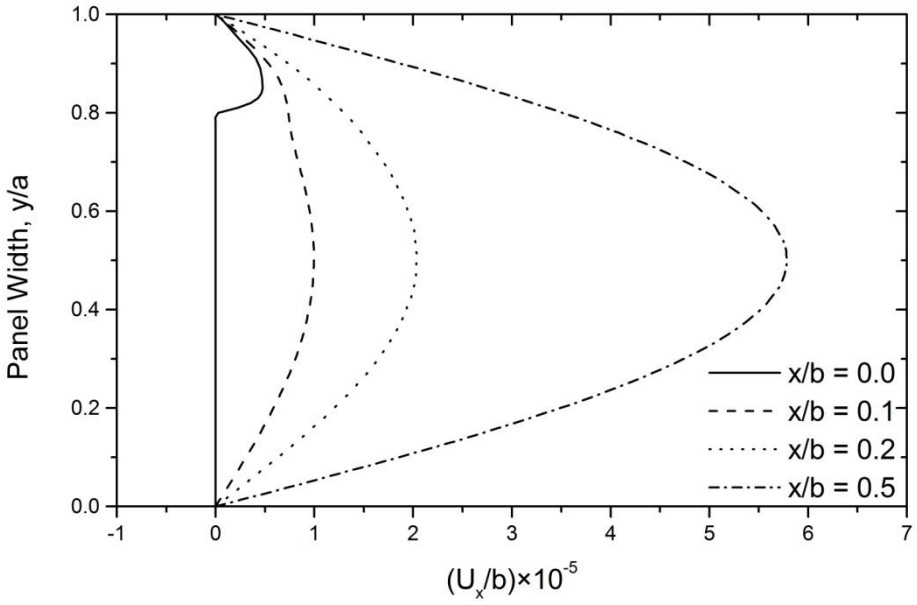

Fig 3.3: Distribution of normalized axial displacement at different sections of the steel panel. (h/a = 0.2, b/a = 1)

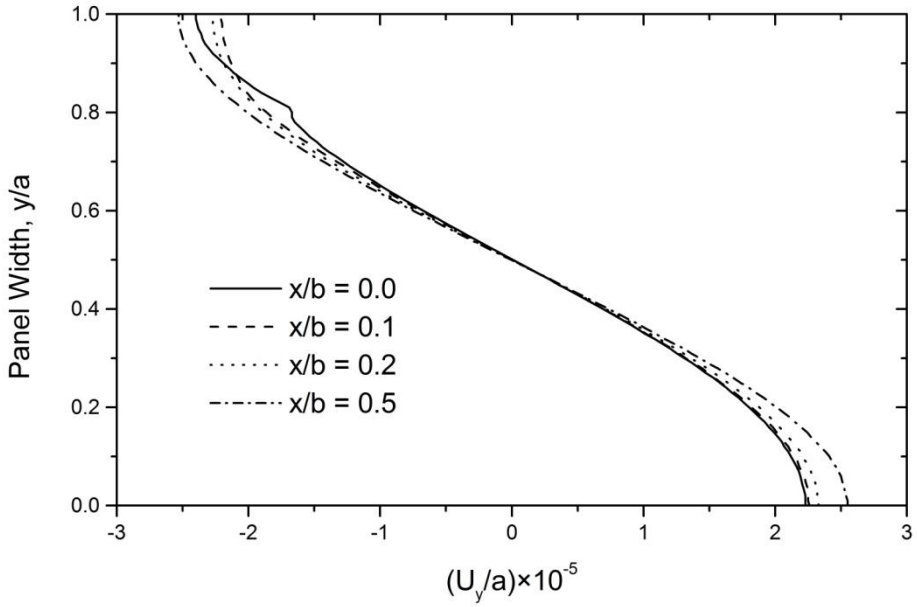

Fig 3.4: Distribution of normalized lateral displacement at different sections of the steel panel. (h/a = 0.2, b/a = 1)

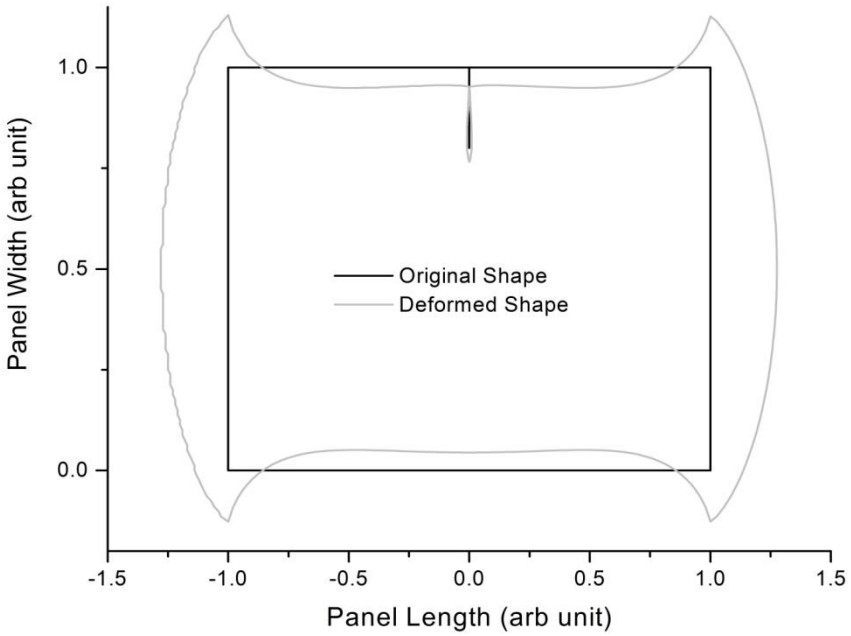

Fig 3.5: Deformed shape of the cracked steel panel, (h/a = 0.2, b/a = 1) (magnification factor×2000).

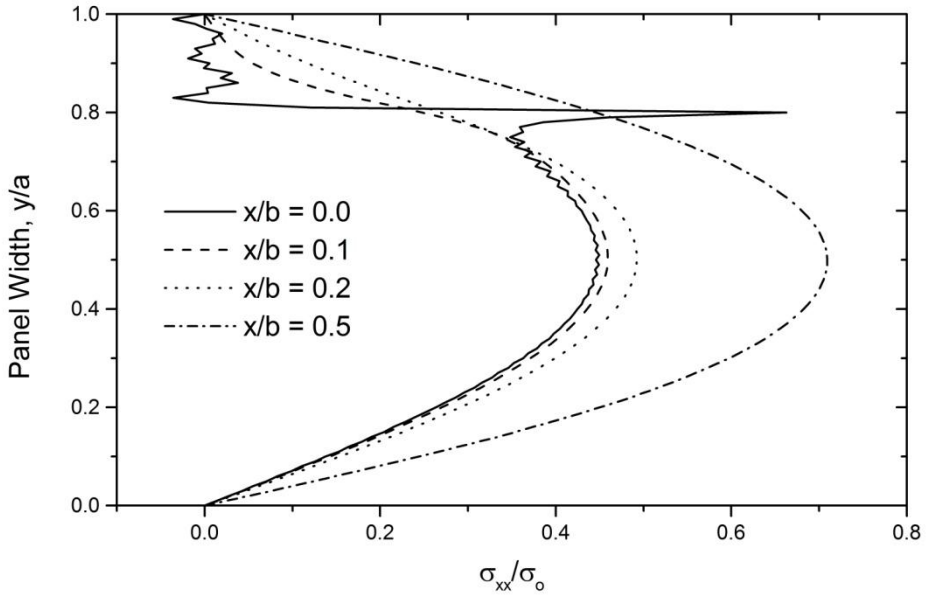

Fig 3.6: Distribution of normalized axial stress at different sections of the steel panel. (h/a = 0.2, b/a = 1)

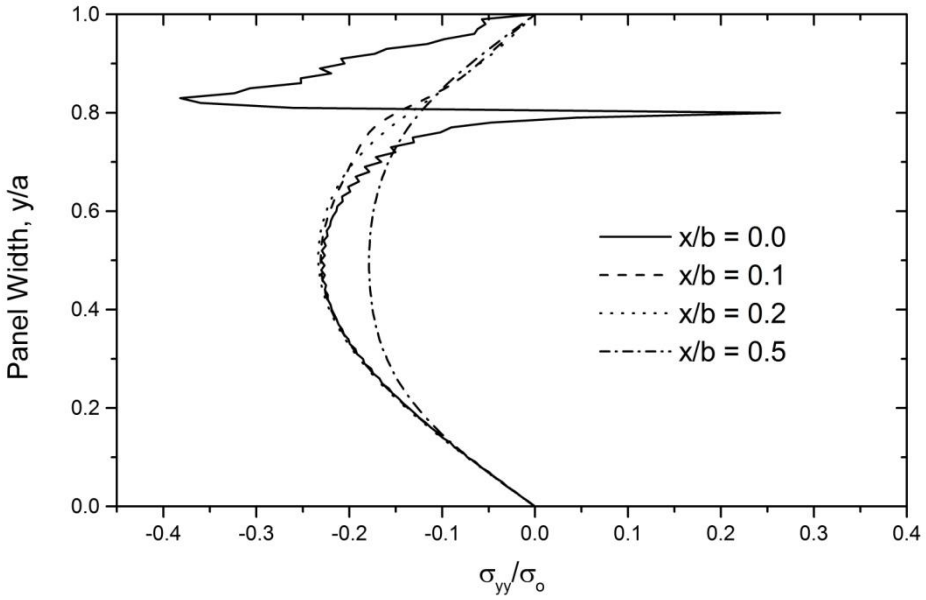

Fig 3.7: Distribution of normalized lateral stress at different sections of the steel panel. (h/a = 0.2, b/a = 1)

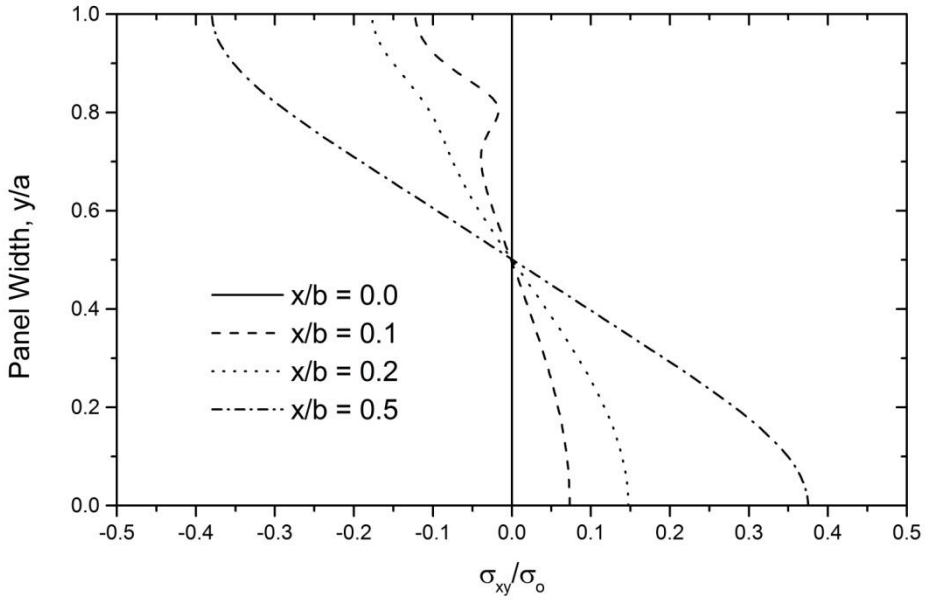

Fig 3.8: Distribution of normalized shear stress at different sections of the steel panel. (h/a = 0.2, b/a = 1)

Distribution of normalized maximum principle stress obtained using the results of displacement potential approach is presented in Fig. 3.9. The relation used in this regard is $\sigma_1 = \frac{\sigma_x+\sigma_y}{2} + \sqrt{\left(\frac{\sigma_x-\sigma_y}{2}\right)^2 + \sigma_{xy}^2}$, where σ_1 is the maximum principle stress. No reference of the principle stress distribution for a guided deep beam could be found. As such the verification of present results remains to be investigated with the availability of any other results. However, the contour pattern of maximum principle stress of the current solution seems to be satisfactory in a general sense of visual basis.

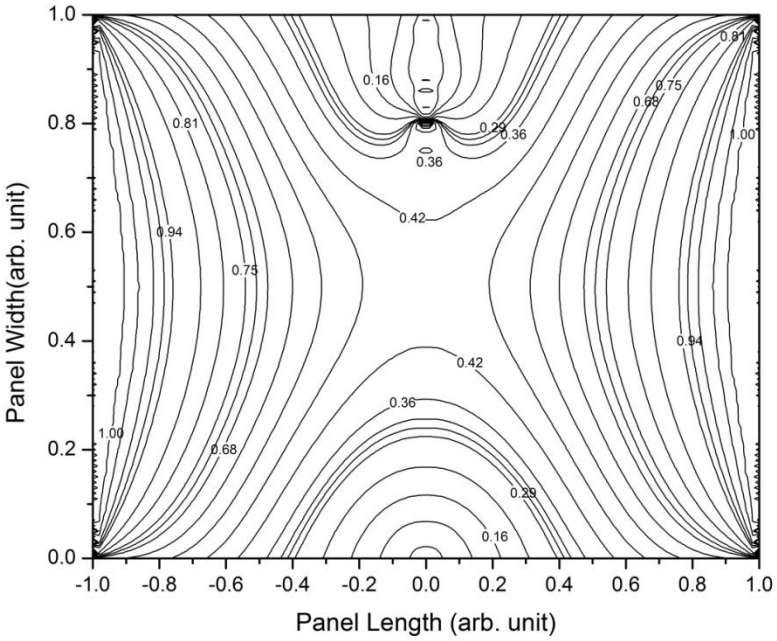

Fig 3.9: Normalized maximum principle stress contour of the cracked stiffened steel panel, (*b/a* = 1, *h/a* = 0.2).

iii. Effect of Crack Length on the Stress and Displacement Fields

In this section the effect of crack length (h/a = 0.0 ~0.4) on the displacement and stress fields of the panel is discussed. The effects are investigated for two sections near the crack. This is because; the effect of presence of crack is most prominent in the neighborhood of the cracked section. From this analysis, it is possible to determine the maximum crack length that can be allowed safely for a particular panel.

Figures 3.10(a) and 3.10(b) reveals the distribution of the normalized axial stress with the variation of crack length at two different sections of the panel (x/b = 0.0 & 0.1). With the increase of the crack length, the fluctuation of the stress at the crack tip increases. It is observed that the percentage of increase of the stress at crack tip increases with crack length. No fluctuation of stress happens if there is no crack presence in the panel. For h/a =0.4 it is almost 1.4 times of the applied load. At section x/b =0.1 it can be seen that the more the crack length the higher is the effect on the stress distribution that is almost parabolic in the case *of* h/a = 0.0.

The distribution of the normalized lateral stress for different crack length is shown in Fig. 3.11(a) and 3.11(b) for two different sections of the panel. The same thing happens as mentioned before for normalized axial stress. But the main difference is that there is a negative fluctuation of lateral stress happened at crack tip that increases with the crack length. For h/a = 0.4 at crack tip the maximum negative and positive value of the stress is almost 0.7 and 0.8 times of the applied load respectively. The smallest value of the lateral stress is found for higher crack length. The graph diverts more for higher crack length from its regular pattern parabolic shape that is happened only for panel with no crack. Another observation is that only near the crack tip lateral stress is only positive but for other region it shows negative value at section x/b = 0.0.

Since at section x/b =0.0 shear stress is zero that's why a different section x/b = 0.5 have been chosen with x/b = 0.1 as shown in Fig. 3.12(a) and 3.12(b). Though at

section x/b =0.5 it can be seen that there is very little effect on the shear stress of crack. But by closer looking it can be found that near the bottom stiffened edge all graphs for different crack length merge with each other, but upper stiffened edge they all shows different value and for h/a = 0.4 it is lower. The shear stress distribution is smooth for no crack but the smoothness disappears with the increase of the crack length. The maximum fluctuation happened for highest crack length.

Figs. 3.13(a) and 3.13(b) show the distribution of the normalized axial displacement for different crack length at two different sections. The maximum value of the axial displacement is obtained for higher crack length that can be easily predicted by only viewing the results of the stress that have already been discussed.

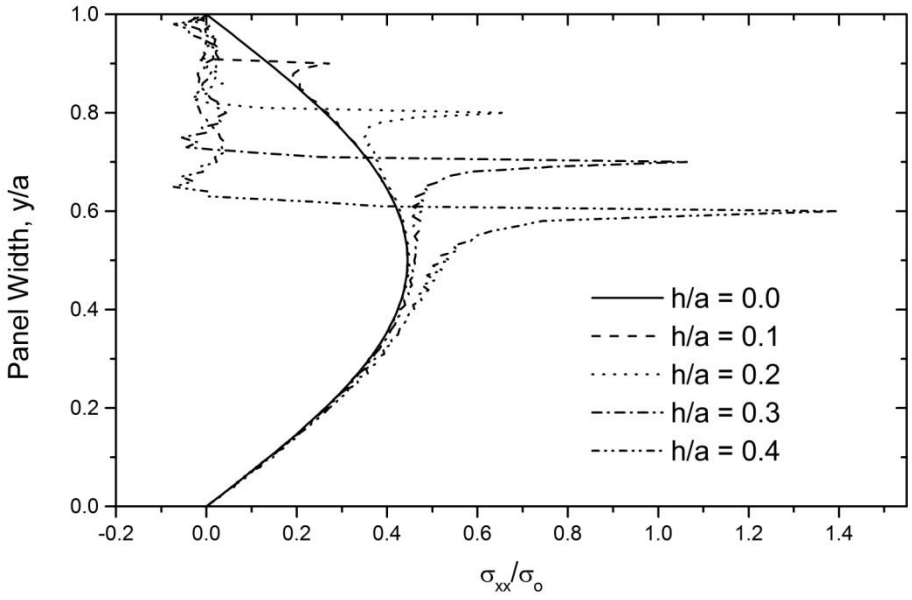

(a)

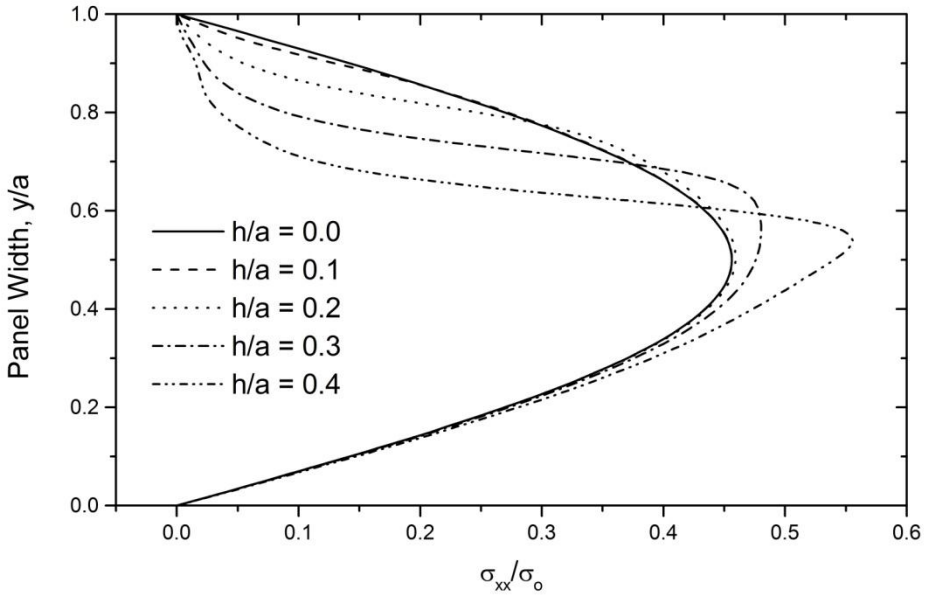

(b)

Fig 3.10: Effect of crack length on the axial stress component at (a) *x/b* = 0.0 and (b) *x/b* = 0.1, (*b/a* = 1).

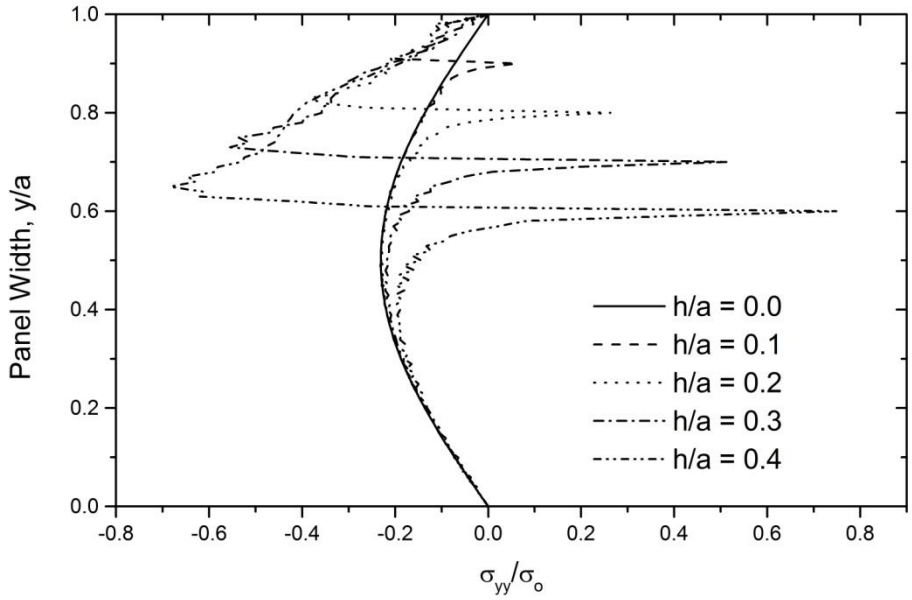

(a)

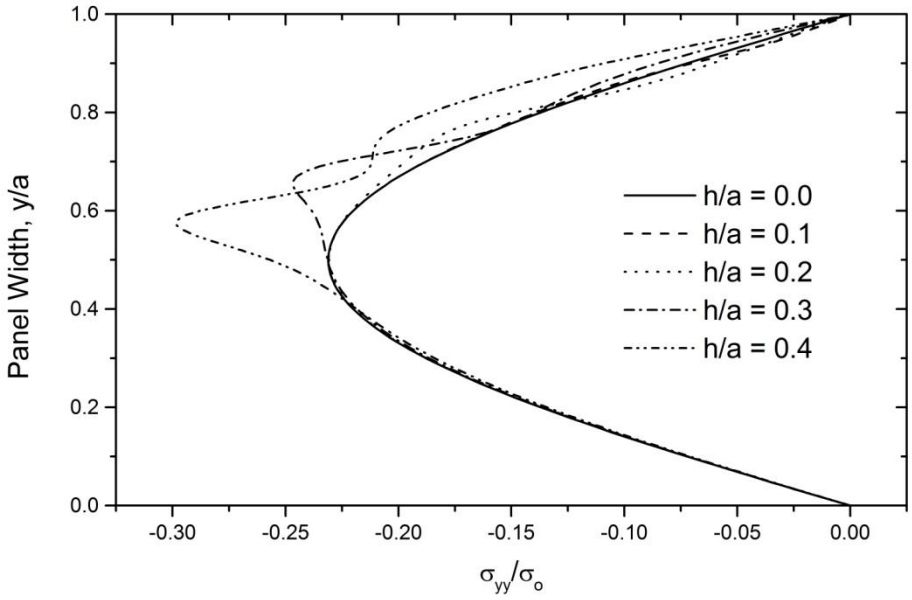

(b)

Fig 3.11: Effect of crack length on the lateral stress component at (a) x/b = 0.0 and (b) x/b = 0.1, (b/a = 1).

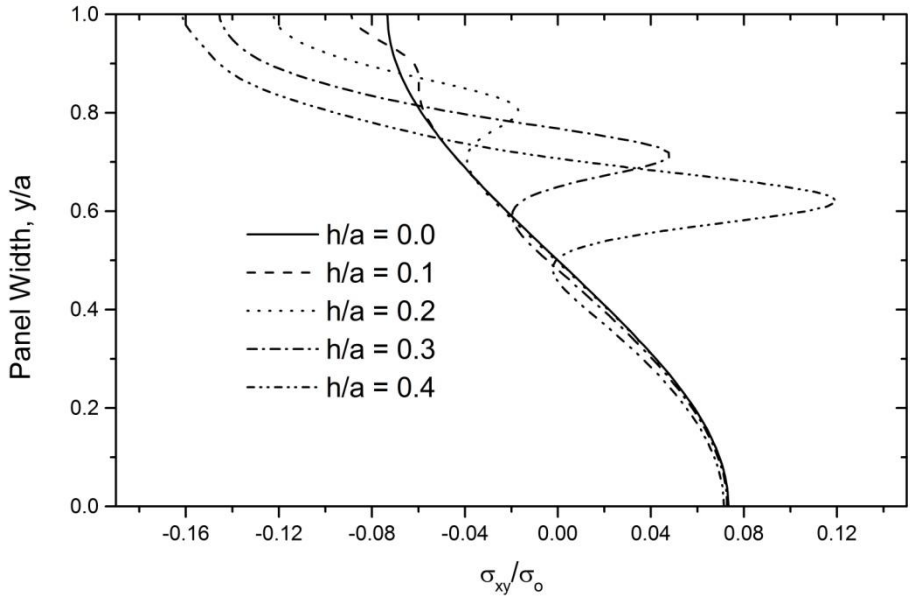

(a)

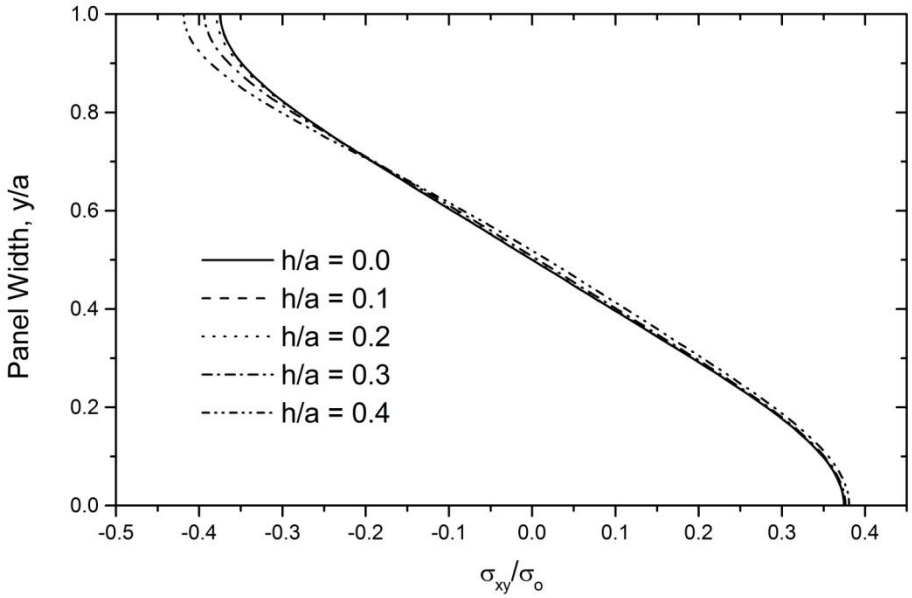

(b)

Fig 3.12: Effect of crack length on the shear stress component at (a) *x/b* = 0.1 and (b) *x/b* = 0.5, (*b/a* = 1).

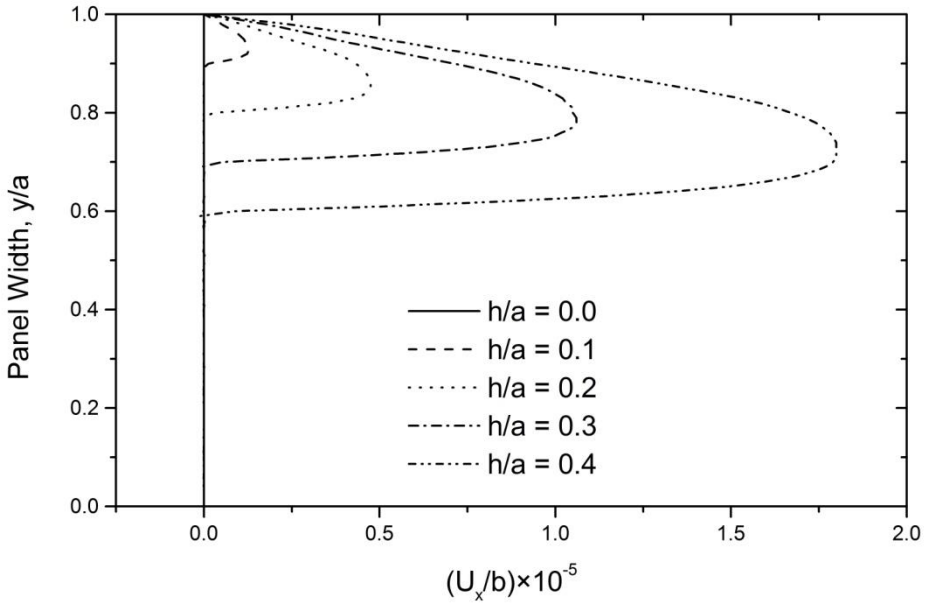

(a)

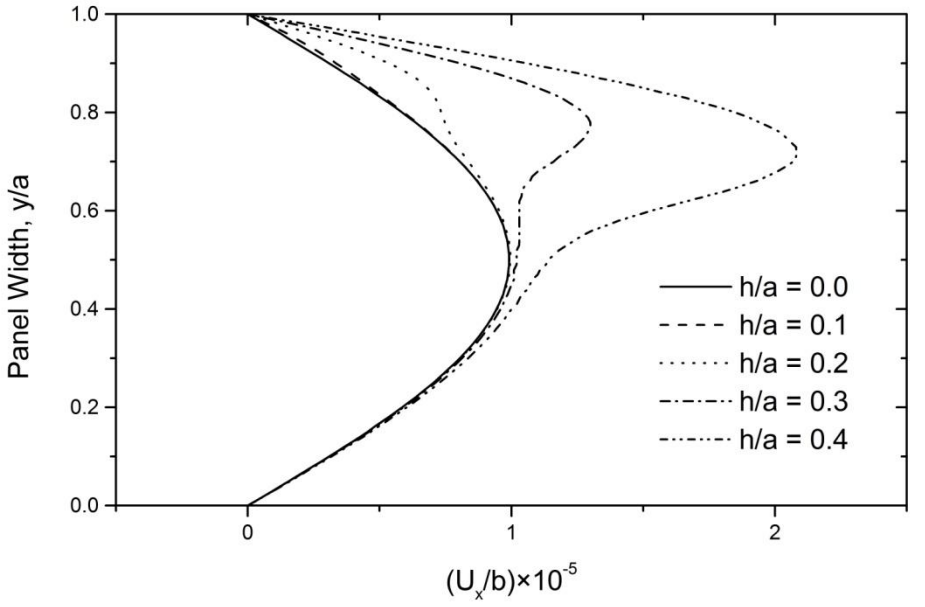

(b)

Fig 3.13: Effect of crack length on the axial displacement component at (a) *x/b* = 0.0 and (b) *x/b* = 0.1, (*b/a* = 1).

iv. Effect of Panel Aspect Ratio on the Stress and Displacement Fields

The effect of the aspect ratio (*b/a*) on the displacement and stress components are discussed in Figs 3.14 to 3.17. Figure 3.14 shows the effect of the aspect ratio on the solution of normal stress. It is observed that stress increases with the decrease of the panel length. According to the Saint Venant's principle, the effect of boundary condition is insignificant for long structure that means with the increase of length of the panel the effect of load on the crack surface decreases. At section $x/b = 0.0$ the fluctuation of the stress at the crack tip increases for the same reason as shown in Fig. 3.14(a). For all aspect ratio of the panel considered, the midsection is found to be under tension since the axial tension is considered. However, the magnitude of the stress is maximum for the smallest panel ($b/a = 0.5$) and minimum for the largest one (b/a = 2.0).

Figure 3.15 depicts that similar trends will happen for the lateral stress component. But for smallest aspect ratio $b/a = 0.5$ a sudden change is happened at the section $x/b = 0.5$ in Fig. 3.15a. As the length of the panel is increased, the mid-section of the panels experiences compressive stress of the lower magnitude in the traverse direction. This is true for only $b/a = 1.0 \sim 2.0$.But for aspect ratio $b/a = 0.5$ the lowest absolute value of the compressive stress is found. Another important point is that the compressive stress does not increase though it increases for the regions $0 \leq y/a \leq 0.2$ and $0.8 \leq y/a \leq 1.0$. Due to its small length of aspect ratio $b/a = 0.5$, upper and lower region of the panel is under higher compression at section $x/b = 0.0$ compared to the middle region for the same section.

The anti-symmetric variation of the shearing stress component at the section, $x/b = 0.1$ and 0.5, is presented as a function of the bar aspect ratio in Fig. 3.16a and 3.16b. The effect of crack is only visible for section $x/b = 0.1$. Due to presence of discontinuity there happens a sudden fluctuation near the crack tip. But the value of peak point increases with the decrease of aspect ratio. But for section $x/b = 0.5$ the magnitude of shearing stress decreases as the aspect ratio *b/a* increases. But for lower aspect ratio $b/a = 0.5$, the distribution is different from the distribution for higher aspect ratio $b/a \geq 1.0$.

The displacement u_x are found to decrease as the length of the panel is increased as can be noted from Figs 3.17a and 3.17b. In Fig. 3.17a, since the crack region is free that's why a distribution of displacement is found at section x/b =0.0 from $0.8 \leq y/a \leq 1.0$.It is noted that the effect of load on the crack decreases with the increase of the panel length. That's why maximum displacement is found for aspect ratio b/a = 0.5.

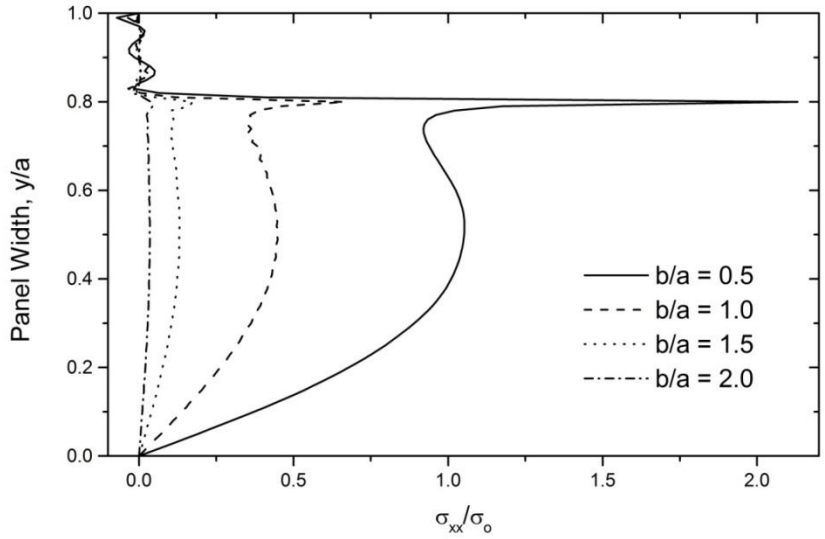

(a)

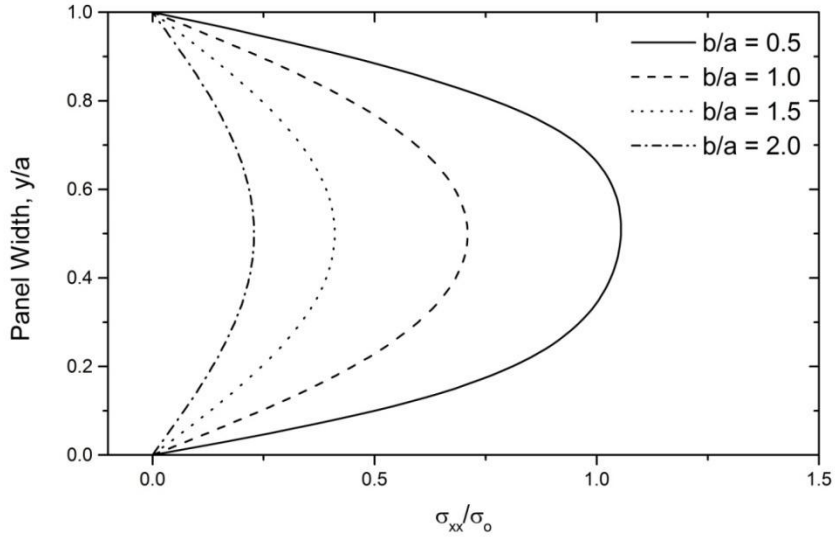

(b)

Fig 3.14: Effect of panel aspect ratio on the axial stress component at (a) $x/b = 0.0$ and (b) $x/b = 0.5$, ($h/a = 0.2$)

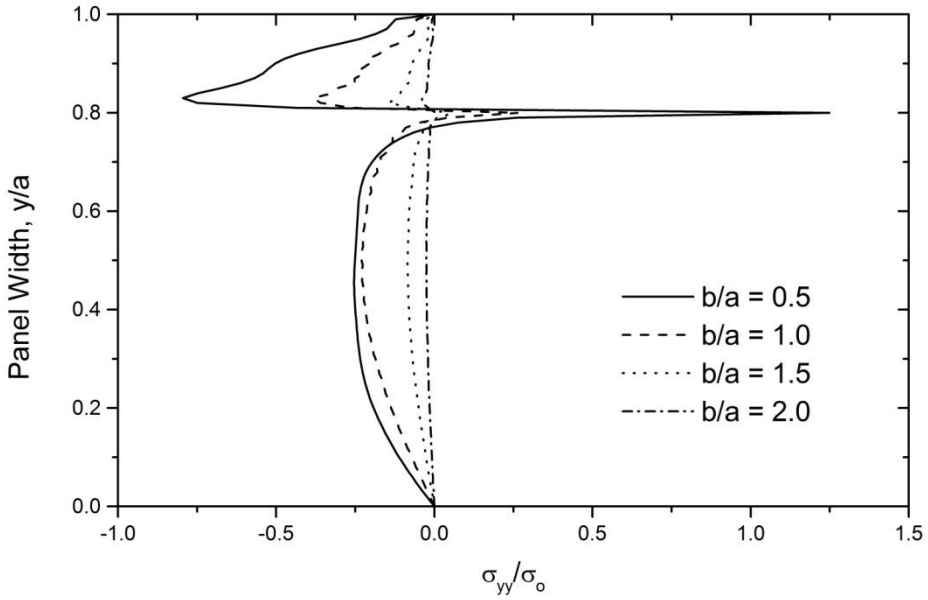

(a)

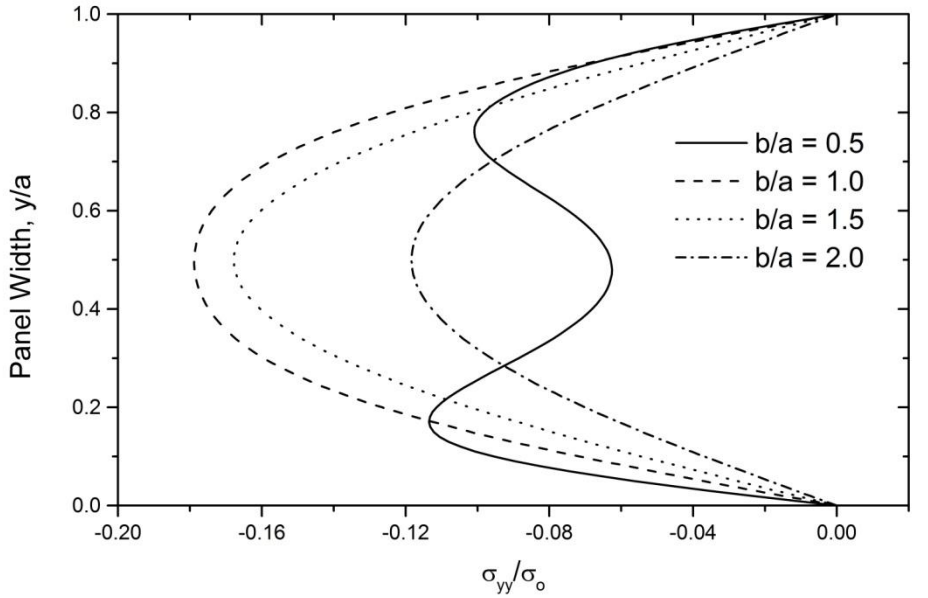

(b)

Fig 3.15: Effect of panel aspect ratio on the lateral stress component at (a) $x/b = 0.0$ and (b) $x/b = 0.5$, ($h/a = 0.2$).

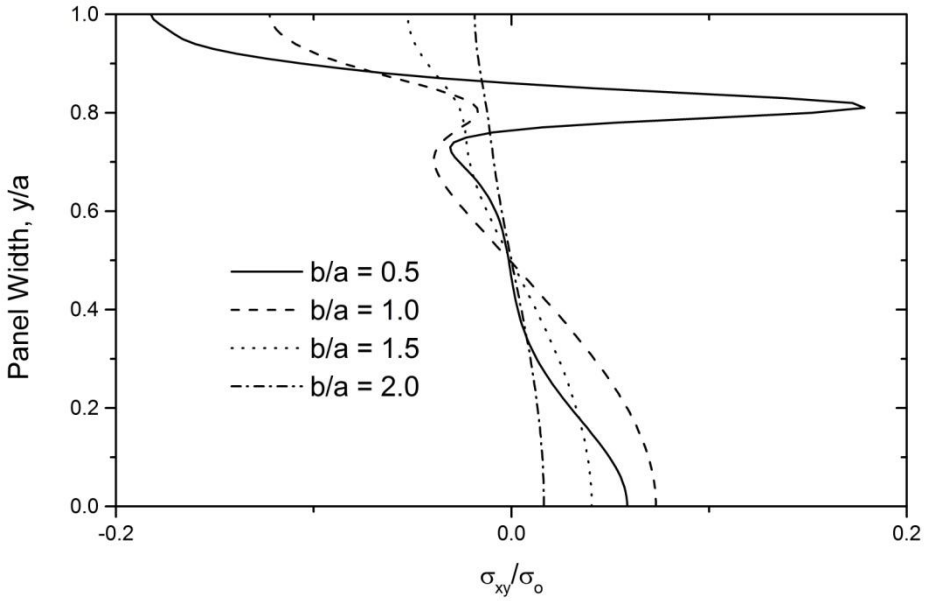

(a)

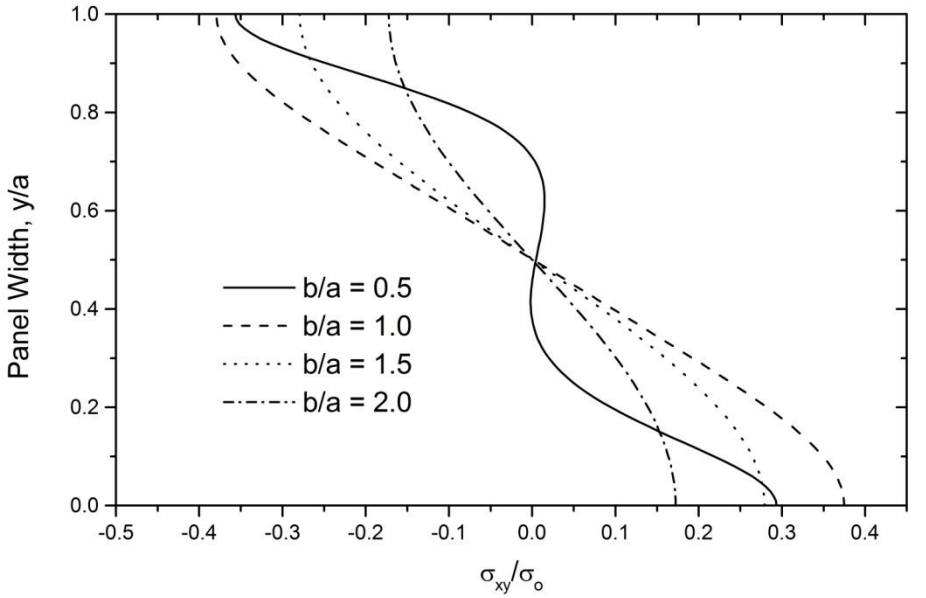

(b)

Fig 3.16: Effect of panel aspect ratio on the shear stress component at (a) $x/b = 0.1$ and (b) $x/b = 0.5$, ($h/a = 0.2$).

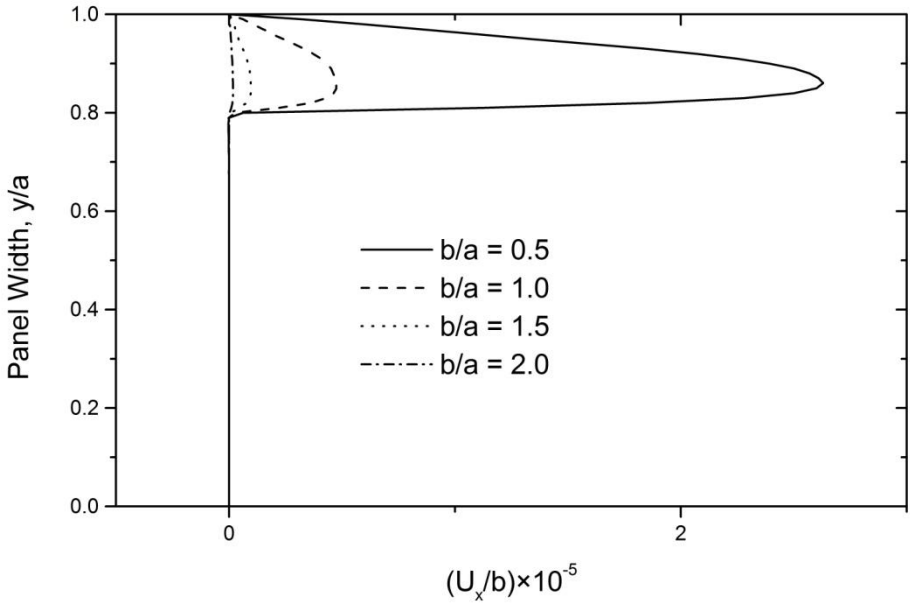

(a)

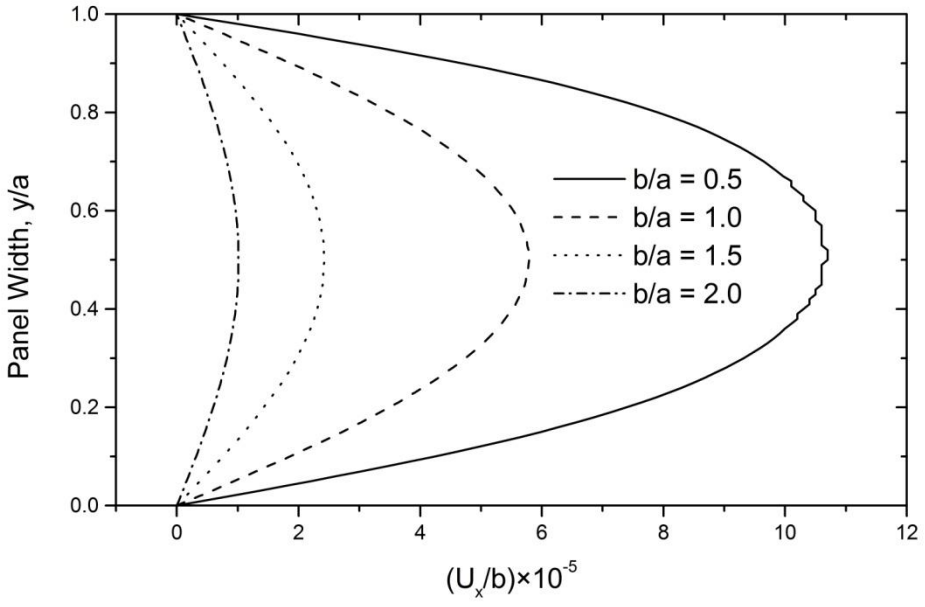

(b)

Fig 3.17: Effect of panel aspect ratio on the axial displacement component at (a) *x/b* = 0.0 and (b) *x/b* = 0.5, (*h/a* = 0.2).

CHAPTER 4

CRACKED PANEL UNDER AXIAL STIFFENERS SUBJECTED TO BENDING

The main focus of this chapter is to find the stress and displacement fields of a problem using potential function approach. In this chapter, a stiffened panel with an edge crack is considered for the analysis under the influence of bending moment. The panel is stiffened by axial stiffeners at its opposing longitudinal edges and is loaded by a bending moment at the opposing lateral ends. The effect of crack length and aspect ratio on the stress field are also discussed at the end of this chapter. .

4.1 Problem Articulation

A metallic stiffened panel with an edge crack emanating from the upper surface subjected to bending load with maximum intensity σ_0 at both lateral ends is considered. The model of the panel with a rectangular frame of reference *x-y* is shown in Fig. 4.2a. The geometrical properties of the panel are: length 2b, height *a* and crack length h. Since the structure is symmetric with reference mid of the panel along y-axis, half of the panel may be considered for the analysis as shown in Fig. 4.2b, i.e., the right half of the panel with the crack was analyzed due to symmetry. Since the thickness of such structures is very small compared to its other dimensions, the plane stress condition is adopted to model the problem for the determination of the corresponding displacement and stress fields. There will be no axial displacement along ligament of the full panel due to the symmetry but the crack surface is free from loading and restraints. No axial displacements will be allowed along the ligament (x=0) over the length $0 \leq y \leq (a-h)$, but the lateral displacements are free to assume any value.

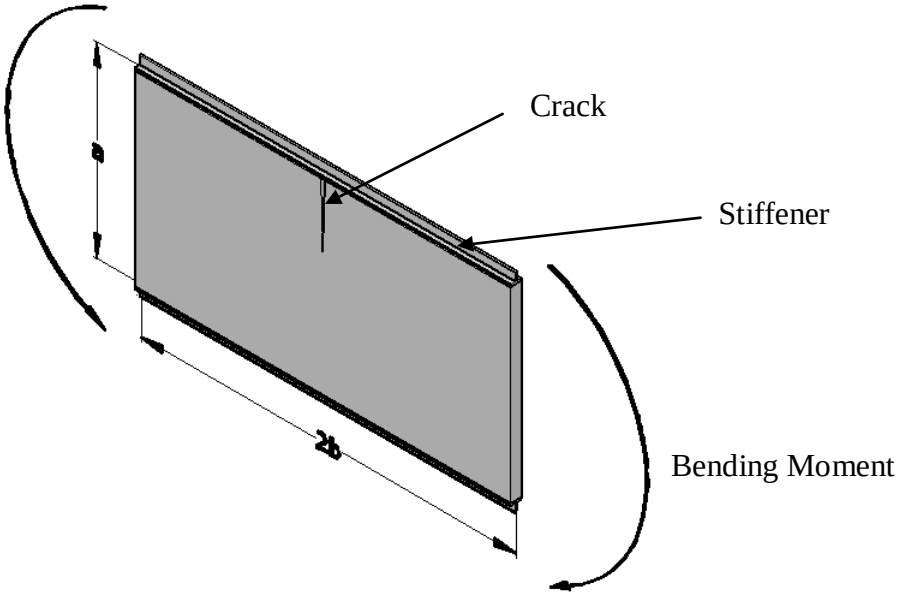

Fig 4.1: 3-D model of the full panel.

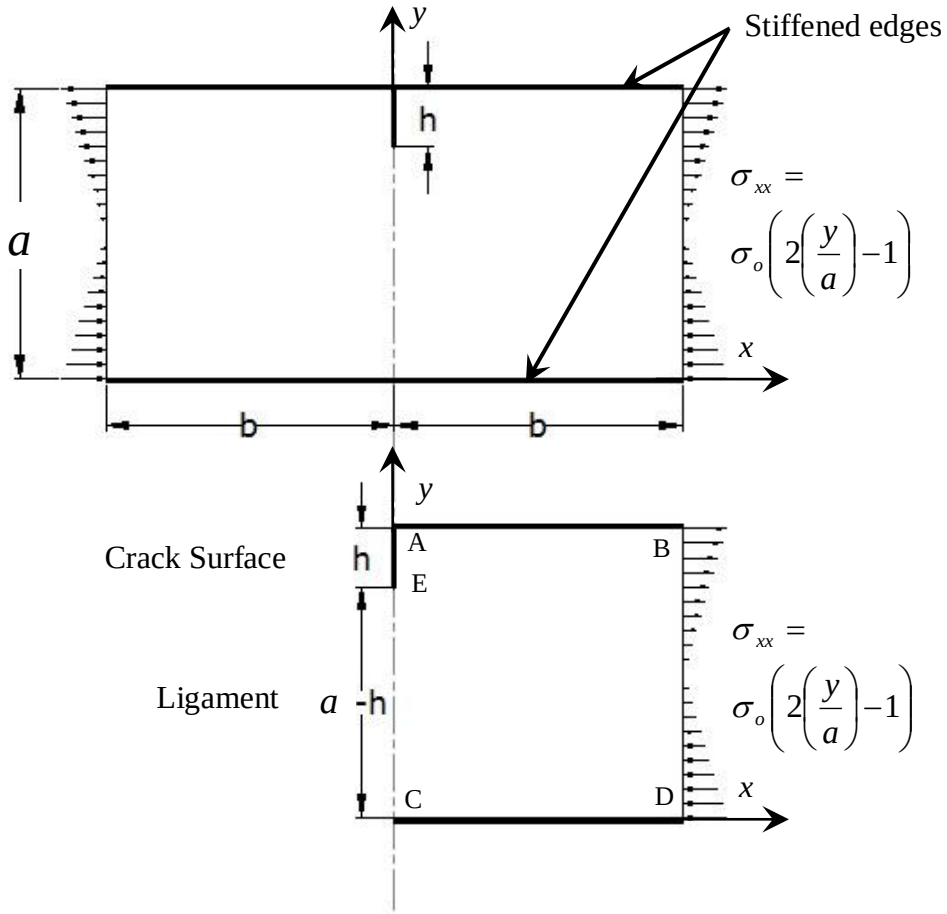

Fig 4.2: Geometry and loading of a stiffened cracked panel: (a) Full model of the panel (b) symmetric model of the panel.

4.2 Boundary Conditions

(i) Stiffened Edge, AB:

Since it is a longitudinal stiffener, there is no axial displacement and lateral stress. Thus,

$u_x(x,a) = 0$ and $\sigma_{yy}(x,a) = 0$ [$0 \le x \le b$]

(ii) Stiffened End, CD:

There is no axial displacement and lateral stress. Thus,

$u_x(x,0) = 0$ and $\sigma_{yy}(x,0) = 0$ [$0 \le x \le b$]

(iii) Ligament, EC:

Due to symmetry of the full model of the panel, axial displacement and shear stresses along this section are assumed to be zero.

$u_x(0,y) = 0$ [$0 \le y \le (a\text{-}h)$] and $\sigma_{xy}(0,y) = 0$ [$0 \le y \le (a\text{-}h)$]

Crack surface, AE:

Since the crack surface is free from loading and restraints, there will be no boundary constraints and shear stress. A Fourier series is assumed at crack surface for the axial displacement distribution.

$\sigma_{xy}(0,y) = 0$ [$(a\text{-}h) \le y \le a$]

$$u_x(0,y) = a_0 + \sum_{i=1}^{3} a_i \cos(i * w * y) + \sum_{i=1}^{3} b_i \sin(i * w * y) \quad [(a\text{-}h) \le y \le a]$$

where a_i and b_i are constants and i = 1 to 3.

(iv) Loading Edge, BD:

The boundary will also be free from shearing stress.. But flexural stresses are there in the regions of the applied bending load, which is the function of load intensity. Thus,

$\sigma_{xx}(b,y) = \sigma_o\left(2\left(\frac{y}{a}\right) - 1\right)$ and $\sigma_{xy}(b,y) = 0$ [$0 \le y \le a$]

4.3 Solution Procedure

For the plane problems of isotropic material, the governing equilibrium equation based on the displacement potential function $\psi(x,y)$ is obtained from Eq. (2.36) as follows:

$$\frac{\partial^4\psi}{\partial x^4}+2\frac{\partial^4\psi}{\partial x^2\partial y^2}+\frac{\partial^4\psi}{\partial y^4}=0 \tag{4.1}$$

The expressions of displacement and stress components in terms of function $\psi(x, y)$ are also obtained from Eqs. (2.37) as follows:

$$u_x(x,y)=\frac{\partial^2\psi}{\partial x\partial y} \tag{4.2a}$$

$$u_y(x,y)=-\frac{1}{1+\mu}\left[2\frac{\partial^2\psi}{\partial x^2}+(1-\mu)\frac{\partial^2\psi}{\partial y^2}\right] \tag{4.2b}$$

$$\sigma_{xx}(x,y)=\frac{E}{(1+\mu)^2}\left[\frac{\partial^3\psi}{\partial x^2\partial y}-\mu\frac{\partial^3\psi}{\partial y^3}\right] \tag{4.2c}$$

$$\sigma_{yy}(x,y)=-\frac{E}{(1+\mu)^2}\left[(2+\mu)\frac{\partial^3\psi}{\partial x^2\partial y}+\frac{\partial^3\psi}{\partial y^3}\right] \tag{4.2d}$$

$$\sigma_{xy}(x,y)=-\frac{E}{(1+\mu)^2}\left[\frac{\partial^3\psi}{\partial x^3}-\mu\frac{\partial^3\psi}{\partial x\partial y^2}\right] \tag{4.2e}$$

In the present analytical approach, the potential function $\psi(x, y)$ is first assumed in a way so that the physical conditions of the two opposing stiffened edges are automatically satisfied. At the same time the solution has to satisfy the governing differential equation of equilibrium. Following a series of long trial and error processes, the solution of the governing equation (4.1), that is the potential function is thus approximated as follows:

$$\psi(x,\ y)\ =\sum_{m=1}^{\infty}X_m(x)\cos\alpha y \tag{4.3}$$

where, $X_m=f(x)$, $\alpha=(m\pi/a)$ and m = 1, 2, 3, …….∞.

Derivatives of equation (4.3) with respect to x and y are

$$\frac{\partial \psi}{\partial x} = \sum_{m=1}^{\infty} X'_m \cos \alpha y$$

$$\frac{\partial^2 \psi}{\partial x^2} = \sum_{m=1}^{\infty} X''_m \cos \alpha y$$

$$\frac{\partial^3 \psi}{\partial x^3} = \sum_{m=1}^{\infty} X'''_m \cos \alpha y$$

$$\frac{\partial^4 \psi}{\partial x^4} = \sum_{m=1}^{\infty} X''''_m \cos \alpha y$$

$$\frac{\partial^2 \psi}{\partial x \partial y} = -\sum_{m=1}^{\infty} X'_m \alpha \sin \alpha y$$

$$\frac{\partial^3 \psi}{\partial x \partial y^2} = -\sum_{m=1}^{\infty} X'_m \alpha^2 \cos \alpha y$$

$$\frac{\partial^3 \psi}{\partial x^2 \partial y} = -\sum_{m=1}^{\infty} X''_m \alpha \cos \alpha y$$

$$\frac{\partial^4 \psi}{\partial x^2 \partial y^2} = -\sum_{m=1}^{\infty} X''_m \alpha^2 \cos \alpha y$$

$$\frac{\partial \psi}{\partial y} = -\sum_{m=1}^{\infty} X_m \alpha \sin \alpha y$$

$$\frac{\partial^2 \psi}{\partial y^2} = -\sum_{m=1}^{\infty} X_m \alpha^2 \cos \alpha y$$

$$\frac{\partial^3 \psi}{\partial y^3} = \sum_{m=1}^{\infty} X_m \alpha^3 \sin \alpha y$$

$$\frac{\partial^4 \psi}{\partial y^4} = \sum_{m=1}^{\infty} X_m \alpha^4 \cos \alpha y$$

Substituting the expressions of above derivatives in Eq. (4.1) following equation is obtained.

$$\sum_{m=1}^{\infty} X''''_m \cos \alpha y - 2\sum_{m=1}^{\infty} X''_m \alpha^2 \cos \alpha y + \sum_{m=1}^{\infty} X_m \alpha^4 \cos \alpha y = 0$$

or, $$\sum_{m=1}^{\infty} \left[X''''_m - 2\alpha^2 X''_m + \alpha^4 X_m \right] \cos \alpha y = 0$$

or, $$X_m'''' - 2\alpha^2 X_m'' + \alpha^4 X_m = 0 \qquad (4.4)$$

The solution of the above 4th order ordinary differential equation with constant coefficients [Eq. (4.4)] can normally be approximated as follows:

$$X_m = A_m e^{r_1 x} + B_m x e^{r_2 x} + C_m e^{r_3 x} + D_m x e^{r_4 x} \tag{4.5}$$

But the ordinary differential equation (4.4) has the complementary function of repeated roots. Thus $r_1 = r_2 = \alpha$ and $r_3 = r_4 = -\alpha$ and the general solution of Eq. (4.4) can be written as

$$X_m = (A_m + B_m x)e^{\alpha x} + (C_m + D_m x)e^{-\alpha x} \tag{4.6}$$

where A_m, B_m, C_m and D_m are arbitrary constants.

Differentiating equation (4.6) following expressions are found

$$X_m^{'} = (A_m\alpha + B_m\alpha x + B_m)e^{\alpha x} + (-C_m\alpha - D_m\alpha x + D_m)e^{-\alpha x}$$

$$X_m^{''} = (A_m\alpha^2 + B_m\alpha^2 x + 2B_m\alpha)e^{\alpha x} + (C_m\alpha^2 + D_m\alpha^2 x - 2D_m\alpha)e^{-\alpha x}$$

$$X_m^{'''} = (A_m\alpha^3 + B_m\alpha^3 x + 3B_m\alpha^3)e^{\alpha x} + (-C_m\alpha^3 - D_m\alpha^3 x + 3D_m\alpha^2)e^{-\alpha x}$$

$$X_m^{''''} = (A_m\alpha^4 + B_m\alpha^4 x + 4B_m\alpha^3)e^{\alpha x} + (C_m\alpha^4 + D_m\alpha^4 x - 4D_m\alpha^3)e^{-\alpha x}$$

Now substituting the derivatives of ψ and X_m in the expressions for displacement and stresses (4.2), following expressions are found.

$$u_x(x,y) = \frac{\partial^2\psi}{\partial x\partial y}$$

$$= -\sum_{m=1}^{\infty} X^{'}{}_m\alpha \sin\alpha y$$

$$= -\sum_{m=1}^{\infty}\left[(A_m\alpha + B_m\alpha x + B_m)e^{\alpha x} + (-C_m\alpha - D_m\alpha x + D_m)e^{-\alpha x}\right]\alpha \sin\alpha y$$

$$= -\sum_{m=1}^{\infty}\left[A_m\alpha e^{\alpha x} + B_m(\alpha x+1)e^{\alpha x} - C_m\alpha e^{-\alpha x} - D_m(\alpha x-1)e^{-\alpha x}\right]\alpha \sin\alpha y \tag{4.7a}$$

$$u_y(x,y) = -\frac{1}{(1+\mu)}\left[2\frac{\partial^2\psi}{\partial x^2} + (1-\mu)\frac{\partial^2\psi}{\partial y^2}\right]$$

$$= -\frac{1}{(1+\mu)}\left[2\left\{ \sum_{m=1}^{\infty} X_m^{''} \cos \alpha y \right\} - (1-\mu)\left\{ \sum_{m=1}^{\infty} X_m \alpha^2 \cos \alpha y \right\} \right]$$

$$= -\frac{1}{(1+\mu)}\left[\begin{array}{l} 2\sum_{m=1}^{\infty} \left\{ \begin{array}{l} \left(A_m \alpha^2 + B_m \alpha^2 x + 2B_m \alpha\right) e^{\alpha x} + \\ \left(C_m \alpha^2 + D_m \alpha^2 x - 2D_m \alpha\right) e^{-\alpha x} \end{array} \right\} \cos \alpha y - (1-\mu) \\ \sum_{m=1}^{\infty} \left\{ \left(A_m + B_m x\right) e^{\alpha x} + \left(C_m + D_m x\right) e^{-\alpha x} \right\} \alpha^2 \cos \alpha y \end{array} \right]$$

$$= \frac{-1}{(1+\mu)}\left[\sum_{m=1}^{\infty} \left\{ \begin{array}{l} A_m (1+\mu) \alpha^2 e^{\alpha x} + \\ B_m (\alpha x + \mu \alpha x + 4) \alpha e^{\alpha x} \\ + C_m (1+\mu) \alpha^2 e^{-\alpha x} + \\ D_m (\alpha x + \mu \alpha x - 4) \alpha e^{-\alpha x} \end{array} \right\} \cos \alpha y \right] \qquad (4.7b)$$

$$\sigma_{xx}(x, y) = \frac{E}{(1+\mu)^2}\left[\frac{\partial^3 \psi}{\partial x^2 \partial y} - \mu \frac{\partial^3 \psi}{\partial y^3} \right]$$

$$= -\frac{E}{(1+\mu)^2}\left[\left\{ \sum_{m=1}^{\infty} X_m^{''} \alpha \ \sin \alpha y \right\} + \mu \left\{ \sum_{m=1}^{\infty} X_m \alpha^3 \sin \alpha y \right\} \right]$$

$$= \frac{-E}{(1+\mu)^2}\left[\begin{array}{l} \sum_{m=1}^{\infty} \left\{ \left(A_m \alpha^2 + B_m \alpha^2 x + 2B_m \alpha\right) e^{\alpha x} + \left(C_m \alpha^2 + D_m \alpha^2 x - 2D_m \alpha\right) e^{-\alpha x} \right\} \alpha^2 \sin \alpha y \\ + \mu \sum_{m=1}^{\infty} \left\{ \left(A_m + B_m x\right) e^{\alpha x} + \left(C_m + D_m x\right) e^{-\alpha x} \right\} \alpha^3 \sin \alpha y \end{array} \right]$$

$$= \frac{-E}{(1+\mu)^2}\left[\sum_{m=1}^{\infty} \left\{ \begin{array}{l} A_m \alpha (1+\mu) e^{\alpha x} + B_m (\alpha x + \mu \alpha x + 2) e^{\alpha x} \\ + C_m \alpha (1+\mu) e^{-\alpha x} + D_m (\alpha x + \mu \alpha x - 2) e^{-\alpha x} \end{array} \right\} \alpha^2 \sin \alpha y \right] \qquad (4.7c)$$

$$\sigma_{yy}(x, y) = \frac{-E}{(1+\mu)^2}\left[(2+\mu) \frac{\partial^3 \psi}{\partial x^2 \partial y} + \frac{\partial^3 \psi}{\partial y^3} \right]$$

$$= \frac{-E}{(1+\mu)^2}\left[-(2+\mu)\left\{ \sum_{m=1}^{\infty} X_m^{''} \alpha \ \sin \alpha y \right\} + \left\{ \sum_{m=1}^{\infty} X_m \alpha^3 \sin \alpha y \right\} \right]$$

$$= \frac{-E}{(1+\mu)^2}\left[\begin{array}{l} -(2+\mu) \sum_{m=1}^{\infty} \left\{ \left(A_m \alpha^2 + B_m \alpha^2 x + 2B_m \alpha\right) e^{\alpha x} + \left(C_m \alpha^2 + D_m \alpha^2 x - 2D_m \alpha\right) e^{-\alpha x} \right\} \alpha \ \sin \alpha y \\ + \sum_{m=1}^{\infty} \left\{ \left(A_m + B_m x\right) e^{\alpha x} + \left(C_m + D_m x\right) e^{-\alpha x} \right\} \alpha^3 \sin \alpha y \end{array} \right]$$

$$= \frac{-E}{(1+\mu)^2}\left[\sum_{m=1}^{\infty}\begin{Bmatrix} A_m\alpha(-1-\mu)e^{\alpha x} + B_m(-\alpha x - \mu\alpha x - 2\mu - 4)e^{\alpha x} + \\ C_m\alpha(-1-\mu)e^{-\alpha x} + D_m(-\alpha y - \mu\alpha x + 2\mu + 4)e^{-\alpha x}\end{Bmatrix}\alpha^2 \sin\alpha y\right] \qquad (4.7d)$$

$$\sigma_{xy}(x,y) = \frac{-E}{(1+\mu)^2}\left[\frac{\partial^3\psi}{\partial x^3} - \mu\frac{\partial^3\psi}{\partial x\partial y^2}\right]$$

$$= \frac{-E}{(1+\mu)^2}\left[\sum_{m=1}^{\infty} X'''_m \cos\alpha y + \mu\left\{\sum_{m=1}^{\infty} X'_m\alpha^2\cos\alpha y\right\}\right]$$

$$= \frac{-E}{(1+\mu)^2}[\sum_{m=1}^{\infty}\left\{\left(A_m\alpha^3 + B_m\alpha^3 x + 3B_m\alpha^2\right)e^{\alpha x} + \left(-C_m\alpha^3 - D_m\alpha^3 x + 3D_m\alpha^2\right)e^{-\alpha x}\right\}\cos\alpha y$$

$$+ \mu\sum_{m=1}^{\infty}\left\{\left(A_m\alpha\ + B_m\alpha\ x + B_m\right)e^{\alpha x} + \left(-C_m\alpha\ - D_m\alpha\ x + D_m\right)e^{-\alpha x}\right\}\alpha^2\cos\alpha y]$$

$$= \frac{-E}{(1+\mu)^2}\left[\sum_{m=1}^{\infty}\begin{Bmatrix} A_m(1+\mu)\alpha e^{\alpha x} + B_m(\alpha x + \mu\alpha x + \mu + 3)e^{\alpha x} \\ -C_m(1+\mu)\alpha e^{-\alpha x} - D_m(\alpha x + \mu\alpha x - \mu - 3)e^{-\alpha x}\end{Bmatrix}\alpha^2\cos\alpha y\right] \qquad (4.7e)$$

Now, the axial loading on the right edge of the panel can be taken as Fourier series in the following manner:

$$\sigma_{xx}(b,y) = \frac{\sigma^o_{xx}}{a}(2y-a) = \sum_{m=1}^{\infty} E_m \sin\alpha y \qquad (4.8)$$

To satisfy both the boundary condition and the loading distribution, Fourier sine series have been considered for the analysis.

$$E_m = \frac{2}{a}\int_0^a \frac{\sigma^o_{xx}}{a}(2y-a)\sin(\alpha y)dy$$

$$= \frac{4\sigma^o_{xx}}{a^2}\int_0^a y\sin(\alpha y)dy - \frac{2\sigma^o_{xx}}{a}\int_0^a \sin(\alpha y)dy$$

$$= -\frac{2\sigma^o_{xx}}{m\pi}[1+\cos(m\pi)], \text{ where m = 1, 2, 3, 4, 5 } \ldots\ldots\ldots\ldots\ldots \infty$$

Due to symmetry, the axial displacement at the left edge from 0 to (a-h) is zero. But at the cracked surface, the distribution of the axial displacement can be expressed as the Fourier series in the following manner:

$$u_x(0,y) = a_0 + \sum_{i=1}^{3} a_i\cos(i*w*y) + \sum_{i=1}^{3} b_i\sin(i*w*y) = \sum_{m=1}^{\infty} I_m\sin(\alpha y) \qquad (4.9)$$

The curve fitted equation as Fourier series up to 7th term have been considered. This is because of up to 7th term we always achieve R^2 value above 0.99. If we increase the term it will make the mathematical calculation more complicated.

Here

$$I_m = \frac{2}{a}\int_{a-h}^{a}(a_0 + \sum_{i=1}^{3} a_i \cos(i*w*y) + \sum_{i=1}^{3} b_i \sin(i*w*y))\sin(\alpha y)dy$$

After performing integration on the above equation, the result is given below:

$$I_m = \left(\frac{2a_o}{m\pi}\left(\cos\left(\frac{(a-h)m\pi}{a}\right) - \cos(m\pi)\right)\right) + \sum_{i=1}^{3} a_i \begin{pmatrix} \left(\frac{1}{m\pi + iwa}\cos\left(\left(\frac{a-h}{a}\right)(m\pi + iwa)\right)\right) + \\ \left(\frac{1}{m\pi - iwa}\cos\left(\left(\frac{a-h}{a}\right)(m\pi - iwa)\right)\right) - \\ \left(\frac{1}{m\pi + iwa}\cos(m\pi + iwa)\right) - \\ \left(\frac{1}{m\pi - iwa}\cos(m\pi - iwa)\right) \end{pmatrix}$$

$$+ \sum_{i=1}^{3} b_i \begin{pmatrix} -\left(\frac{1}{m\pi - iwa}\sin(m\pi + iwa)\right) + \\ \left(\frac{1}{m\pi - iwa}\sin(m\pi - iwa)\right) + \\ \left(\frac{1}{m\pi + iwa}\sin\left(\left(\frac{a-h}{a}\right)(m\pi + iwa)\right)\right) - \\ \left(\frac{1}{m\pi - iwa}\sin\left(\left(\frac{a-h}{a}\right)(m\pi - iwa)\right)\right) \end{pmatrix}$$

Using boundary condition $\sigma_{xy}(0, y) = 0$ at the edge of $x = 0$, it is found that

$$\frac{-E}{(1+\mu)^2}\left[\sum_{m=1}^{\infty}\left\{A_m(1+\mu)\alpha + B_m(\mu+3) - C_m(1+\mu)\alpha - D_m(-\mu-3)\right\}\alpha^2\cos\alpha y\right] = 0$$

$$or, \left[A_m\alpha(1+\mu) + B_m(\mu+3) - C_m\alpha(1+\mu) + D_m(\mu+3)\right] = 0 \quad (4.10)$$

Using boundary condition $\sigma_{xy}(b, y) = 0$ at the edge of $x = b$, it is found that

$$\frac{-E}{(1+\mu)^2}\left[\sum_{m=1}^{\infty}\left\{\begin{matrix} A_m\alpha(1+\mu)e^{\alpha b} + B_m(\alpha b + \mu\alpha b + \mu + 3)e^{\alpha b} \\ -C_m(1+\mu)\alpha e^{-\alpha b} - D_m(\alpha b + \mu\alpha b - \mu - 3)e^{-\alpha b} \end{matrix}\right\}\alpha^2\cos\alpha y\right] = 0$$

$$or,\begin{bmatrix} A_m\alpha(1+\mu)e^{\alpha b} + B_m(\alpha b+\mu\alpha b+\mu+3)e^{\alpha b} \\ -C_m\alpha(1+\mu)e^{-\alpha b} - D_m(\alpha b+\mu\alpha b-\mu-3)e^{-\alpha b} \end{bmatrix} = 0 \tag{4.11}$$

Using boundary condition $u_x(0,y) = a_0 + \sum_{i=1}^{3} a_i \cos(i*w*y) + \sum_{i=1}^{3} b_i \sin(i*w*y)$ at the edge of $x = 0$, it is found that

$$-\sum_{m=1}^{\infty}[A_m\alpha + B_m - C_m\alpha + D_m]\alpha \sin\alpha y = \sum_{m=1}^{\infty} I_m \sin(\alpha y)$$

$$or,-[A_m\alpha + B_m - C_m\alpha + D_m]\alpha = I_m \tag{4.12}$$

Using boundary condition $\sigma_{xx}(b,y) = \sigma_{xx}^{o}$ at the edge of $x = b$, it is found

$$\frac{-E}{(1+\mu)^2}\left[\sum_{m=1}^{\infty}\begin{Bmatrix} A_m\alpha(1+\mu)e^{\alpha b} + B_m(\alpha b+\mu\alpha b+2)e^{\alpha b} \\ +C_m\alpha(1+\mu)e^{-\alpha b} + D_m(\alpha b+\mu\alpha b-2)e^{-\alpha b} \end{Bmatrix}\alpha^2 \sin\alpha y\right] = \sum_{m=1}^{\infty} E_m \sin\alpha y$$

$$or,\frac{-E\alpha^2}{(1+\mu)^2}\begin{bmatrix} A_m\alpha(1+\mu)e^{\alpha b} + B_m(\alpha b+\mu\alpha b+2)e^{\alpha b} \\ +C_m\alpha(1+\mu)e^{-\alpha b} + D_m(\alpha b+\mu\alpha b-2)e^{-\alpha b} \end{bmatrix} = E_m \tag{4.13}$$

The simultaneous equations (4.10), (4.11), (4.12) and (4.13) can be realized in a simplified matrix form for the solution of unknown terms like A_m , B_m , C_m and D_m as follows:

$$\begin{bmatrix} DD_1 & DD_2 & DD_3 & DD_2 \\ FF_1 & FF_2 & FF_3 & FF_4 \\ HH_1 & HH_2 & HH_3 & HH_2 \\ KK_1 & KK_2 & KK_3 & KK_4 \end{bmatrix}\begin{bmatrix} A_m \\ B_m \\ C_m \\ D_m \end{bmatrix} = \begin{bmatrix} 0 \\ 0 \\ I_m \\ E_m \end{bmatrix} \tag{4.14}$$

Where

$$DD_1 = \alpha(1+\mu)$$

$$DD_2 = (\mu+3)$$

$$DD_3 = -\alpha(1+\mu)$$

$$FF_1 = \alpha(1+\mu)e^{\alpha b}$$

$$FF_2 = (\alpha b+\mu\alpha b+\mu+3)e^{\alpha b}$$

$$FF_3 = -\alpha(1+\mu)e^{-\alpha b}$$

$$FF_4 = -(\alpha b + \mu\alpha b - \mu - 3)e^{-\alpha b}$$

$$HH_1 = -\alpha^2$$

$$HH_2 = -\alpha$$

$$HH_3 = \alpha^2$$

$$KK_1 = Z_{11}\alpha(1+\mu)e^{\alpha b}$$

$$KK_2 = Z_{11}(\alpha b + \mu\alpha b + 2)e^{\alpha b}$$

$$KK_3 = Z_{11}\alpha(1+\mu)e^{-\alpha b}$$

$$KK_4 = Z_{11}(\alpha b + \mu\alpha b - 2)e^{-\alpha b}$$

$$Z_{11} = \frac{-E\alpha^2}{(1+\mu)^2}$$

Solution of the above matrix Eq. (4.14) yields the unknown constants A_m , B_m , C_m and D_m . Once the value of the unknowns are determined, they are directly substituted in Eqs.[4.7(a)-4.7(e)] to obtain the explicit expressions for the different parameters of interest, namely, the two displacement and the three stress components at various points.

3.5 Analysis of Elastic Field

The solutions of displacement and stress components using displacement potential approach are obtained for steel panel (Poisson ratio μ = 0.3 and Modulus of Elasticity E = 209 GPa), aspect ratio b/a = 1.0, crack length ratio h/a = 0.3 and the maximum intensity loading parameter, σ_o = 40 N/mm. The results is presented in a sequence of axial displacement (u_x), lateral displacement (u_y), bending stress (σ_{xx}), normal stress (σ_{yy}) and shearing stress (σ_{xy}). In order to make the results non-dimensional, the displacements are expressed as the ratio of actual displacement to the actual dimension of the bar, and the stresses are expressed as the ratio of the actual stress to the applied loading parameter. Finally the effects of panel aspect ratio and crack length ratio on the elastic fields are analyzed.

i. Displacement Field

The variation of normalized displacement component u_x/a with x is shown in Fig. 4.3. As the symmetric bending loading is applied on the right edge of the panel, the displacement u_x should be negative throughout the bottom half the panel and positive throughout the rest of panel. It will be higher at the loaded section which will decrease as we move towards the crack surface section of the panel. Due to symmetry no axial displacement happened at mid section of full panel (x=0) but axial displacement happens due to presence of crack throughout the region of $y/a \geq 0.7$. That's why axial displacement is not symmetric below the region of $x/b \leq 0.2$. This phenomenon is totally reflected in Fig. 4.3. It is zero at both the stiffened edges which satisfies the physical characteristics of the problem.

The distribution of normalized lateral components u_y/a with respect to y at different sections the panel is shown in Fig. 4.4. From figure 4.3 and 4.5, it is observed that contraction of column occurs in the region $0.75 \leq y/a \leq 1.0$ while expansion occurs in the region of $0.0 \leq y/a \leq 0.25$. Since tensile loading in x direction at upper half of panel has normally led to contraction in y direction due to the effect of Possion's ratio, the lateral displacement is positive over the region of $0.5 \leq y/a \leq 0.75$. The lateral displacement is also positive for the region $0.25 \leq y/a \leq 0.5$ due to the compressive loading at lower half of the panel. The effect of crack on lateral displacement is only visible below the region of $x/b \leq 0.2$.

Fig 4.5 shows the deformed shape of the bar under bending loading at the left and right edges with the magnification of 5000 times of displacement. The displacement at the crack surface is found insignificant as compared to the axial loading condition that was discussed at the previous chapter.

ii. Stress Field

Fig. 4.6 and 4.7 illustrates the distribution of normalized normal stress components σ_{xx}/σ_o and σ_{yy}/σ_o at different sections of the panel. As the normal stress component σ_{xx} and σ_{yy} are functions of the displacement components u_x and u_y ,

both of the stresses will decrease towards the supporting edge because the displacement components u_x and u_y decrease towards the supporting edge as shown in Figs. 4.6 and 4.7. A sudden fluctuation of stress happens near the crack. But the influence of crack is noticeable over the region $0.0 \leq x/b \leq 0.2$. The stress component σ_{xx} is almost 0.045 times of the applied load. This fluctuation is much lower than considering axial loading at the right end of the beam. It reveals that bending loading has lower effect on crack tip of this panel. As appears from the distribution, the above half of the present isotropic panel is always in tension in the x-direction whereas the lower half is subjected to compression. The stress at the stiffened edge is completely zero which is good agreement with boundary condition.

Fig. 4.7 shows that bending load makes the lateral stress component σ_{yy} lower significant over the region of x/b <0.5 because the largest value of σ_{yy} is only 0.06 times of the maximum intensity of the applied load. But at crick tip it is almost 0.025 times of the applied load.

Fig. 4.8 presents the normalized shear stress component σ_{xy}/σ_o at different sections of the panel. At the left edge the shear stress is zero, which is in good agreement with the physical characteristics of the problem. The maximum shear stress is found at sections x/b = 0.5.It concludes from the Fig. 4.8 that the shear stress is maximum near the right edge and near the stiffened edges.

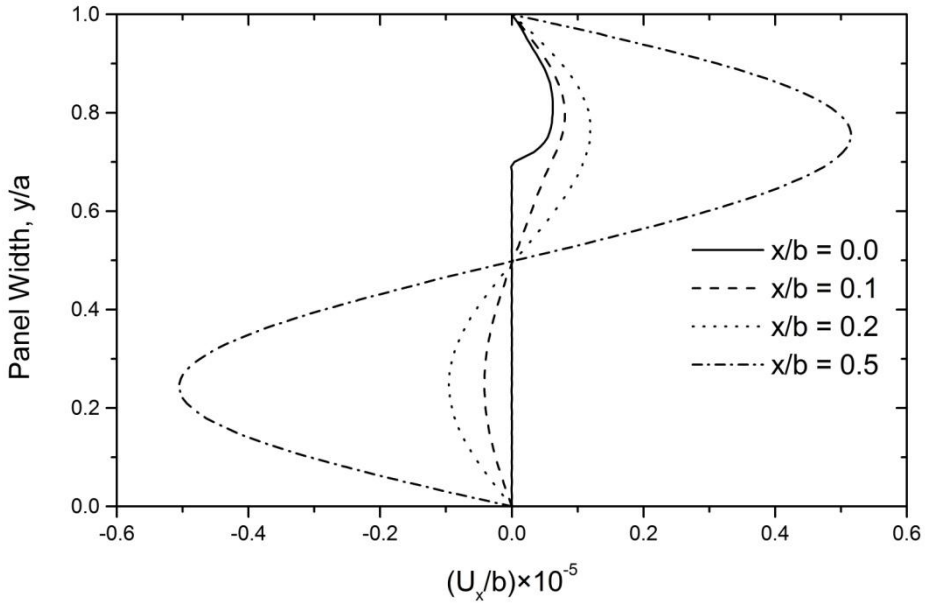

Fig 4.3: Distribution of normalized axial displacement at different sections of the steel panel. (*b/a* =1, *h/a* =0.3)

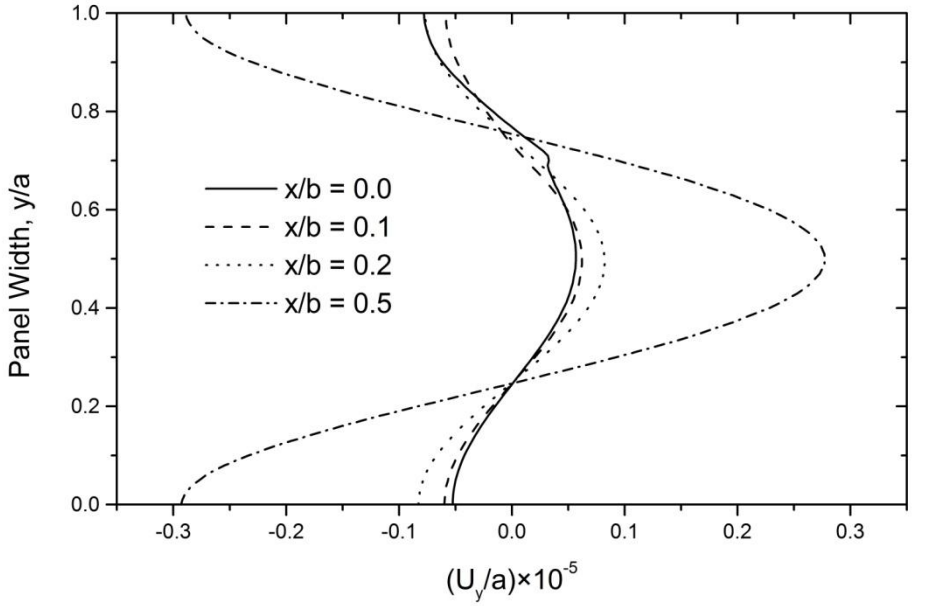

Fig 4.4: Distribution of normalized lateral displacement at different sections of the steel panel. (*b/a* =1, *h/a* =0.3)

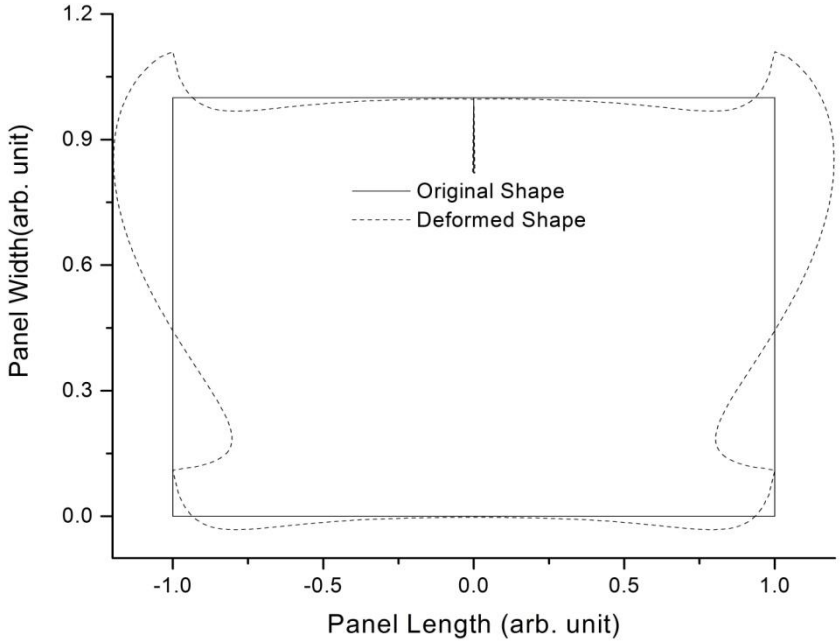

Fig 4.5: Deformed shape of the cracked steel panel, (*b/a* =1, *h/a* =0.3) (magnification factor×5000).

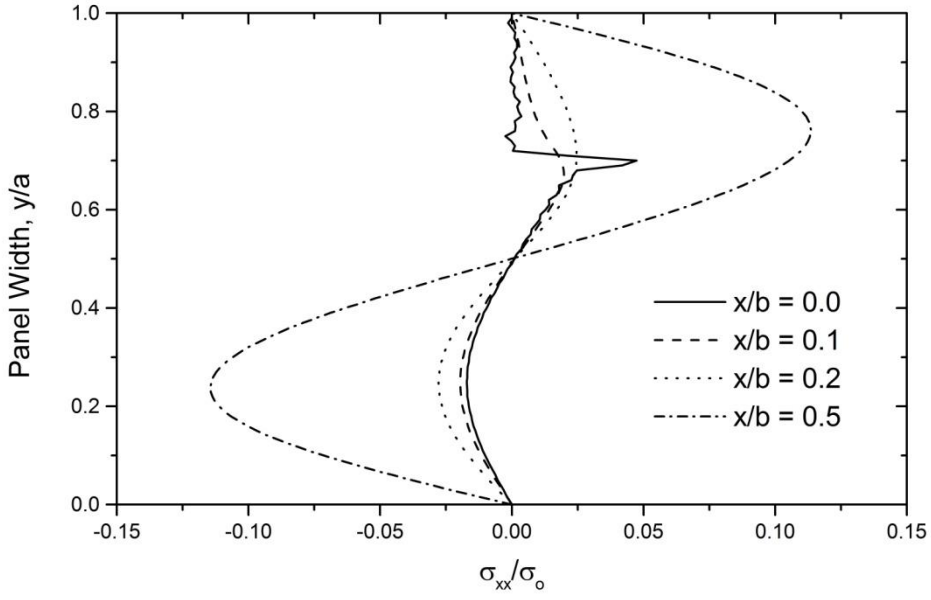

Fig 4.6: Distribution of normalized axial stress at different sections of the steel panel. (*b/a* =1, *h/a* =0.3)

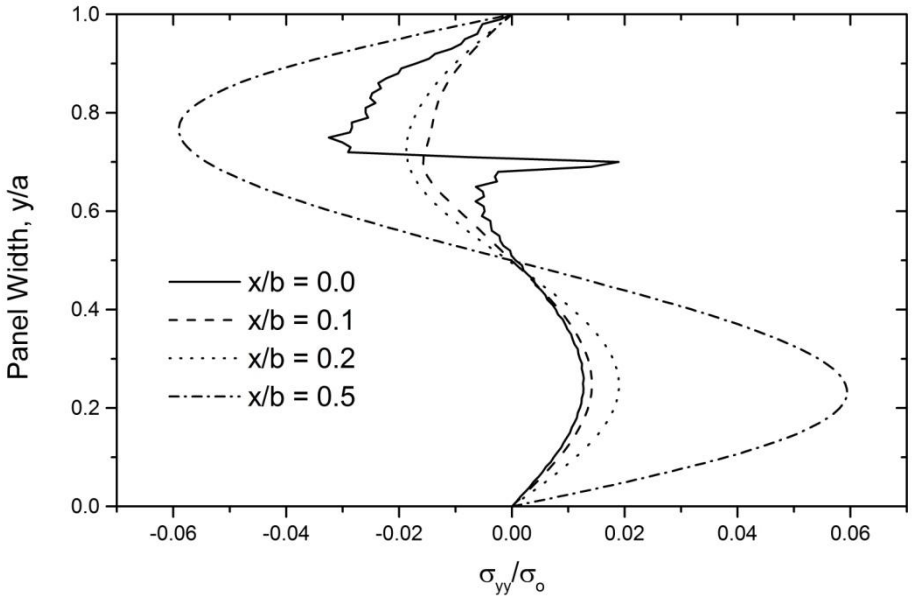

Fig 4.7: Distribution of normalized lateral stress at different sections of the steel panel. (b/a = 1, h/a = 0.3)

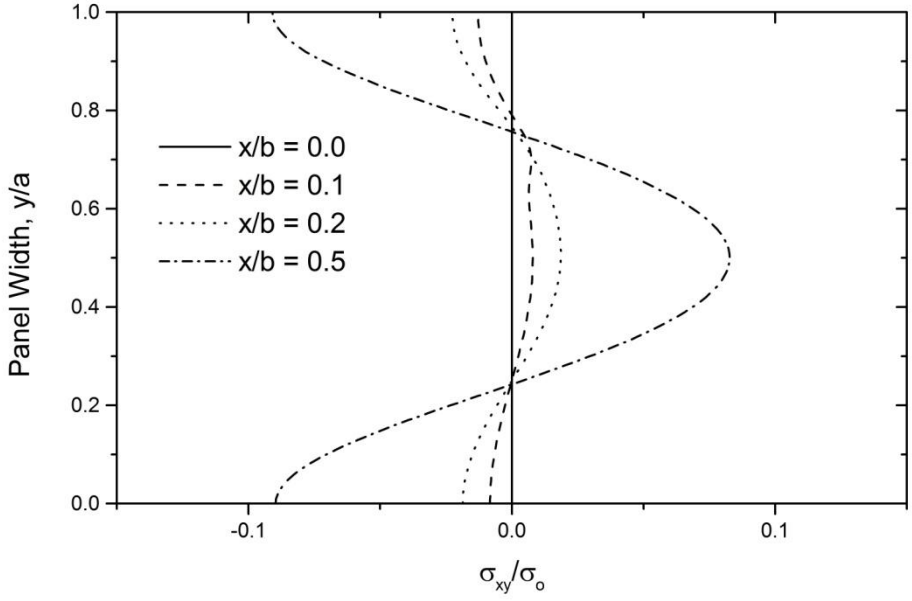

Fig 4.8: Distribution of normalized shear stress at different sections of the steel panel. (b/a = 1, h/a = 0.3)

Distribution of normalized maximum principle stress obtained using the results of displacement potential approach is presented in Fig. 4.9. The relation used in this regard is $\sigma_1 = \frac{\sigma_x+\sigma_y}{2} + \sqrt{\left(\frac{\sigma_x-\sigma_y}{2}\right)^2 + \sigma_{xy}^2}$, where σ_1 is the maximum principle stress. No reference of the principle stress distribution for a guided deep beam could be found. As such the verification of present results remains to be investigated with the availability of any other results. However, the contour pattern of maximum principle stress of the current solution seems to be satisfactory in a general sense of visual basis.

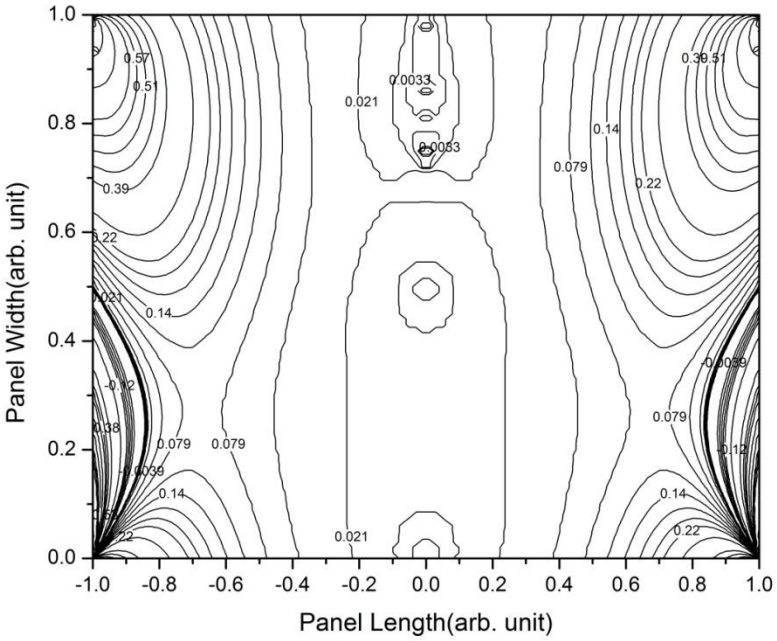

Fig 4.9: Normalized maximum principle stress contour of cracked stiffened steel panel, (*b/a* = 1, *h/a* = 0.3).

iii. Effect of Crack Length on the Stress and Displacement Fields

In this section the effect of crack length ratio (*h/a* = 0.0 ~0.4) on the isotropic panel is discussed. Note that the crack depth ratio is always considered to be less than 0.6 which is quite reasonable for industrial applications [7].

The distribution of normalized axial stress with the variation of crack length is shown in Fig. 4.10 for two different sections. Normally with the increase of crack length, the fluctuation of the axial stress increases. This happens as our knowledge has up to crack length ratio of h/a = 0.3. Then fluctuation decreases that is also reflected at sections x/b = 0.1. This phenomenon is in contrast to our general intuition and may be attributed to the conditions of bending loading. No fluctuation of stress happens if there is no crack presence in the panel.

The distribution of lateral stress for different crack length did not follow the same pattern that has been found in case of axial stress. It is observed from Fig. 4.11 that the percentage of increase of the stress at crack tip increases with crack length. For h/a = 0.4 at crack tip the maximum positive value of the stress is almost 0.025 times of the maximum intensity of load. The graph diverts more for higher crack length from its regular pattern parabolic shape that is happened only for panel with no crack.

Due to zero shear stress at section x/b =0.0 a different section x/b = 0.5 have been chosen with x/b = 0.1 as shown in Fig. 4.12(a) and 4.12(b). Though at section x/b =0.5 it can be seen that there is very little effect on the shear stress of crack. But by\closer looking it can be found that near the bottom stiffened edge all graphs for different crack length merge with each other, but upper stiffened edge they all shows different value and for h/a = 0.4 it is lower. The shear stress distribution is smooth for no crack but the smoothness disappears with the increase of the crack length. The maximum fluctuation happens for highest crack length.

Figs. 4.13(a) and 4.13(b) illustrates the distribution of the normalized axial displacement for different crack length at two different sections. The maximum value of the axial displacement is obtained for higher crack length.

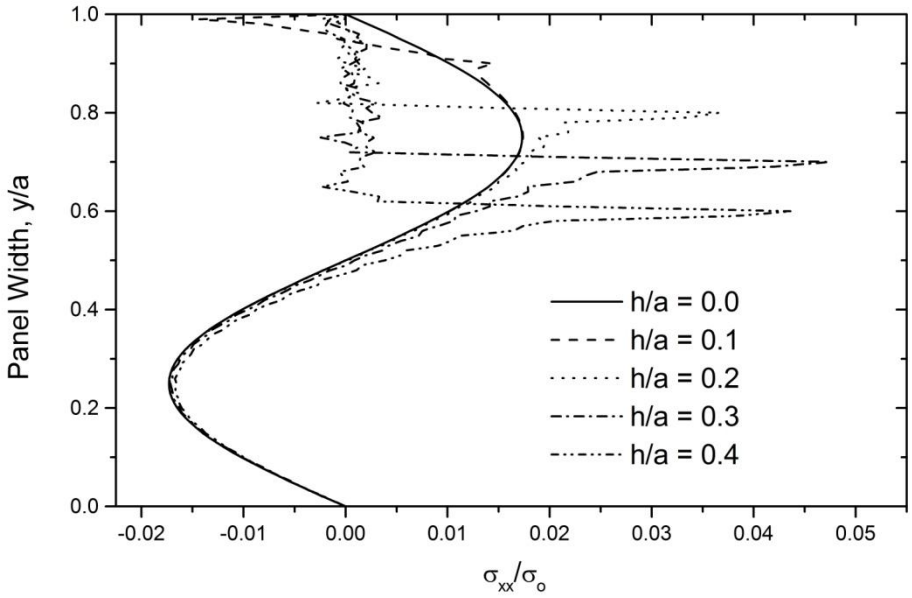

(a)

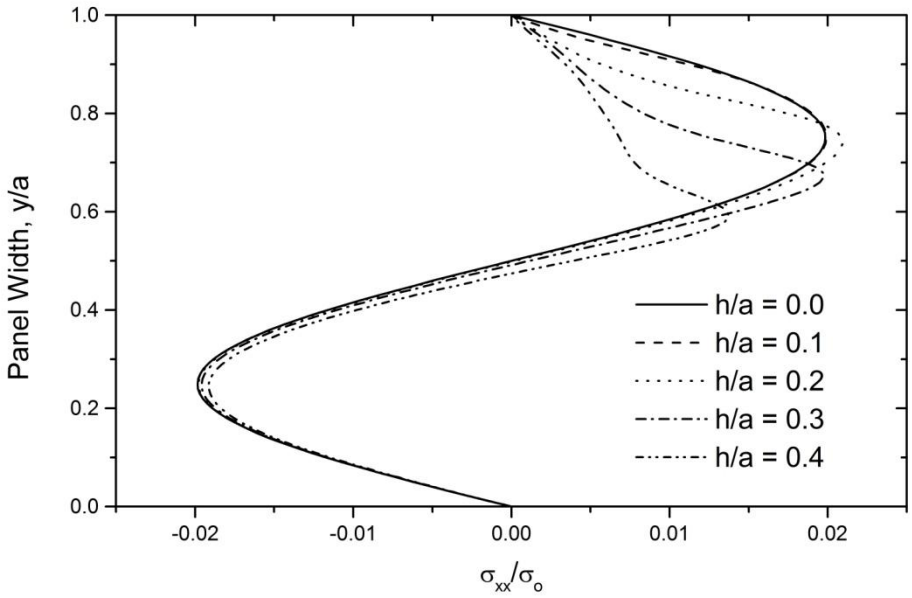

(b)

Fig 4.10: Effect of crack length on the axial stress component at (a) *x/b* = 0.0 and (b) *x/b* = 0.1, (*b/a* = 1).

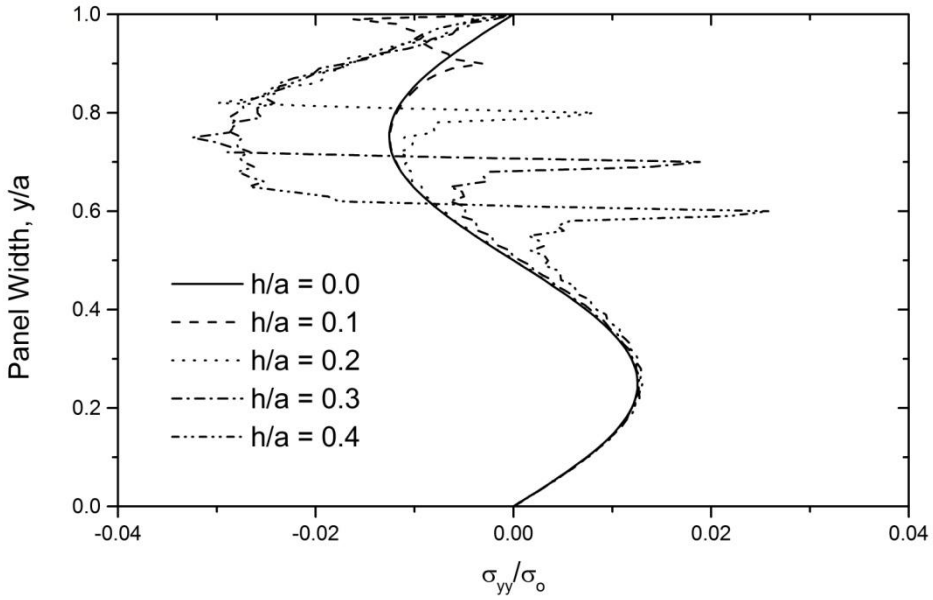

(a)

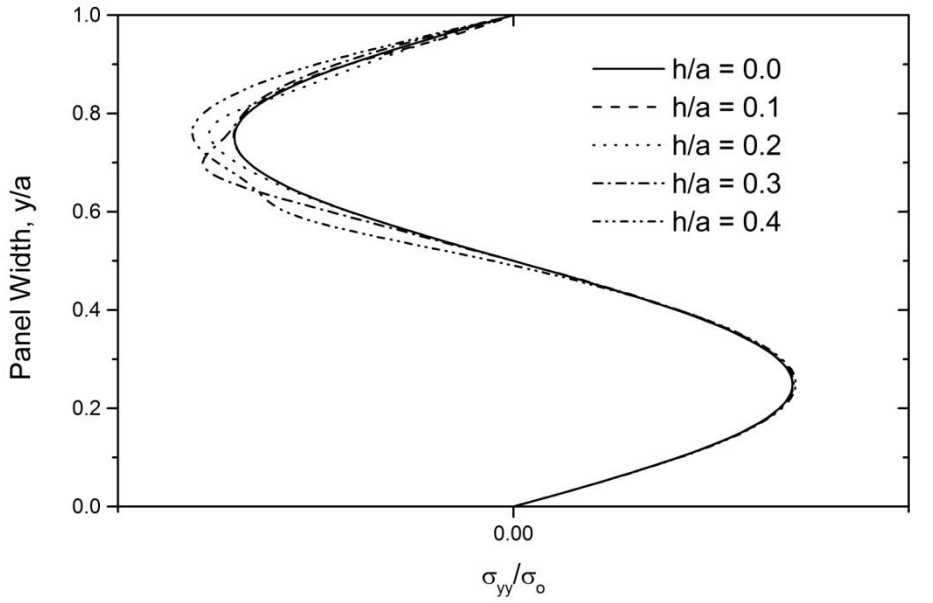

(b)

Fig 4.11: Effect of crack length on the lateral stress component at (a) *x/b* = 0.0 and (b) *x/b* = 0.1, (*b/a* = 1).

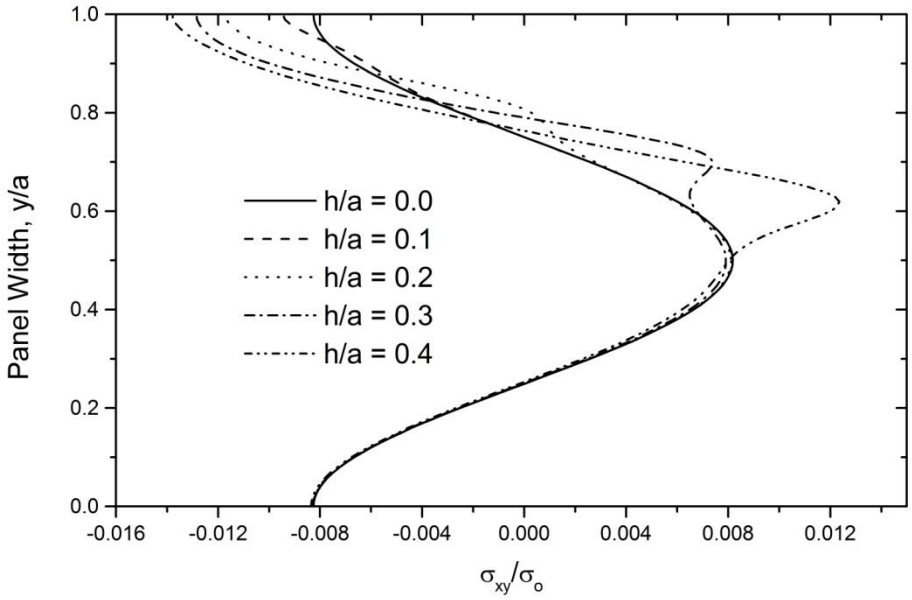

(a)

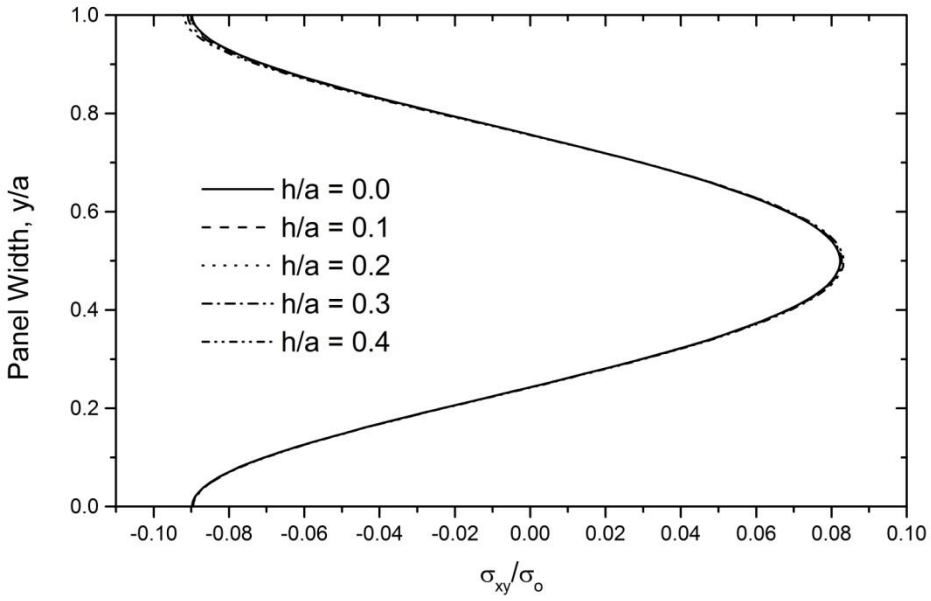

(b)

Fig 4.12: Effect of crack length on the shear stress component at (a) *x/b* = 0.1 and (b) *x/b* = 0.5, (*b/a* = 1).

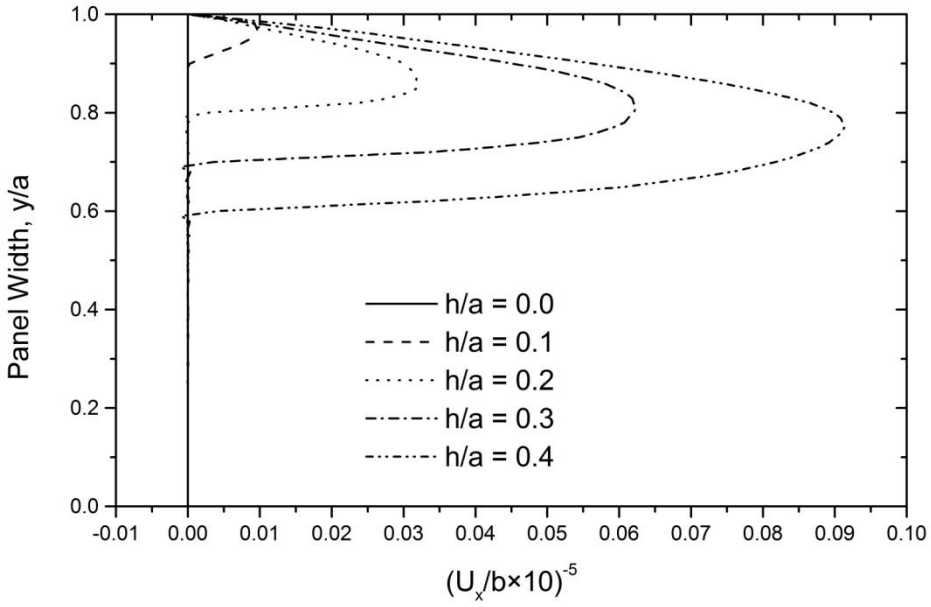

(a)

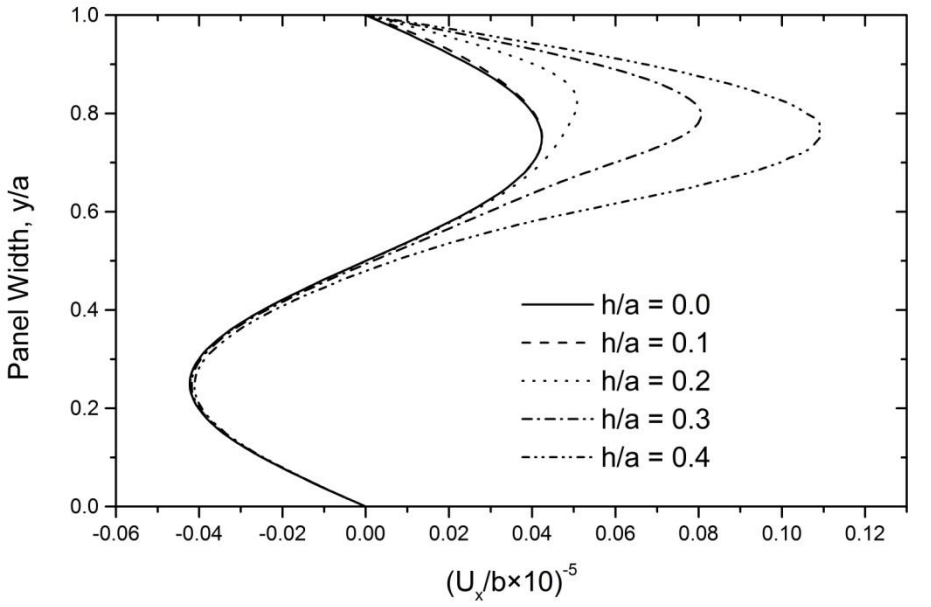

(b)

Fig 4.13: Effect of crack length on the axial displacement component at (a) x/b = 0.0 and (b) x/b = 0.1, (b/a = 1).

iv. Effect of Panel Aspect Ratio on the Stress and Displacement Fields

Figs. 4.14, 4.15 and 4.16 portrait the distribution normalized stress components σ_{xx}/σ_o, σ_{yy}/σ_o and σ_{xy}/σ_o as a function of the aspect ratio of the isotropic panel. As seen from the figures, all the stress components vary inversely with the aspect ratio *b/a*, i.e. the magnitude of stress components decreases as the aspect ratio increases. Thus, a section whose distance is more from the applied load will have a stress of lower magnitude.

From Fig. 4.14, it can be seen that applied load has so lower effect on crack for aspect ratio *b/a* =1.5 that fluctuation of stress is barely noticeable. The magnitude of maximum stress is maximum for the smallest panel and minimum for the largest one.

Similar trends happened for the lateral stress component as shown in the Fig. 4.15. Fig. 4.16 represents the variation of shearing stress with aspect ratio. The anti symmetric variation of shearing stress is found at lower aspect ratio. The fluctuation of shear stress is so high at crack tip for lower aspect ratio that it is very negligible for high aspect ratio. The variation of shear stress is almost symmetric in case of higher aspect ratio.

Fig. 4.17 exhibits the axial displacement u_x as a function of aspect ratio. This displacement component is influenced by the aspect ratio b/a in the same manner as stress components discussed in the preceding paragraph.

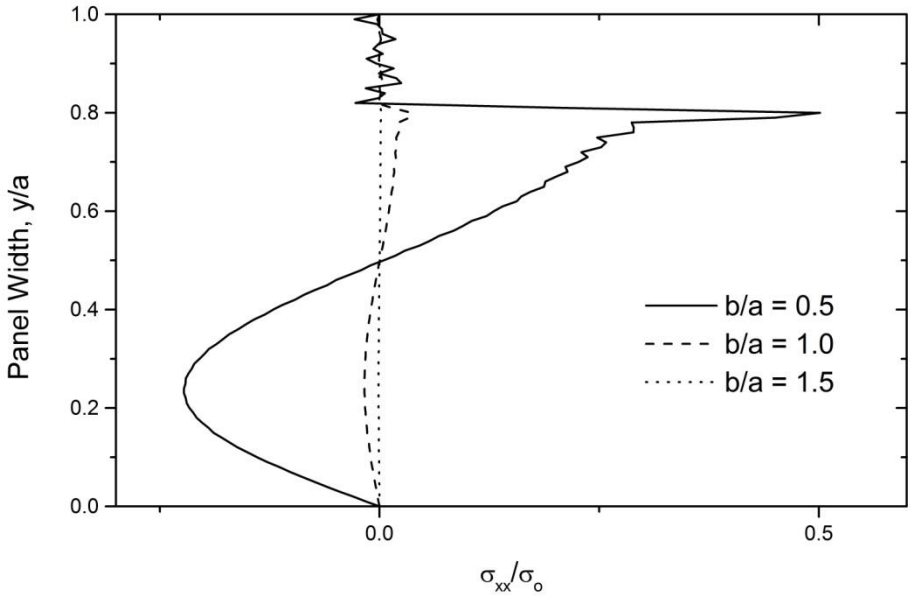

(a)

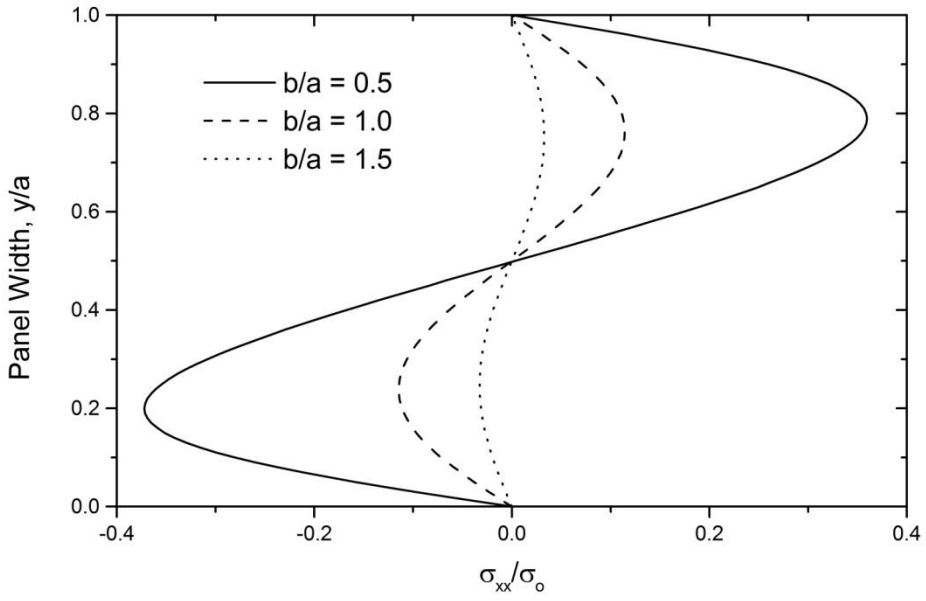

(b)

Fig 4.14: Effect of aspect ratio on the axial stress component at (a) *x/b* = 0.0 and (b) *x/b* = 0.5, (*h/a* = 0.3)

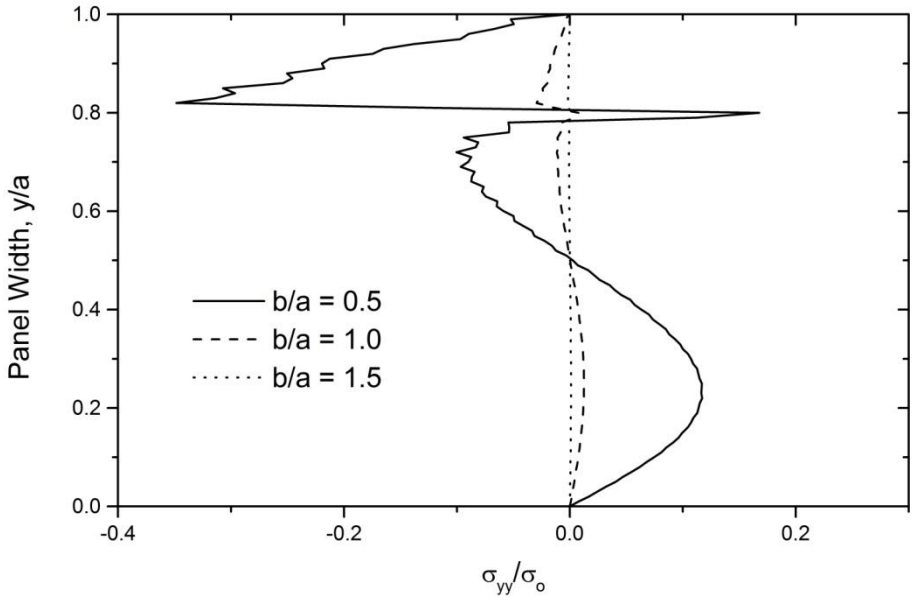

(a)

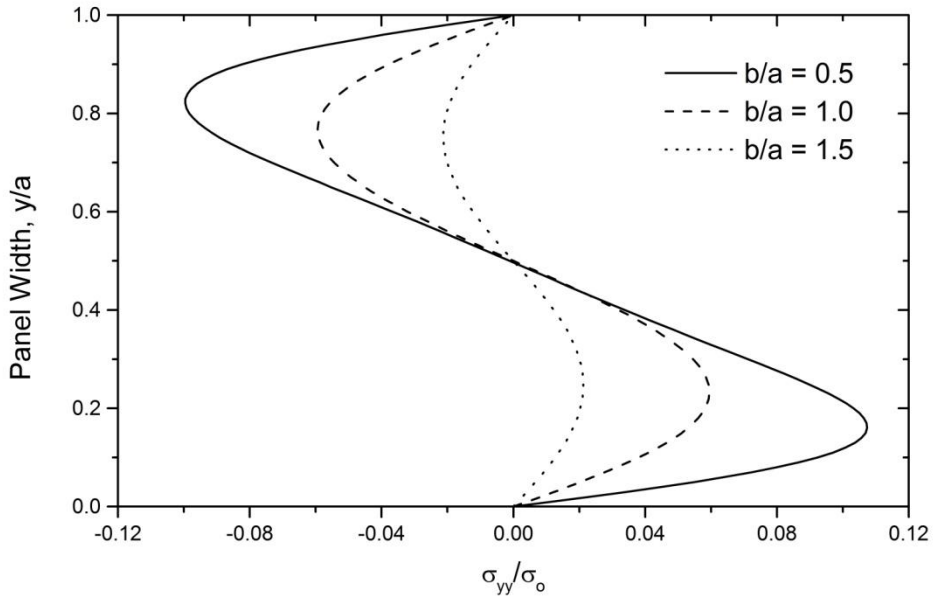

(b)

Fig 4.15: Effect of aspect ratio on the lateral stress component at (a) *x/b* = 0.0 and (b) *x/b* = 0.5, (*h/a* = 0.3).

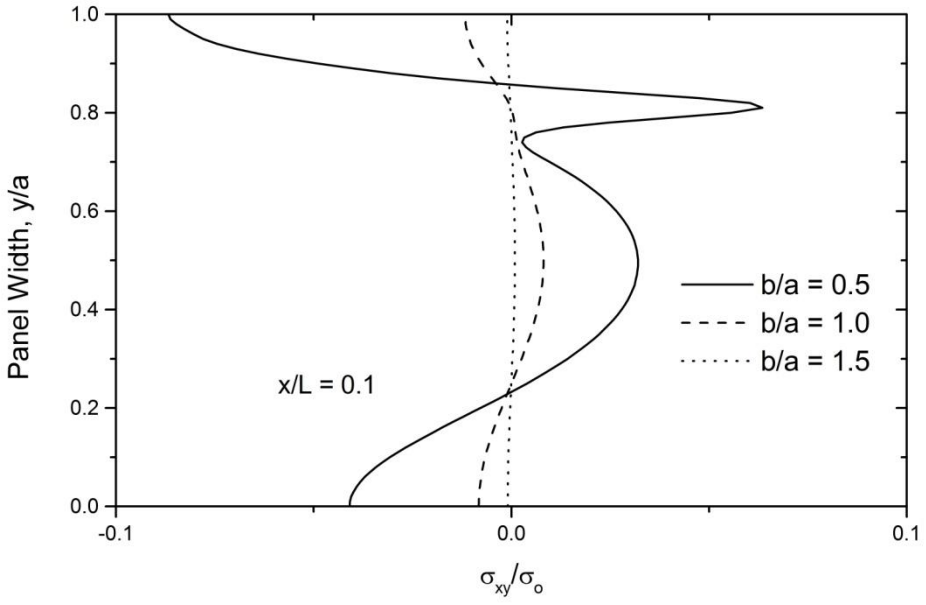

(a)

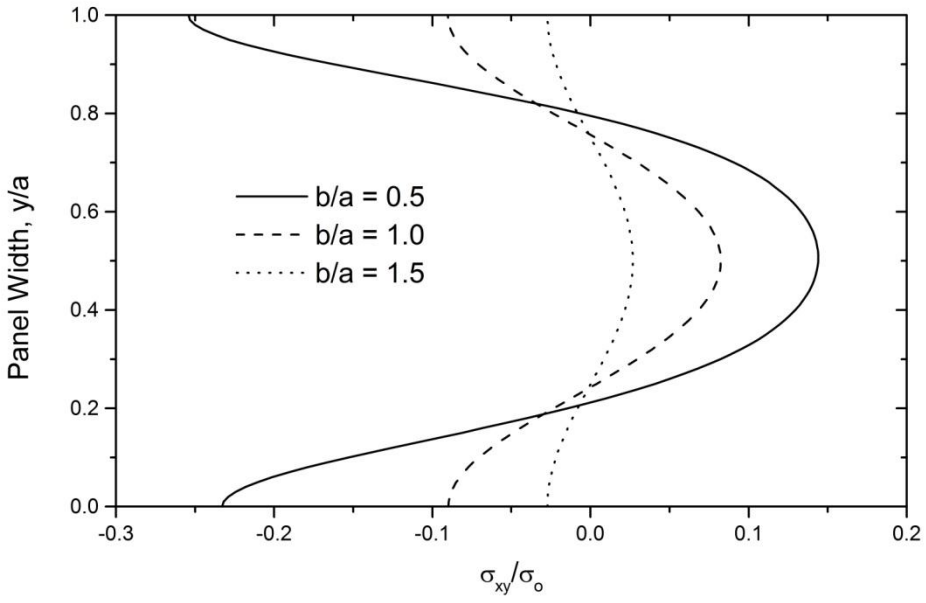

(b)

Fig 4.16: Effect of aspect ratio on the shear stress component at (a) *x/b* = 0.1 and (b) *x/b* = 0.5, (*h/a* = 0.3).

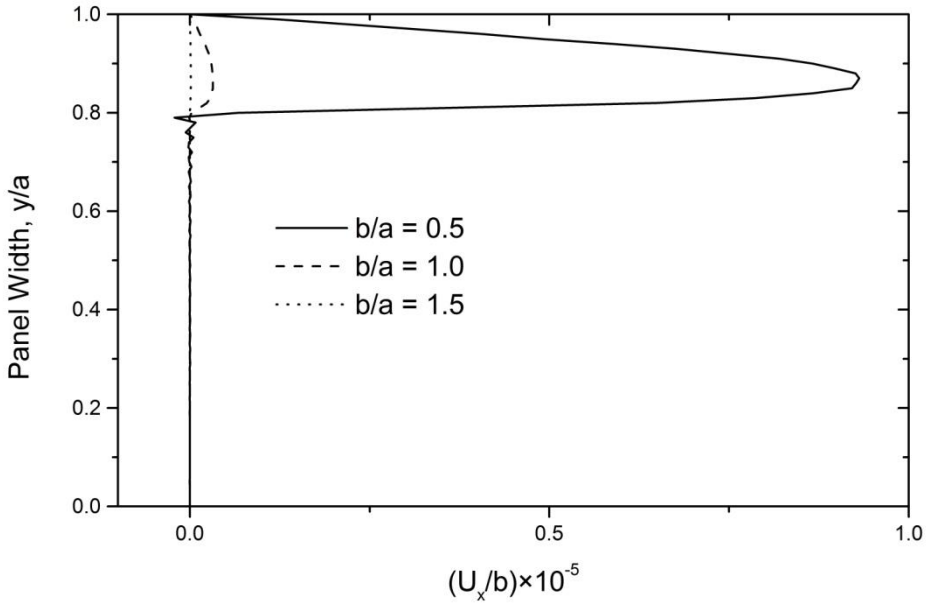

(a)

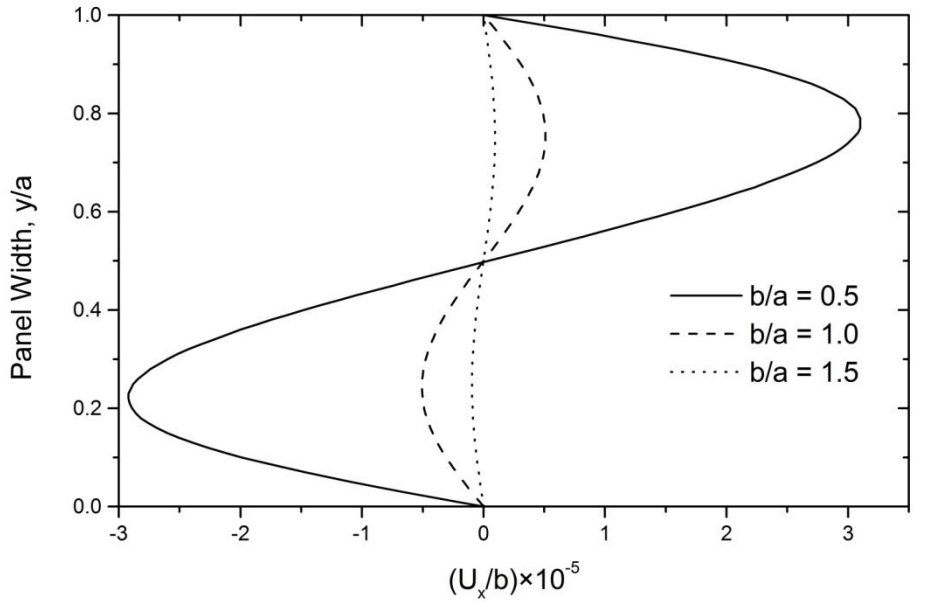

(b)

Fig 4.17: Effect of aspect ratio on the axial displacement component at (a) x/b = 0.0 and (b) x/b = 0.5, (h/a = 0.3).

CHAPTER 5

CRACKED PANEL UNDER LATERAL STIFFENERS SUBJECTED TO AXIAL TENSION

This chapter discusses the solution of a cracked panel stiffened by lateral stiffeners at its opposing longitudinal edges and is loaded axially by a uniform tension. In the previous two chapters, axial stiffeners were considered. The main difference between the two stiffeners is, lateral stiffener restraints the lateral displacement whereas axial stiffener restraints the axial displacement.

5.1 Problem Articulation

A metallic stiffened panel of isotropic material with an edge crack emanating from the upper surface subjected to uniform tensile loading σ_0 at both lateral ends is considered. The analytical model of the panel with a rectangular frame of reference *x-y* is shown in Fig. 5.2a. The geometrical properties of the panel are: length 2b, height *a* and crack length h. Since the structure is symmetric with reference to mid-section of the panel along y-axis, half of the panel may be considered for the analysis as shown in Fig. 5.2b, i.e., the right half of the panel with the crack was analyzed due to symmetry. Since the thickness of such structures is very small compared to its other dimensions, the plane stress condition is adopted to model the problem for the determination of the corresponding displacement and stress fields. There will be no axial displacement along the ligament of the full panel due to the symmetry but the crack will be free from loading and restraints. No allowance will be allowed for the axial displacements along the ligament (x=0) over the length $0 \leq y \leq (a-h)$, but the lateral displacements are free to assume any value.

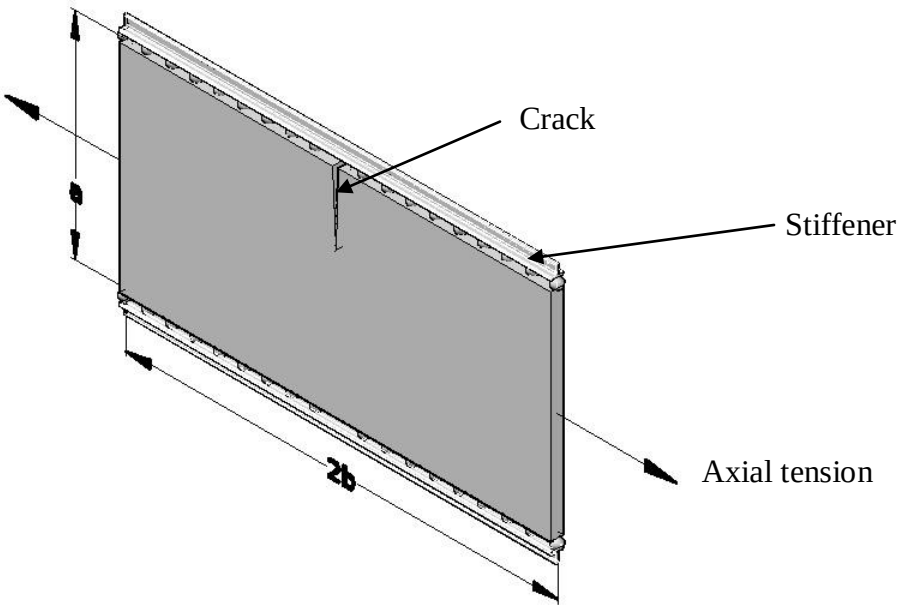

Fig 5.1: 3-D model of the full panel.

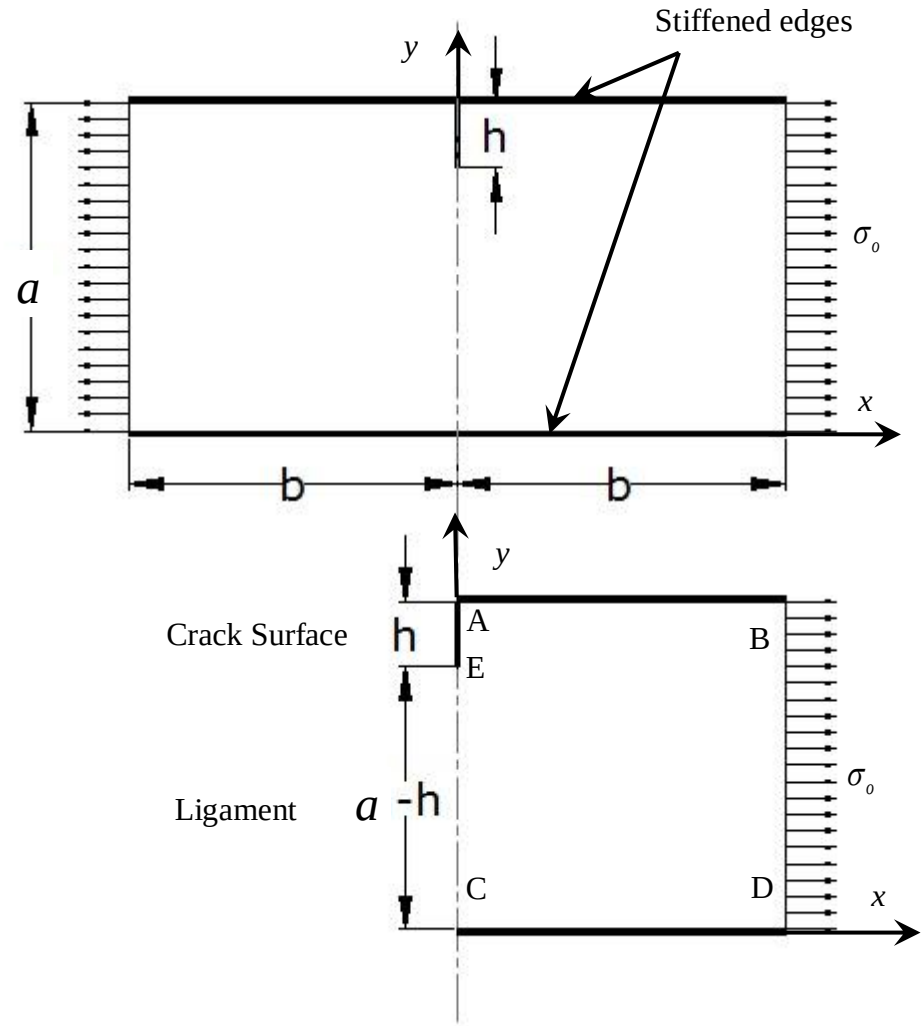

Fig 5.2: Geometry and loading of a stiffened cracked isotropic panel: (a) Full model of the panel (b) symmetric model of the panel.

5.2 Boundary Conditions

(i) Stiffened Edge, AB:

Since it is a lateral stiffener, there is no axial displacement and shear stress. Thus,

$u_y(x,a)=0$ and $\sigma_{xy}(x,a)=0$ [$0 \le x \le b$]

(ii) Stiffened Edge, CD:

There is no lateral displacement and shear stress. Thus,

$u_y(x,0)=0$ and $\sigma_{xy}(x,0)=0$ [$0 \le x \le b$]

(iii) Ligament, EC:

Due to symmetry of the full model of the panel, axial displacement and shear stresses along this section are assumed to be zero.

$u_x(0,y)=0$ [$0 \le y \le (a-h)$] and $\sigma_{xy}(0,y)=0$ [$0 \le y \le a$]

Crack surface, AE:

Since the crack surface is free from loading and restraints, there will be no boundary constraints and shear stress. A Fourier series is assumed at crack surface for the axial displacement distribution.

$\sigma_{xy}(0,y)=0$ [$(a-h) \le y \le a$]

$$u_x(0,y)=a_0+\sum_{i=1}^{3} a_i \cos(i*w*y)+\sum_{i=1}^{3} b_i \sin(i*w*y) \quad [(a-h) \le y \le a]$$

where a_i and b_i are constants and i = 1~3.

(iv) Loading End, BD:

The axial tension of the panel is realized by assigning a uniform value to the axial stress component. The boundary will also be free from shearing stress. Thus,

$\sigma_{xx}(b,y)=\sigma_{xx}^{o}$ and $\sigma_{xy}(b,y)=0$ [$0 \le y \le a$]

5.3 Solution Procedure

The analytical solution is employed in this section. For the plane problems of isotropic material, the governing equilibrium equation based on the displacement potential function $\psi(x,y)$ is obtained from Eq. (2.36) as follows:

$$\frac{\partial^4 \psi}{\partial x^4} + 2\frac{\partial^4 \psi}{\partial x^2 \partial y^2} + \frac{\partial^4 \psi}{\partial y^4} = 0 \tag{5.1}$$

The expressions of displacement and stress components in terms of function $\psi(x, y)$ are also obtained from Eq. (2.37) as follows:

$$u_x(x,y) = \frac{\partial^2 \psi}{\partial x \partial y} \tag{5.2a}$$

$$u_y(x,y) = -\frac{1}{1+\mu}\left[2\frac{\partial^2 \psi}{\partial x^2} + (1-\mu)\frac{\partial^2 \psi}{\partial y^2}\right] \tag{5.2b}$$

$$\sigma_{xx}(x,y) = \frac{E}{(1+\mu)^2}\left[\frac{\partial^3 \psi}{\partial x^2 \partial y} - \mu\frac{\partial^3 \psi}{\partial y^3}\right] \tag{5.2c}$$

$$\sigma_{yy}(x,y) = -\frac{E}{(1+\mu)^2}\left[(2+\mu)\frac{\partial^3 \psi}{\partial x^2 \partial y} + \frac{\partial^3 \psi}{\partial y^3}\right] \tag{5.2d}$$

$$\sigma_{xy}(x,y) = -\frac{E}{(1+\mu)^2}\left[\frac{\partial^3 \psi}{\partial x^3} - \mu\frac{\partial^3 \psi}{\partial x \partial y^2}\right] \tag{5.2e}$$

In the present analytical approach, the potential function $\psi(x, y)$ is first assumed in a way so that the physical conditions of the two opposing stiffened edges are automatically satisfied. At the same time the solution has to satisfy the governing differential equation of equilibrium. Following a series of long trial and error process, the solution of the governing equation (5.1), that is the potential function is thus approximated as follows:

$$\psi(x,\ y) = \sum_{m=1}^{\infty} X_m(x)\sin\alpha y + By^3 + Ax^2 y + Cxy \tag{5.3}$$

where, $X_m = f(x)$, $\alpha = (m\pi/a)$ and m = 1, 2, 3, …….. ∞. And B, C & D are arbitrary constants.

Derivatives of equation (5.3) with respect to x and y are

$$\frac{\partial \psi}{\partial x} = \sum_{m=1}^{\infty} X'_m \sin \alpha y + 2Axy + Cy$$

$$\frac{\partial^2 \psi}{\partial x^2} = \sum_{m=1}^{\infty} X''_m \sin \alpha y + 2Ay$$

$$\frac{\partial^3 \psi}{\partial x^3} = \sum_{m=1}^{\infty} X'''_m \sin \alpha y$$

$$\frac{\partial^4 \psi}{\partial x^4} = \sum_{m=1}^{\infty} X''''_m \sin \alpha y$$

$$\frac{\partial^2 \psi}{\partial x \partial y} = \sum_{m=1}^{\infty} X'_m \alpha \cos \alpha y + 2Ax + C$$

$$\frac{\partial^3 \psi}{\partial x \partial y^2} = -\sum_{m=1}^{\infty} X'_m \alpha^2 \sin \alpha y$$

$$\frac{\partial^3 \psi}{\partial x^2 \partial y} = \sum_{m=1}^{\infty} X''_m \alpha \quad \cos \alpha y + 2A$$

$$\frac{\partial^4 \psi}{\partial x^2 \partial y^2} = -\sum_{m=1}^{\infty} X''_m \alpha^2 \sin \alpha y$$

$$\frac{\partial \psi}{\partial y} = \sum_{m=1}^{\infty} X_m \alpha \cos \alpha y + 3By^2 + Ax^2 + Cx$$

$$\frac{\partial^2 \psi}{\partial y^2} = -\sum_{m=1}^{\infty} X_m \alpha^2 \sin \alpha y + 6By$$

$$\frac{\partial^3 \psi}{\partial y^3} = \sum_{m=1}^{\infty} X_m \alpha^3 \cos \alpha y + 6B$$

$$\frac{\partial^4 \psi}{\partial y^4} = \sum_{m=1}^{\infty} X_m \alpha^4 \sin \alpha y$$

Substituting the expressions of above derivatives in Eq. (5.1) following equation is obtained.

$$\sum_{m=1}^{\infty} X''''_m \sin \alpha y - 2\sum_{m=1}^{\infty} X''_m \alpha^2 \sin \alpha y + \sum_{m=1}^{\infty} X_m \alpha^4 \sin \alpha y = 0$$

or, $$\sum_{m=1}^{\infty} \left[X''''_m - 2\alpha^2 X''_m + \alpha^4 X_m \right] \sin \alpha y = 0$$

or, $$X_m'''' - 2\alpha^2 X_m'' + \alpha^4 X_m = 0 \qquad (5.4)$$

The solution of the above 4th order ordinary differential equation with constant coefficients [Eq. (5.4)] can normally be approximated as follows:

$$X_m = A_m e^{r_1 x} + B_m x e^{r_2 x} + C_m e^{r_3 x} + D_m x e^{r_4 x} \tag{5.5}$$

But the ordinary differential equation (5.4) has the complementary function of repeated roots. Thus $r_1 = r_2 = \alpha$ and $r_3 = r_4 = -\alpha$ and the general solution of Eq. (5.4) can be written as

$$X_m = (A_m + B_m x)e^{\alpha x} + (C_m + D_m x)e^{-\alpha x} \tag{5.6}$$

where A_m, B_m, C_m and D_m are arbitrary constants.

Differentiating equation (5.6) following expressions are found

$$X_m' = (A_m\alpha + B_m\alpha x + B_m)e^{\alpha x} + (-C_m\alpha - D_m\alpha x + D_m)e^{-\alpha x}$$

$$X_m'' = (A_m\alpha^2 + B_m\alpha^2 x + 2B_m\alpha)e^{\alpha x} + (C_m\alpha^2 + D_m\alpha^2 x - 2D_m\alpha)e^{-\alpha x}$$

$$X_m''' = (A_m\alpha^3 + B_m\alpha^3 x + 3B_m\alpha^3)e^{\alpha x} + (-C_m\alpha^3 - D_m\alpha^3 x + 3D_m\alpha^2)e^{-\alpha x}$$

$$X_m'''' = (A_m\alpha^4 + B_m\alpha^4 x + 4B_m\alpha^3)e^{\alpha x} + (C_m\alpha^4 + D_m\alpha^4 x - 4D_m\alpha^3)e^{-\alpha x}$$

Now substituting the derivatives of ψ and X_m in the expressions for displacement and stresses (5.2), following expressions are found.

$$u_x(x,y) = \frac{\partial^2\psi}{\partial x \partial y}$$

$$= \sum_{m=1}^{\infty} X'_m \alpha \cos\alpha y + 2Ax + C$$

$$= \sum_{m=1}^{\infty} \left[(A_m\alpha + B_m\alpha x + B_m)e^{\alpha x} + (-C_m\alpha - D_m\alpha x + D_m)e^{-\alpha x}\right]\alpha \cos\alpha y + 2Ax + C$$

$$= \sum_{m=1}^{\infty} \left[A_m\alpha e^{\alpha x} + B_m(\alpha x + 1)e^{\alpha x} - C_m\alpha e^{-\alpha x} - D_m(\alpha x - 1)e^{-\alpha x}\right]\alpha \cos\alpha y + 2Ax + C \tag{5.7a}$$

$$u_y(x,y) = -\frac{1}{(1+\mu)}\left[2\frac{\partial^2\psi}{\partial x^2} + (1-\mu)\frac{\partial^2\psi}{\partial y^2}\right]$$

$$= -\frac{1}{(1+\mu)}\left[2\left\{\sum_{m=1}^{\infty} X_m'' \sin\alpha y\right\} + 4Ay - (1-\mu)\left\{\sum_{m=1}^{\infty} X_m \alpha^2 \sin\alpha y - 6By\right\}\right]$$

$$= -\frac{1}{(1+\mu)}\left[\begin{array}{l} 2\sum_{m=1}^{\infty}\left\{\begin{array}{l}(A_m\alpha^2 + B_m\alpha^2 x + 2B_m\alpha)e^{\alpha x} + \\ (C_m\alpha^2 + D_m\alpha^2 x - 2D_m\alpha)e^{-\alpha x}\end{array}\right\}\cos\alpha y - (1-\mu) \\ \sum_{m=1}^{\infty}\left\{(A_m + B_m x)e^{\alpha x} + (C_m + D_m x)e^{-\alpha x}\right\}\alpha^2\cos\alpha y \end{array}\right] - \frac{6B(1-\mu)}{(1+\mu)}$$

$$- \frac{4Ay}{(1+\mu)}$$

$$= \frac{-1}{(1+\mu)}\left[\sum_{m=1}^{\infty}\left\{\begin{array}{l} A_m(1+\mu)\alpha^2 e^{\alpha x} + \\ B_m(\alpha x + \mu\alpha x + 4)\alpha e^{\alpha x} \\ + C_m(1+\mu)\alpha^2 e^{-\alpha x} + \\ D_m(\alpha x + \mu\alpha x - 4)\alpha e^{-\alpha x}\end{array}\right\}\sin\alpha y\right] - \frac{6B(1-\mu)}{(1+\mu)} - \frac{4Ay}{(1+\mu)} \quad (5.7b)$$

$$\sigma_{xx}(x,y) = \frac{E}{(1+\mu)^2}\left[\frac{\partial^3\psi}{\partial x^2\partial y} - \mu\frac{\partial^3\psi}{\partial y^3}\right]$$

$$= \frac{E}{(1+\mu)^2}\left[\left\{\sum_{m=1}^{\infty} X_m''\alpha \cos\alpha y\right\} + 2A + \mu\left\{\sum_{m=1}^{\infty} X_m\alpha^3\cos\alpha y\right\} - 6B\right]$$

$$= \frac{E}{(1+\mu)^2}\left[\begin{array}{l}\sum_{m=1}^{\infty}\left\{(A_m\alpha^2 + B_m\alpha^2 x + 2B_m\alpha)e^{\alpha x} + (C_m\alpha^2 + D_m\alpha^2 x - 2D_m\alpha)e^{-\alpha x}\right\}\alpha \\ \cos\alpha y + \mu\sum_{m=1}^{\infty}\left\{(A_m + B_m x)e^{\alpha x} + (C_m + D_m x)e^{-\alpha x}\right\}\alpha^3\cos\alpha y\end{array}\right]$$

$$+ \frac{2AE}{(1+\mu)^2} - \frac{6BE}{(1+\mu)^2}$$

$$= \frac{E}{(1+\mu)^2}\left[\sum_{m=1}^{\infty}\left\{\begin{array}{l} A_m\alpha(1+\mu)e^{\alpha x} + B_m(\alpha x + \mu\alpha x + 2)e^{\alpha x} \\ + C_m\alpha(1+\mu)e^{-\alpha x} + D_m(\alpha x + \mu\alpha x - 2)e^{-\alpha x}\end{array}\right\}\alpha^2\cos\alpha y\right] \quad (5.7c)$$

$$+ \frac{2AE}{(1+\mu)^2} - \frac{6BE}{(1+\mu)^2}$$

$$\sigma_{yy}(x,y) = \frac{-E}{(1+\mu)^2}\left[(2+\mu)\frac{\partial^3\psi}{\partial x^2\partial y} + \frac{\partial^3\psi}{\partial y^3}\right]$$

$$= \frac{-E}{(1+\mu)^2}\left[(2+\mu)\left\{\sum_{m=1}^{\infty} X_m^{''}\alpha \quad \cos\alpha y + 2A\right\} - \left\{\sum_{m=1}^{\infty} X_m \alpha^3 \cos\alpha y - 6B\right\}\right]$$

$$= \frac{E}{(1+\mu)^2}\left[\begin{array}{l}(2+\mu)\sum_{m=1}^{\infty}\left\{\left(A_m\alpha^2 + B_m\alpha^2 x + 2B_m\alpha\right)e^{\alpha x} + \left(C_m\alpha^2 + D_m\alpha^2 x - 2D_m\alpha\right)e^{-\alpha x}\right\} \\ \alpha \quad \cos\alpha y + 2(2+\mu)A + \sum_{m=1}^{\infty}\left\{\begin{array}{l}(A_m + B_m x)e^{\alpha x} + \\ (C_m + D_m x)e^{-\alpha x}\end{array}\right\}\alpha^3 \cos\alpha y + 6B\end{array}\right]$$

$$= \frac{E}{(1+\mu)^2}\left[\sum_{m=1}^{\infty}\left\{\begin{array}{l}A_m\alpha(-1-\mu)e^{\alpha x} + B_m\left(-\alpha x - \mu\alpha x - 2\mu - 4\right)e^{\alpha x} + \\ C_m\alpha(-1-\mu)e^{-\alpha x} + D_m\left(-\alpha y - \mu\alpha x + 2\mu + 4\right)e^{-\alpha x}\end{array}\right\}\alpha^2 \cos\alpha y\right] \qquad (5.7d)$$

$$-\frac{2A(2+\mu)}{(1+\mu)^2} - \frac{6BE}{(1+\mu)^2}$$

$$\sigma_{xy}(x,y) = \frac{-E}{(1+\mu)^2}\left[\frac{\partial^3\psi}{\partial x^3} - \mu\frac{\partial^3\psi}{\partial x\partial y^2}\right]$$

$$= \frac{-E}{(1+\mu)^2}\left[\sum_{m=1}^{\infty} X_m^{'''}\sin\alpha y + \mu\left\{\sum_{m=1}^{\infty} X_m^{'}\alpha^2 \sin\alpha y\right\}\right]$$

$$= \frac{-E}{(1+\mu)^2}[\sum_{m=1}^{\infty}\left\{\left(A_m\alpha^3 + B_m\alpha^3 x + 3B_m\alpha^2\right)e^{\alpha x} + \left(-C_m\alpha^3 - D_m\alpha^3 x + 3D_m\alpha^2\right)e^{-\alpha x}\right\}\sin\alpha y$$

$$+ \mu\sum_{m=1}^{\infty}\left\{\left(A_m\alpha \quad + B_m\alpha \;\; x + B_m\right)e^{\alpha x} + \left(-C_m\alpha \quad - D_m\alpha \;\; x + D_m\right)e^{-\alpha x}\right\}\alpha^2 \sin\alpha y]$$

$$= \frac{-E}{(1+\mu)^2}\left[\sum_{m=1}^{\infty}\left\{\begin{array}{l}A_m(1+\mu)\alpha e^{\alpha x} + B_m\left(\alpha x + \mu\alpha x + \mu + 3\right)e^{\alpha x} \\ -C_m(1+\mu)\alpha e^{-\alpha x} - D_m\left(\alpha x + \mu\alpha x - \mu - 3\right)e^{-\alpha x}\end{array}\right\}\alpha^2 \sin\alpha y\right] \qquad (5.7e)$$

Now, the axial loading on the right edge of the panel can be taken as Fourier series in the following manner:

$$\sigma_{xx}(b,y) = \sigma_{xx}^{o} = \sum_{m=1}^{\infty} E_m \cos\alpha y + E_o \qquad (5.8)$$

To satisfy the boundary condition and loading distribution, Fourier cosine series have been considered for the analysis.

$$E_m = \frac{2}{a}\int_0^a \sigma_{xx}^{o}\cos(\alpha y)dy$$

$$= \frac{2\sigma_{xx}^{o}}{a^2}\int_0^a \cos(\alpha y)dy \quad = 0$$

And $E_o = \frac{1}{a}\int_0^a \sigma_{xx}^{o} dy = \frac{\sigma_{xx}^{o}}{a}\int_0^a dy = \sigma_{xx}^{o}$

Due to symmetry, the axial displacement at the left edge from 0 to (a-h) is zero. But at the cracked edge, the distribution of the axial displacement can be expressed as the Fourier series in the following manner:

$$u_x(0,y) = a_0 + \sum_{i=1}^{3} a_i \cos(i*w*y) + \sum_{i=1}^{3} b_i \sin(i*w*y) = I_o + \sum_{m=1}^{\infty} I_m \cos(\alpha y) \qquad (5.9)$$

The curve fitted equation as Fourier series up to 7th term have been considered. This is because of up to 7th term we always achieve R^2 value above 0.99. If we increase the term it will make the mathematical calculation more complicated.

Here

$$I_m = \frac{2}{a}\int_{a-h}^{a} (a_0 + \sum_{i=1}^{3} a_i \cos(i*w*y) + \sum_{i=1}^{3} b_i \sin(i*w*y))\cos(\alpha y)dy$$

After performing integration of the above equation, the result is given below:

$$I_m = \left(\frac{2a_o}{m\pi}\left(-\sin\left(\frac{(a-h)m\pi}{a}\right)\right)\right) + \sum_{i=1}^{3} a_i \begin{pmatrix} -\left(\frac{1}{m\pi+iwa}\sin\left(\left(\frac{a-h}{a}\right)(m\pi+iwa)\right)\right) \\ -\left(\frac{1}{m\pi-iwa}\sin\left(\left(\frac{a-h}{a}\right)(m\pi-iwa)\right)\right) \\ +\left(\frac{1}{m\pi+iwa}\sin(m\pi+iwa)\right) \\ +\left(\frac{1}{m\pi-iwa}\sin(m\pi-iwa)\right) \end{pmatrix}$$

$$+\sum_{i=1}^{3} b_i \begin{pmatrix} -\left(\frac{1}{m\pi+iwa}\cos(m\pi+iwa)\right)+ \\ \left(\frac{1}{m\pi-iwa}\cos(m\pi-iwa)\right)+ \\ \left(\frac{1}{m\pi+iwa}\cos\left(\left(\frac{a-h}{a}\right)(m\pi+iwa)\right)\right)- \\ \left(\frac{1}{m\pi-iwa}\cos\left(\left(\frac{a-h}{a}\right)(m\pi-iwa)\right)\right) \end{pmatrix}$$

$$I_0 = \frac{1}{a}\int_{a-h}^{a}(a_0 + \sum_{i=1}^{3} a_i \cos(i*w*y) + \sum_{i=1}^{3} b_i \sin(i*w*y))dy$$

After performing integration, the result is given below:

$$I_o = \left(\frac{ha_o}{a}\right) + \sum_{i=1}^{3} a_i \left(\left(\frac{1}{iw}\sin(iwa)\right) - \left(\frac{1}{iw}\sin\left(\left(\frac{a-h}{a}\right)iwa\right)\right)\right) - \sum_{i=1}^{3} b_i \left(\begin{array}{l}\left(\left(\frac{1}{iw}\cos(iwa)\right) - \\ \left(\frac{1}{iw}\cos\left(\left(\frac{a-h}{a}\right)iwa\right)\right)\end{array}\right)$$

Using boundary condition $\sigma_{xy}(0, y) = 0$ at the edge of $x = 0$, it is found that

$$\frac{-E}{(1+\mu)^2}\left[\sum_{m=1}^{\infty}\{A_m(1+\mu)\alpha + B_m(\mu+3) - C_m(1+\mu)\alpha - D_m(-\mu-3)\}\alpha^2 \sin\alpha y\right] = 0$$

$$or, [A_m\alpha(1+\mu) + B_m(\mu+3) - C_m\alpha(1+\mu) + D_m(\mu+3)] = 0 \qquad (5.10)$$

Using boundary condition $\sigma_{xy}(b, y) = 0$ at the edge of $x = b$, it is found that

$$\frac{-E}{(1+\mu)^2}\left[\sum_{m=1}^{\infty}\left\{\begin{array}{l}A_m\alpha(1+\mu)e^{\alpha b} + B_m(\alpha b + \mu\alpha b + \mu + 3)e^{\alpha b} \\ -C_m(1+\mu)\alpha e^{-\alpha b} - D_m(\alpha b + \mu\alpha b - \mu - 3)e^{-\alpha b}\end{array}\right\}\alpha^2 \sin\alpha y\right] = 0$$

$$or, \left[\begin{array}{l}A_m\alpha(1+\mu)e^{\alpha b} + B_m(\alpha b + \mu\alpha b + \mu + 3)e^{\alpha b} \\ -C_m\alpha(1+\mu)e^{-\alpha b} - D_m(\alpha b + \mu\alpha b - \mu - 3)e^{-\alpha b}\end{array}\right] = 0 \qquad (5.11)$$

Using boundary condition $u_x(0, y) = a_0 + \sum_{i=1}^{3} a_i \cos(i*w*y) + \sum_{i=1}^{3} b_i \sin(i*w*y)$ at the edge of $x = 0$, it is found that

$$\sum_{m=1}^{\infty}[A_m\alpha + B_m - C_m\alpha + D_m]\alpha\cos\alpha y + C = I_o + \sum_{m=1}^{\infty} I_m \cos(\alpha y)$$

$$or, [A_m\alpha + B_m - C_m\alpha + D_m]\alpha = I_m \qquad (5.12)$$

Using boundary condition $\sigma_{xx}(b, y) = \sigma_{xx}^{o}$ at the edge of $x = b$, it is found

$$\frac{E}{(1+\mu)^2}\left[\sum_{m=1}^{\infty}\left\{\begin{array}{l}A_m\alpha(1+\mu)e^{\alpha b} + B_m(\alpha b + \mu\alpha b + 2)e^{\alpha b} \\ +C_m\alpha(1+\mu)e^{-\alpha b} + D_m(\alpha b + \mu\alpha b - 2)e^{-\alpha b}\end{array}\right\}\alpha^2 \cos\alpha y\right]$$

$$+\frac{2AE}{(1+\mu)^2} - \frac{6BE}{(1+\mu)^2} = E_0 + \sum_{m=1}^{\infty} E_m \cos\alpha y$$

$$or, \frac{E\alpha^2}{(1+\mu)^2}\begin{bmatrix} A_m\alpha(1+\mu)e^{\alpha b} + B_m(\alpha b + \mu\alpha b + 2)e^{\alpha b} \\ + C_m\alpha(1+\mu)e^{-\alpha b} + D_m(\alpha b + \mu\alpha b - 2)e^{-\alpha b} \end{bmatrix} = E_m \tag{5.13}$$

The simultaneous equations (5.10), (5.11), (5.12) and (5.13) can be arranged in a simplified matrix form for the solution of unknown terms like A_m , B_m , C_m and D_m as follows:

$$\begin{bmatrix} DD_1 & DD_2 & DD_3 & DD_2 \\ FF_1 & FF_2 & FF_3 & FF_4 \\ HH_1 & HH_2 & HH_3 & HH_2 \\ KK_1 & KK_2 & KK_3 & KK_4 \end{bmatrix}\begin{bmatrix} A_m \\ B_m \\ C_m \\ D_m \end{bmatrix} = \begin{bmatrix} 0 \\ 0 \\ I_m \\ E_m \end{bmatrix} \tag{5.14}$$

Where

$$DD_1 = \alpha(1+\mu)$$

$$DD_2 = (\mu + 3)$$

$$DD_3 = -\alpha(1+\mu)$$

$$FF_1 = \alpha(1+\mu)e^{\alpha b}$$

$$FF_2 = (\alpha b + \mu\alpha b + \mu + 3)e^{\alpha b}$$

$$FF_3 = -\alpha(1+\mu)e^{-\alpha b}$$

$$FF_4 = -(\alpha b + \mu\alpha b - \mu - 3)e^{-\alpha b}$$

$$HH_1 = \alpha^2$$

$$HH_2 = \alpha$$

$$HH_3 = -\alpha^2$$

$$KK_1 = Z_{11}\alpha(1+\mu)e^{\alpha b}$$

$$KK_2 = Z_{11}(\alpha b + \mu\alpha b + 2)e^{\alpha b}$$

$$KK_3 = Z_{11}\alpha(1+\mu)e^{-\alpha b}$$

$$KK_4 = Z_{11}(\alpha b + \mu\alpha b - 2)e^{-\alpha b}$$

$$Z_{11} = \frac{E\alpha^2}{(1+\mu)^2}$$

And

$$A = \frac{\sigma_{xx}^{o}(1+\mu)(1-\mu^2)}{E(3-\mu)}$$

$$B = \frac{-2\sigma_{xx}^{o}(1+\mu)^2}{E(9-3\mu)}$$

$$C = I_o$$

Solution of the above matrix Eq. (5.14) yields the unknown constants A_m , B_m , C_m and D_m . Once the value of the unknowns are determined, they are directly substituted in Eqs.[5.7(a)-5.7(e)] to obtain the explicit expressions for the different parameters of interest, namely, the two displacement and the three stress components at various points.

5.4 Analysis of Elastic Field

The solutions of displacement and stress components using displacement potential approach are obtained for steel beam (Poisson ratio μ = 0.3 and Modulus of Elasticity E = 209 GPa), aspect ratio *b/a* = 1.0, crack length ratio *h/a* = 0.2 and the loading parameter, σ_o= 40 N/mm. The results is presented in a sequence of axial displacement (u_x), lateral displacement (u_y), bending stress (σ_{xx}), normal stress (σ_{yy}) and shearing stress (σ_{xy}).). In order to make the results non-dimensional, the displacements are expressed as the ratio of actual displacement to the actual dimension of the bar, and the stresses are expressed as the ratio of the actual stress to the applied loading parameter. Finally the effects of panel aspect ratio and crack length ratio on the elastic fields are analyzed.

i. Displacement Field

The distribution of normalized displacement components u_x/b and u_y/a with respect to y at different sections of the panel is shown in Figs 5.3 and 5.4. The lateral

displacement u_y is zero at the two stiffened edges which satisfies the physical characteristics of the problem. At the loaded section *x/b* = 1.0, the axial displacement is maximum and towards the supporting edge the displacement decreases. According to Saint-Venant's Principle, towards the supporting edges the effect of load decreases. The same thing happens also for crack i.e. the effect of crack decreases towards the load. But at section *x/b* = 1.0, the effect of load is higher. The effect of crack on displacement is clearly visible in Fig. 5.3. From fig. 5.4 it can be seen that for section x/b = 0.5 and 1.0 the lateral displacement is negative that means since the panel is subjected to axial loading the length of the panel increases as a result of decreasing area which refers it is subjected to compressive loading. But for section *x/b* = 0.1 and 0.2 most of the area is under tension though near the crack it is compressive. But at section *x/L* = 0.0, only tension happens.

Fig. 5.5 shows the deformed shape of the panel which is good agreement with the loading. Since the panel is subject ted to uniform axial loading, the length of the panel will increase. Here another observation is that the opening of the crack increases.

ii. Stress Field

Fig. 5.6 illustrates the distribution of the normalized stress component σ_{xx}/σ_o at different sections of the column. The distribution of normal stress σ_{xx} at the loaded region $x/b = 1.0$is constant which is in good agreement with loading. The effect of crack is dominant near the crack surface. Due to presence of discontinuity i.e. crack a sudden fluctuation of stress happens at the crack tip(*x*=0 and *y*=0.8a) of the panel. The effect is noticeable up to the region of $x/b \leq 0.5$. As appears from the distribution, the normal stress σ_{xx} is positive throughout the panel which means that the panel is under tension. But at crack region the stress is nearly zero because it is free. But at crack tip the stress becomes almost 5.2 times of the applied load which is much higher than longitudinal stress where it was only 0.6 times of the applied load.

It concluded that longitudinal stiffened panel is safer than lateral stiffened panel for design purpose.

Fig. 5.7 describes the distribution of the normalized stress distribution σ_{yy}/σ_o at different sections of the panel. The lateral stress for the current problem is not zero at the two stiffened edges but which it happened in the case of longitudinal stiffened edges. The value of the normalized lateral stress is found 0.3 times of the maximum intensity of load at the loading edge but it increases when moves toward the crack except at the crack surface. There is a sudden fluctuation of lateral stress at the crack tip due to stress concentration. But at crack surface it is negative. The maximum value of the lateral stress at crack tip is almost 4.4 times of the applied load which also reflects the differences between two different types of stiffeners.

The distribution of normalized shearing stress σ_{xy}/σ_o at various section of the panel is presented in Fig. 5.8. It is observed that there is very huge effect of the crack near the support end which is found less in case of longitudinal stiffened panel. The shearing stress at the right, left boundary and two lateral stiffened is found to be zero which verifies the physical boundary conditions of the problem. In the region near the crack $x/b = 0.0$ the shear stress is maximum gradually decreases as moving towards the loading edge at $x/b = 1.0$

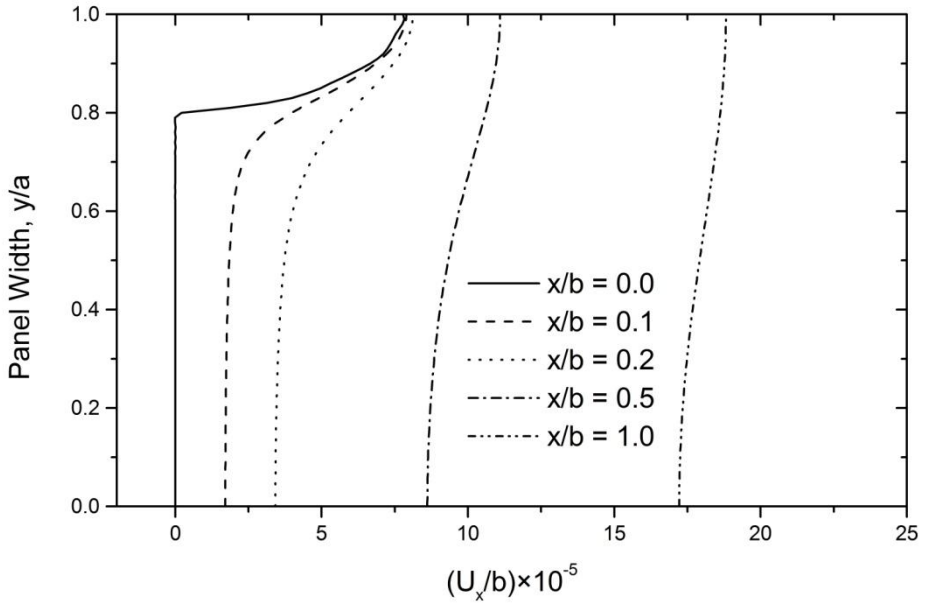

Fig 5.3: Distribution of normalized axial displacement at different sections of the steel panel. (*b/a* =1, *h/a* =0.2)

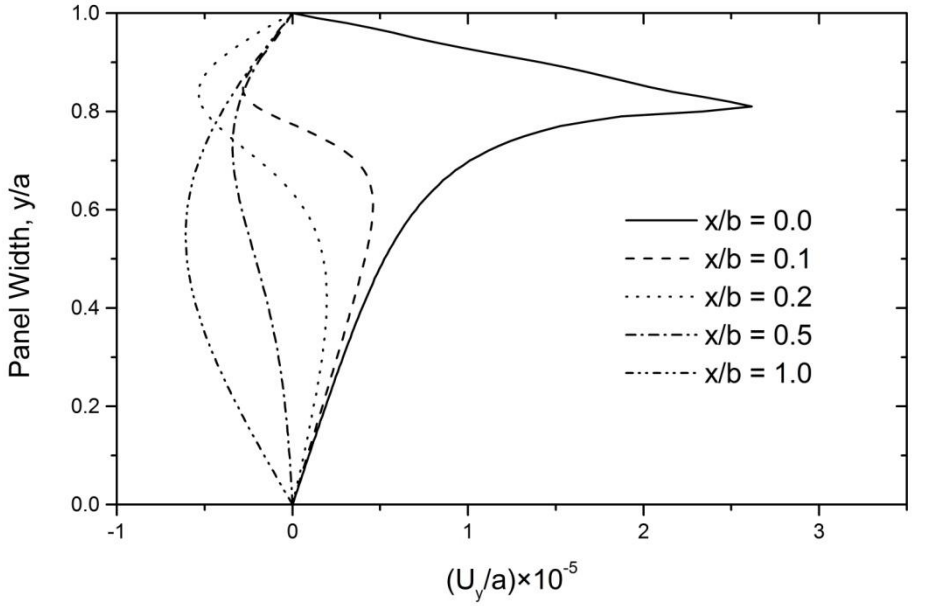

Fig 5.4: Distribution of normalized lateral displacement at different sections of the steel panel. (*b/a* =1, *h/a* =0.2)

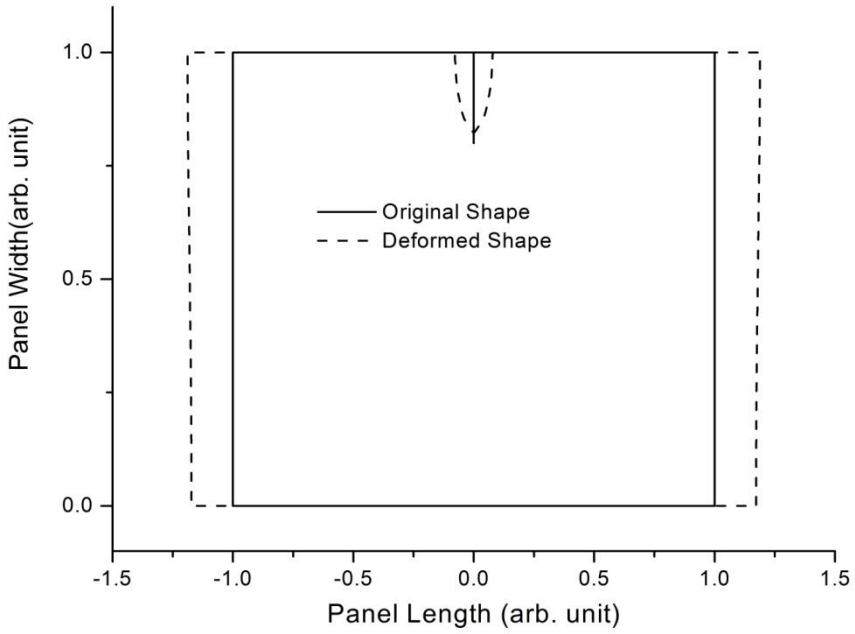

Fig 5.5: Deformed shape of the cracked steel panel, *b/a* = 1 (magnification factor ×1000).

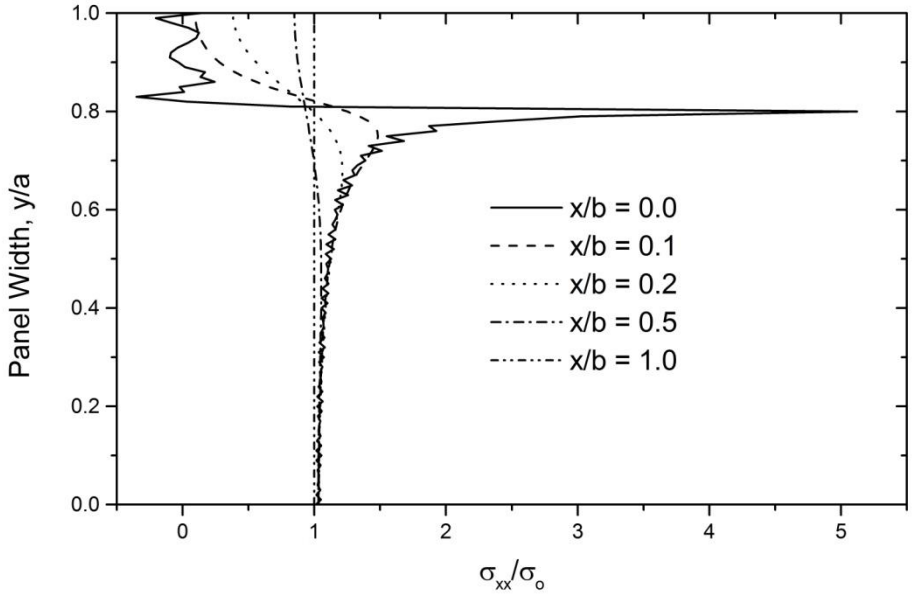

Fig 5.6: Distribution of normalized axial stress at different sections of the steel panel. (*b/a* =1, *h/a* =0.2)

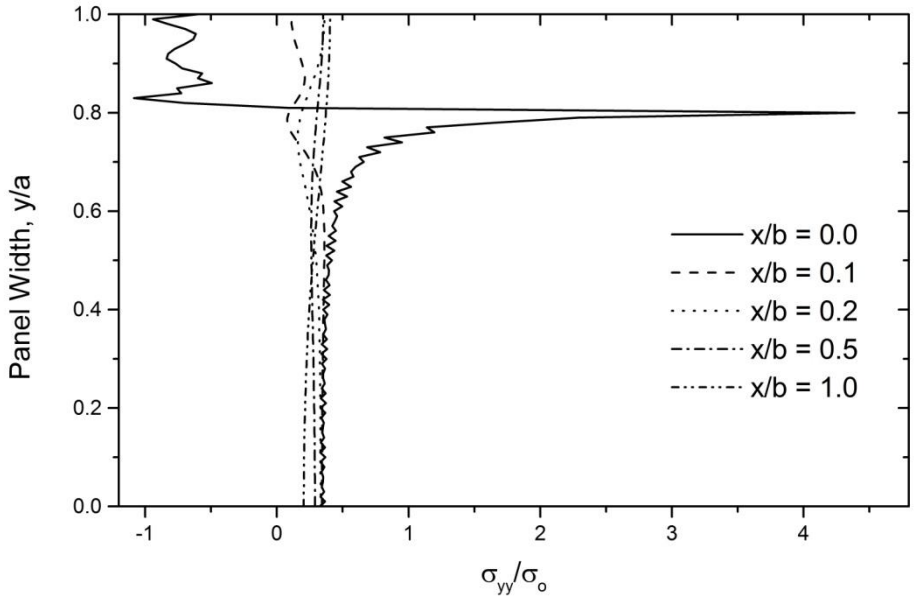

Fig 5.7: Distribution of normalized lateral stress at different sections of the panel. (*b/a* =1, *h/a* =0.2)

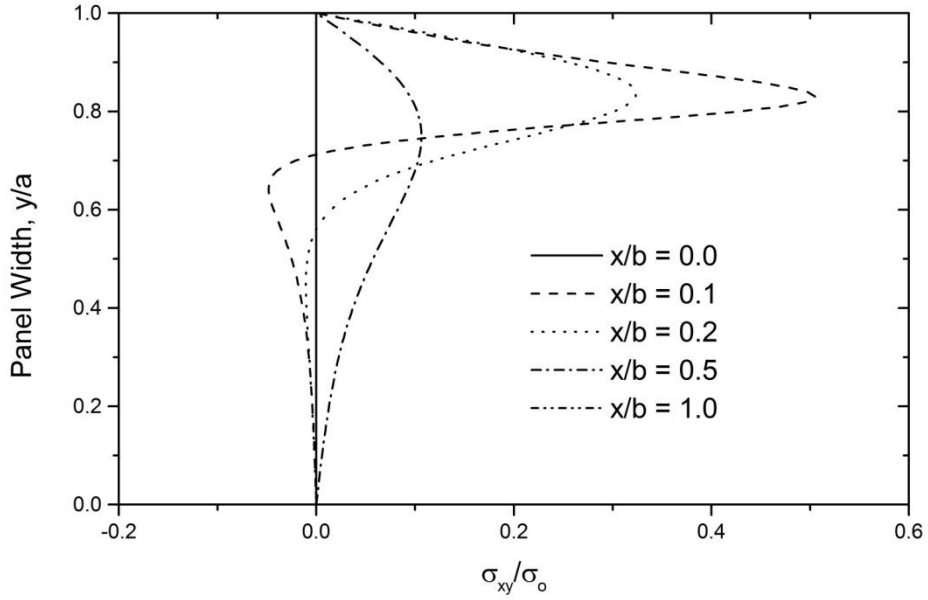

Fig 5.8: Distribution of normalized shear stress at different sections of the panel. (*b/a* =1, *h/a* =0.2)

Distribution of normalized maximum principle stress obtained using the results of displacement potential approach is presented in Fig. 5.9. The relation used in this regard is $\sigma_1 = \frac{\sigma_x+\sigma_y}{2} + \sqrt{\left(\frac{\sigma_x-\sigma_y}{2}\right)^2 + \sigma_{xy}^2}$, where σ_1 is the maximum principle stress. No reference of the principle stress distribution for a guided deep beam could be found. As such the verification of present results remains to be investigated with the availability of any other results. However, the contour pattern of maximum principle stress of the current solution seems to be satisfactory in a general sense of visual basis.

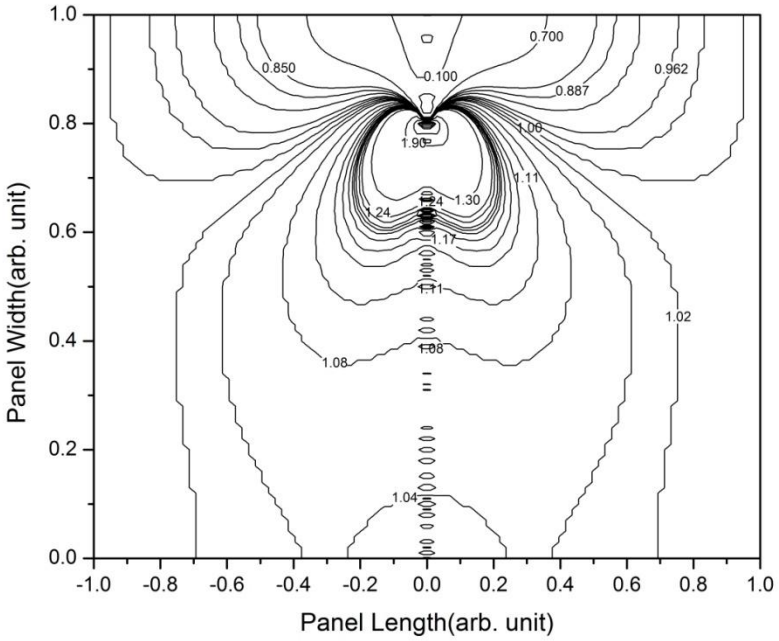

Fig 5.9: Normalized maximum principle stress contour of the cracked stiffened steel panel, (*b/a* = 1, *h/a* = 0.2).

iii. Effect of Crack Length on the Stress and Displacement Fields

The effect of crack length ratio on a structure is now becoming a major concern for failure analysis because a structure starts to fail at what crack length, it must be considered where a structure could not be thought without a crack. In this section the effect of crack length ratio (*h/a* = 0.0 ~0.4) on the panel is discussed, though only two sections near the crack is investigated.

The distribution of the normalized axial stress with the variation of crack length at two different sections of the panel (*x/b* = 0.0 & 0.1) is presented in Figures 5.10(a) and 5.10(b). These two figures reflected the same phenomena that we have found in chapter 3 i.e. with the increase of the crack length, the fluctuation of the stress at the crack tip increases. But fluctuation value of the stress is much higher. For *h/a* =0.4 it is almost 7 times of the applied load. At section x/b =0.1 it can be seen that the more the crack length the higher is the effect on the stress distribution that is constant value one in the case *of h/a* = 0.0. The highest value of the axial stress increases with the increase of the crack length.

The distribution of the normalized lateral stress for different crack length is shown in Fig. 5.11(a) and 5.11(b). The normalized lateral is constant in the case of *h/a* = 0.0 but at crack surface it represents a value that is negative of the applied load. For *h/a* = 0.4 at crack tip the maximum normalized value of the stress is almost 6.4 times of the applied load. At section *x/b* = 0.1 the distribution pattern is almost similar in case of crack length ratio *h/a* = 0.2 ~0.4 and the normalized lateral stress is negative at the upper stiffened edge. The smallest value of the lateral stress is found for higher crack length.

Fig. 5.12(a) and 5.12(b) depicts the distribution of normalized shear stress at sections (*x/b* = 0.1 & 0.5). It can be seen that the value of shear stress is zero for two different sections in case of zero crack length ratio i.e. there is no crack present in the structure. Whenever crack is present crack in structure fluctuation happens. The value of that fluctuation increases with increasing the value of the crack length ratio. Though the distribution of normalized shear stress is different at two different sections but same incidents can be seen from the two figures that we have discussed already.

Figs. 5.13(a) and 5.13(b) shows the distribution of the normalized axial displacement for different crack length at two different sections. The maximum value of the axial displacement happened for higher crack length that can be easily predicted by only viewing the results of the stress that have already discussed.

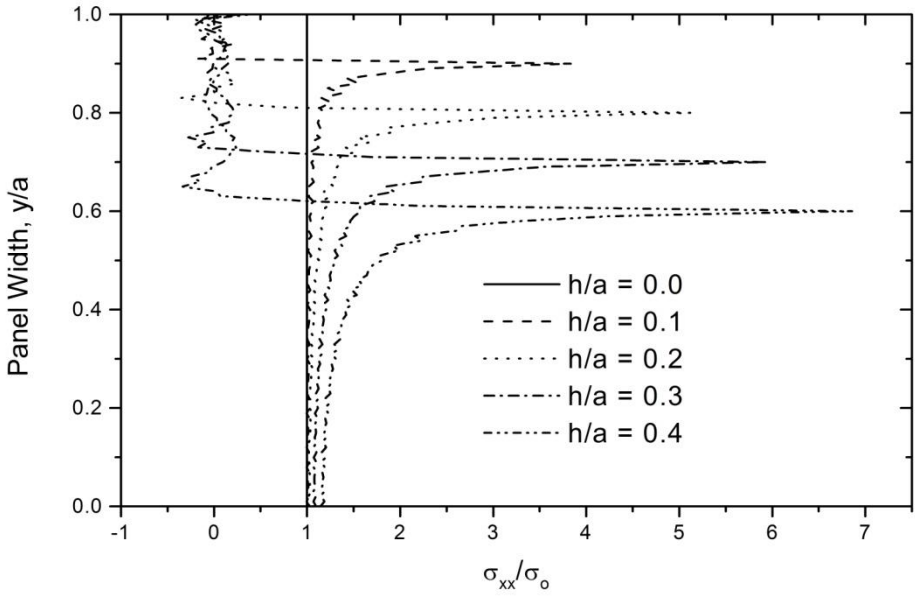

(a)

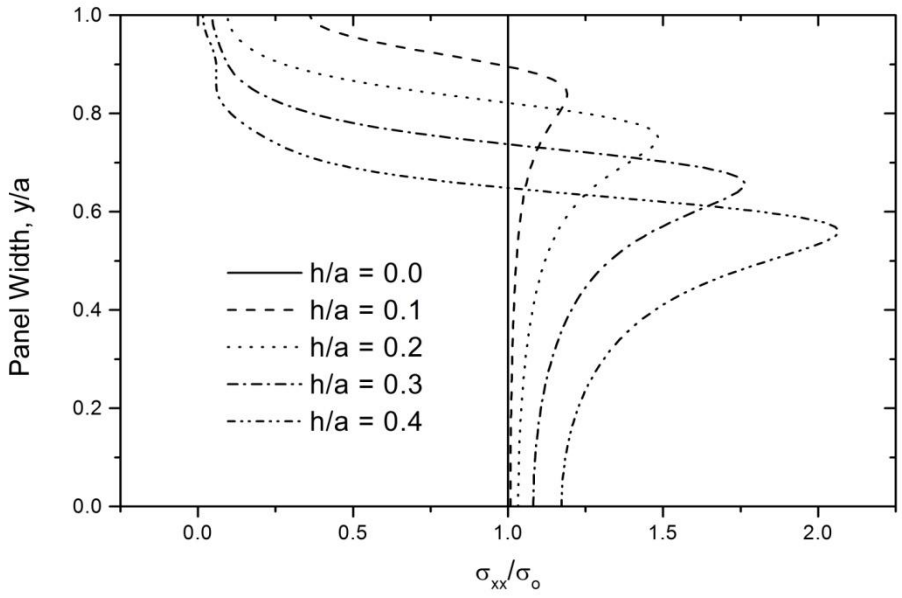

(b)

Fig 5.10: Effect of crack length on the axial stress component at (a) *x/b* = 0.0 and (b) *x/b* = 0.1, (*b/a* = 1.0).

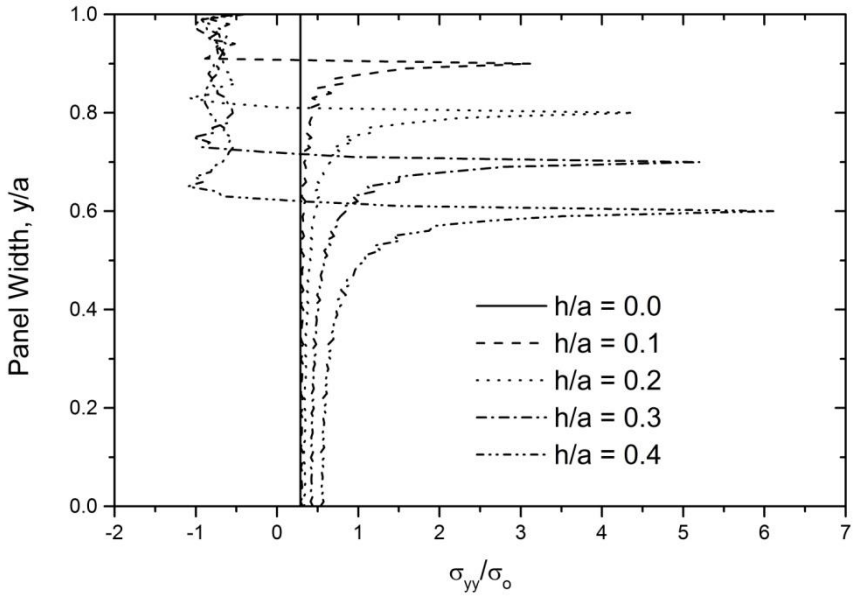

(a)

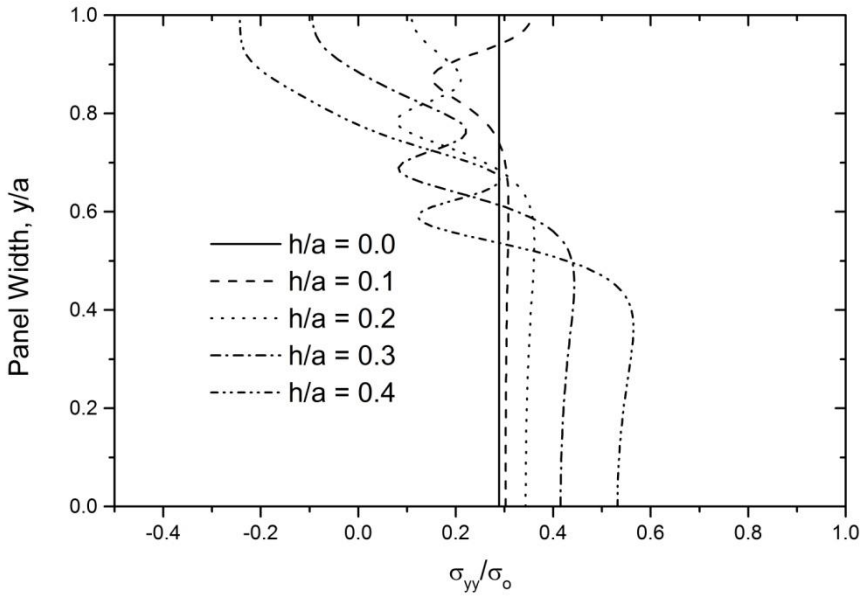

(b)

Fig 5.11: Effect of crack length on the lateral stress component at (a) *x/b* = 0.0 and (b) *x/b* = 0.1, (*b/a* = 1.0).

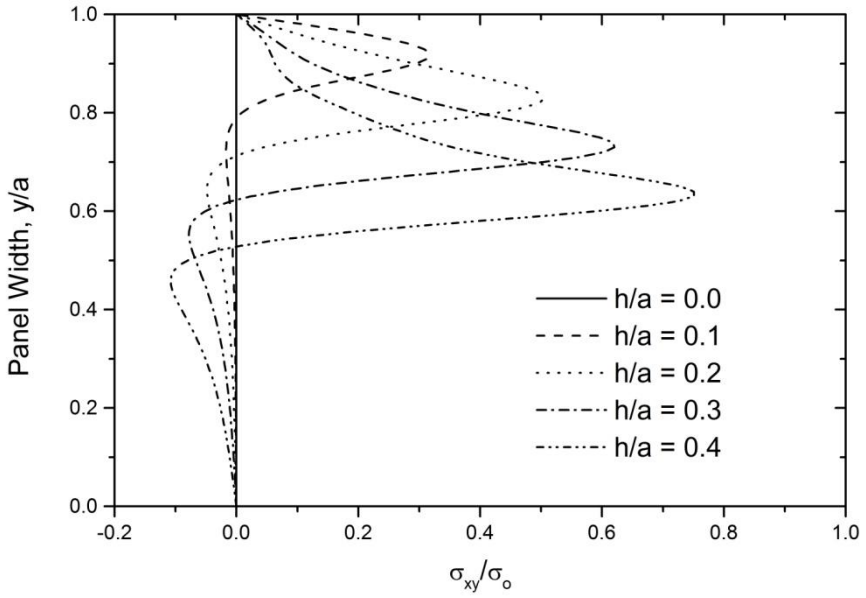

(a)

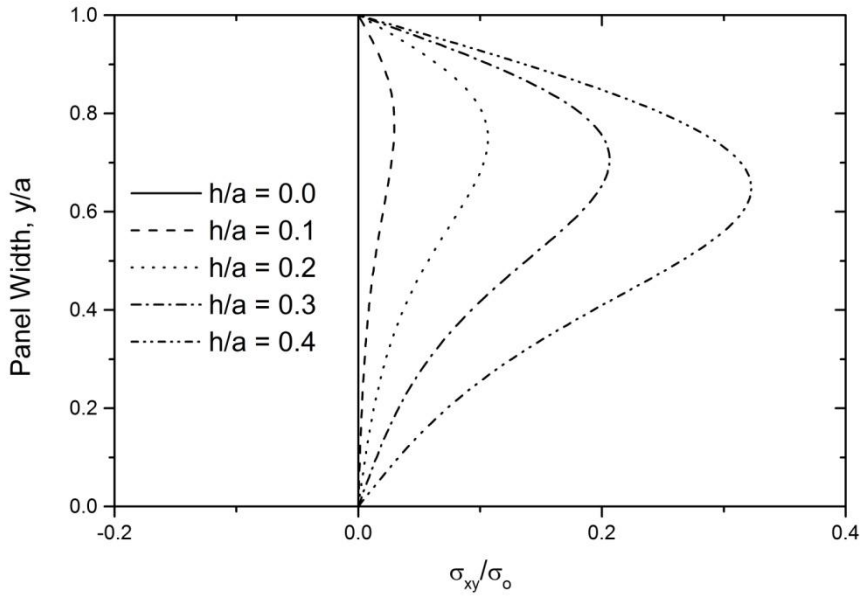

(b)

Fig 5.12: Effect of crack length on the shear stress component at (a) *x/b* = 0.1 and (b) *x/b* = 0.5, (*b/a* = 1.0).

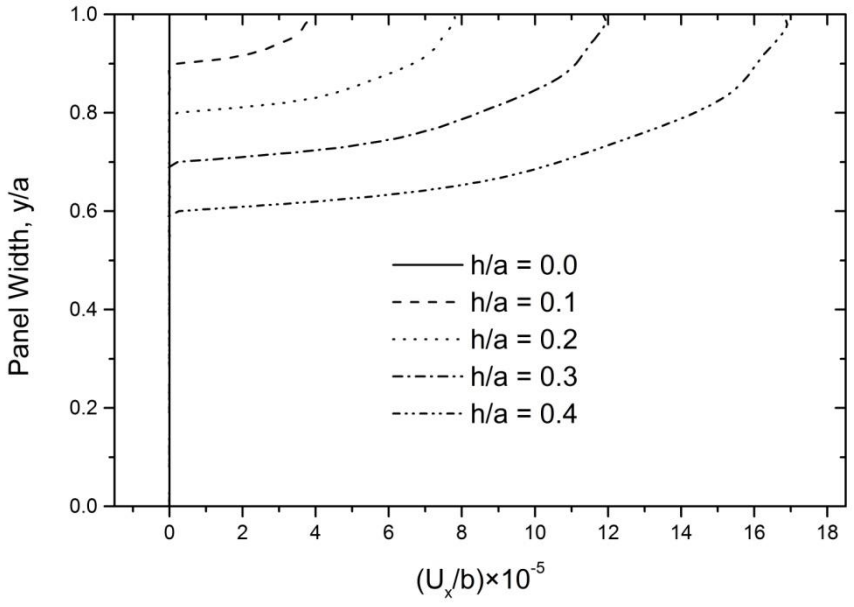

(a)

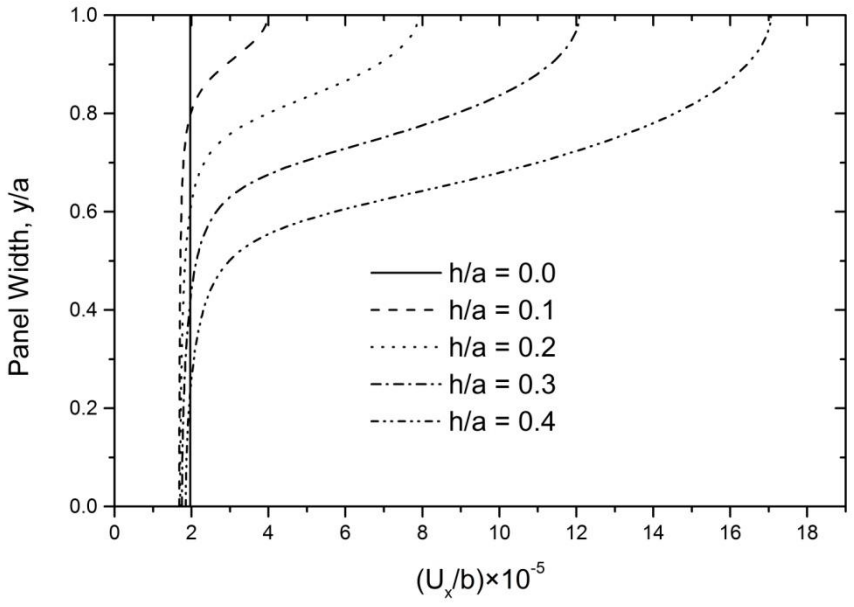

(b)

Fig 5.13: Effect of crack length on the axial displacement component at (a) *x/b* = 0.0 and (b) *x/b* = 0.1, (*b/a* = 1.0).

iv. Effect of Panel Aspect Ratio on the Stress and Displacement Fields

The displacement and stress components of a structure depend on the aspect ratio *b/a* as a large extent which are shown in Figs 5.14 to 5.17. With increasing the aspect ratio, the distance between the loading edge and crack surface increases. The loading has higher effect on crack for lower aspect ratio than higher aspect ratio. All the parameters decrease with increasing the aspect ratio *b/a*.

Figs. 5.14 through 5.16 portrait the stress components σ_{xx}, σ_{yy} and σ_{xy} at sections *x/b* = 0.0, 0.5 and 0.1 for normalized shear stress as a function of the aspect ratio *b/a* of the column. The pattern of normalized axial stress distribution at section *x/b* = 0.0 is almost similar for different aspect ratio but peak value of the fluctuation is not same as shown in Fig. 5.14(a).But for section *x/b* = 0.1 the trend of the distribution for different aspect ratio is noticeable. Fig. 5.15 reflects the same characteristics in case of normalized lateral stress.

For no crack case, shear stress will be zero at section *x/b* = 0.0 but normalized shear stress distribution diverts from its regular pattern if a crack is present in that section. From all the previous three chapters stress components would be severe if the upper and bottom edges are lateral stiffened. Fig. 5.16 represents the normalized shear stress. It has observed that the effect of crack is more severe in case of lower aspect ratio.

The normalized axial displacement is shown in Fig. 5.17. The axial displacement increases at crack surface with decreasing the aspect ratio that can be easily predicted by observing the graph of normalized axial stress.

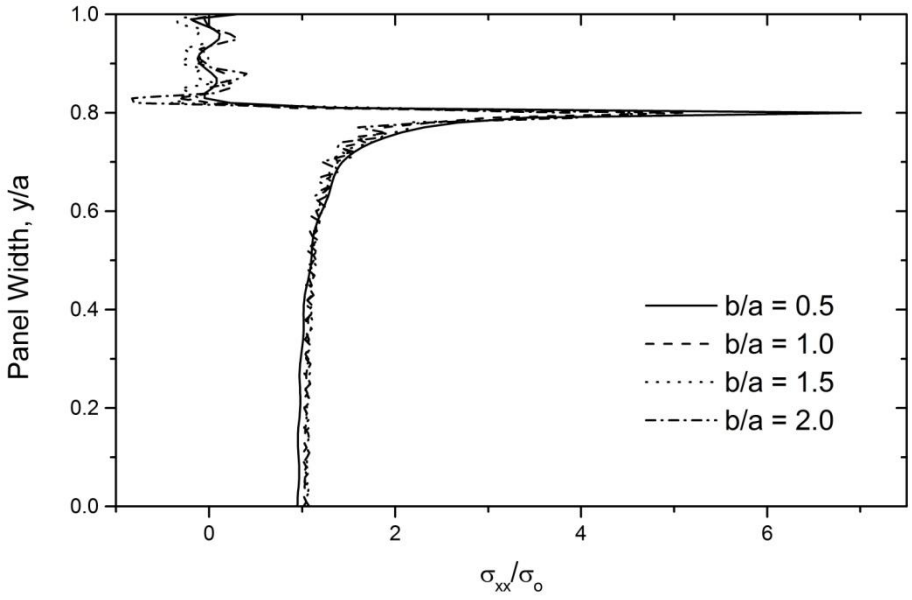

(a)

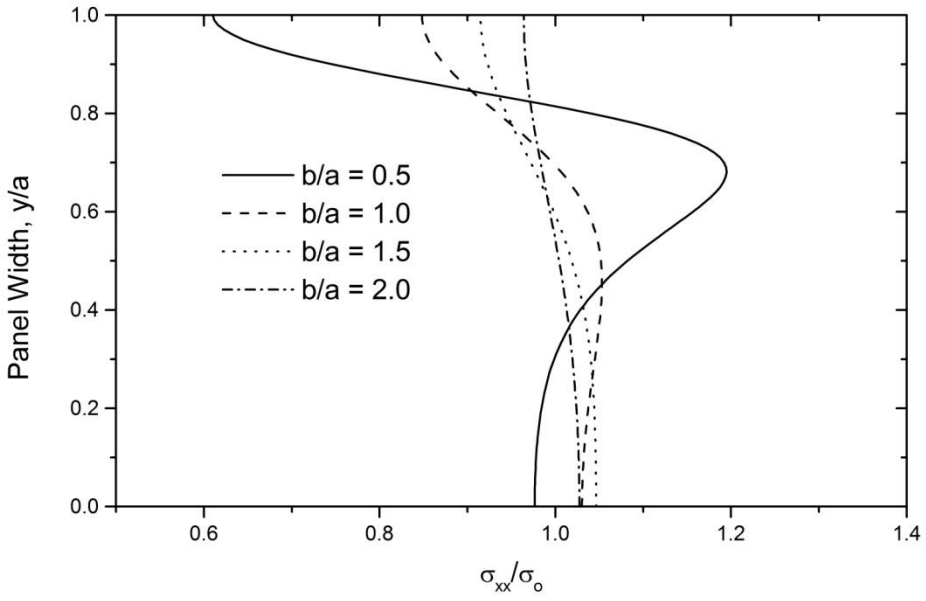

(b)

Fig 5.14: Effect of aspect ratio on the axial stress component at (a) *x/b* = 0.0 and (b) *x/b* = 0.5, (*h/a* = 0.2).

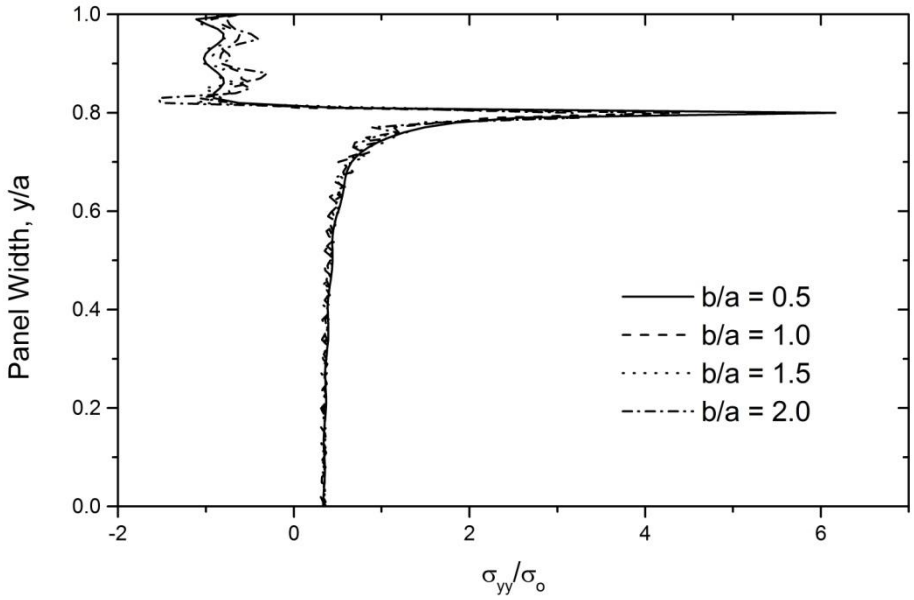

(a)

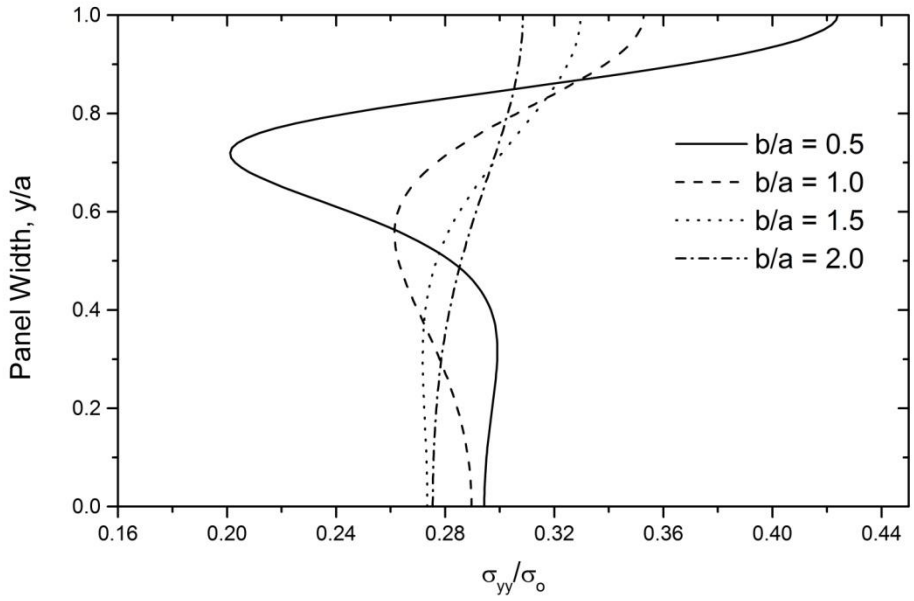

(b)

Fig 5.15: Effect of aspect ratio on the lateral stress component at (a) *x/b* = 0.0 and (b) *x/b* = 0.5, (*h/a* = 0.2).

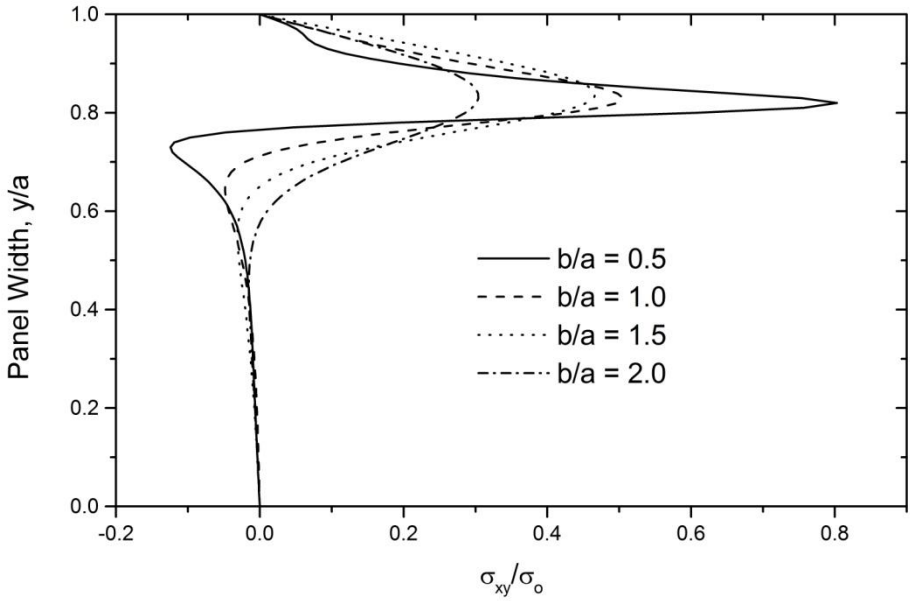

(a)

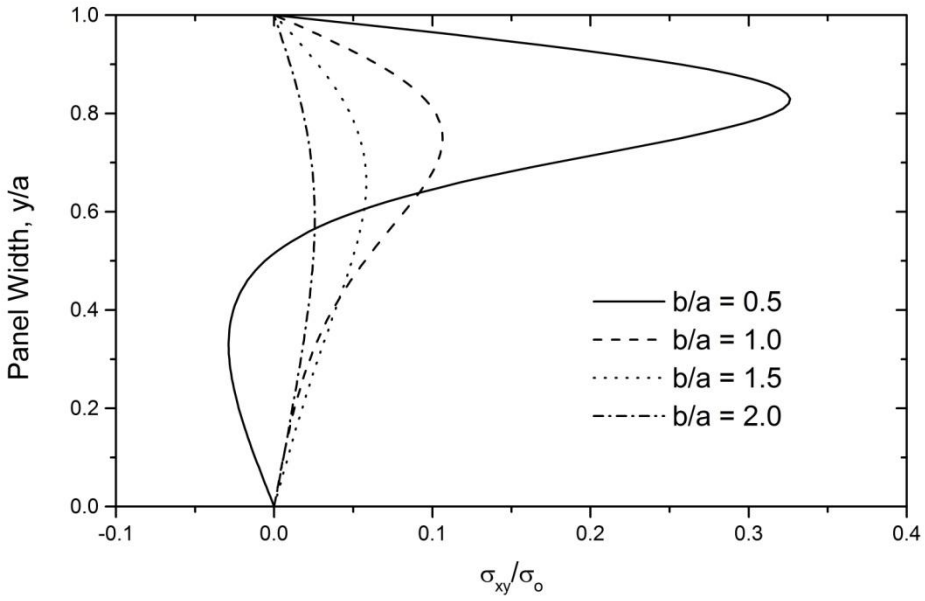

(b)

Fig 5.16: Effect of aspect ratio on the shear stress component at (a) *x/b* = 0.1 and (b) *x/b* = 0.5, (*h/a* = 0.2).

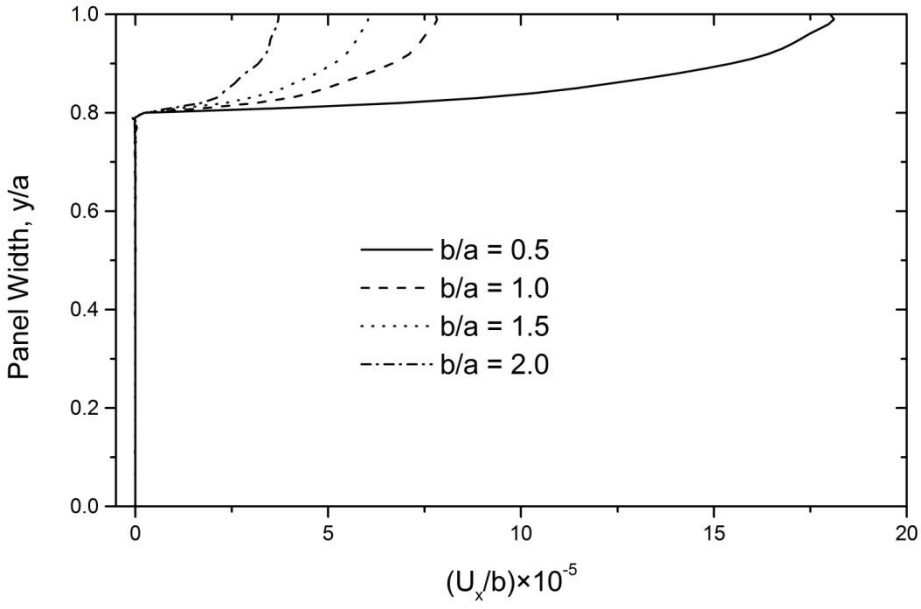

(a)

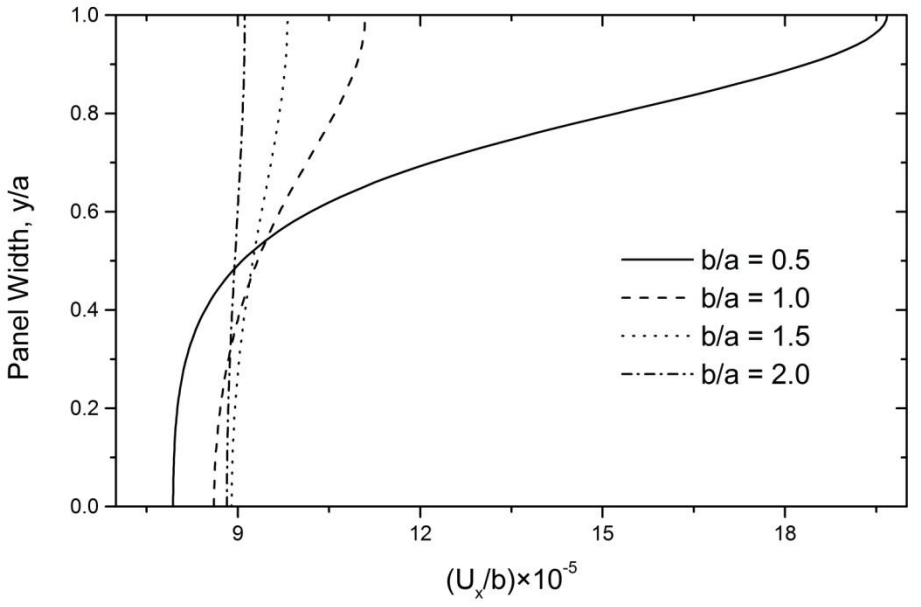

(b)

Fig 5.17: Effect of aspect ratio on the axial displacement component at (a) $x/b = 0.0$ and (b) $x/b = 0.5$, ($h/a = 0.2$).

CHAPTER 6

CRACKED COMPOSITE PANEL UNDER AXIAL STIFFENERS SUBJECTED TO AXIAL TENSION

In this chapter, the stress and displacement fields of a stiffened composite panel with an edge crack are analyzed under uniform axial tension loading. The effect of fiber orientation on the stress and displacements at different sections of the composite panel is also analyzed. The solution is obtained using displacement potential approach for the two limiting cases of fiber orientations of the panel. It is observed that fiber orientation has significant effect on the state of stresses at the crack surface as well as other sections of the panel.

6.1 Problem Articulation

Stiffened panels with symmetric edge-cracked orthotropic panel with reference to a two dimensional Cartesian coordinate system *x*-*y* are shown in Figs 6.1 and 6.2. The fibers are oriented along the *x*-axis that represent the first case with $\theta=0^{o}$ (Case-A) as shown in Fig. 6.1. In the second case the fiber are oriented along the *y*-axis for which $\theta=90^{o}$ (Case-B) as shown in Fig. 6.2.

6.2 Boundary Conditions

(i) Stiffened Edge, AB:

Since it is a longitudinal stiffener, there is no axial displacement and shear stress. Thus,

$u_x(x,a)=0$ and $\sigma_{yy}(x,a)=0$ [$0 \le x \le b$]

(ii) Stiffened Edge, CD:

There is no axial displacement and lateral stress. Thus,

$u_x(x,0)=0$ and $\sigma_{yy}(x,0)=0$ [$0 \le x \le b$]

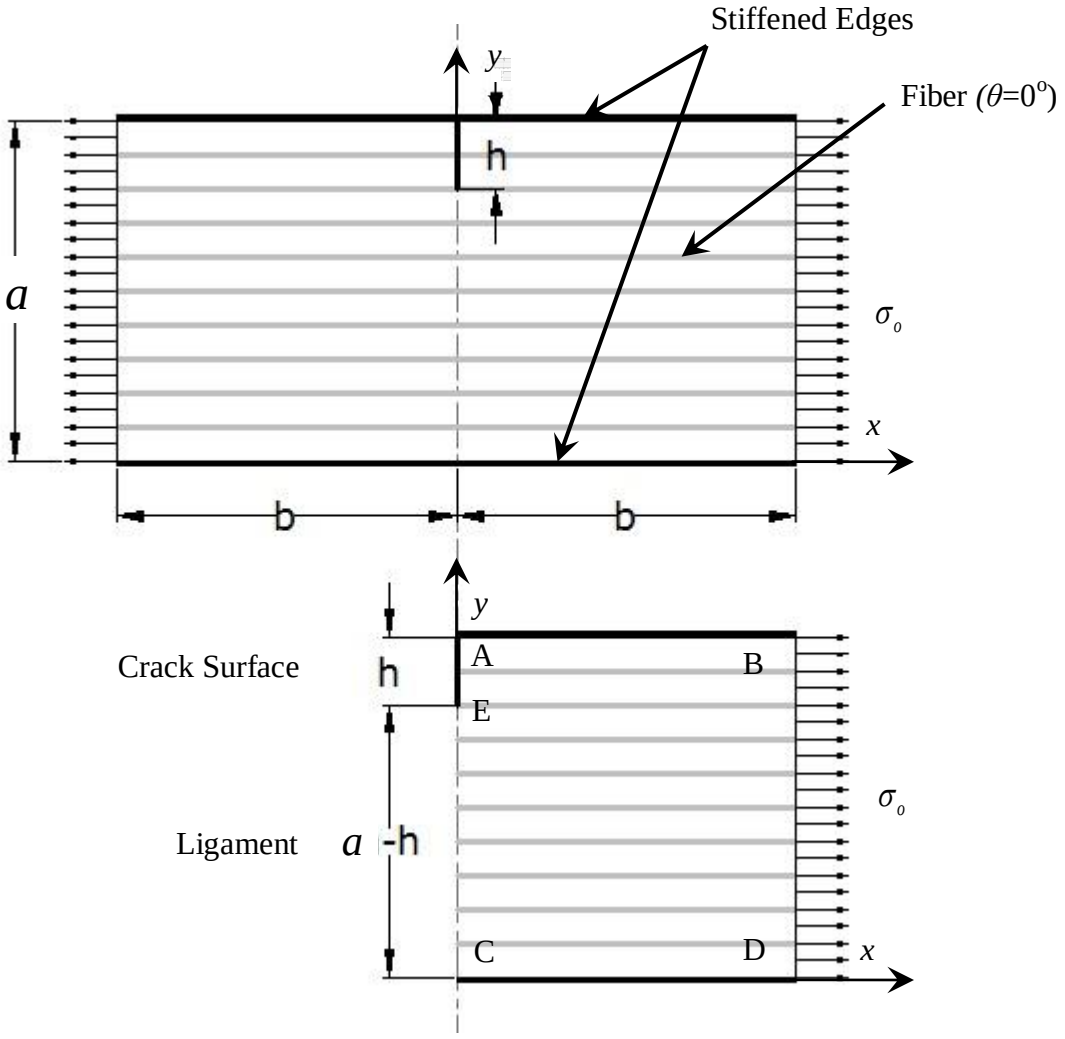

Fig 6.1: Geometry and loading of a cracked stiffened composite panel (Case-A) (a) Full model of the panel (b) symmetric model of the panel.

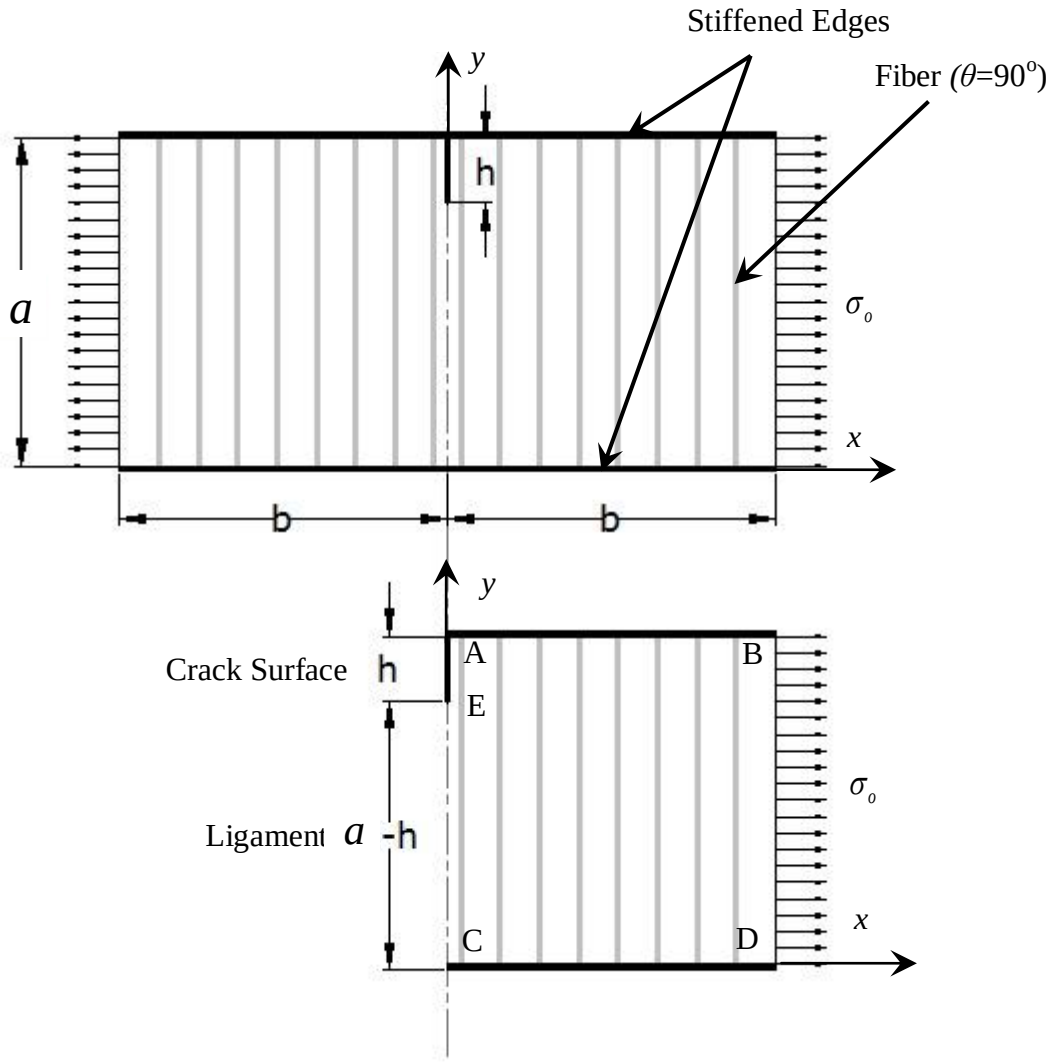

Fig 6.2: Geometry and loading of a cracked stiffened composite panel (Case-B) (a) Full model of the panel (b) symmetric model of the panel.

.

(iii) Ligament, EC:

Due to symmetry of the full model of the panel, axial displacement and shear stresses along this section are assumed to be zero.

$u_x(0,y) = 0$ [$0 \le y \le (a\text{-}h)$] and $\sigma_{xy}(0,y) = 0$ [$0 \le y \le (a\text{-}h)$]

Crack surface, AE:

Since the crack surface is free from loading and restraints, there will be no boundary constraints and shear stress. A Fourier series is assumed along the crack surface for the axial displacement distribution.

$\sigma_{xy}(0,y) = 0$ [$(a\text{-}h) \le y \le a$]

$$u_x(0,y) = a_0 + \sum_{i=1}^{3} a_i \cos(i * w * y) + \sum_{i=1}^{3} b_i \sin(i * w * y) \quad [(a\text{-}h) \le y \le a]$$

where a_i and b_i are constants and i = 1~3.

(iv) Loading Edge, BD:

The axial tension of the panel is realized by assigning a uniform value to the axial stress component which is the function of load intensity. The boundary will also free from shearing stress.

$\sigma_{xx}(b,y) = \sigma_{xx}^{o}$ and $\sigma_{xy}(b,y) = 0$ [$0 \le y \le a$]

6.3 Solution Procedure

Case-A : θ = 0° (Fibers are parallel to the direction of loading)

Mathematical model here is the partial differential equation derived from the equations of equilibrium and equations of compatibility based on Displacement Potential Function $\psi(x,y)$ obtained from Eq. (2.30) as follows.

$$E_1 G_{12} \frac{\partial^4 \psi}{\partial x^4} + E_2 (E_1 - 2\mu_{12} G_{12}) \frac{\partial^4 \psi}{\partial x^2 \partial y^2} + E_2 G_{12} \frac{\partial^4 \psi}{\partial y^4} = 0 \qquad (6.1)$$

In this case the displacement and stress components are also obtained from Eq. (2.31) as follows:

$$u_x(x,y)=\frac{\partial^2\psi}{\partial x\partial y} \tag{6.2a}$$

$$u_y(x,y)=-\frac{1}{Z_{11}}\left[E_1^2\frac{\partial^2\psi}{\partial x^2}+G_{12}\left(E_1-\mu_{12}^2E_2\right)\frac{\partial^2\psi}{\partial y^2}\right] \tag{6.2b}$$

$$\sigma_{xx}(x,y)=\frac{E_1G_{12}}{Z_{11}}\left[E_1\frac{\partial^3\psi}{\partial x^2\partial y}-\mu_{12}E_2\frac{\partial^3\psi}{\partial y^3}\right] \tag{6.2c}$$

$$\sigma_{yy}(x,y)=\frac{E_1E_2}{Z_{11}}\left[\left(\mu_{12}G_{12}-E_1\right)\frac{\partial^3\psi}{\partial x^2\partial y}-G_{12}\frac{\partial^3\psi}{\partial y^3}\right] \tag{6.2d}$$

$$\sigma_{xy}(x,y)=-\frac{E_1G_{12}}{Z_{11}}\left[E_1\frac{\partial^3\psi}{\partial x^3}-\mu_{12}E_2\frac{\partial^3\psi}{\partial x\partial y^2}\right] \tag{6.2e}$$

where $Z_{11}=\mu_{12}E_1E_2+G_{12}\left(E_1-\mu_{12}^2E_2\right)$

The displacement potential trial function is assumed in such a way that the boundary conditions at the stiffened edges are satisfied automatically. Actually, the trial function should be in terms of cosine function so that its first derivative and third derivative with respect to x can be found in terms of sine function. By this way the requirement of physical conditions of the two opposing stiffened ends are automatically satisfied, i.e., automatic satisfaction of boundary conditions of (a) and (b). At the same time the expression for ψ should also be compatible to the distribution of load on the right boundary and reactions on the supports. Considering all these factors the expression for ψ may be approximated as follows:

$$\psi(x,\ y)=\sum_{m=1}^{\infty}X_m(x)\cos\alpha y \tag{6.3}$$

where, $X_m=f(x)$, $\alpha=(m\pi/a)$ and m = 1, 2, 3, …….∞.

Derivatives of equation (6.3) with respect to x and y are

$$\frac{\partial\psi}{\partial x}=\sum_{m=1}^{\infty}X'_m\cos\alpha y$$

$$\frac{\partial^2\psi}{\partial x^2}=\sum_{m=1}^{\infty}X''_m\cos\alpha y$$

$$\frac{\partial^3\psi}{\partial x^3}=\sum_{m=1}^{\infty}X'''_m\cos\alpha y$$

$$\frac{\partial^4\psi}{\partial x^4}=\sum_{m=1}^{\infty}X''''_m\cos\alpha y$$

$$\frac{\partial^2\psi}{\partial x\partial y}=-\sum_{m=1}^{\infty}X'_m\alpha\sin\alpha y$$

$$\frac{\partial^3\psi}{\partial x\partial y^2}=-\sum_{m=1}^{\infty}X'_m\alpha^2\cos\alpha y$$

$$\frac{\partial^3\psi}{\partial x^2\partial y}=-\sum_{m=1}^{\infty}X''_m\alpha\cos\alpha y$$

$$\frac{\partial^4\psi}{\partial x^2\partial y^2}=-\sum_{m=1}^{\infty}X''_m\alpha^2\cos\alpha y$$

$$\frac{\partial\psi}{\partial y}=-\sum_{m=1}^{\infty}X_m\alpha\sin\alpha y$$

$$\frac{\partial^2\psi}{\partial y^2}=-\sum_{m=1}^{\infty}X_m\alpha^2\cos\alpha y$$

$$\frac{\partial^3\psi}{\partial y^3}=\sum_{m=1}^{\infty}X_m\alpha^3\sin\alpha y$$

$$\frac{\partial^4\psi}{\partial y^4}=\sum_{m=1}^{\infty}X_m\alpha^4\cos\alpha y$$

Using the derivatives of equation (6.3) equation (6.1) yields

$$E_1G_{12}\sum_{m=1}^{\infty}X''''_m\cos\alpha y-E_2(E_1-2\mu_{12}G_{12})\sum_{m=1}^{\infty}X''_m\alpha^2\cos\alpha y+E_2G_{12}\sum_{m=1}^{\infty}X_m\alpha^4\cos\alpha y=0$$

$$or,E_1G_{12}\sum_{m=1}^{\infty}\left[X''''_m-\frac{E_2(E_1-2\mu_{12}G_{12})}{E_1G_{12}}X''_m\alpha^2+\frac{E_2G_{12}}{E_1G_{12}}X_m\alpha^4\right]\cos\alpha y=0$$

$$or,X''''_m-\frac{E_2(E_1-2\mu_{12}G_{12})}{E_1G_{12}}X''_m\alpha^2+\frac{E_2G_{12}}{E_1G_{12}}X_m\alpha^4=0$$

$$or, X_m'''' - \left(\frac{E_2}{G_{12}} - \frac{2\mu_{12}E_2}{E_1}\right)X_m''\alpha^2 + \frac{E_2}{E_1}X_m\alpha^4 = 0 \tag{6.4}$$

The general solution to the above ordinary differential equation be

$$X_m = A_m e^{r_1 x} + B_m e^{r_2 x} + C_m e^{r_3 x} + D_m e^{r_4 x} \tag{6.5}$$

where A_m, B_m, C_m and D_m are arbitrary constants and r_1, r_2, r_3 and r_4 are the roots of following equation

$$r^4 - \left(\frac{E_2}{G_{12}} - \frac{2\mu_{12}E_2}{E_1}\right)\alpha^2 r^2 + \frac{E_2}{E_1}\alpha^4 = 0$$

Where

$$r_1, r_2 = \frac{\alpha}{\sqrt{2}}\left[\left(\frac{E_2}{G_{12}} - \frac{2\mu_{12}E_2}{E_1}\right) \pm \sqrt{\left(\frac{E_2}{G_{12}} - \frac{2\mu_{12}E_2}{E_1}\right)^2 - 4\frac{E_2}{E_1}}\right]^{\frac{1}{2}} \tag{6.6a}$$

$$r_3, r_4 = -\frac{\alpha}{\sqrt{2}}\left[\left(\frac{E_2}{G_{12}} - \frac{2\mu_{12}E_2}{E_1}\right) \pm \sqrt{\left(\frac{E_2}{G_{12}} - \frac{2\mu_{12}E_2}{E_1}\right)^2 - 4\frac{E_2}{E_1}}\right]^{\frac{1}{2}} \tag{6.6b}$$

Now substituting the derivatives of ψ and Y_m using equation (6.3) and (6.5) respectively in the expressions for displacement and stresses (6.2a, 6.2b, 6.2c, 6.2d and 6.2e).

$$u_x(x,y) = \frac{\partial^2\psi}{\partial x \partial y}$$

$$= -\sum_{m=1}^{\infty} X'_m \alpha \sin \alpha y$$

$$= -\sum_{m=1}^{\infty}\left(A_m r_1 e^{r_1 x} + B_m r_2 e^{r_2 x} + C_m r_3 e^{r_3 x} + D_m r_4 e^{r_4 x}\right)\alpha \sin \alpha y \tag{6.7a}$$

$$u_y(x,y) = -\frac{1}{Z_{11}}\left[E_1^2 \frac{\partial^2\psi}{\partial x^2} + G_{12}\left(E_1 - \mu_{12}^2 E_2\right)\frac{\partial^2\psi}{\partial y^2}\right]$$

$$= \frac{1}{Z_{11}}\left[-E_1^2\left\{\sum_{m=1}^{\infty} X_m'' \cos \alpha y\right\} + G_{12}\left(E_1 - \mu_{12}^2 E_2\right)\left\{\sum_{m=1}^{\infty} X_m \alpha^2 \cos \alpha y\right\}\right]$$

$$= \left[\sum_{m=1}^{\infty} \begin{Bmatrix} \left(\frac{Z_{12}}{Z_{11}} \alpha^2 - \frac{E_1^2}{Z_{11}} r_1^2 \right) e^{r_1 x} A_m + \left(\frac{Z_{12}}{Z_{11}} \alpha^2 - \frac{E_1^2}{Z_{11}} r_2^2 \right) e^{r_2 x} B_m + \\ \left(\frac{Z_{12}}{Z_{11}} \alpha^2 - \frac{E_1^2}{Z_{11}} r_3^2 \right) e^{r_3 x} C_m + \left(\frac{Z_{12}}{Z_{11}} \alpha^2 - \frac{E_1^2}{Z_{11}} r_4^2 \right) e^{r_4 x} D_m \end{Bmatrix} \cos \alpha y \right] \quad (6.7b)$$

$$\sigma_{xx}(x,y) = \frac{E_1 G_{12}}{Z_{11}} \left[E_1 \frac{\partial^3 \psi}{\partial x^2 \partial y} - \mu_{12} E_2 \frac{\partial^3 \psi}{\partial y^3} \right]$$

$$= \frac{E_1 G_{12}}{Z_{11}} \left[E_1 \left\{ - \sum_{m=1}^{\infty} X_m'' \alpha \sin \alpha y \right\} - \mu_{12} E_2 \left\{ \sum_{m=1}^{\infty} X_m \alpha^3 \sin \alpha y \right\} \right]$$

$$= - \frac{E_1 G_{12}}{Z_{11}} \left[\sum_{m=1}^{\infty} \begin{Bmatrix} \left(E_1 \alpha r_1^2 + E_2 \mu_{12} \alpha^3 \right) A_m e^{r_1 x} + \left(E_1 \alpha r_2^2 + E_2 \mu_{12} \alpha^3 \right) B_m e^{r_2 x} + \\ \left(E_1 \alpha r_3^2 + E_2 \mu_{12} \alpha^3 \right) A_m e^{r_3 x} + \left(E_1 \alpha r_4^2 + E_2 \mu_{12} \alpha^3 \right) B_m e^{r_4 x} \end{Bmatrix} \sin \alpha y \right] \quad (6.7c)$$

$$\sigma_{yy}(x,y) = \frac{E_1 E_2}{Z_{11}} \left[\left(\mu_{12} G_{12} - E_1 \right) \frac{\partial^3 \psi}{\partial x^2 \partial y} - G_{12} \frac{\partial^3 \psi}{\partial y^3} \right]$$

$$= \frac{E_1 E_2}{Z_{11}} \left[\left(\mu_{12} G_{12} - E_1 \right) \left\{ - \sum_{m=1}^{\infty} X_m'' \alpha \sin \alpha y \right\} - G_{12} \left\{ \sum_{m=1}^{\infty} X_m \alpha^3 \sin \alpha y \right\} \right]$$

$$= - \frac{E_1 E_2}{Z_{11}} \left[\sum_{m=1}^{\infty} \begin{Bmatrix} (\alpha r_1^2 (\mu_{12} G_{12} - E_1) + G_{12} \alpha^3) A_m e^{r_1 x} + \\ (\alpha r_2^2 (\mu_{12} G_{12} - E_1) + G_{12} \alpha^3) A_m e^{r_2 x} + \\ (\alpha r_3^2 (\mu_{12} G_{12} - E_1) + G_{12} \alpha^3) A_m e^{r_3 x} + \\ (\alpha r_4^2 (\mu_{12} G_{12} - E_1) + G_{12} \alpha^3) A_m e^{r_4 x} \end{Bmatrix} \sin \alpha y \right] \quad (6.7d)$$

$$\sigma_{xy}(x,y) = - \frac{E_1 G_{12}}{Z_{11}} \left[E_1 \frac{\partial^3 \psi}{\partial x^3} - \mu_{12} E_2 \frac{\partial^3 \psi}{\partial x \partial y^2} \right]$$

$$= - \frac{E_1 G_{12}}{Z_{11}} \left[\sum_{m=1}^{\infty} E_1 X_m''' \cos \alpha y + \mu_{12} E_2 \left\{ \sum_{m=1}^{\infty} X_m' \alpha^2 \cos \alpha y \right\} \right]$$

$$= - \frac{E_1 G_{12}}{Z_{11}} \left[\sum_{m=1}^{\infty} \begin{Bmatrix} \left(E_1 r_1^3 + \mu_{12} E_2 \alpha^2 r_1 \right) A_m e^{r_1 x} + \left(E_1 r_2^3 + \mu_{12} E_2 \alpha^2 r_2 \right) B_m e^{r_2 x} + \\ \left(E_1 r_3^3 + \mu_{12} E_2 \alpha^2 r_3 \right) C_m e^{r_3 x} + \left(E_1 r_4^3 + \mu_{12} E_2 \alpha^2 r_4 \right) D_m e^{r_4 x} \end{Bmatrix} \cos \alpha y \right] \quad (6.7e)$$

Where $Z_{12} = G_{12}(E_1 - \mu_{12}^2 E_2)$

Now, the axial loading on the right edge of the panel can be taken as Fourier series in the following manner:

$$\sigma_{xx}(b, y) = \sigma_{xx}^{o} = \sum_{m=1}^{\infty} E_m \sin \alpha y \tag{6.8}$$

To satisfy the boundary condition and the loading distribution, Fourier sine series have been considered for the analysis.

$$E_m = \frac{2}{a}\int_0^a \sigma_{xx}^{o} \sin(\alpha y)dy$$

$$= \frac{2\sigma_{xx}^{o}}{a}\int_0^a \sin(\alpha y)dy$$

$$= \frac{2\sigma_{xx}^{0}}{\alpha a}[-\cos(\alpha y)]_0^a$$

$$= \frac{2\sigma_{xx}^{o}}{m\pi}[1-\cos(m\pi)], \text{ where m = 1, 2, 3, 4, 5 } \ldots\ldots\ldots\ldots\ldots\infty$$

Due to symmetry, the axial displacement at the left edge from 0 to (a-h) is zero. But at the cracked edge, the distribution of the axial displacement can be expressed as the Fourier series in the following manner:

$$u_x(0, y) = a_0 + \sum_{i=1}^{3} a_i \cos(i*w*y) + \sum_{i=1}^{3} b_i \sin(i*w*y) = \sum_{m=1}^{\infty} I_m \sin(\alpha y) \tag{6.9}$$

The curve fitted equation as Fourier series up to 7th term have been considered. This is because of up to 7^{th} term we always achieve R^2 value above 0.99. If we increase the term it will make the mathematical calculation more complicated.

Here

$$I_m = \frac{2}{a}\int_{a-h}^{a} (a_0 + \sum_{i=1}^{3} a_i \cos(i*w*y) + \sum_{i=1}^{3} b_i \sin(i*w*y))\sin(\alpha y)dy$$

After performing integration, the result is given below:

$$I_m = \left(\frac{2a_o}{m\pi} \left(\cos\left(\frac{(a-h)m\pi}{a} \right) - \cos(m\pi) \right) \right) + \sum_{i=1}^{3} a_i \begin{pmatrix} \left(\frac{1}{m\pi + iwa} \cos\left(\left(\frac{a-h}{a} \right) (m\pi + iwa) \right) \right) + \\ \left(\frac{1}{m\pi - iwa} \cos\left(\left(\frac{a-h}{a} \right) (m\pi - iwa) \right) \right) - \\ \left(\frac{1}{m\pi + iwa} \cos(m\pi + iwa) \right) - \\ \left(\frac{1}{m\pi - iwa} \cos(m\pi - iwa) \right) \end{pmatrix}$$

$$+ \sum_{i=1}^{3} b_i \begin{pmatrix} -\left(\frac{1}{m\pi - iwa} \sin(m\pi + iwa) \right) + \\ \left(\frac{1}{m\pi - iwa} \sin(m\pi - iwa) \right) + \\ \left(\frac{1}{m\pi + iwa} \sin\left(\left(\frac{a-h}{a} \right) (m\pi + iwa) \right) \right) - \\ \left(\frac{1}{m\pi - iwa} \sin\left(\left(\frac{a-h}{a} \right) (m\pi - iwa) \right) \right) \end{pmatrix}$$

Using boundary condition $\sigma_{xy}(0, y) = 0$ at the edge of $x = 0$, it is found that

$$-\frac{E_1 G_{12}}{Z_{11}} \left[\sum_{m=1}^{\infty} \begin{Bmatrix} \left(E_1 r_1^3 + \mu_{12} E_2 \alpha^2 r_1 \right) A_m + \left(E_1 r_2^3 + \mu_{12} E_2 \alpha^2 r_2 \right) B_m + \\ \left(E_1 r_3^3 + \mu_{12} E_2 \alpha^2 r_3 \right) C_m + \left(E_1 r_4^3 + \mu_{12} E_2 \alpha^2 r_4 \right) D_m \end{Bmatrix} \cos \alpha y \right] = 0$$

$$or, \begin{Bmatrix} \left(-E_1^2 G_{12} r_1^3 - \mu_{12} E_1 E_2 G_{12} \alpha^2 r_1 \right) A_m + \left(-E_1^2 G_{12} r_2^3 - \mu_{12} E_1 E_2 G_{12} \alpha^2 r_2 \right) B_m + \\ \left(-E_1^2 G_{12} r_3^3 - \mu_{12} E_1 E_2 G_{12} \alpha^2 r_3 \right) C_m + \left(-E_1^2 G_{12} r_4^3 - \mu_{12} E_1 E_2 G_{12} \alpha^2 r_4 \right) D_m \end{Bmatrix} = 0 \quad (6.10)$$

Using boundary condition $\sigma_{xy}(b, y) = 0$ at the edge of $x = b$, it is found that

$$-\frac{E_1 G_{12}}{Z_{11}} \left[\sum_{m=1}^{\infty} \begin{Bmatrix} \left(E_1 r_1^3 + \mu_{12} E_2 \alpha^2 r_1 \right) A_m e^{r_1 b} + \left(E_1 r_2^3 + \mu_{12} E_2 \alpha^2 r_2 \right) B_m e^{r_2 b} + \\ \left(E_1 r_3^3 + \mu_{12} E_2 \alpha^2 r_3 \right) C_m e^{r_3 b} + \left(E_1 r_4^3 + \mu_{12} E_2 \alpha^2 r_4 \right) D_m e^{r_4 b} \end{Bmatrix} \cos \alpha y \right] = 0$$

$$or, \begin{Bmatrix} \left(-E_1^2 G_{12} r_1^3 - \mu_{12} E_1 E_2 G_{12} \alpha^2 r_1 \right) A_m e^{r_1 b} + \left(-E_1^2 G_{12} r_2^3 - \mu_{12} E_1 E_2 G_{12} \alpha^2 r_2 \right) B_m e^{r_2 b} + \\ \left(-E_1^2 G_{12} r_3^3 - \mu_{12} E_1 E_2 G_{12} \alpha^2 r_3 \right) C_m e^{r_3 b} + \left(-E_1^2 G_{12} r_4^3 - \mu_{12} E_1 E_2 G_{12} \alpha^2 r_4 \right) D_m e^{r_4 b} \end{Bmatrix} = 0 \quad (6.11)$$

Using boundary condition $u_x(0,y) = a_0 + \sum_{i=1}^{3} a_i \cos(i*w*y) + \sum_{i=1}^{3} b_i \sin(i*w*y)$ at the edge of $x = 0$, it is found that

$$-\sum_{m=1}^{\infty}(A_m r_1 + B_m r_2 + C_m r_3 + D_m r_4)\alpha \sin \alpha y = \sum_{m=1}^{\infty} I_m \sin(\alpha y)$$

$$or, -(A_m r_1 + B_m r_2 + C_m r_3 + D_m r_4)\alpha = I_m \tag{6.12}$$

Using boundary condition $\sigma_{xx}(b,y) = \sigma_{xx}^{o}$ at the edge of $x = b$, it is found

$$-\frac{E_1 G_{12}}{Z_{11}}\left[\sum_{m=1}^{\infty}\begin{Bmatrix}\left(E_1\alpha r_1^2 + E_2\mu_{12}\alpha^3\right)A_m e^{r_1 b} + \left(E_1\alpha r_2^2 + E_2\mu_{12}\alpha^3\right)B_m e^{r_2 b} + \\ \left(E_1\alpha r_3^2 + E_2\mu_{12}\alpha^3\right)A_m e^{r_3 b} + \left(E_1\alpha r_4^2 + E_2\mu_{12}\alpha^3\right)B_m e^{r_4 b}\end{Bmatrix}\sin\alpha y\right] = \sum_{m=1}^{\infty} E_m \sin\alpha y$$

$$or, \begin{Bmatrix}\left(\frac{-E_1^2 G_{12}\alpha r_1^2 - \mu_{12}E_1E_2G_{12}\alpha^3}{Z_{11}}\right)A_m e^{r_1 b} + \left(\frac{-E_1^2 G_{12}\alpha r_2^2 - \mu_{12}E_1E_2G_{12}\alpha^3}{Z_{11}}\right)B_m e^{r_2 b} + \\ \left(\frac{-E_1^2 G_{12}\alpha r_3^2 - \mu_{12}E_1E_2G_{12}\alpha^3}{Z_{11}}\right)C_m e^{r_3 b} + \left(\frac{-E_1^2 G_{12}\alpha r_4^2 - \mu_{12}E_1E_2G_{12}\alpha^3}{Z_{11}}\right)D_m e^{r_4 b}\end{Bmatrix} = E_m \tag{6.13}$$

The simultaneous equations (6.10), (6.11), (6.12) and (6.13) can be realized in a simplified matrix form for the solution of unknown terms like A_m, B_m, C_m and D_m as follows:

$$\begin{bmatrix} DD_1 & DD_2 & DD_3 & DD_4 \\ FF_1 & FF_2 & FF_3 & FF_4 \\ HH_1 & HH_2 & HH_3 & HH_4 \\ KK_1 & KK_2 & KK_3 & KK_4 \end{bmatrix}\begin{bmatrix} A_m \\ B_m \\ C_m \\ D_m \end{bmatrix} = \begin{bmatrix} 0 \\ 0 \\ I_m \\ E_m \end{bmatrix} \tag{6.14}$$

Where

$$DD_i = -E_1^2 G_{12} r_i^3 - \mu_{12}E_1E_2G_{12}\alpha^2 r_i$$

$$FF_i = \left(-E_1^2 G_{12} r_i^3 - \mu_{12}E_1E_2G_{12}\alpha^2 r_i\right)e^{r_i b}$$

$$HH_i = -\alpha r_i$$

$$KK_i = \left(\frac{-E_1^2 G_{12} \alpha r_i^2 - \mu_{12} E_1 E_2 G_{12} \alpha^3}{Z_{11}} \right) e^{r_i b}$$

Solution of the above matrix Eq. (6.14) yields the unknown constants A_m , B_m , C_m and D_m . Once the value of the unknowns are determined, they are directly substituted in Eqs.[6.7(a)-6.7(e)] to obtain the explicit expressions for the different parameters of interest, namely, the two displacement and the three stress components at various points.

Case-B : θ = 90^o (Fibers are perpendicular to the direction of loading)

The governing equation for fiber orientation $\theta = 90^o$ is derived from the equations of equilibrium and equations of compatibility based on Displacement Potential Function $\psi(x,y)$ obtained from Eq. (2.32) as follows.

$$E_2 G_{12} \frac{\partial^4 \psi}{\partial x^4} + E_2 \left(E_1 - 2\mu_{12} G_{12} \right) \frac{\partial^4 \psi}{\partial x^2 \partial y^2} + E_1 G_{12} \frac{\partial^4 \psi}{\partial y^4} = 0 \tag{6.15}$$

In this case the displacement and stress components are also obtained from Eq. (2.33) as follows:

$$u_x(x,y) = \frac{\partial^2 \psi}{\partial x \partial y} \tag{6.16a}$$

$$u_y(x,y) = -\frac{1}{Z_{11}} \left[E_1 E_2 \frac{\partial^2 \psi}{\partial x^2} + G_{12} \left(E_1 - \mu_{12}^2 E_2 \right) \frac{\partial^2 \psi}{\partial y^2} \right] \tag{6.16b}$$

$$\sigma_{xx}(x,y) = \frac{E_1 E_2 G_{12}}{Z_{11}} \left[\frac{\partial^3 \psi}{\partial x^2 \partial y} - \mu_{12} \frac{\partial^3 \psi}{\partial y^3} \right] \tag{6.16c}$$

$$\sigma_{yy}(x,y) = \frac{E_1}{Z_{11}} \left[E_2 \left(\mu_{12} G_{12} - E_1 \right) \frac{\partial^3 \psi}{\partial x^2 \partial y} - E_1 G_{12} \frac{\partial^3 \psi}{\partial y^3} \right] \tag{6.16d}$$

$$\sigma_{xy}(x,y) = -\frac{E_1 E_2 G_{12}}{Z_{11}} \left[\frac{\partial^3 \psi}{\partial x^3} - \mu_{12} \frac{\partial^3 \psi}{\partial x \partial y^2} \right] \tag{6.16e}$$

The expression for ψ may be approximated as follows:

$$\psi(x, y) = \sum_{m=1}^{\infty} X_m(x) \cos \alpha y \tag{6.17}$$

where, $X_m = f(x)$, $\alpha = (m\pi / a)$ and m = 1, 2, 3, …….. ∞.

Derivatives of equation (6.17) with respect to x and y have already mentioned in the first case.

Using the derivatives of equation (6.17) equation (6.15) yields

$$E_2 G_{12} \sum_{m=1}^{\infty} X_m'''' \cos \alpha y - E_2 \left(E_1 - 2\mu_{12} G_{12}\right) \sum_{m=1}^{\infty} X_m'' \alpha^2 \cos \alpha y + E_1 G_{12} \sum_{m=1}^{\infty} X_m \alpha^4 \cos \alpha y = 0$$

$$or, E_2 G_{12} \sum_{m=1}^{\infty} \left[X_m'''' - \frac{E_2 \left(E_1 - 2\mu_{12} G_{12}\right)}{E_2 G_{12}} X_m'' \alpha^2 + \frac{E_1 G_{12}}{E_2 G_{12}} X_m \alpha^4 \right] \cos \alpha y = 0$$

$$or, X_m'''' - \frac{\left(E_1 - 2\mu_{12} G_{12}\right)}{G_{12}} X_m'' \alpha^2 + \frac{E_1}{E_2} X_m \alpha^4 = 0$$

$$or, X_m'''' - \left(\frac{E_1}{G_{12}} - 2\mu_{12} \right) X_m'' \alpha^2 + \frac{E_1}{E_2} X_m \alpha^4 = 0 \tag{6.18}$$

The general solution of ordinary differential equation be

$$X_m = A_m e^{r_1 x} + B_m e^{r_2 x} + C_m e^{r_3 x} + D_m e^{r_4 x} \tag{6.19}$$

where A_m, B_m, C_m and D_m are arbitrary constants and r_1, r_2, r_3 and r_4 are the roots of following equation

$$r^4 - \left(\frac{E_1}{G_{12}} - 2\mu_{12} \right) \alpha^2 r^2 + \frac{E_1}{E_2} \alpha^4 = 0$$

Where

$$r_1, r_2 = \frac{\alpha}{\sqrt{2}} \left[\left(\frac{E_1}{G_{12}} - 2\mu_{12} \right) \pm \sqrt{\left(\frac{E_1}{G_{12}} - 2\mu_{12} \right)^2 - 4 \frac{E_1}{E_2}} \right]^{\frac{1}{2}} \tag{6.20a}$$

$$r_3, r_4 = -\frac{\alpha}{\sqrt{2}} \left[\left(\frac{E_1}{G_{12}} - 2\mu_{12} \right) \pm \sqrt{\left(\frac{E_1}{G_{12}} - 2\mu_{12} \right)^2 - 4 \frac{E_1}{E_2}} \right]^{\frac{1}{2}} \tag{6.20b}$$

Now substituting the derivatives of ψ and Y_m using equation (6.17) and (6.19) respectively in the expressions for displacement and stresses (6.16a, 6.16b, 6.16c, 6.16d and 6.16e).

$$u_x(x,y)=\frac{\partial^2\psi}{\partial x\partial y}$$

$$=-\sum_{m=1}^{\infty}X'_m\alpha\sin\alpha y$$

$$=-\sum_{m=1}^{\infty}\left(A_m r_1 e^{r_1 x}+B_m r_2 e^{r_2 x}+C_m r_3 e^{r_3 x}+D_m r_4 e^{r_4 x}\right)\alpha\sin\alpha y \qquad (6.21a)$$

$$u_y(x,y)=-\frac{1}{Z_{11}}\left[E_1E_2\frac{\partial^2\psi}{\partial x^2}+G_{12}\left(E_1-\mu_{12}^2E_2\right)\frac{\partial^2\psi}{\partial y^2}\right]$$

$$=\frac{1}{Z_{11}}\left[-E_1E_2\left\{\sum_{m=1}^{\infty}X''_m\cos\alpha y\right\}+G_{12}\left(E_1-\mu_{12}^2E_2\right)\left\{\sum_{m=1}^{\infty}X_m\alpha^2\cos\alpha y\right\}\right]$$

$$=\left[\sum_{m=1}^{\infty}\begin{Bmatrix}\left(\frac{Z_{12}}{Z_{11}}\alpha^2-\frac{E_1E_2}{Z_{11}}r_1^2\right)e^{r_1x}A_m+\left(\frac{Z_{12}}{Z_{11}}\alpha^2-\frac{E_1E_2}{Z_{11}}r_2^2\right)e^{r_2x}B_m+\\ \left(\frac{Z_{12}}{Z_{11}}\alpha^2-\frac{E_1E_2}{Z_{11}}r_3^2\right)e^{r_3x}C_m+\left(\frac{Z_{12}}{Z_{11}}\alpha^2-\frac{E_1E_2}{Z_{11}}r_4^2\right)e^{r_4x}D_m\end{Bmatrix}\cos\alpha y\right] \qquad (6.21b)$$

$$\sigma_{xx}(x,y)=\frac{E_1E_2G_{12}}{Z_{11}}\left[\frac{\partial^3\psi}{\partial x^2\partial y}-\mu_{12}\frac{\partial^3\psi}{\partial y^3}\right]$$

$$=\frac{E_1E_2G_{12}}{Z_{11}}\left[\left\{-\sum_{m=1}^{\infty}X''_m\alpha\sin\alpha y\right\}-\mu_{12}\left\{\sum_{m=1}^{\infty}X_m\alpha^3\sin\alpha y\right\}\right]$$

$$=-\frac{E_1E_2G_{12}}{Z_{11}}\left[\sum_{m=1}^{\infty}\begin{Bmatrix}\left(\alpha r_1^2+\mu_{12}\alpha^3\right)A_m e^{r_1x}+\left(\alpha r_2^2+\mu_{12}\alpha^3\right)B_m e^{r_2x}+\\ \left(\alpha r_3^2+\mu_{12}\alpha^3\right)A_m e^{r_3x}+\left(\alpha r_4^2+\mu_{12}\alpha^3\right)B_m e^{r_4x}\end{Bmatrix}\sin\alpha y\right] \qquad (6.21c)$$

$$\sigma_{yy}(x,y)=\frac{E_1}{Z_{11}}\left[E_2\left(\mu_{12}G_{12}-E_1\right)\frac{\partial^3\psi}{\partial x^2\partial y}-E_1G_{12}\frac{\partial^3\psi}{\partial y^3}\right]$$

$$=\frac{E_1}{Z_{11}}\left[E_2\left(\mu_{12}G_{12}-E_1\right)\left\{-\sum_{m=1}^{\infty}X''_m\alpha\sin\alpha y\right\}-E_1G_{12}\left\{\sum_{m=1}^{\infty}X_m\alpha^3\sin\alpha y\right\}\right]$$

$$=-\frac{E_1}{Z_{11}}\left[\sum_{m=1}^{\infty}\begin{Bmatrix}(\alpha E_2r_1^2(\mu_{12}G_{12}-E_1)+E_1G_{12}\alpha^3)A_m e^{r_1x}+\\ (\alpha E_2r_2^2(\mu_{12}G_{12}-E_1)+E_1G_{12}\alpha^3)A_m e^{r_2x}+\\ (\alpha E_2r_3^2(\mu_{12}G_{12}-E_1)+E_1G_{12}\alpha^3)A_m e^{r_3x}+\\ (\alpha E_2r_4^2(\mu_{12}G_{12}-E_1)+E_1G_{12}\alpha^3)A_m e^{r_4x}\end{Bmatrix}\sin\alpha y\right] \qquad (6.21d)$$

$$\sigma_{xy}(x,y) = -\frac{E_1 E_2 G_{12}}{Z_{11}}\left[-\frac{\partial^3 \psi}{\partial x^3} + \mu_{12}\frac{\partial^3 \psi}{\partial x \partial y^2}\right]$$

$$= -\frac{E_1 E_2 G_{12}}{Z_{11}}\left[\sum_{m=1}^{\infty} X_m''' \cos\alpha y + \mu_{12}\left\{\sum_{m=1}^{\infty} X_m' \alpha^2 \cos\alpha y\right\}\right]$$

$$= -\frac{E_1 E_2 G_{12}}{Z_{11}}\left[\sum_{m=1}^{\infty}\begin{Bmatrix}\left(r_1^3 + \mu_{12}\alpha^2 r_1\right)A_m e^{r_1 x} + \left(r_2^3 + \mu_{12}\alpha^2 r_2\right)B_m e^{r_2 x} + \\ \left(r_3^3 + \mu_{12}\alpha^2 r_3\right)C_m e^{r_3 x} + \left(r_4^3 + \mu_{12}\alpha^2 r_4\right)D_m e^{r_4 x}\end{Bmatrix}\cos\alpha y\right] \qquad (6.21e)$$

Now, the axial loading on the right edge of the panel can be taken as Fourier series in the following manner:

$$\sigma_{xx}(b,y) = \sigma_{xx}^{o} = \sum_{m=1}^{\infty} E_m \sin\alpha y \qquad (6.22)$$

To satisfy the boundary condition and the loading distribution, Fourier sine series have been considered for the analysis.

$$E_m = \frac{2}{a}\int_0^a \sigma_{xx}^{o} \sin(\alpha y)dy$$

$$= \frac{2\sigma_{xx}^{o}}{a}\int_0^a \sin(\alpha y)dy$$

$$= \frac{2\sigma_{xx}^{0}}{\alpha a}[-\cos(\alpha y)]_0^a$$

$$= \frac{2\sigma_{xx}^{o}}{m\pi}[1-\cos(m\pi)], \text{ where m = 1, 2, 3, 4, 5 } \ldots\ldots\ldots\ldots\ldots \infty$$

Due to symmetry, the axial displacement at the left edge from 0 to (a-h) is zero. But at the cracked edge, the distribution of the axial displacement can be expressed as the Fourier series in the following manner:

$$u_x(0,y) = a_0 + \sum_{i=1}^{3} a_i \cos(i*w*y) + \sum_{i=1}^{3} b_i \sin(i*w*y) = \sum_{m=1}^{\infty} I_m \sin(\alpha y) \qquad (6.23)$$

The curve fitted equation as Fourier series up to 7th term have been considered. This is because of up to 7th term we always achieve R^2 value above 0.99. If we increase the term it will make the mathematical calculation more complicated.

Here

$$I_m = \frac{2}{a}\int_{a-h}^{a}(a_0 + \sum_{i=1}^{3} a_i \cos(i*w*y) + \sum_{i=1}^{3} b_i \sin(i*w*y))\sin(\alpha y)dy$$

After performing integration of the above equation, the result is given below:

$$I_m = \left(\frac{2a_o}{m\pi}\left(\cos\left(\frac{(a-h)m\pi}{a}\right) - \cos(m\pi)\right)\right) + \sum_{i=1}^{3} a_i \begin{pmatrix} \left(\frac{1}{m\pi + iwa}\cos\left(\left(\frac{a-h}{a}\right)(m\pi + iwa)\right)\right) + \\ \left(\frac{1}{m\pi - iwa}\cos\left(\left(\frac{a-h}{a}\right)(m\pi - iwa)\right)\right) - \\ \left(\frac{1}{m\pi + iwa}\cos(m\pi + iwa)\right) - \\ \left(\frac{1}{m\pi - iwa}\cos(m\pi - iwa)\right) \end{pmatrix}$$

$$+ \sum_{i=1}^{3} b_i \begin{pmatrix} -\left(\frac{1}{m\pi - iwa}\sin(m\pi + iwa)\right) + \\ \left(\frac{1}{m\pi - iwa}\sin(m\pi - iwa)\right) + \\ \left(\frac{1}{m\pi + iwa}\sin\left(\left(\frac{a-h}{a}\right)(m\pi + iwa)\right)\right) - \\ \left(\frac{1}{m\pi - iwa}\sin\left(\left(\frac{a-h}{a}\right)(m\pi - iwa)\right)\right) \end{pmatrix}$$

Using boundary condition $\sigma_{xy}(0, y) = 0$ at the edge of $x = 0$, it is found that

$$-\frac{E_1E_2G_{12}}{Z_{11}}\left[\sum_{m=1}^{\infty}\begin{Bmatrix}\left(r_1^3 + \mu_{12}\alpha^2 r_1\right)A_m + \left(r_2^3 + \mu_{12}\alpha^2 r_2\right)B_m + \\ \left(r_3^3 + \mu_{12}\alpha^2 r_3\right)C_m + \left(r_4^3 + \mu_{12}\alpha^2 r_4\right)D_m\end{Bmatrix}\cos\alpha y\right] = 0$$

$$or, \begin{Bmatrix}\left(-E_1E_2G_{12}r_1^3 - \mu_{12}E_1E_2G_{12}\alpha^2 r_1\right)A_m + \left(-E_1E_2G_{12}r_2^3 - \mu_{12}E_1E_2G_{12}\alpha^2 r_2\right)B_m + \\ \left(-E_1E_2G_{12}r_3^3 - \mu_{12}E_1E_2G_{12}\alpha^2 r_3\right)C_m + \left(-E_1E_2G_{12}r_4^3 - \mu_{12}E_1E_2G_{12}\alpha^2 r_4\right)D_m\end{Bmatrix} = 0$$

(6.24)

Using boundary condition $\sigma_{xy}(b,y)=0$ at the edge of $x=b$, it is found that

$$-\frac{E_1E_2G_{12}}{Z_{11}}\left[\sum_{m=1}^{\infty}\begin{Bmatrix}\left(r_1^3+\mu_{12}\alpha^2r_1\right)A_me^{r_1b}+\left(r_2^3+\mu_{12}\alpha^2r_2\right)B_me^{r_2b}+\\ \left(r_3^3+\mu_{12}\alpha^2r_3\right)C_me^{r_3b}+\left(r_4^3+\mu_{12}\alpha^2r_4\right)D_me^{r_4b}\end{Bmatrix}\cos\alpha y\right]=0$$

$$or,\begin{Bmatrix}\left(-E_1E_2G_{12}r_1^3-\mu_{12}E_1E_2G_{12}\alpha^2r_1\right)A_me^{r_1b}+\left(-E_1E_2G_{12}r_2^3-\mu_{12}E_1E_2G_{12}\alpha^2r_2\right)B_me^{r_2b}+\\ \left(-E_1E_2G_{12}r_3^3-\mu_{12}E_1E_2G_{12}\alpha^2r_3\right)C_me^{r_3b}+\left(-E_1E_2G_{12}r_4^3-\mu_{12}E_1E_2G_{12}\alpha^2r_4\right)D_me^{r_4b}\end{Bmatrix}=0$$

(6.25)

Using boundary condition $u_x(0,y)=a_0+\sum_{i=1}^{3}a_i\cos(i*w*y)+\sum_{i=1}^{3}b_i\sin(i*w*y)$ at the edge of $x=0$, it is found that

$$-\sum_{m=1}^{\infty}\left(A_mr_1+B_mr_2+C_mr_3+D_mr_4\right)\alpha\sin\alpha y=\sum_{m=1}^{\infty}I_m\sin(\alpha y)$$

$$or,-\left(A_mr_1+B_mr_2+C_mr_3+D_mr_4\right)\alpha=I_m$$

(6.26)

Using boundary condition $\sigma_{xx}(b,y)=\sigma_{xx}^{o}$ at the edge of $x=b$, it is found

$$-\frac{E_1E_2G_{12}}{Z_{11}}\left[\sum_{m=1}^{\infty}\begin{Bmatrix}\left(\alpha r_1^2+\mu_{12}\alpha^3\right)A_me^{r_1b}+\left(\alpha r_2^2+\mu_{12}\alpha^3\right)B_me^{r_2b}+\\ \left(\alpha r_3^2+\mu_{12}\alpha^3\right)A_me^{r_3b}+\left(\alpha r_4^2+\mu_{12}\alpha^3\right)B_me^{r_4b}\end{Bmatrix}\sin\alpha y\right]=\sum_{m=1}^{\infty}E_m\sin\alpha y$$

$$or,\begin{Bmatrix}\left(\frac{-E_1E_2G_{12}\alpha r_1^2-\mu_{12}E_1E_2G_{12}\alpha^3}{Z_{11}}\right)A_me^{r_1b}+\left(\frac{-E_1E_2G_{12}\alpha r_2^2-\mu_{12}E_1E_2G_{12}\alpha^3}{Z_{11}}\right)B_me^{r_2b}+\\ \left(\frac{-E_1E_2G_{12}\alpha r_3^2-\mu_{12}E_1E_2G_{12}\alpha^3}{Z_{11}}\right)C_me^{r_3b}+\left(\frac{-E_1E_2G_{12}\alpha r_4^2-\mu_{12}E_1E_2G_{12}\alpha^3}{Z_{11}}\right)D_me^{r_4b}\end{Bmatrix}=E_m$$

(6.27)

The simultaneous equations (6.24), (6.25), (6.26) and (6.27) can be realized in a simplified matrix form for the solution of unknown terms like A_m, B_m, C_m and D_m as follows:

$$\begin{bmatrix}DD_1 & DD_2 & DD_3 & DD_4\\ FF_1 & FF_2 & FF_3 & FF_4\\ HH_1 & HH_2 & HH_3 & HH_4\\ KK_1 & KK_2 & KK_3 & KK_4\end{bmatrix}\begin{bmatrix}A_m\\ B_m\\ C_m\\ D_m\end{bmatrix}=\begin{bmatrix}0\\ 0\\ I_m\\ E_m\end{bmatrix}$$

(6.28)

Where

$$DD_i = -E_1E_2G_{12}r_i^3 - \mu_{12}E_1E_2G_{12}\alpha^2 r_i$$

$$FF_i = \left(-E_1E_2G_{12}r_i^3 - \mu_{12}E_1E_2G_{12}\alpha^2 r_i\right)e^{r_i b}$$

$$HH_i = \alpha r_i$$

$$KK_i = \left(\frac{-E_1E_2G_{12}\alpha r_i^2 - \mu_{12}E_1E_2G_{12}\alpha^3}{Z_{11}}\right)e^{r_i b}$$

Solution of the above matrix Eq. (6.28) yields the unknown constants A_m , B_m , C_m and D_m . Once the value of the unknowns are determined, they are directly substituted in Eqs.[6.21(a)-6.21(e)] to obtain the explicit expressions for the different parameters of interest, namely, the two displacement and the three stress components at various points.

6.4 Analysis of Elastic Field

The stress and displacement fields of the composite panel are discussed in this section. For this we have considered on the fiber orientation θ=0^o. In this case the Boron-epoxy has been chosen as the material of the composite panel and its properties are given below:

Table 1: Effective properties of boron/epoxy composite

Young's modulus (MPa)		Shear modulus (MPa)	Poisson's ratio	
E_1	E_2	G_{12}	μ_{12}	μ_{21}
204×10^3	18.5×10^3	5.59×10^3	0.23	0.021

It is worthy to mention that although the formulation can be applied to any composites, boron/epoxy is chosen merely as an example. As the present study primarily focuses on the effect of the fiber orientation on the elastic field of the panel, all results are calculated for the constant value of the crack length ratio h/a = 0.25 and the aspect ratio b/a = 1.0, i.e., the effect of aspect ratio is not analyzed in the

study. Furthermore, all the results presented in the study correspond to the value of applied uniform tensile load σ_o = 40 MPa.

Fig. 6.3 illustrates the normalized axial displacement component u_x/b with respect to *y* at different sections of the panel. The displacement u_x is zero at both upper and bottom stiffened edges. The magnitude of the displacement u_x is maximum at the right lateral edge *x/b* = 1.0. Here an important observation is that the effect of crack is noticeable for all sections of the panel. The effect is higher near the crack surfaces than it decreases towards the loading edges. It is shown that displacement is positive at all sections that mean the panel is subjected to tension. Fig. 6.4 describes the normalized displacement component u_y/a at different sections of the panel. It can be seen that the effect of edge crack is significant up to $x/b \leq 0.2$ on the normalized lateral displacement component. For sections $0 \leq y/a \leq 0.5$, the displacement u_y/a is positive and for sections $0.5 \leq y/a \leq 1.0$, it is negative for all sections except *x/b* = 1.0. That indicates that the panel is under contraction along *y*-axis that complies with Poisson's formula. But at section *x/b* = 1.0 the reverse is found i.e. the panel is expanded in the *y*-direction, which is in contrast to our general intuition and may be attributed to the physical conditions of the stiffened under tension.

The distribution of normalized axial stress component σ_{xx}/σ_o at different sections of the panel is shown in Fig. 6.5.There is a huge fluctuation of stress due to stress concentration near the crack tip at section *x/b* = 0.0. Then fluctuation diminishes as moving towards the loading edges. At the right lateral the normalized value of axial stress is constant one that complies with the physical condition of the panel. Fig. 6.6 presents the distribution of normalized lateral stress component σ_{yy}/σ_o which reflects the same incident at the crack tip as discussed earlier. The axial displacement at mid region of the panel over the region of $0.25 \leq y/a \leq 0.75$ is almost equal to one but for that region lateral displacement is nearly equal to zero except section of *x/b* = 1.0. That's why the stress component σ_{xx} is more significant than the stress σ_{yy}.

Fig. 6.7 reveals the distribution of normalized shear stress component σ_{xy}/σ_o at different sections of the panel. The shear stress distribution would be symmetric with

respect to y but that did not happened for this panel due to presence of crack. That's why the distribution is not symmetric. Due to singularity effect of crack a fluctuation of shear stress happens near the crack tip. Besides that the magnitude of the shear stresses increases near the stiffened edges. But that magnitude is higher near the upper stiffened edge because of the presence of crack. At the sections x/b = 0.0 and x/b = 1.0, the magnitude of the shearing stress is zero which satisfies the physical boundary conditions of the problem. Here another observation is that over the region $0.25 \leq y/a \leq 0.65$ the normalized shear stress is nearly zero which we have also found in case of normalized lateral stress component.

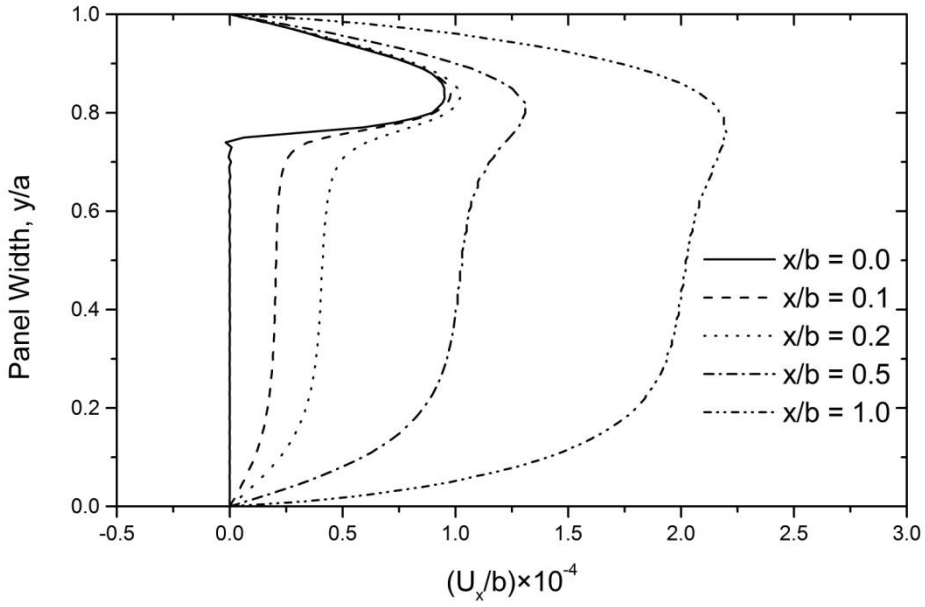

Fig 6.3: Distribution of normalized axial displacement at different sections of the composite panel. ($\theta = 0^o$, b/a =1, h/a =0.25)

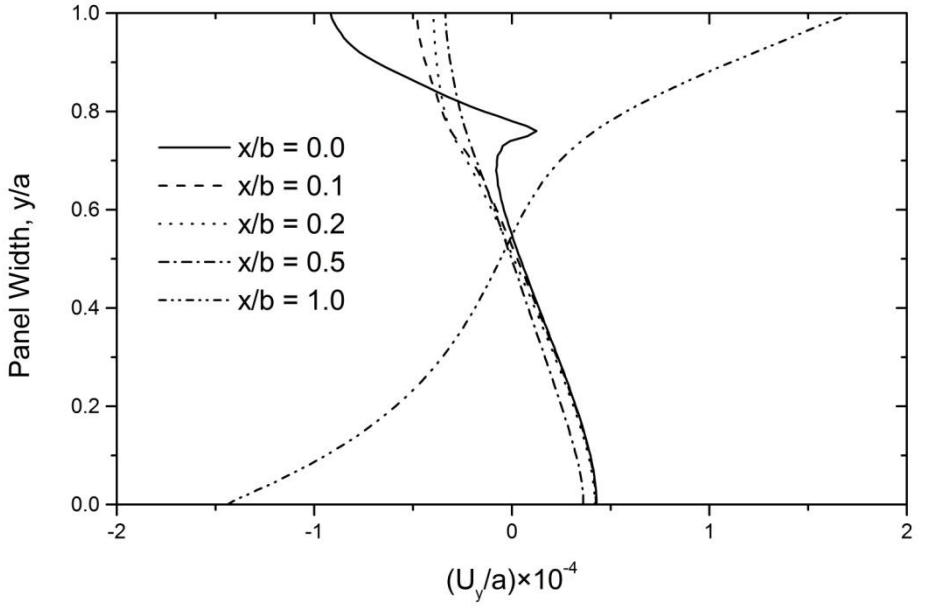

Fig 6.4: Distribution of normalized lateral displacement at different sections of the composite panel.($\theta = 0^o$, b/a =1, h/a =0.25)

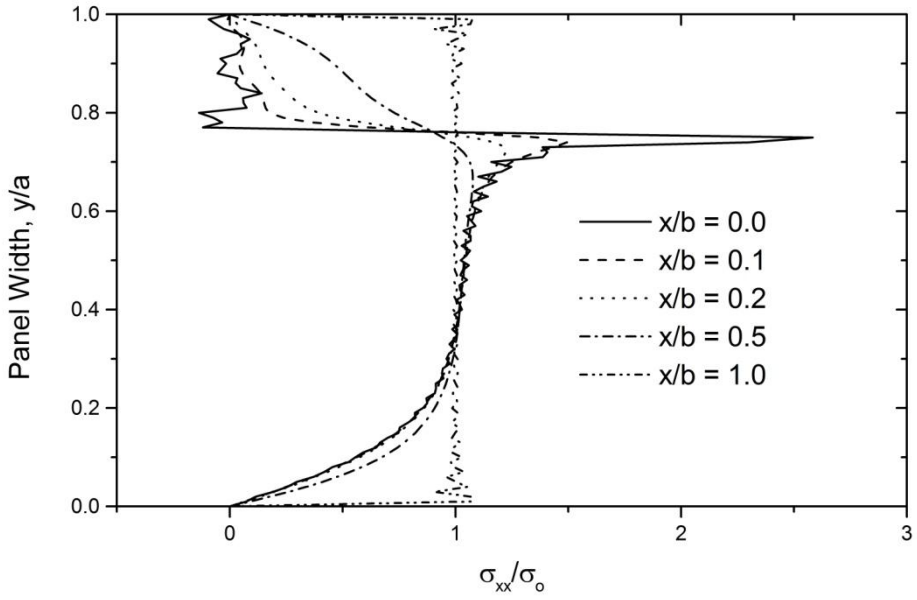

Fig 6.5: Distribution of normalized axial stress at different sections of the composite panel. ($\theta = 0^o$, b/a =1, h/a =0.25)

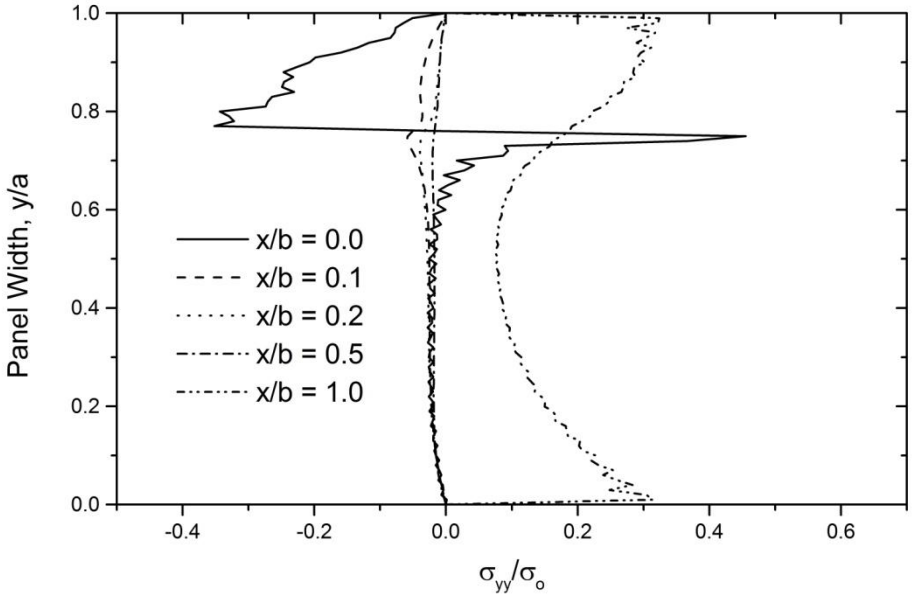

Fig 6.6: Distribution of normalized lateral stress at different sections of the composite panel. ($\theta = 0^o$, b/a =1, h/a =0.25)

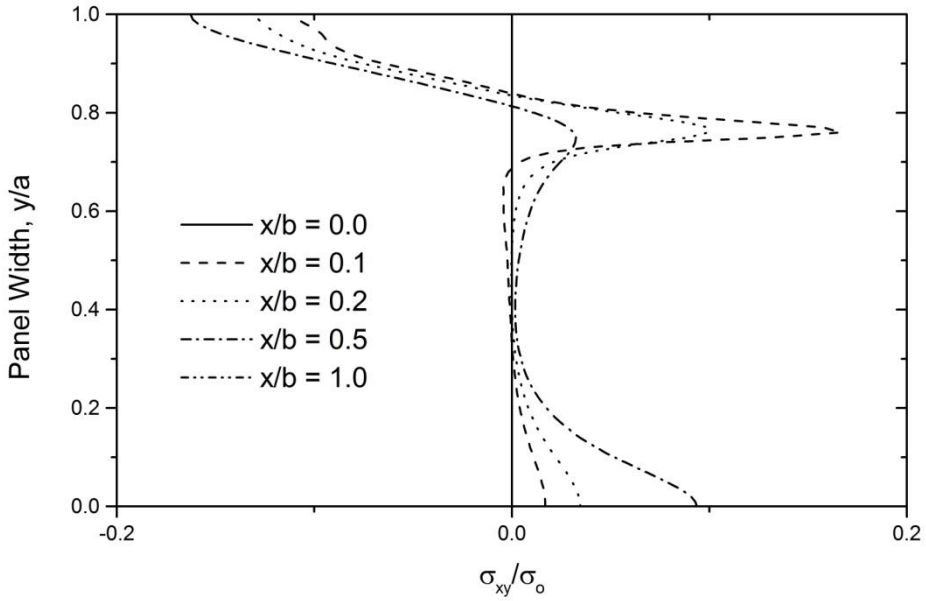

Fig. 6.7: Distribution of normalized shear stress at different sections of the composite panel. ($\theta = 0^o$, b/a =1, h/a =0.25)

6.5 Effect of Fiber Orientation

Effect of fiber orientation on displacement and stress are analyzed in this article. Two different orientations, θ = 0^o and 90^o, are taken into account for the purpose of analysis. Fig. 6.8 shows the comparison of the normalized axial stress component σ_{xx}/σ_o at the sections *x/b* = 0.0, 0.1, 0.5 and 1.0 for two different fiber orientations. At the two stiffened edges, the axial stress σ_{xx} is zero, which is in good agreement with physical conditions applied to the panel. It is noted that the axial stress σ_{xx} is much higher for θ = 0^o fiber orientation at all sections except *x/b* = 1.0. This conforms to the fact that the stiffness of the panel is much higher in the fiber direction which causes less deformation in that direction. The higher magnitude of σ_{xx} is attributed to the higher stiffness in the fiber direction i.e. a small displacement causes a higher stress to develop in the fiber direction. At section *x/b* = 1.0 the magnitude of σ_{xx} is same for both the fiber orientation. But from those figures, another important point can be observed that effect of crack on the normalized axial stress is noticeable section at sections *x/b* = 0.0, 0.1 and 1.0 for θ = 0^o fiber orientation but at section *x/b* = 0.5 it effects vanishes for θ = 90^o fiber orientation. The lower stiffness material i,e, softer material absorbs large amount of energy at the expense of large deformation as quickly that have been happened in this case due to presence of crack. The fluctuation of axial stress near the crack tip is much less for 90^o fiber orientation.

Fig. 6.9 presents the distribution of normalized lateral stress component σ_{yy}/σ_o at the sections *x/b* = 0.0, 0.1, 0.5 and 1.0. The magnitude of the lateral stress is higher for 90^o fiber orientation because of the same reason discussed earlier for Fig. 6.8. In general, the stress is higher in fiber direction while the displacement is lower in fiber direction. It can be seen that the effect of crack on lateral stress is not visible for θ = 90^o fiber orientation at section *x/b* = 0.5 which is in contrast to what have been discussed earlier. This is because of crack surface is parallel to the fiber orientation for θ = 90^o fiber orientation. At loading edge, the normalized lateral stress is huge compared to the axial stress and even that stress induced at the crack tip that is almost 3.5 times of the applied load.

The magnitude of shear stress at section of x/b = 0.5 is higher for θ = 90^o fiber orientation as shown in Fig. 6.10(b). But at section of x/b = 0.0 shear stress is higher over the region 0.6≤ $y/a \leq 1.0$ for 0^o fiber orientation but it is less for the rest of region at the same section for same fiber orientation.

The normalized displacement component u_x/b at the sections x/b = 0.0, 0.1, 0.5 and 1.0 is shown in Fig. 6.11. At the two stiffened edges, the axial displacement component is zero, which satisfies the physical boundary conditions of the problem. The magnitude of u_x is much higher for θ = 90^o fiber orientation as the fibers are not aligned in the displacement direction. At crack surface, the axial displacement is same for two different fiber orientations.

Shown in Fig. 6.12 is the normalized displacement component u_y/b at different sections of the panel for two different fiber orientations. The displacement is greater for θ = 0^o fiber orientation at all sections except x/b = 1.0 because the stiffness in perpendicular to fiber direction is lower than that of fiber direction. Thus, the displacement in low stiffness direction will be obviously higher. But at sections, the graph shows an unlikely phenomenon that is the lateral displacement is higher for 90^o fiber orientation but it reversed.

Figure 6.13 shows the deformed shape of the panel under uniform loading at the left and right edges with the magnification of 200 times of displacement. Since the panel is subjected to axial loading it must be obvious that it is elongated with the reduction of the width due to the effect of Poisson's ratio. The panel with θ = 90^o fiber orientation is elongated more in *x*-direction compared to θ = 0^o fiber orientation which is significant than the deformation happened in *y*-direction.

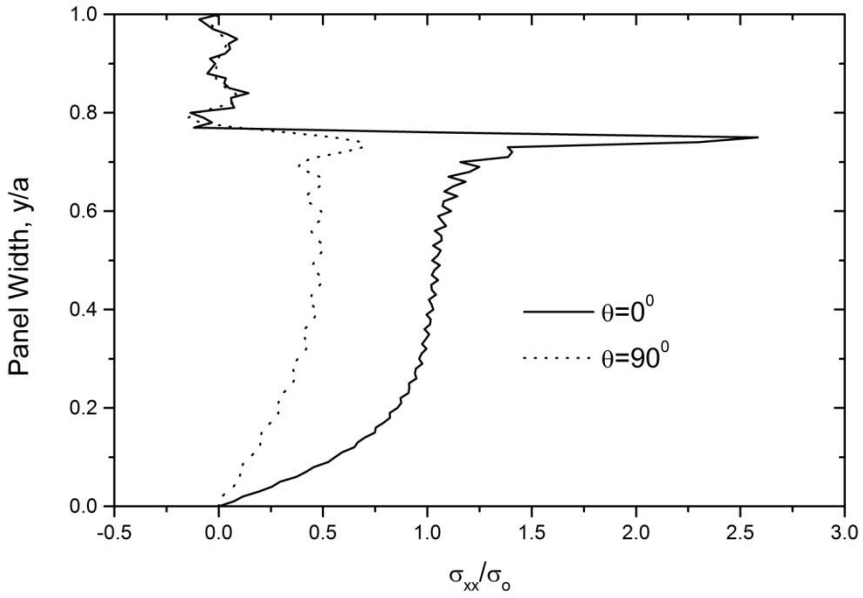
Panel Width, y/a
1.0
0.8
0.6
0.4
0.2
0.0
-0.5
0.0
0.5
1.0
1.5
2.0
2.5
3.0
θ=0⁰
θ=90⁰
σxx/σo

(a)

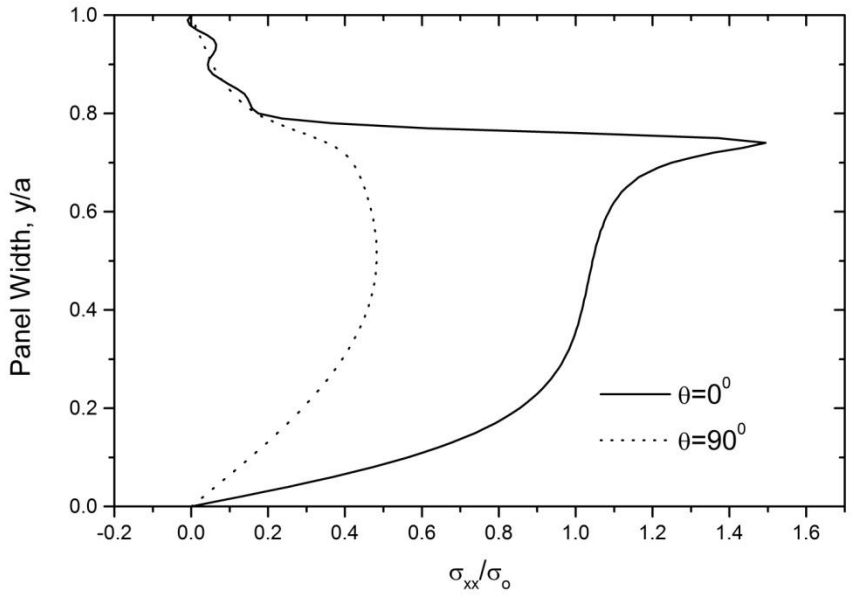
Panel Width, y/a
1.0
0.8
0.6
0.4
0.2
0.0
-0.2
0.0
0.2
0.4
0.6
0.8
1.0
1.2
1.4
1.6
θ=0⁰
θ=90⁰
σxx/σo

(b)

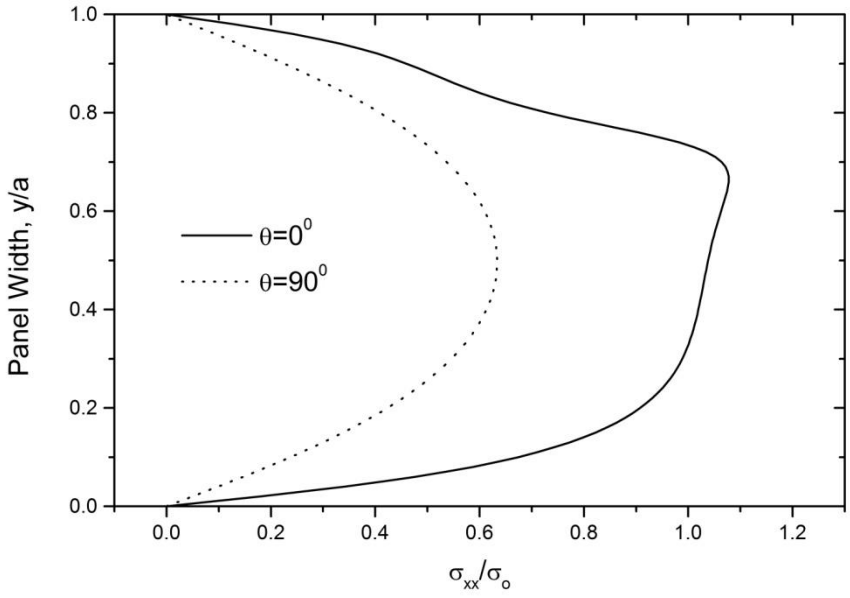

(c)

Fig 6.8: Distribution of Normalized Axial Stress at sections (a) *x/b* = 0.0, (b) *x/b* = 0.1 and (c) *x/b* = 0.5 of the composite panel (*b/a* = 1, *h/a* = 0.25).

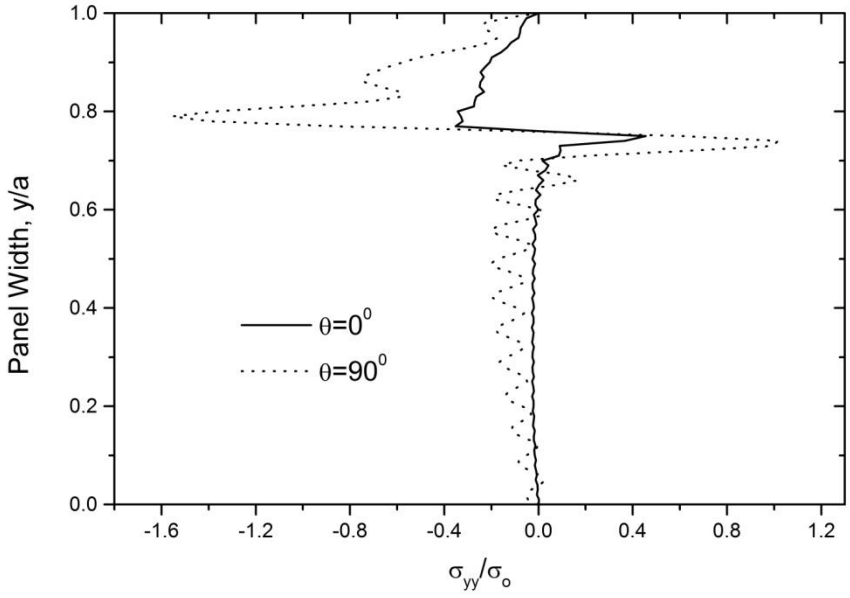

(a)

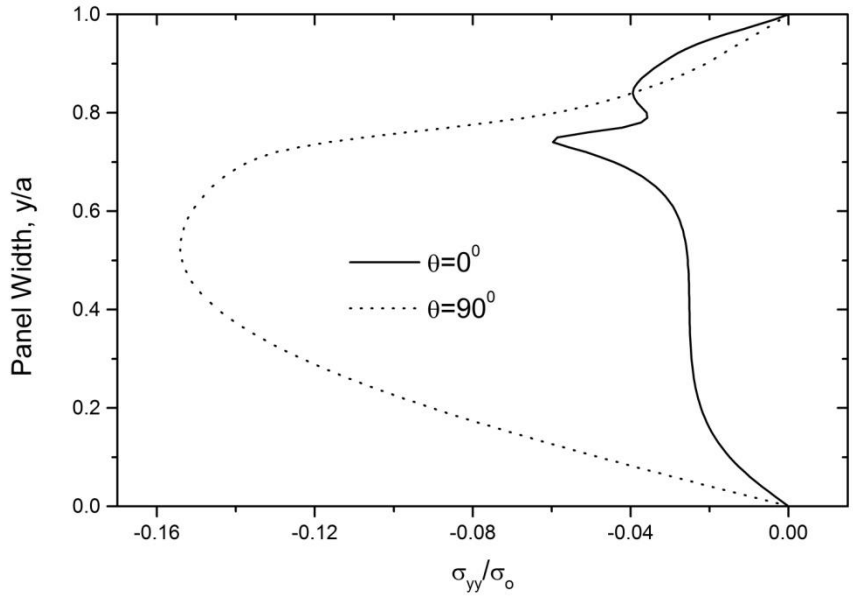

(b)

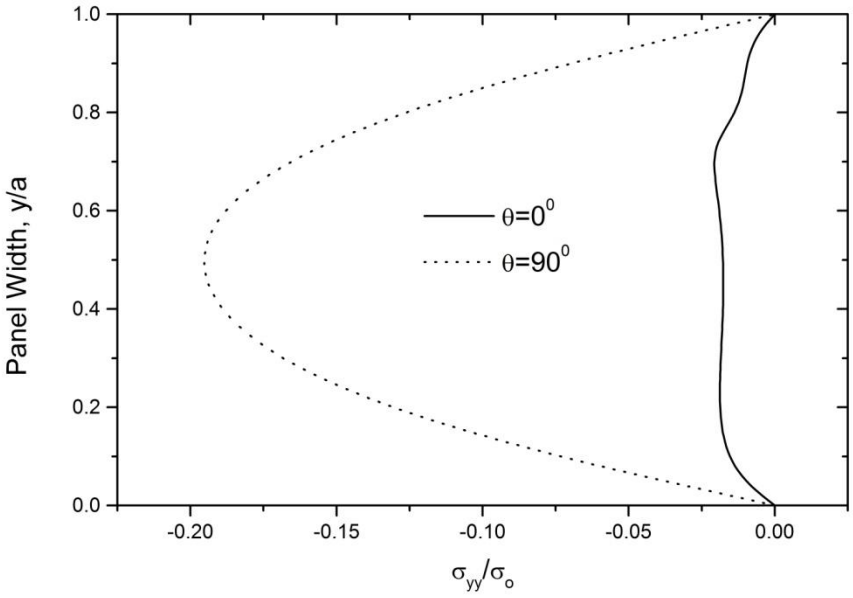

(c)

Fig 6.9: Distribution of Normalized Lateral Stress at sections (a) *x/b* = 0.0, (b) *x/b* = 0.1 and (c) *x/b* = 0.5 of the composite panel (*b/a* = 1, *h/a* = 0.25).

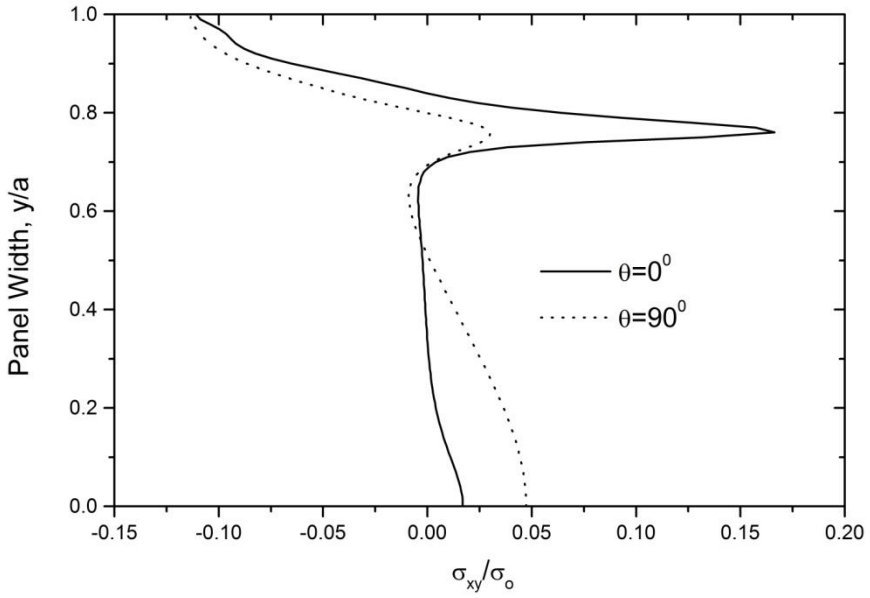

(a)

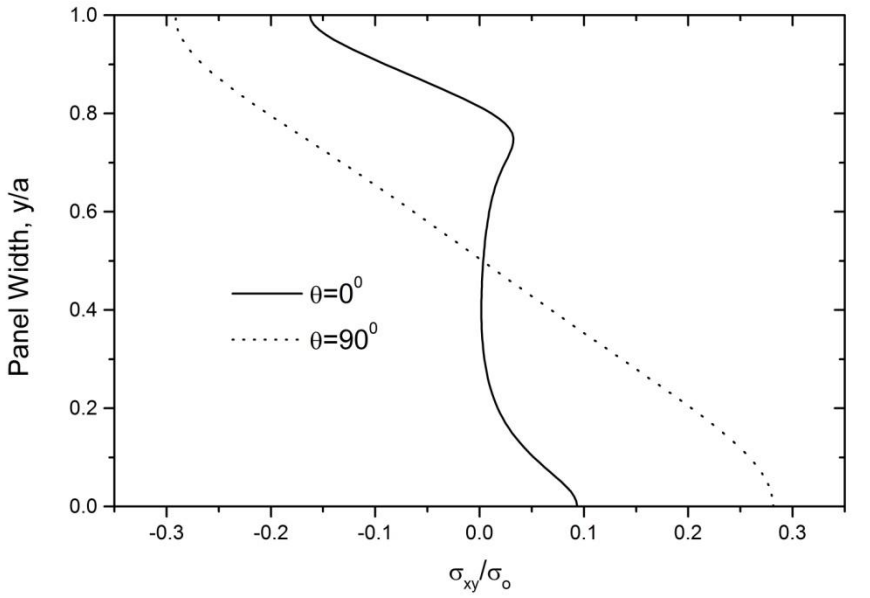

(b)

Fig 6.10: Distribution of Normalized Shear Stress at sections (a) *x/b* = 0.1 and (b) *x/b* = 0.5 of the composite panel (*b/a* = 1, *h/a* = 0.25).

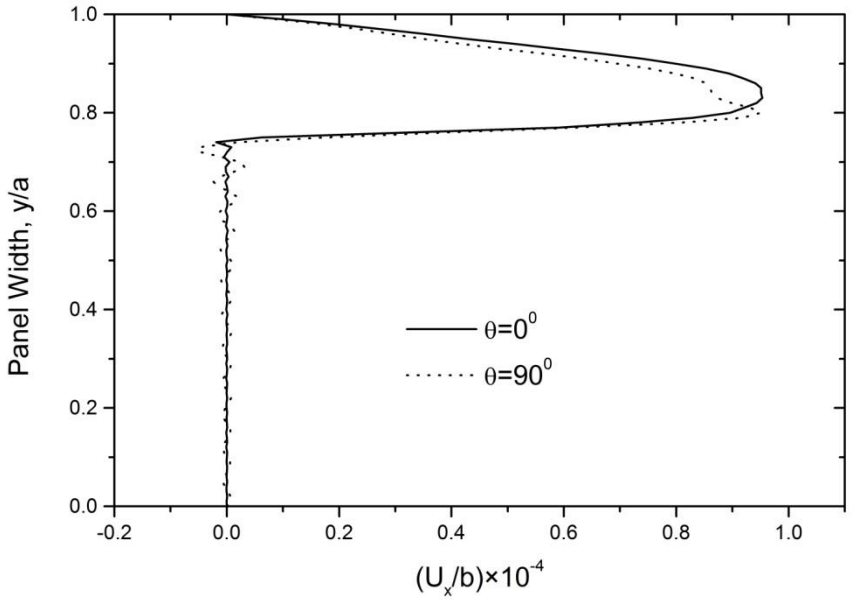
Panel Width, y/a
θ=0⁰
θ=90⁰
(Ux/b)×10⁻⁴

(a)

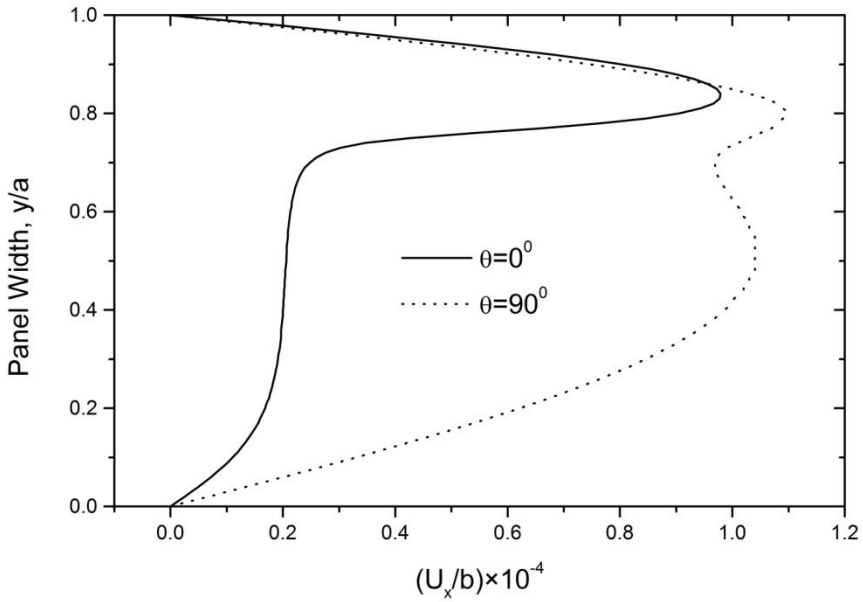
Panel Width, y/a
θ=0⁰
θ=90⁰
(Ux/b)×10⁻⁴

(b)

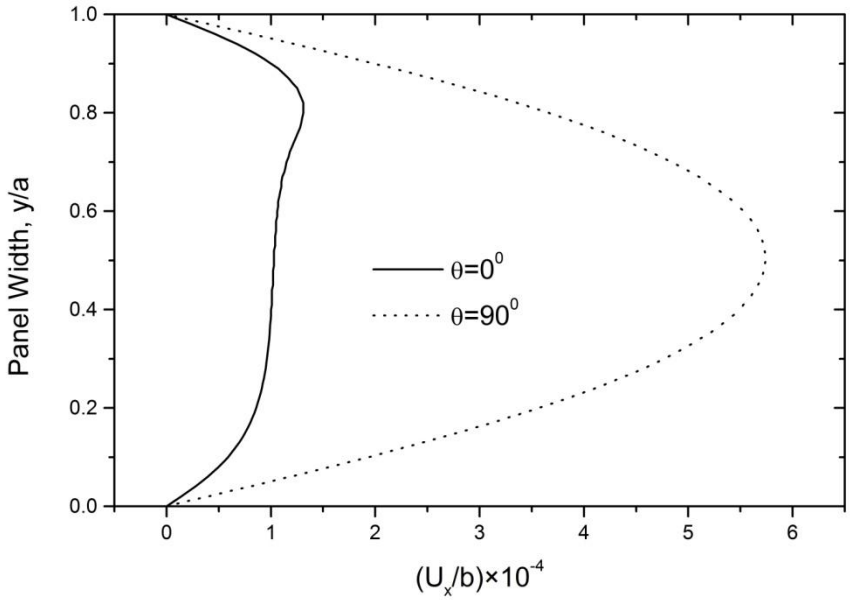

(c)

Fig 6.11: Distribution of Normalized Axial Displacement at sections (a) *x/b* = 0.5, (b) *x/b* = 0.5 and (c) *x/b* = 1.0 of the composite panel (*b/a* = 1, *h/a* = 0.25).

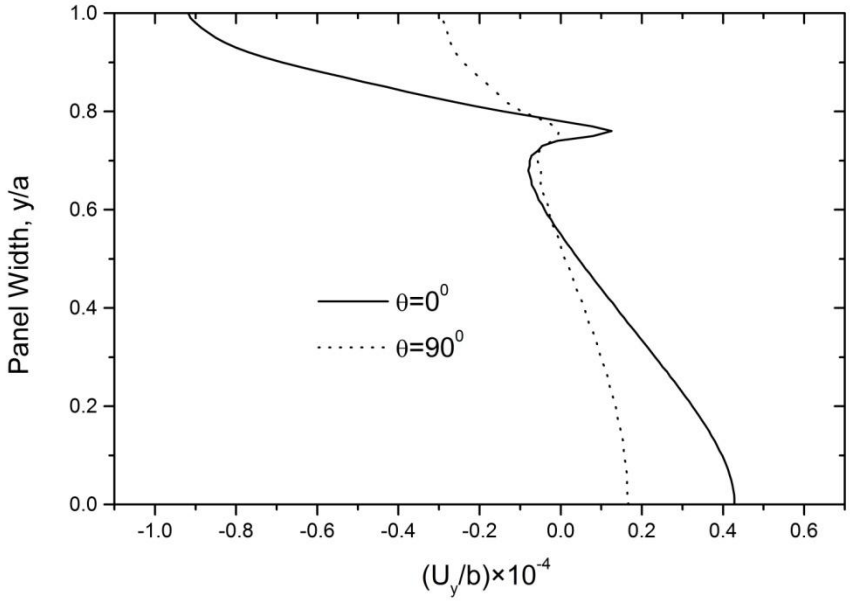

(a)

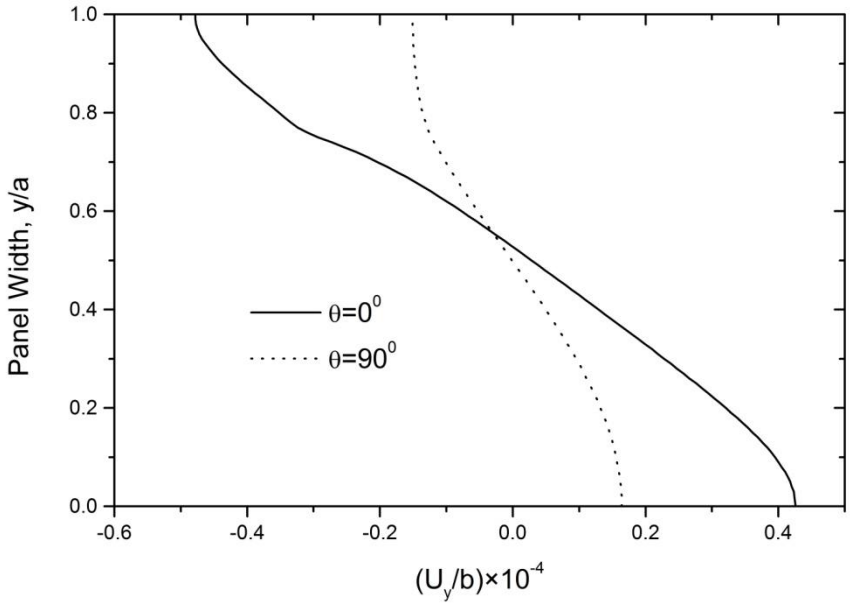

(b)

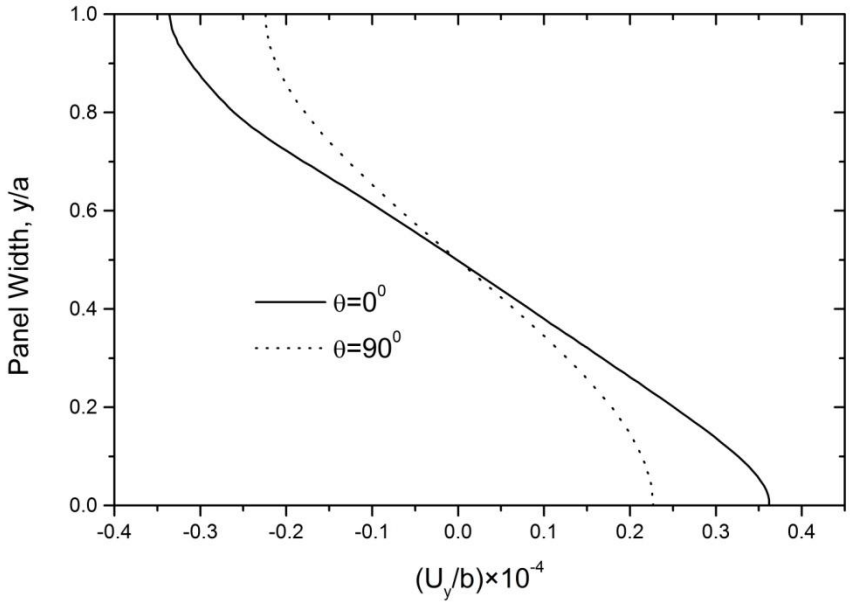

(c)

Fig 6.12: Distribution of Normalized Lateral Displacement at sections (a) *x/b* = 0.0, (b) *x/b* = 0.1 and (d) *x/b* = 0.5 of the composite panel (*b/a* = 1, *h/a* = 0.25).

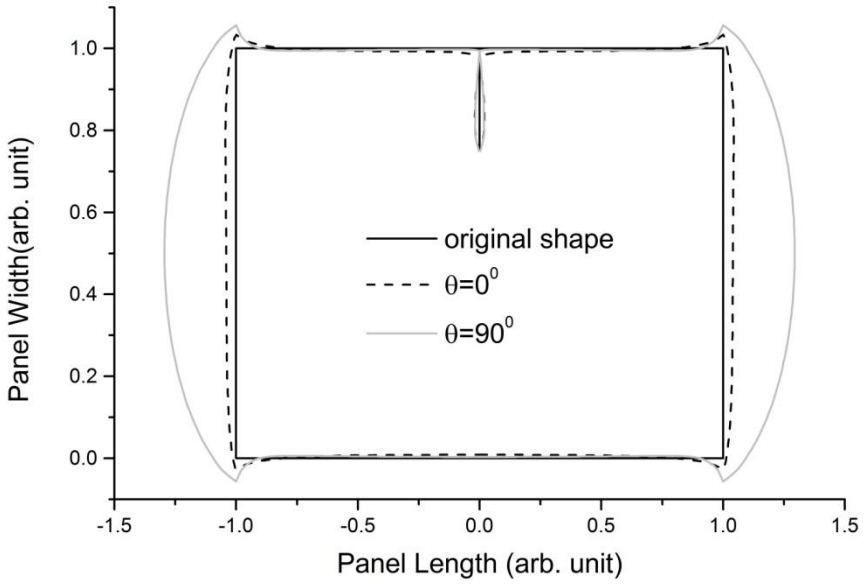

.

Fig 6.13: Deformed shape of the cracked stiffened panel of Boron-epoxy, (*b/a* = 1, *h/a* = 0.25) ,(magnification factor × 200).

6.6 Effect of Crack Length on the Stress and Displacement Fields (Case-A)

The effect of crack length (h/a = 0.0 ~ 0.4) on the displacement and stress fields of the panel for fiber orientation ($\theta = 0^o$) is discussed in this section. As the result have found in the previous chapters, the same trends are found in this sections i.e. the effect of crack length on displacement and stress fields increases with the increase of crack length.

Figs. 6.14 to 6.16 present the distribution of stress with the variation of crack length at two different sections of the panel. No fluctuation of stress happens without presence of crack. Crack tip induces higher axial stress than the value found in case of isotropic material. Because composite material posses higher strength along the fiber direction. As a result of this, axial displacement is lower compared to isotropic material.

At crack length, h/a = 0.1, its effect on the stress and displacement fields is less noticeable and shows a slight deviation from the solution for zero crack length. Crack length effect gradually increases with its length. The distribution of normalized axial displacement for different crack length is shown in Fig. 6.17.

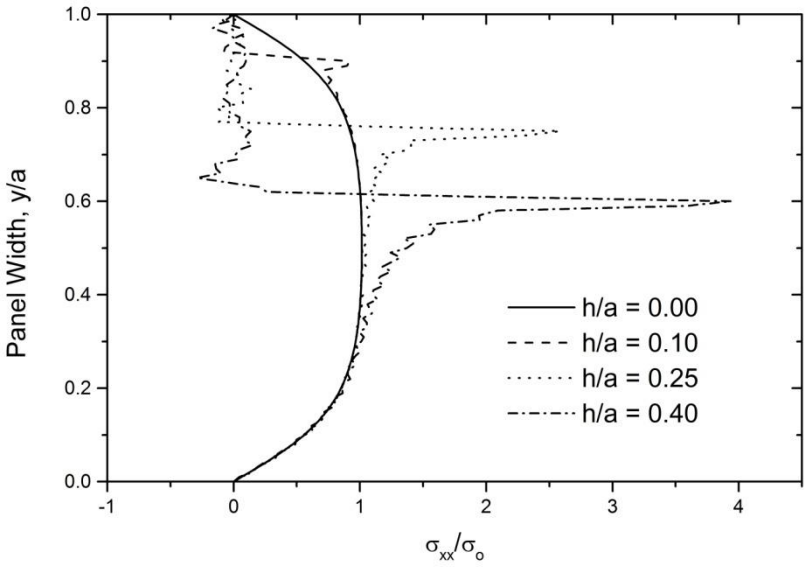

(a)

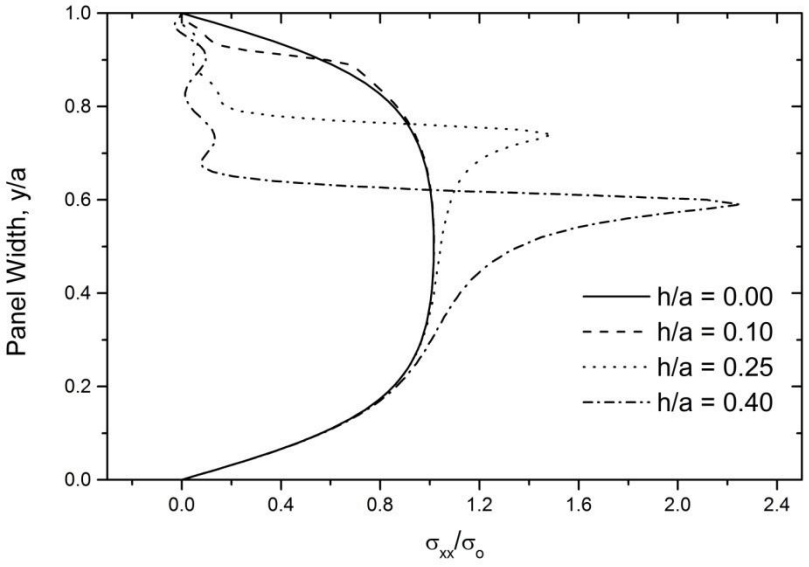

(b)

Fig 6.14: Effect of crack length on the axial stress component at (a) *x/b* = 0.0 and (b) *x/b* = 0.1 ($\theta=0^o$).

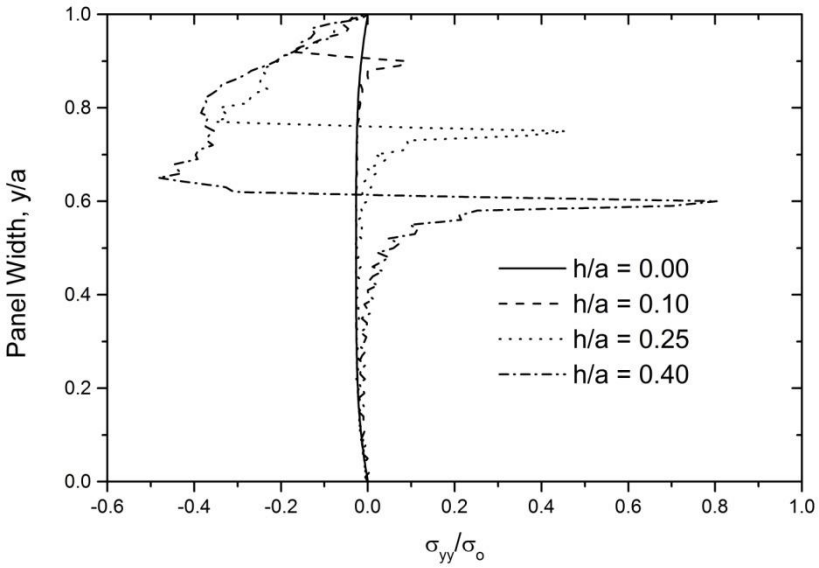

(a)

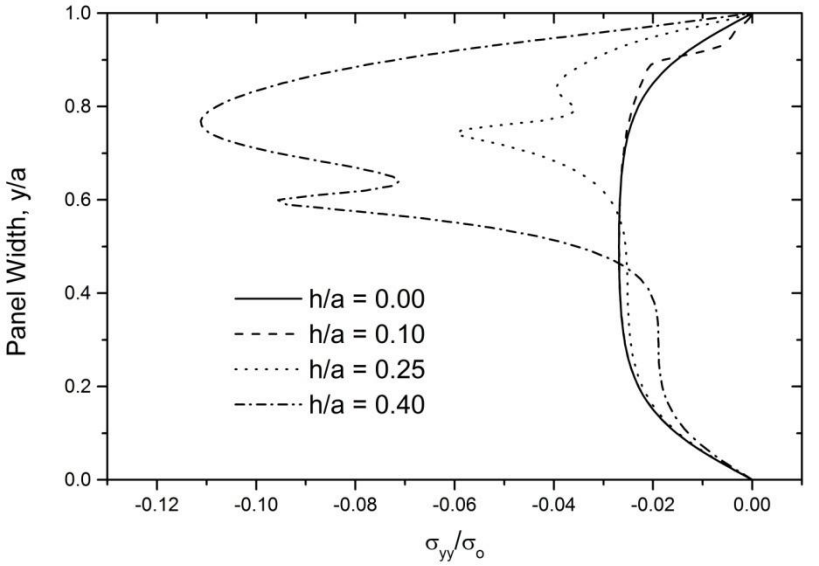

(b)

Fig 6.15: Effect of crack length on the lateral stress component at (a) x/b = 0.0 and (b) x/b = 0.1 ($\theta=0^o$).

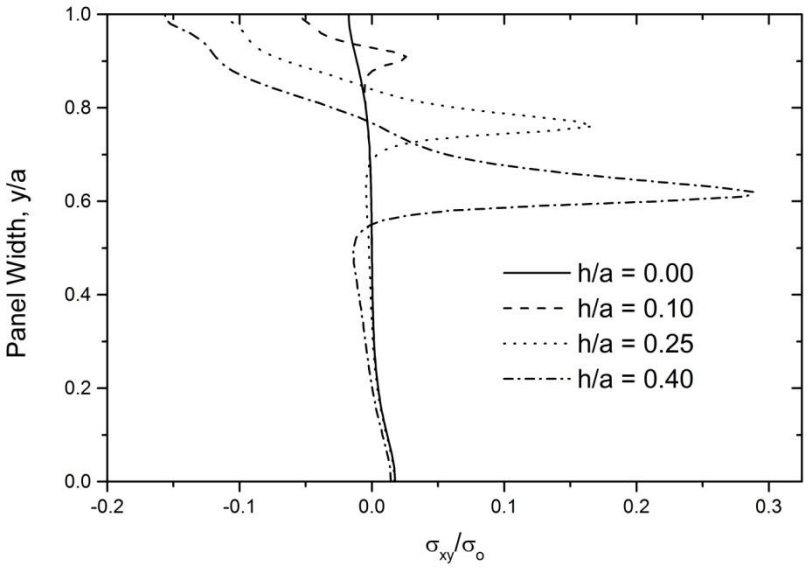

(a)

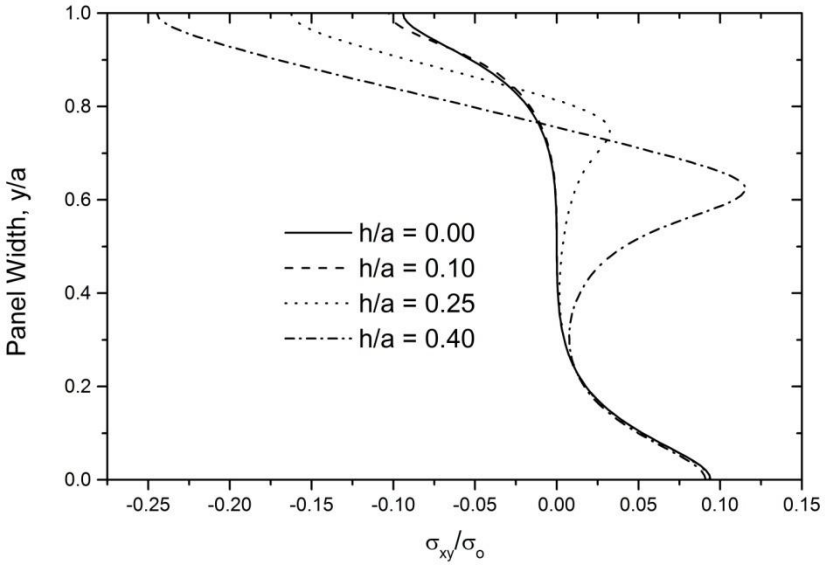

(b)

Fig 6.16: Effect of crack length on the shear stress component at (a) x/b = 0.1 and (b) x/b = 0.5 ($\theta=0^o$).

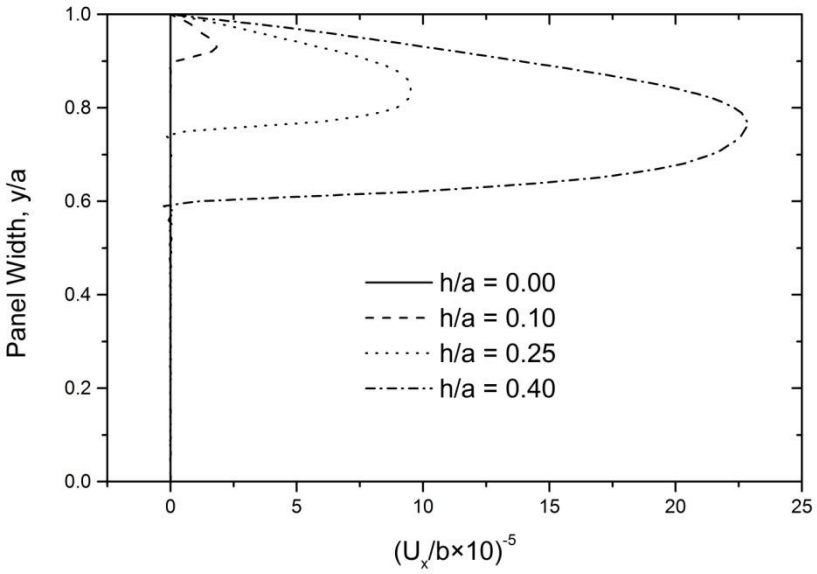

(a)

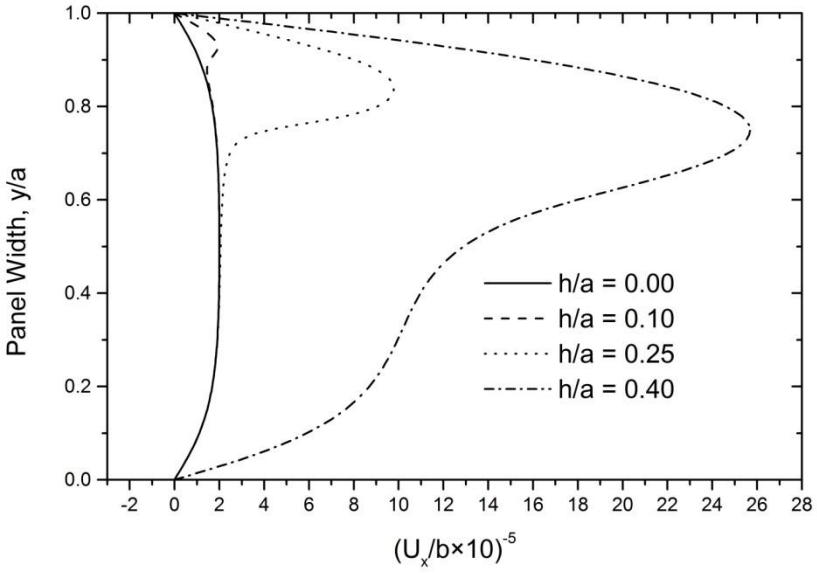

(b)

Fig 6.17: Effect of crack length on the axial displacement component at (a) x/b = 0.0 and (b) x/b = 0.1 ($\theta=0^o$).

CHAPTER 7

COMPARISON OF RESULTS

To verify the accuracy and reliability of the method proposed, a number of problems are analyzed. For all the problems the results obtained by Potential Function approach are now compared with the corresponding numerical solutions obtained by FEM and FDM. Finite difference formulation will be slightly discussed here because it is not the major concern in this study that had been already formulated in several previous works [22]. Those works of FDM formulation have been used to find the solution of elastic field of all problems.

Furthermore, as the analytical results have been discussed in details in the previous chapter, this chapter analyses basically the agreement of the results of the displacement potential method and numerical methods without paying attention to the characteristics of the results.

7.1 Finite Difference Method

Finite difference solutions are obtained on the basis of present displacement potential approach. The region of interest in which the potential function ψ is to be evaluated is divided into a desirable number of mesh points and the values of the function are sought only at these points. A uniform rectangular mesh network is used to discretize the panel domain. The number of meshes used in the *x* and *y* directions are 61 and 41 respectively. An imaginary boundary, exterior to the physical boundary of the panel, is considered for the present discretization. The fourth-order partial derivatives of the governing differential equation (Eqns. 2.30, 2.32 and 2.34) are expressed by their corresponding central difference formulae whereas, in an attempt to avoid the inclusion of points exterior to the imaginary boundary, the second and third-order derivatives associated with the boundary expressions are replaced by their

corresponding backward or forward difference formulae, keeping the order of local truncation error the same. The discrete values of the potential function $\psi(x,y)$ are solved from the system of linear algebraic equations by the direct method of solution (triangular decomposition method). Since all the components of stress and displacements are expressed in terms of function ψ, the parameters of interest are readily calculated from the values of ψ obtained at the mesh points of the domain. The detailed computational scheme for the discretization of the domain, management of boundary conditions, evaluations of the parameters of interest are given in references [17-19, 22].

7.2 Finite Element Method

Finite-element method is widely used all over the world for various computational purposes in lab and commercial areas. In this study, ANSYS has been used to solve several problems in order to compare and verify the analytical results. The relevant boundary conditions used are the same as those used in the analytical solution. Four noded rectangular plane elements are used to construct the corresponding mesh network of the panel. The total number of finite elements used to construct the element mesh network for all problems is 10000 (100×100). All the elements are of the same size and their distribution is kept uniform all over the domain. The convergence and accuracy of the solution has been verified by varying the number of finite elements used to model the panel.

7.3 Cracked Panel under Axial Stiffeners Subjected To Axial Tension

A steel panel with aspect ratio b/a = 1, crack length ratio h/a =0.2 and the uniform loading parameter,σ_o = 40 MPa has been chosen for the comparison. As it can be seen form Fig. 7.1 the deflection is defined among the results obtained by FEM, FDM and those calculated by Displacement Potential Method is small. A good agreement between the analytical and numerical results can be realized from Figs. 7.1-7.5. Those figures show the comparison of normalized displacement components

and normalized stress components at four different sections of the panel. One can see that even at the crack tip, which is a point of singularity, the results are almost the same. Basically the ψ-solution and FEM indicate that the axial and lateral stresses at the crack tip fluctuate to highest value. But the effect is less noticeable for the FDM solution. These discrepancies are also found at the load termination end even though it follows the similar trends of FEM and ψ-solution. Slight discrepancies of the results of FEM with those of the present analytical and FEM solution can be attributed to the fact that the FDM solutions are obtained using a relatively lower mesh density compared to that of FEM solution. The result of the present method exactly conforms to the results of FEM. The present ψ-solution is free from the limitation and provides reliable and accurate results at any section of the isotropic panel. But there is a good agreement found among all the methods for axial and lateral displacement, which are shown in Figs. 7.4 and 7.5.

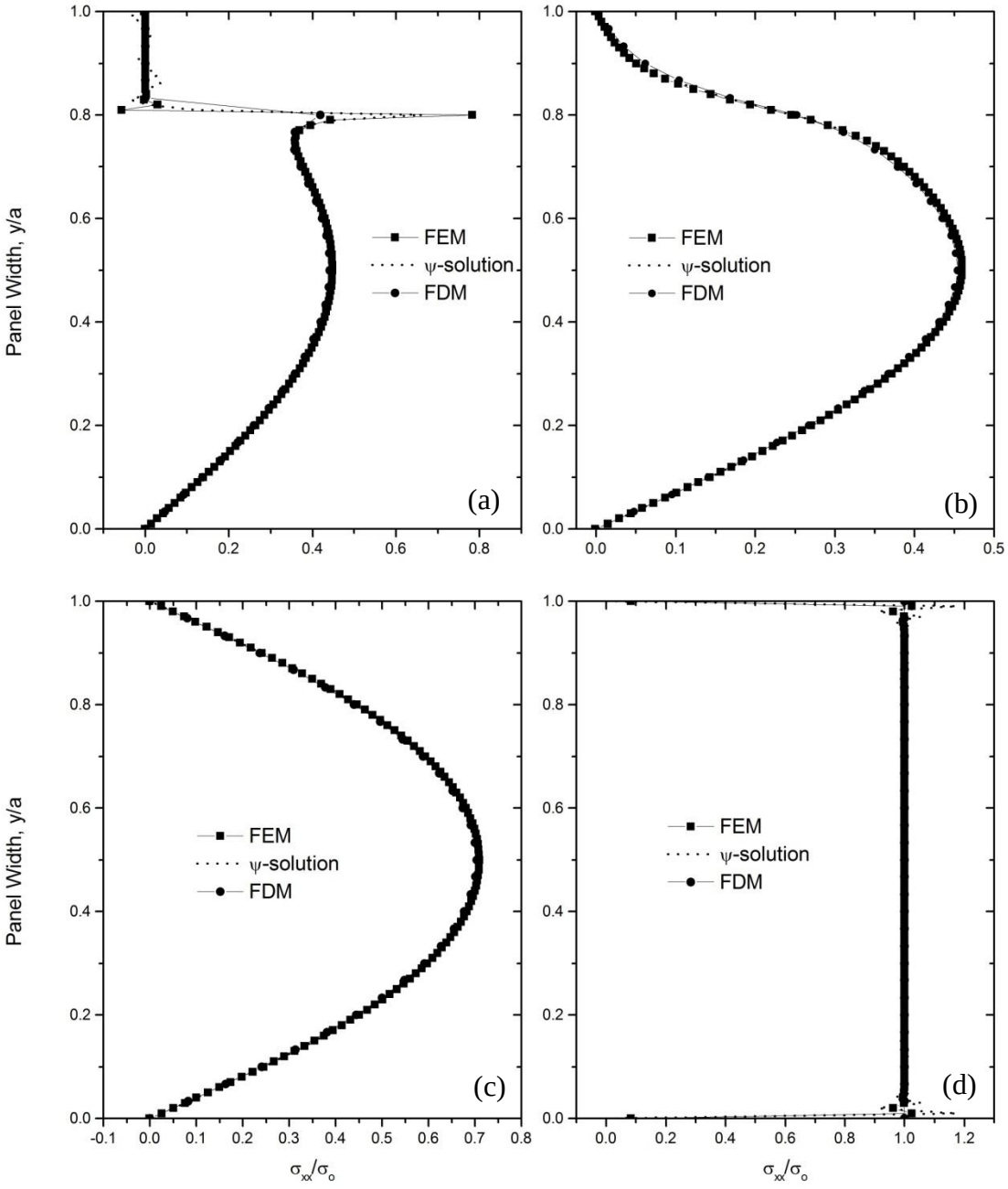

Fig. 7.1: Comparison of normalized axial stress at section (a) *x/b* = 0.0 (b) *x/b* = 0.1 (c) *x/b* = 0.5 and (d) *x/b* = 1.0 of the stiffened (axial) steel panel (*b/a* = 1, *h/a* = 0.2).

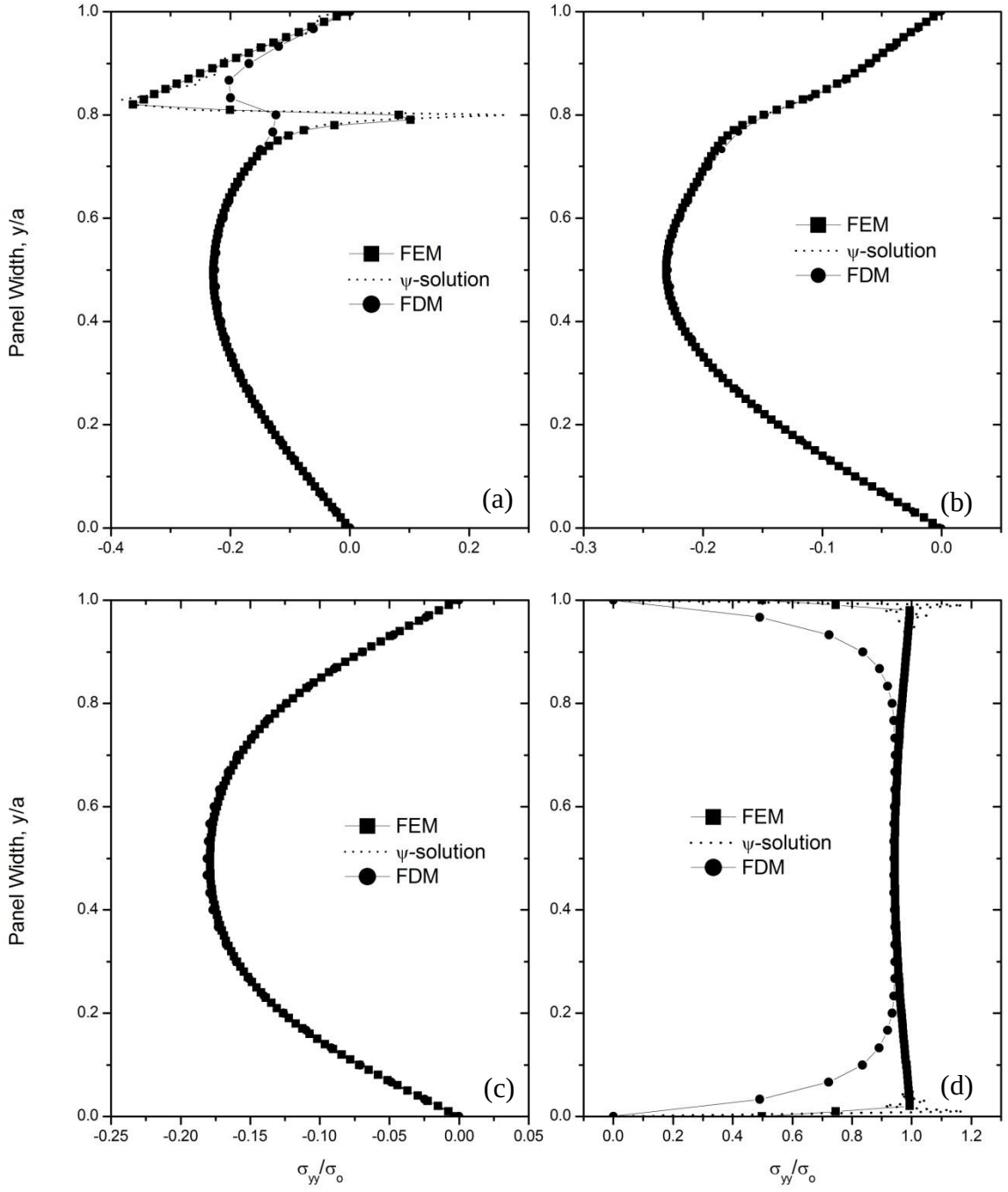

Fig. 7.2: Comparison of normalized lateral stress at section (a) *x/b* = 0.0 (b) *x/b* = 0.1 (c) *x/b* = 0.5 and (d) *x/b* = 1.0 of the stiffened (axial) steel panel (*b/a* = 1, *h/a* = 0.2).

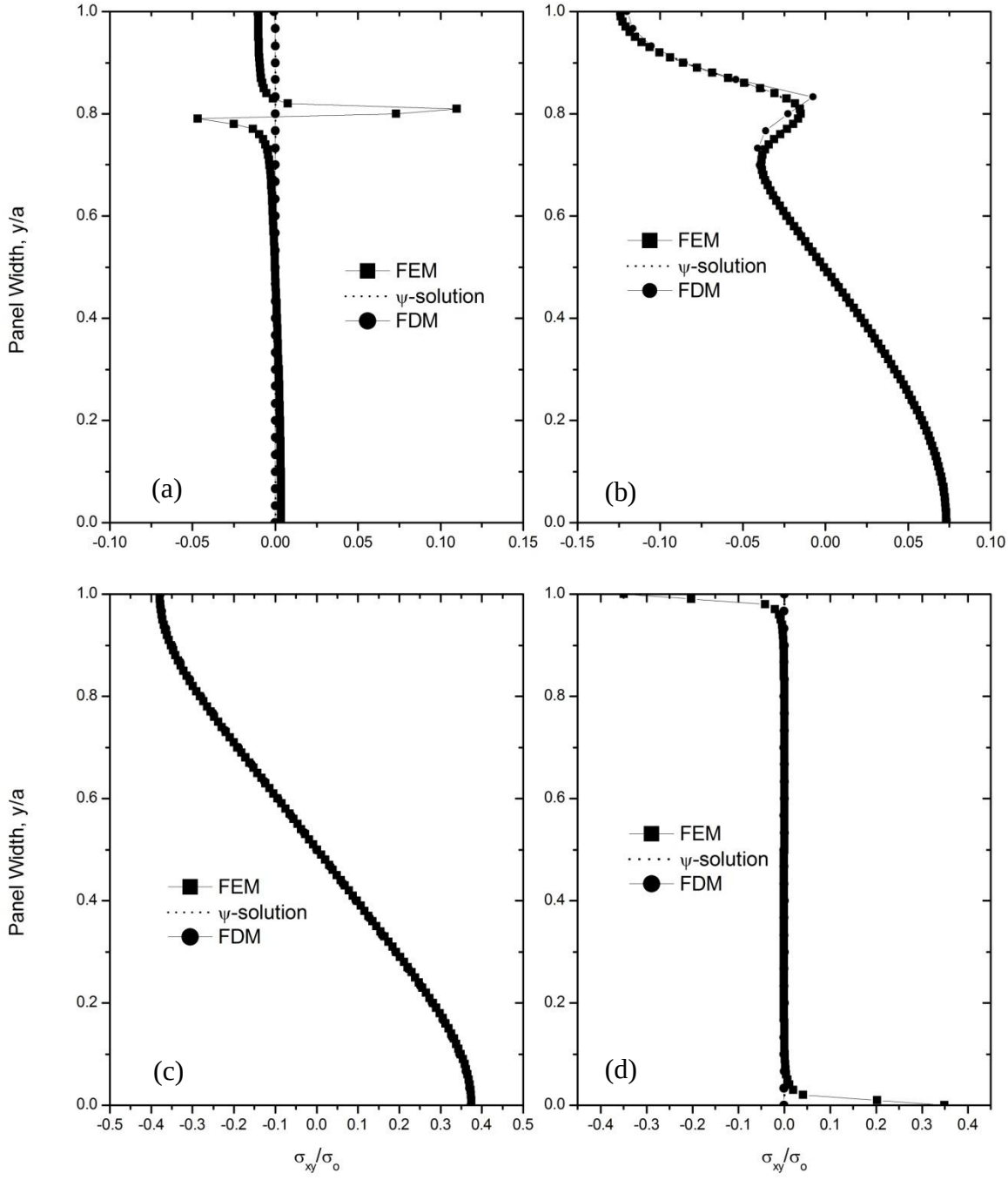

Fig. 7.3: Comparison of normalized shear stress at section (a) *x/b* = 0.0 (b) *x/b* = 0.1 (c) *x/b* = 0.5 and (d) *x/b* = 1.0 of the stiffened (axial) steel panel (*b/a* = 1, *h/a* = 0.2).

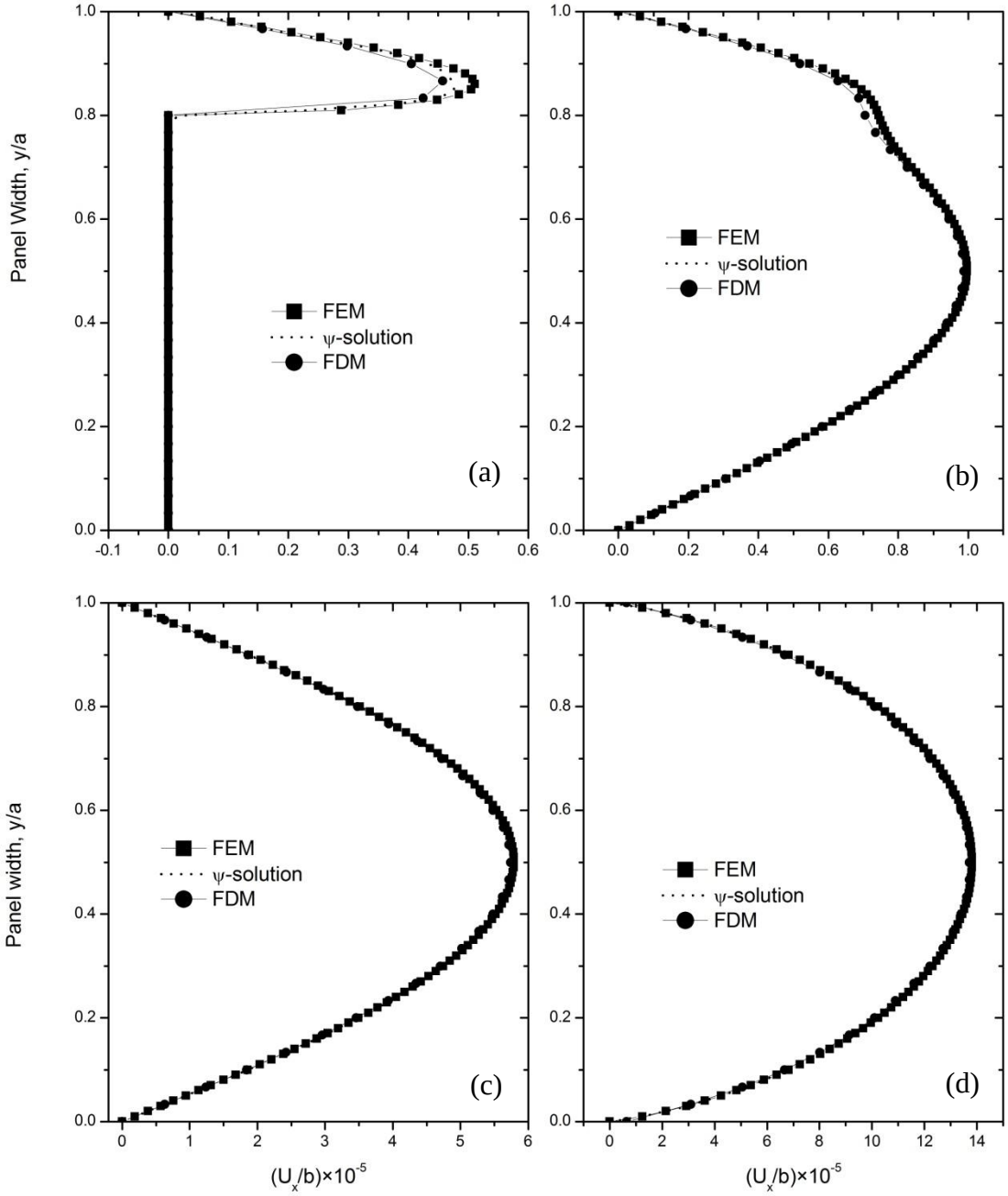

Fig. 7.4: Comparison of normalized axial displacement at section (a) *x/b* = 0.0 (b) *x/b* = 0.1 (c) *x/b* = 0.5 and (d) *x/b* = 1.0 of the stiffened (axial) steel panel (*b/a* = 1, *h/a* = 0.2).

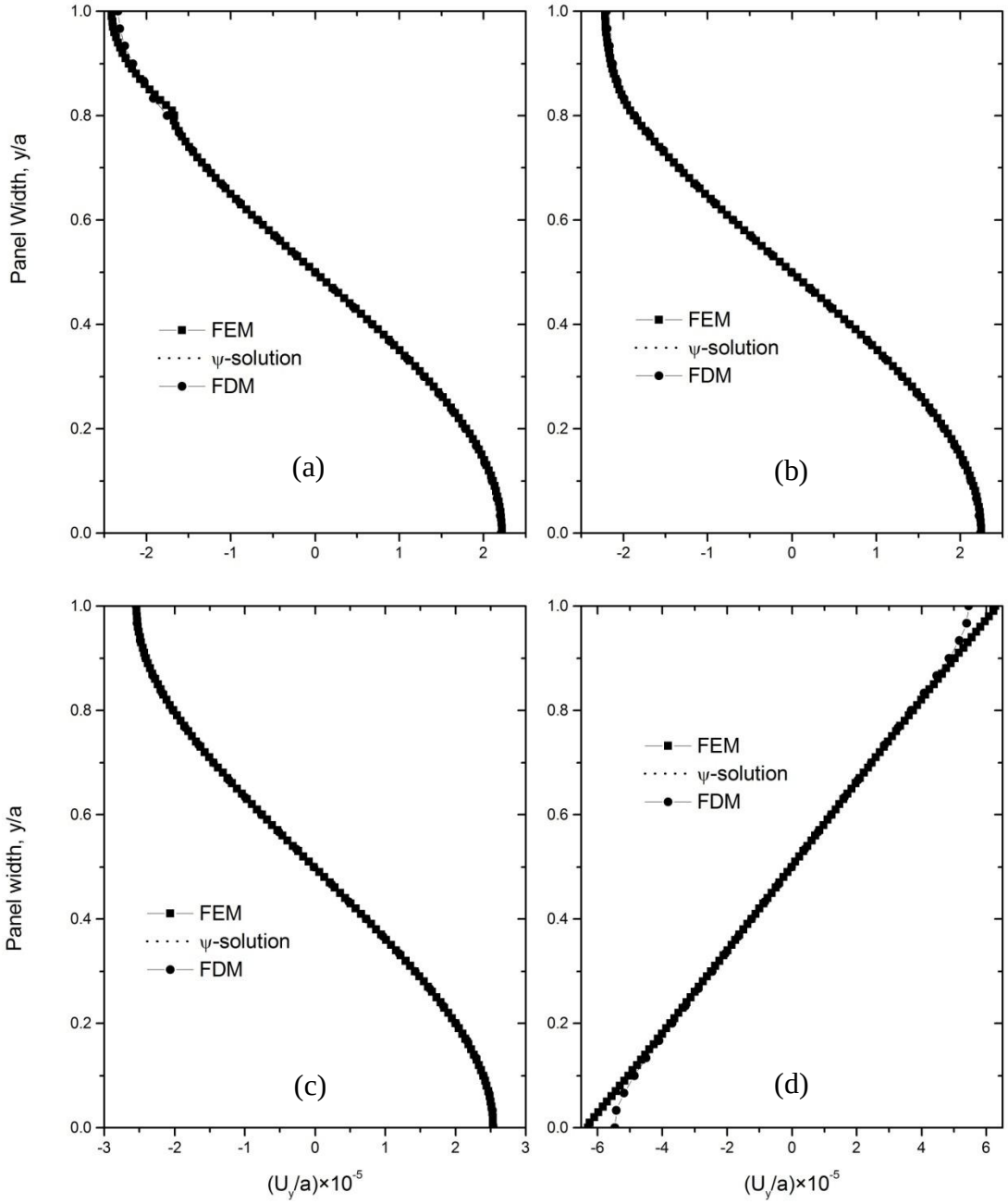

Fig. 7.5: Comparison of normalized lateral displacement at section (a) x/b = 0.0 (b) x/b = 0.1 (c) x/b = 0.5 and (d) x/b = 1.0 of the stiffened (axial) steel panel (b/a = 1, h/a = 0.2).

7.4 Cracked Panel under Axial Stiffeners Subjected To Bending

The parameters chosen for the comparison of the results of the present panel are, aspect ratio *b/a* = 1, crack length ratio *h/a* =0.3 and the maximum intensity of the bending load σ_o = 40 MPa. It was found that bending loading has less effect on crack tip compared to that caused by the axial tension. That's why, longer crack length has been chosen for the current analysis. The comparison of normalized displacement components, u_x/b, u_y/a and normalized stress components, σ_{xx}/σ_o, σ_{yy}/σ_o and σ_{xy}/σ_o are displayed in Figs. 7.6, 7.7, 7.8,7.9 and 7.10, respectively at four different sections of the panel. It is noted that all the results obtained by ψ –solution, FDM and FEM agree well within acceptable limit. The slight discrepancy associated with FDM, which was discussed in section 7.3, has also found in the current problem.

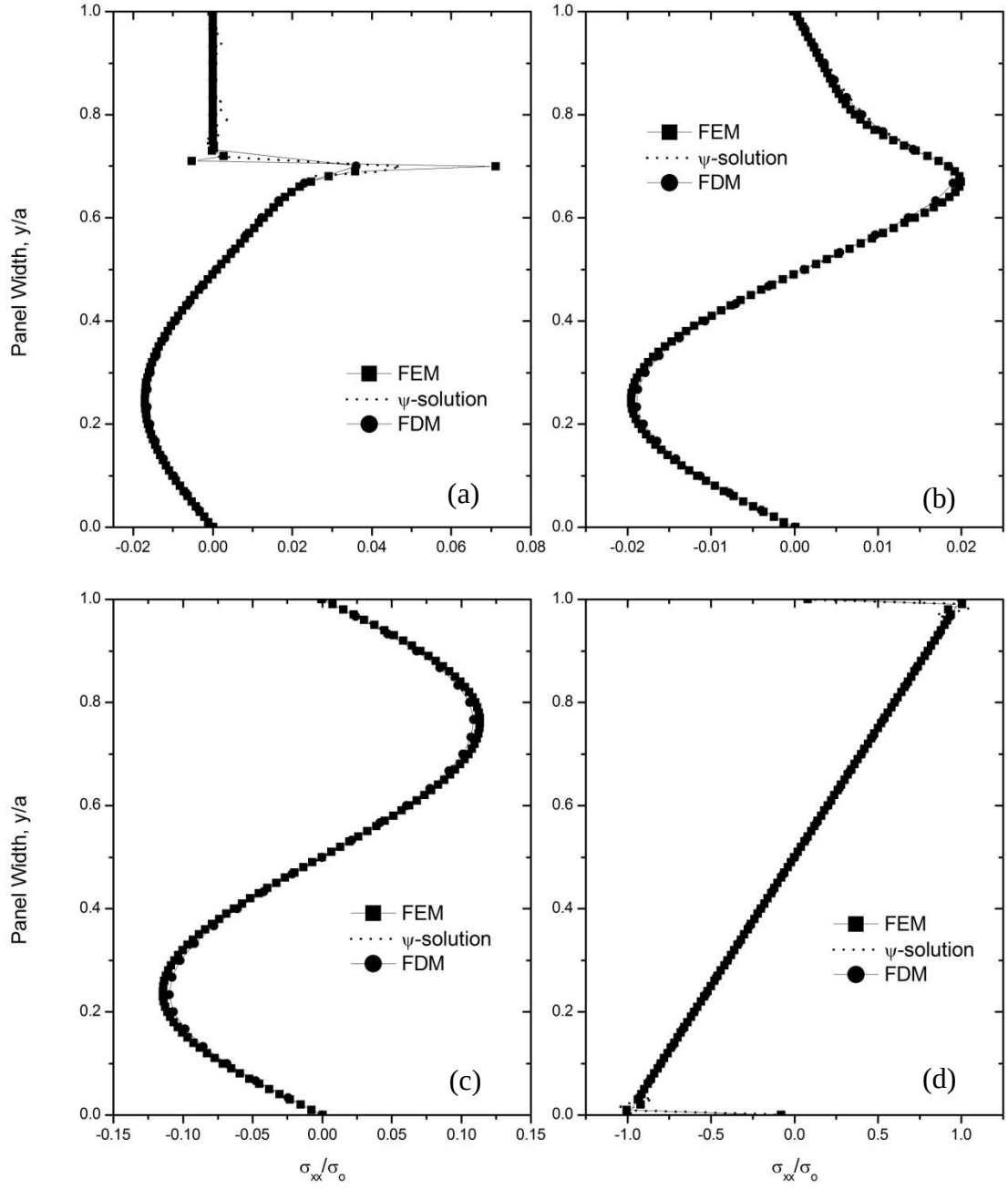

Fig. 7.6: Comparison of normalized axial stress at section (a) *x/b* = 0.0 (b) *x/b* = 0.1 (c) *x/b* = 0.5 and (d) *x/b* = 1.0 of the stiffened (axial) steel panel (*b/a* = 1, *h/a* = 0.3).

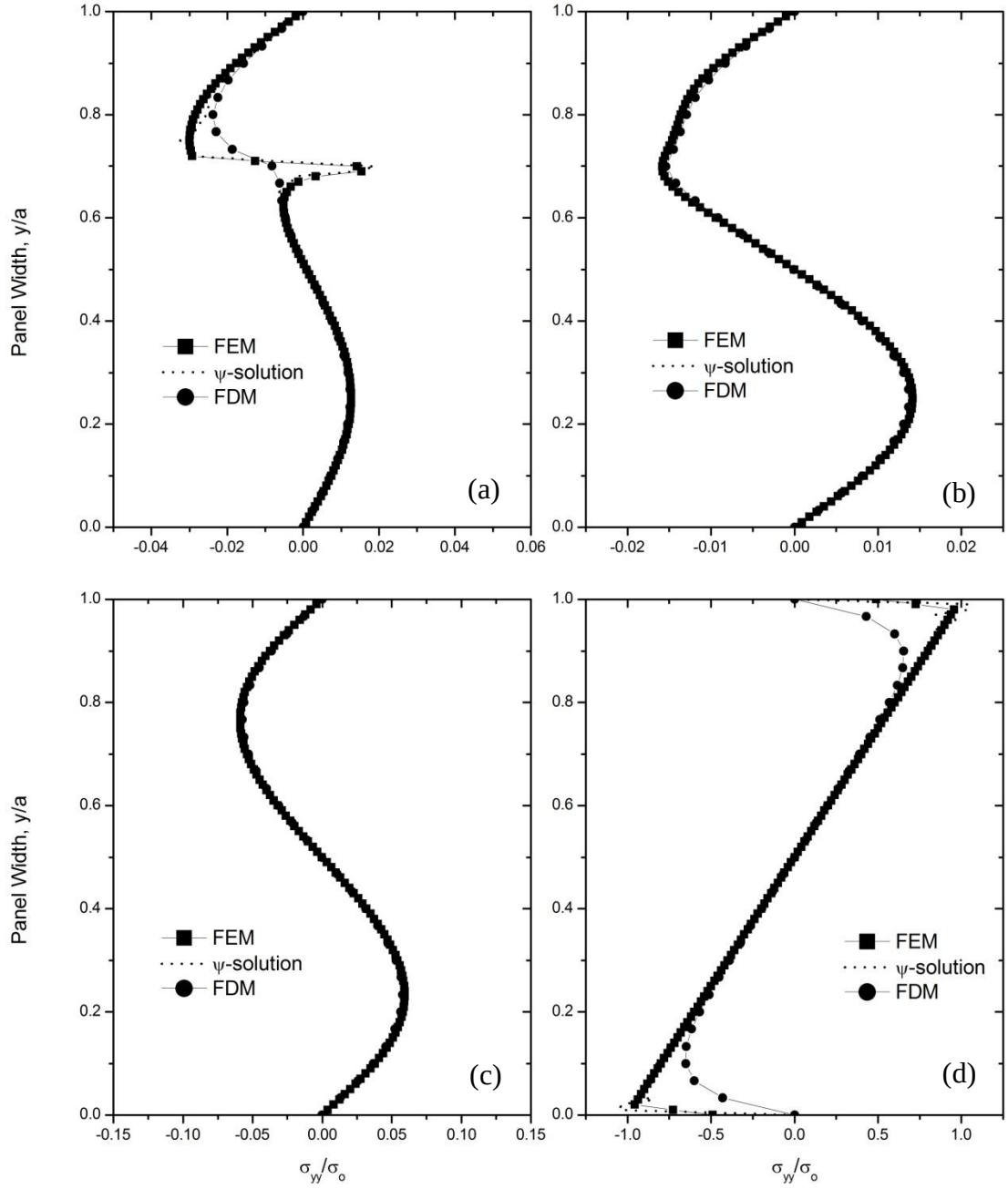

Fig. 7.7: Comparison of normalized lateral stress at section (a) *x/b* = 0.0 (b) *x/b* = 0.1 (c) *x/b* = 0.5 and (d) *x/b* = 1.0 of the stiffened (axial) steel panel (*b/a* = 1, *h/a* = 0.3).

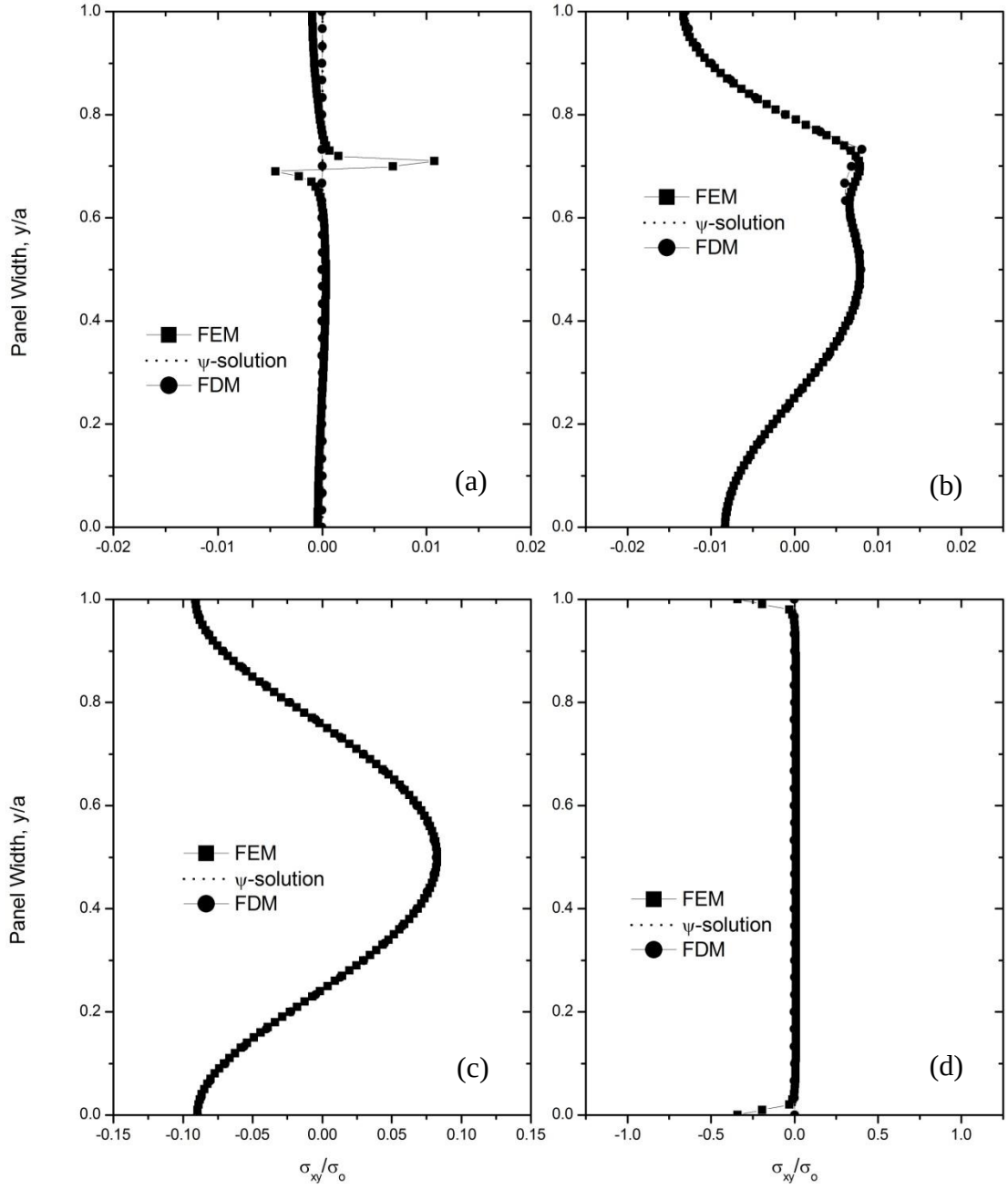

Fig. 7.8: Comparison of normalized shear stress at section (a) *x/b* = 0.0 (b) *x/b* = 0.1 (c) *x/b* = 0.5 and (d) *x/b* = 1.0 of the stiffened (axial) steel panel (*b/a* = 1, *h/a* = 0.3).

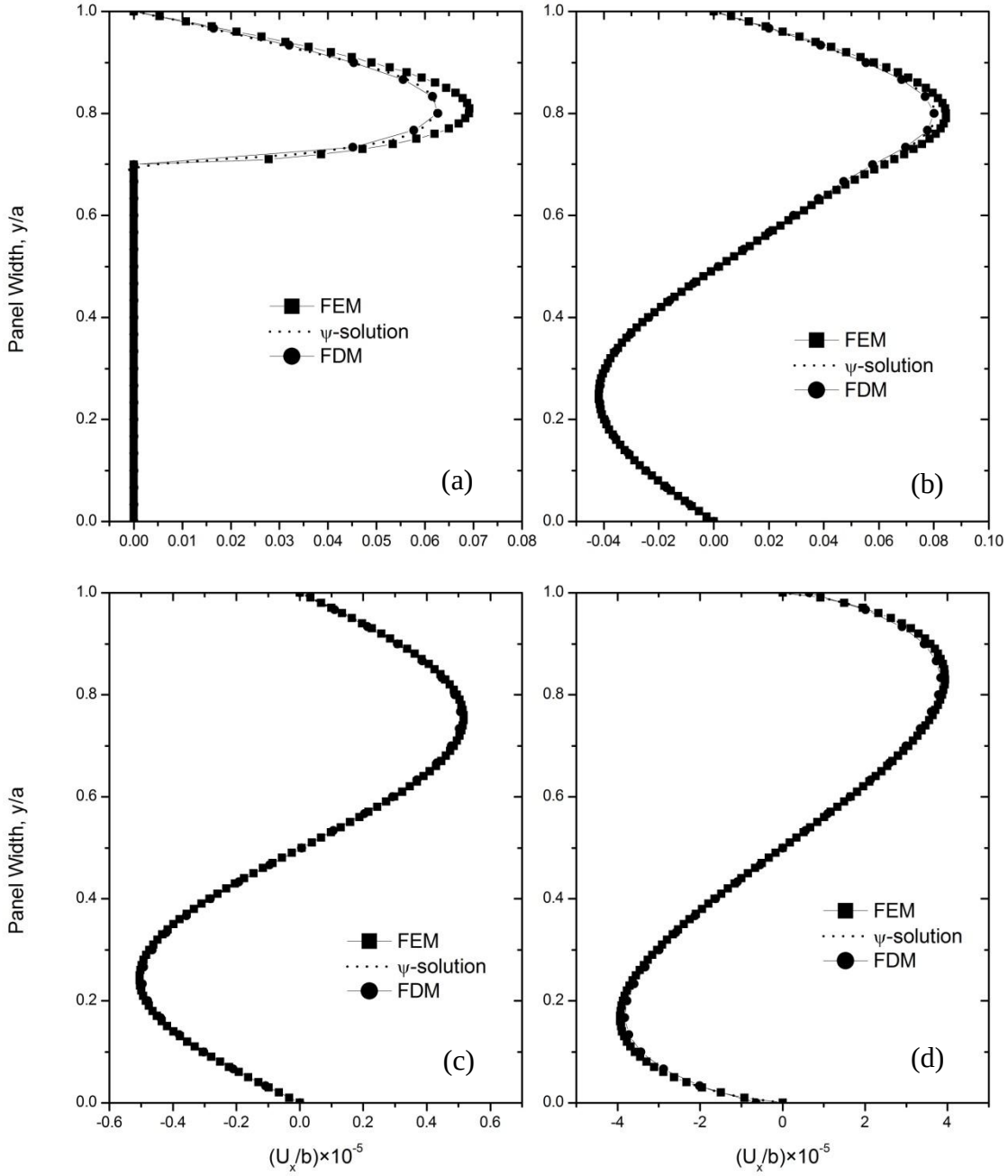

Fig. 7.9: Comparison of normalized axial displacement at section (a) *x/b* = 0.0 (b) *x/b* = 0.1 (c) *x/b* = 0.5 and (d) *x/b* = 1.0 of the stiffened (axial) steel panel (*b/a* = 1, *h/a* = 0.3).

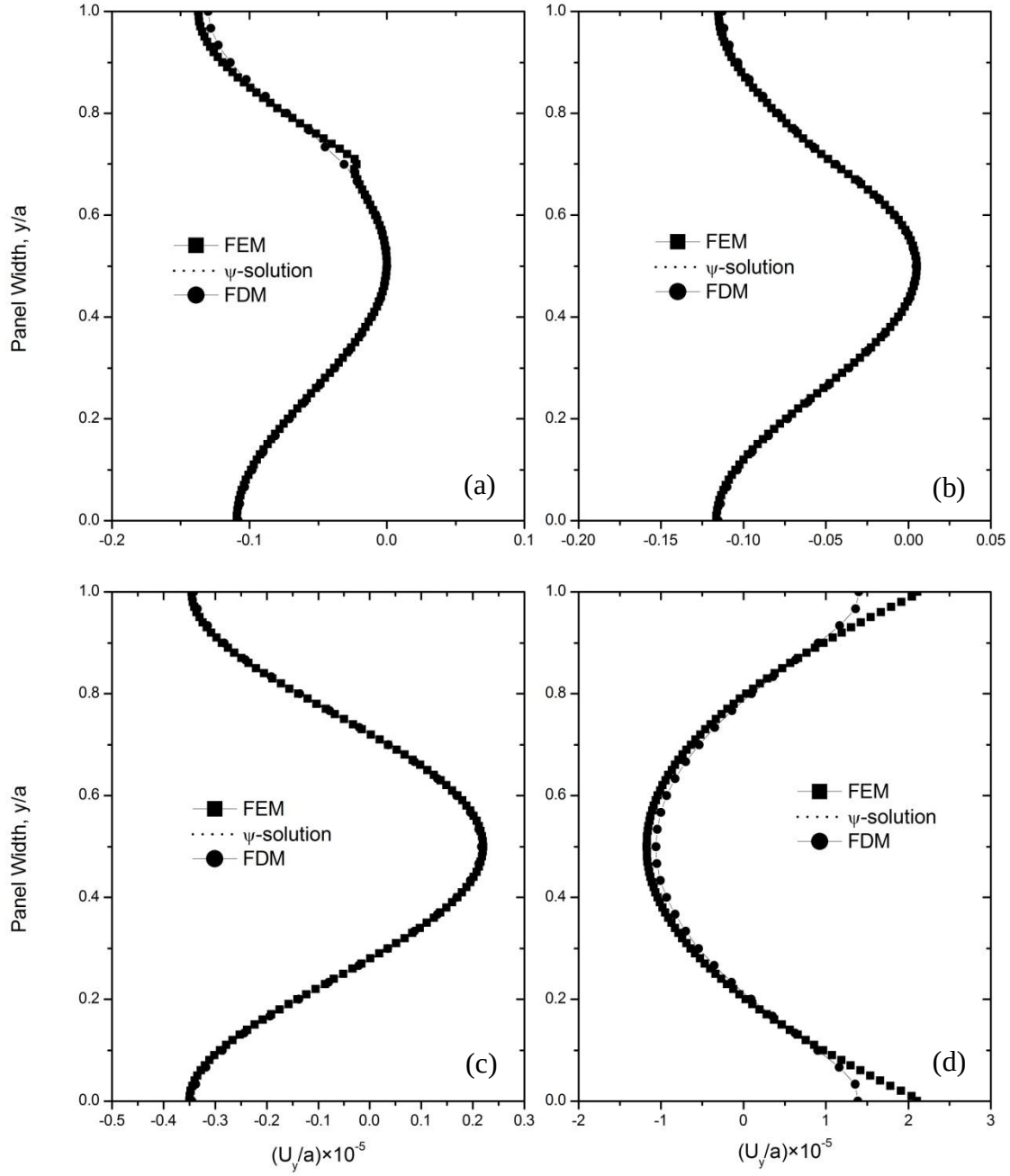

Fig. 7.10: Comparison of normalized lateral displacement at section (a) *x/b* = 0.0 (b) *x/b* = 0.1 (c) *x/b* = 0.5 and (d) *x/b* = 1.0 of the stiffened (axial) steel panel (*b/a* = 1, *h/a* = 0.3).

7.5 Cracked Panel under Lateral Stiffeners Subjected To Axial Tension

The same panel of section 7.3 is considered with different stiffener, i.e., instead of axial stiffener, lateral stiffeners are considered at the bottom and upper edges of the panel. The comparison of normalized stress components σ_{xx}/σ_o, σ_{yy}/σ_o and σ_{xy}/σ_o are shown in Figs. 7.11, 7.12 and 7.13 which clarify that the results of the present method and FEM method are in good agreement with each other at sections *x/b* = 0.0, 0.1 and 1.0 with slight deviation from that obtained by FDM at crack surface and loading termination end. The deviation from FDM has been discussed earlier. But at sections *x/b* = 0.5, the deviation among all the methods is noticeable in Figs. 7.12 and 7.13. At that section the shear stress is almost same for all methods. The reason behind these is the lateral stiffener that has been chosen for the current analysis. Since the lateral stiffener only restricts the lateral displacement and the loading is axial, boundary condition for that stiffener is completely immaterial for FEM method. But BPA method counts these boundary effect so does the FDM method. That's these discrepancy happens which also be confirmed by observing the Fig. 7.14 of normalized axial displacement. But in case of normalized lateral displacement the results for all method are found to be good agreement with slight deviation that obtained by FEM.

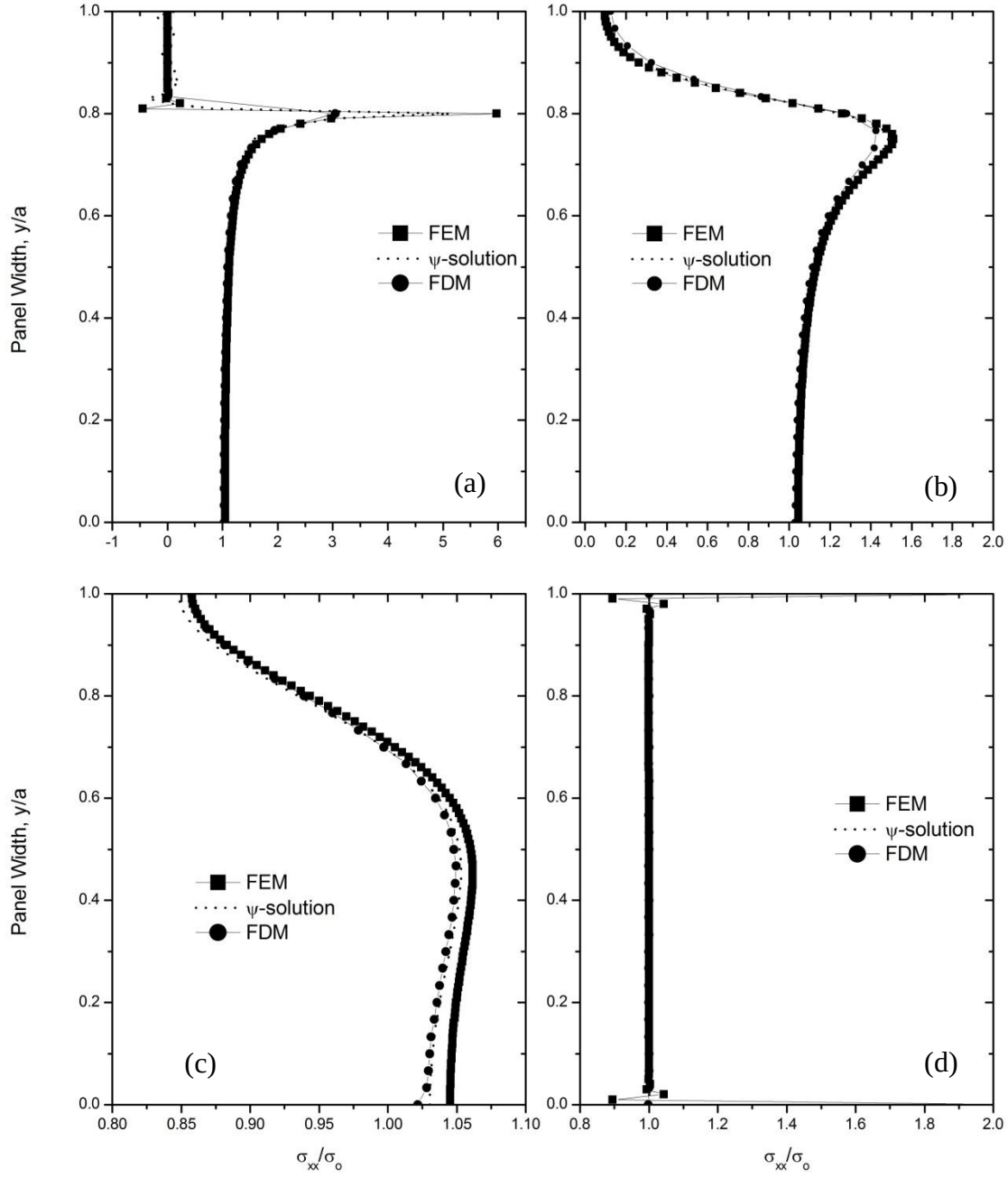

Fig. 7.11: Comparison of normalized axial stress at section (a) *x/b* = 0.0 (b) *x/b* = 0.1 (c) *x/b* = 0.5 and (d) *x/b* = 1.0 of the stiffened (lateral) steel panel (*b/a* = 1, *h/a* = 0.2).

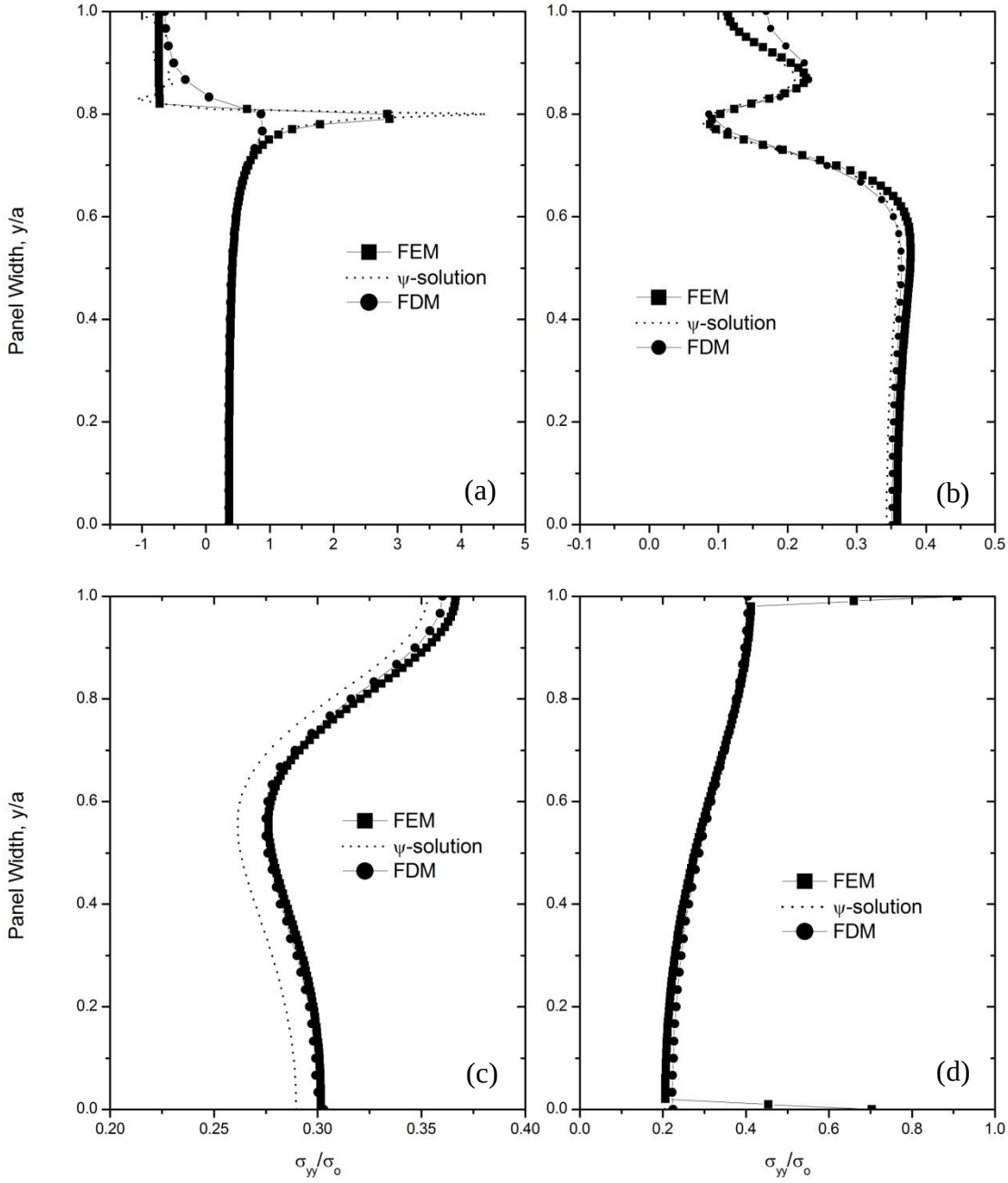

Fig. 7.12: Comparison of normalized lateral stress at section (a) *x/b* = 0.0 (b) *x/b* = 0.1 (c) *x/b* = 0.5 and (d*) x/b* = 1.0 of the stiffened (lateral) steel panel (*b/a* = 1, *h/a* = 0.2).

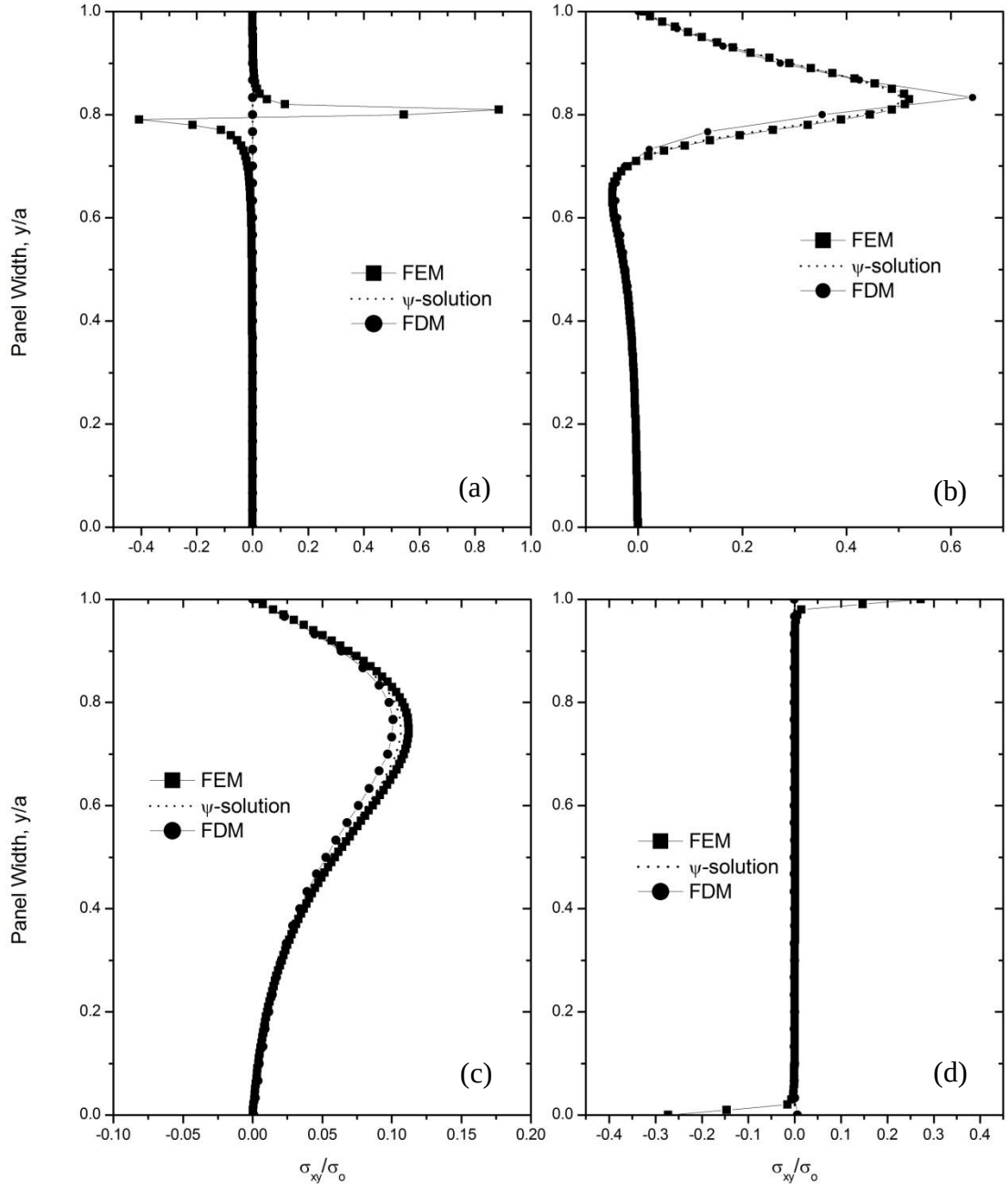

Fig. 7.13: Comparison of normalized shear stress at section (a) *x/b* = 0.0 (b) *x/b* = 0.1 (c) *x/b* = 0.5 and (d) *x/b* = 1.0 of the stiffened (lateral) steel panel (*b/a* = 1, *h/a* = 0.2).

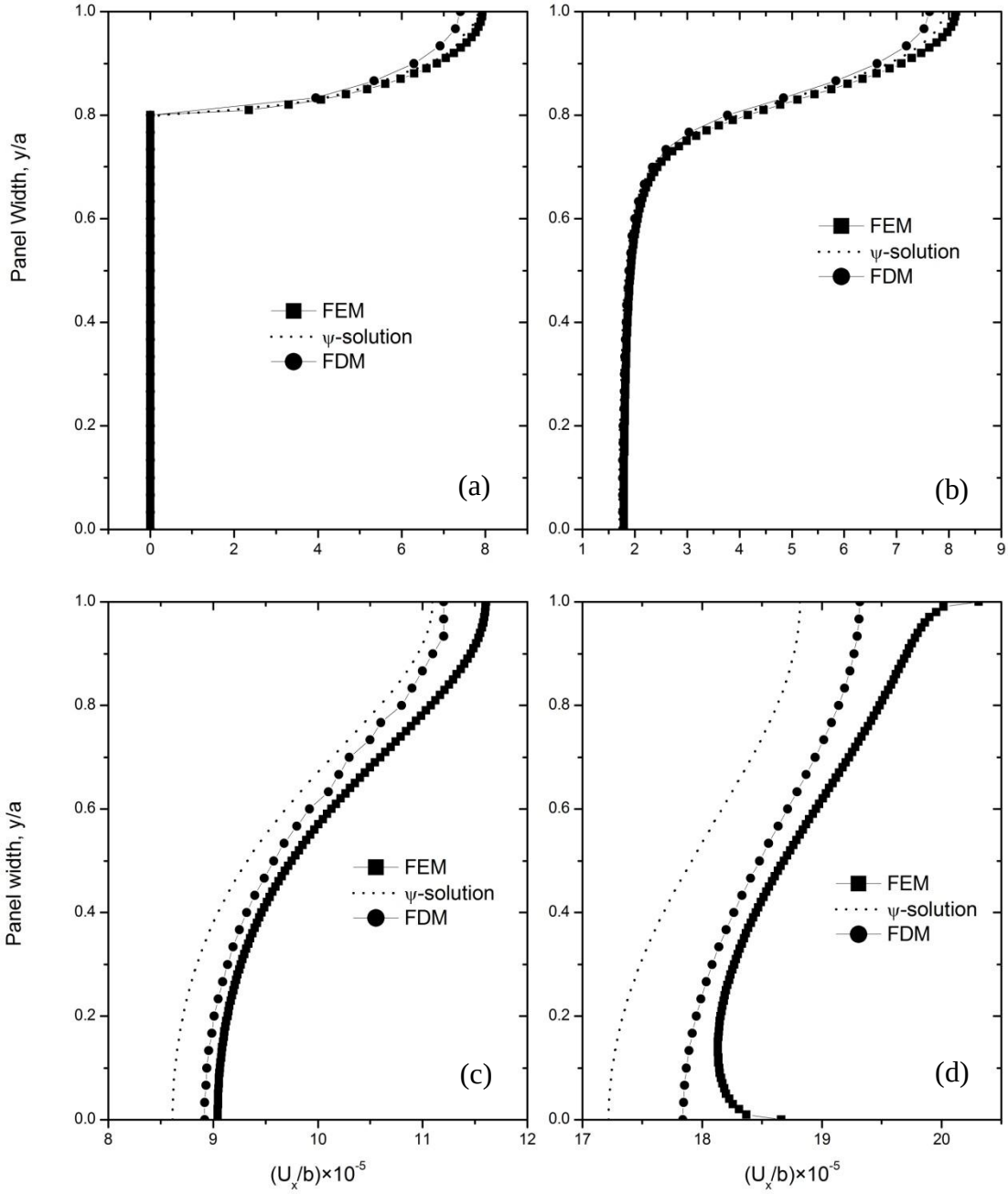

Fig. 7.14: Comparison of normalized axial displacement at section (a) *x/b* = 0.0 (b) *x/b* = 0.1 (c) *x/b* = 0.5 and (d) *x/b* = 1.0 of the stiffened (lateral) steel panel (*b/a* = 1, *h/a* = 0.2).

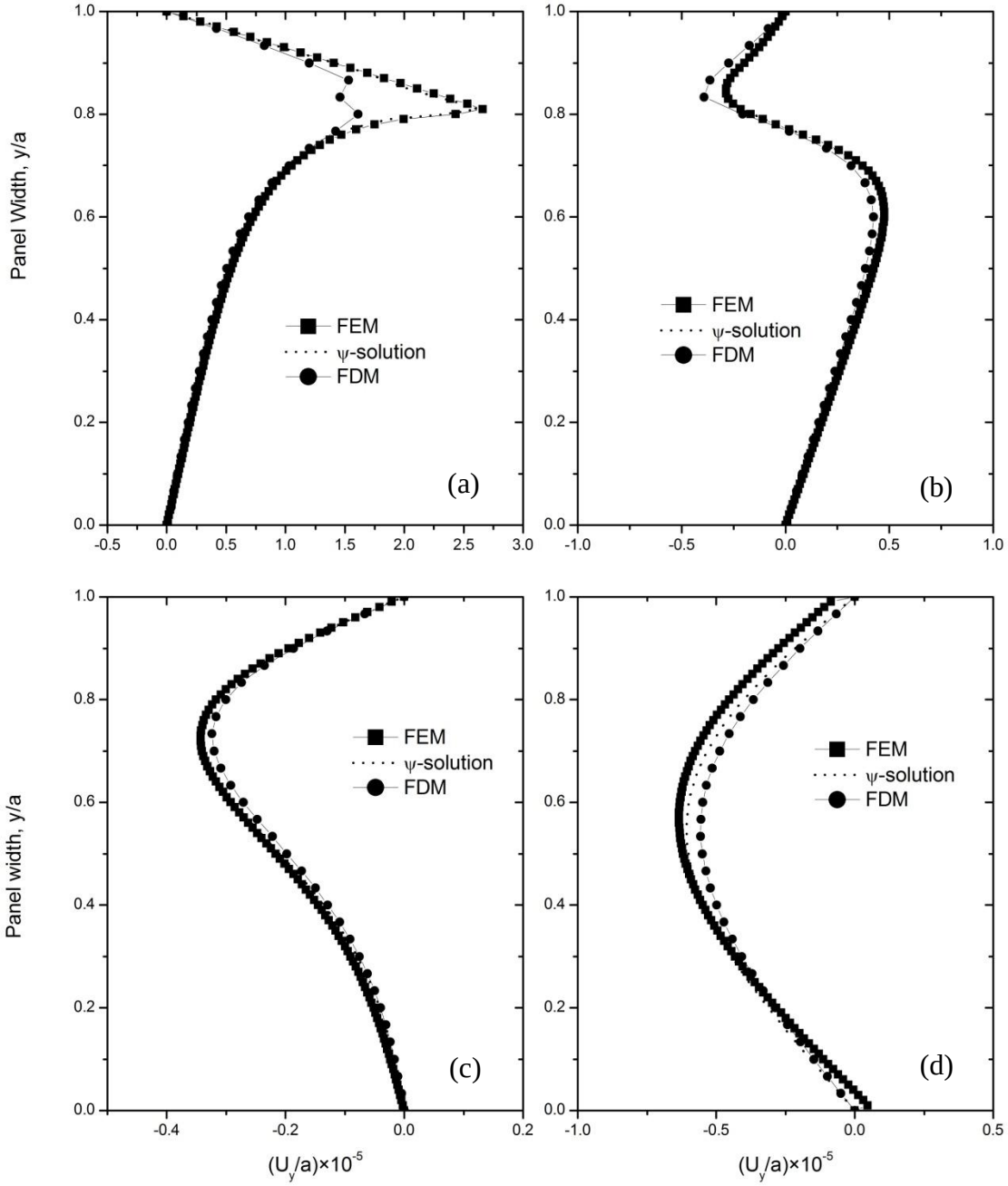

Fig. 7.15: Comparison of normalized lateral displacement at section (a) *x/b* = 0.0 (b) *x/b* = 0.1 (c) *x/b* = 0.5 and (d) *x/b* = 1.0 of the stiffened (lateral) steel panel (*b/a* = 1, *h/a* = 0.2).

7.6 Cracked Composite Panel under Axial Stiffeners Subjected To Axial Tension

The previous three problems that have been discussed earlier were analyzed considering the material as isotropic (steel). In this case, orthotropic material (boron-epoxy) has been considered. The parameters for the composite panels are: aspect ratio b/a = 1, crack length ratio h/a = 0.2, fiber orientation $\theta = 0^o$ and the intensity of loading σ_o = 40 MPa. From observing the normalized displacements $u_x/b, u_y/a$ graphs and normalized stresses σ_{xx}/σ_o, σ_{yy}/σ_o and σ_{xy}/σ_o graphs, it can be seen that three solutions which are obtained based on three philosophies, are very close to each other. There is a slight deviation of the results of FDM solution because of local effects of crack surface and load termination end. Similar slight discrepancies are also observed for FEM solution, especially at the crack tip and the corner points of the right loaded boundary.

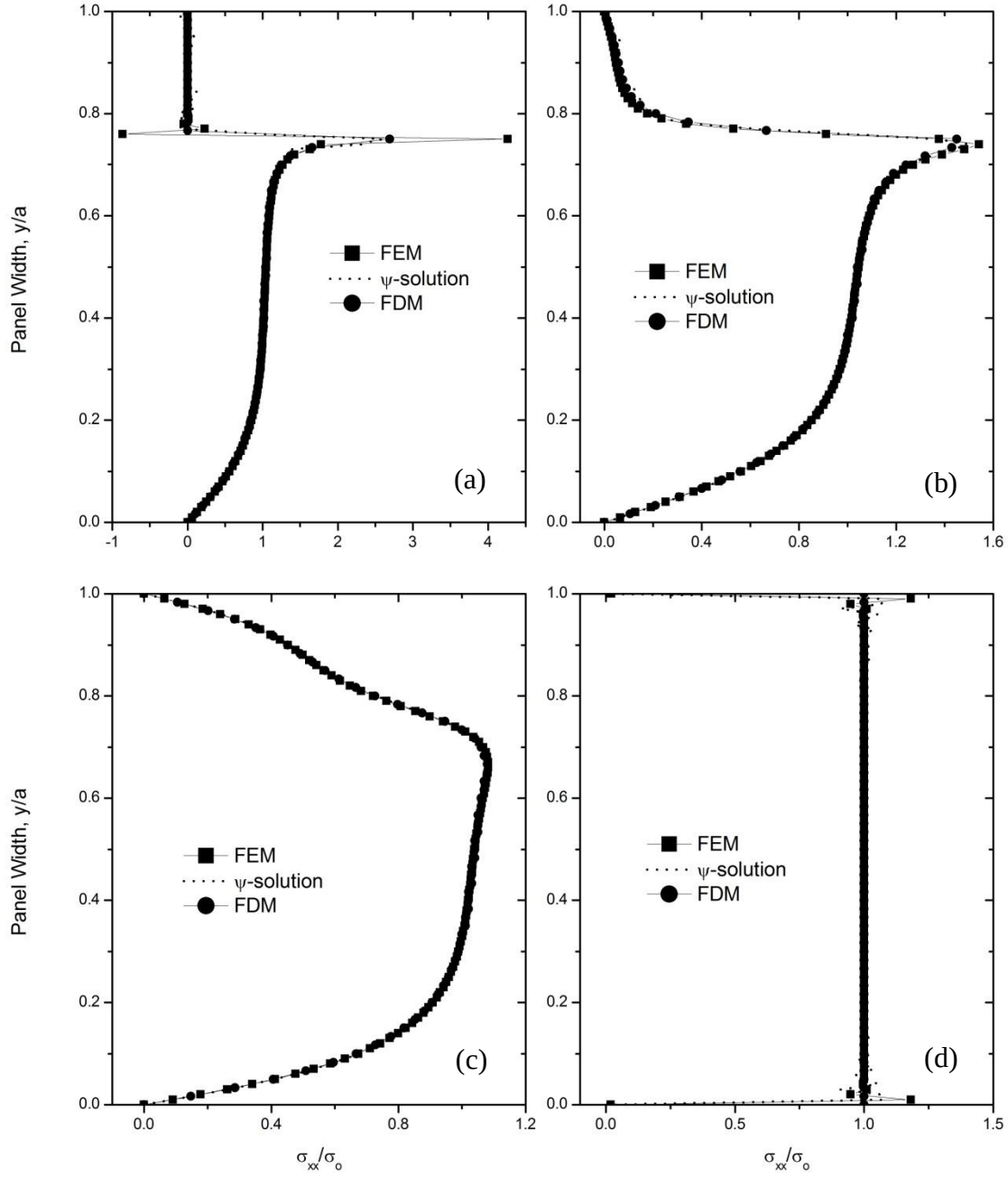

Fig. 7.16: Comparison of normalized axial stress at section (a) *x/b* = 0.0 (b) *x/b* = 0.1 (c) *x/b* = 0.5 and (d) *x/b* = 1.0 of the stiffener (axial) composite ($\theta = 0^o$) panel (*b/a* = 1, *h/a* = 0.25).

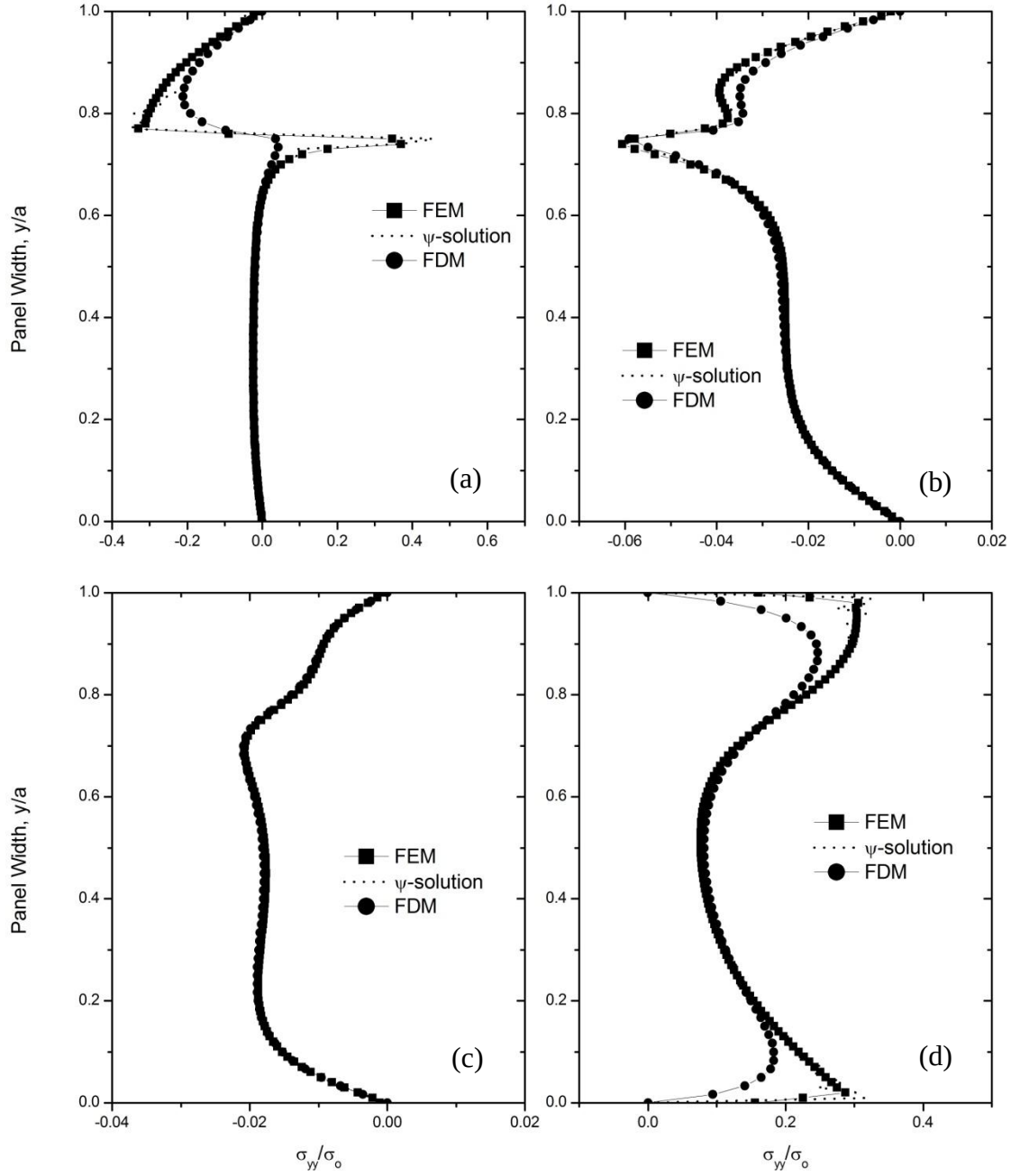

Fig. 7.17: Comparison of normalized lateral stress at section (a) *x/b* = 0.0 (b) *x/b* = 0.1 (c) *x/b* = 0.5 and (d) *x/b* = 1.0 of the stiffener (axial) composite ($\theta = 0^o$) panel (*b/a* = 1, *h/a* = 0.25).

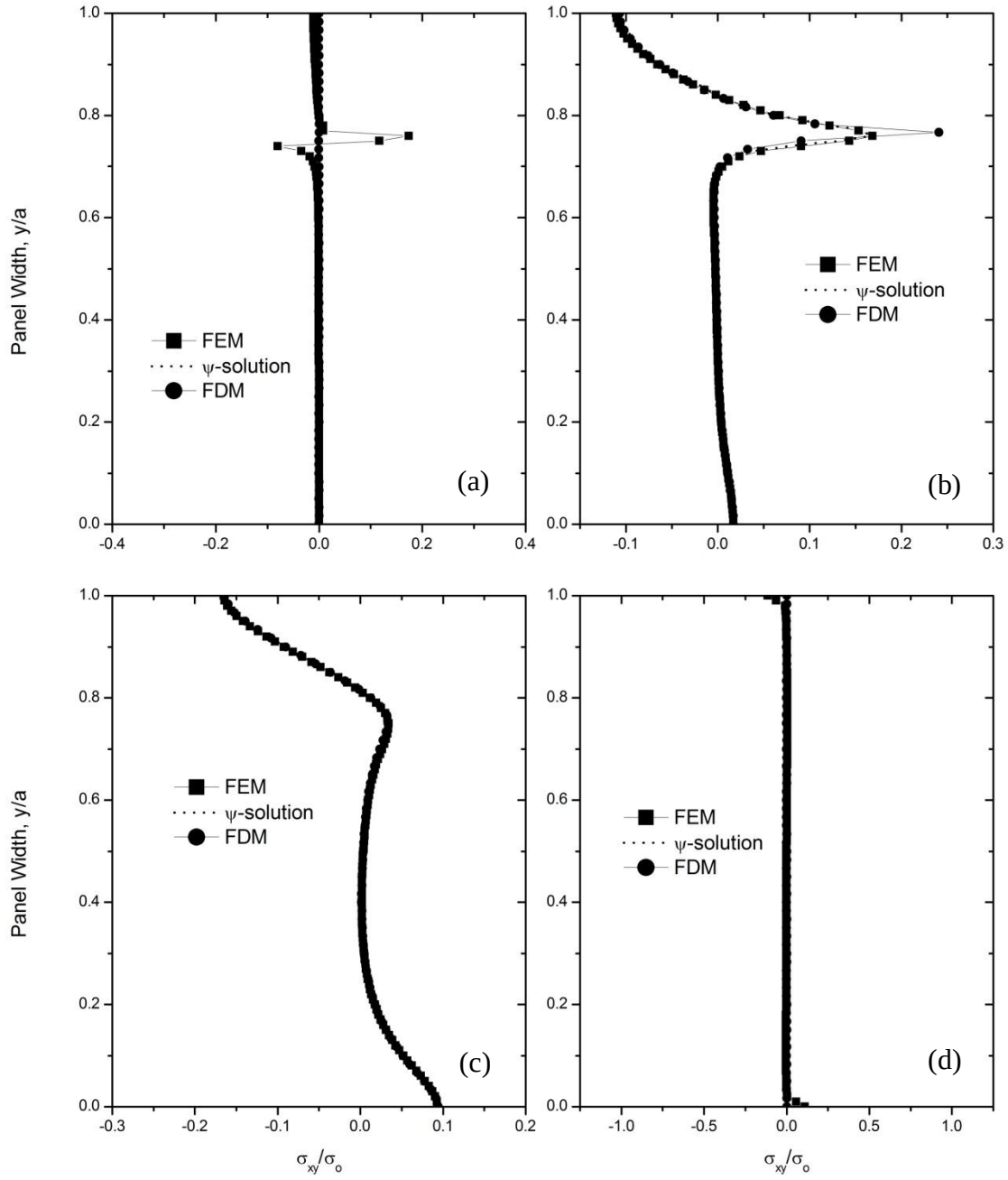

Fig. 7.18: Comparison of normalized shear stress at section (a) *x/b* = 0.0 (b) *x/b* = 0.1 (c) *x/b* = 0.5 and (d) *x/b* = 1.0 of the stiffener (axial) composite ($\theta = 0^o$) panel (*b/a* = 1, *h/a* = 0.25).

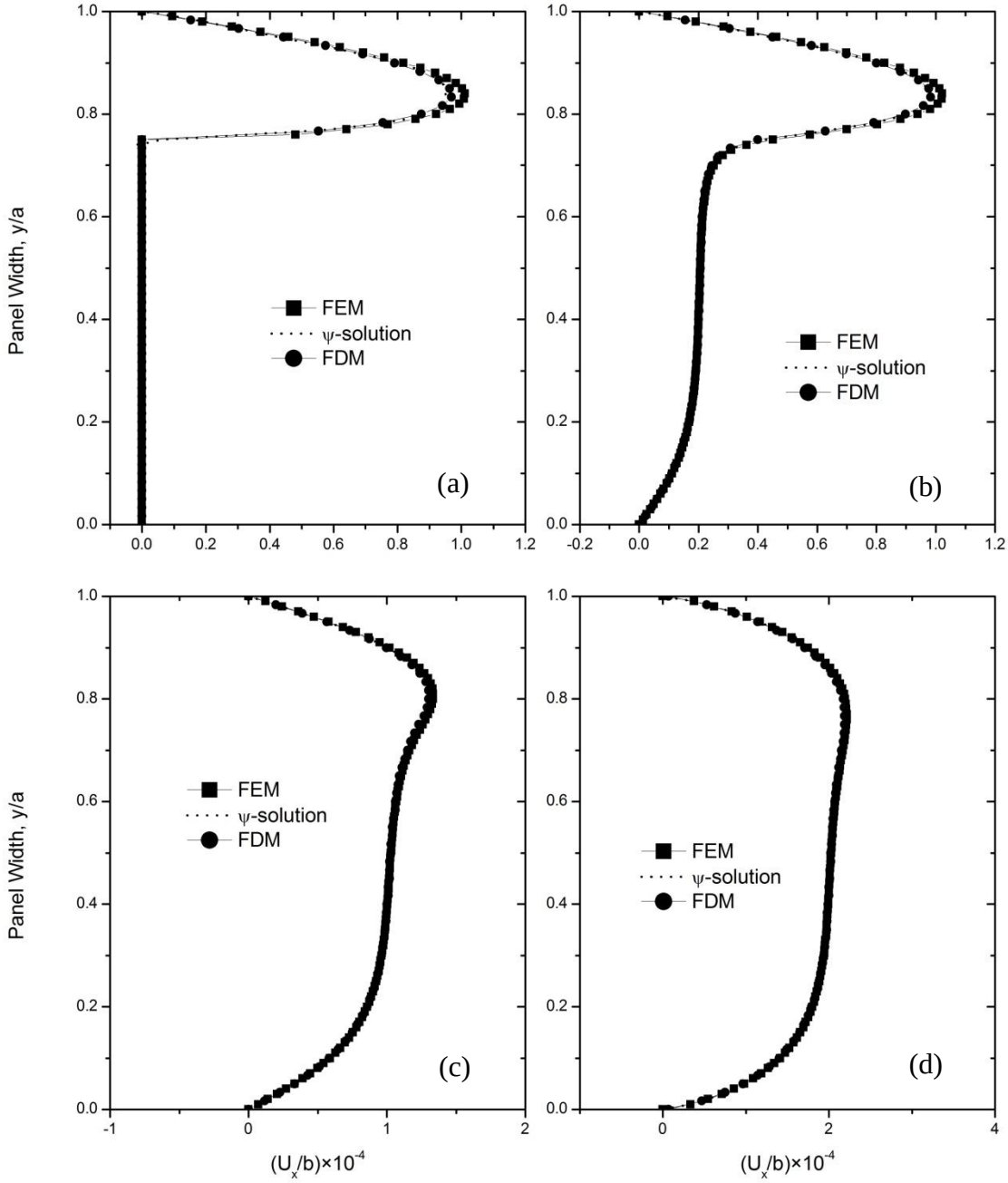

Fig. 7.19: Comparison of normalized axial displacement at section (a) *x/b* = 0.0 (b) *x/b* = 0.1 (c) *x/b* = 0.5 and (d) *x/b* = 1.0 of the stiffener (axial) composite ($\theta = 0^o$) panel (*b/a* = 1, *h/a* = 0.25).

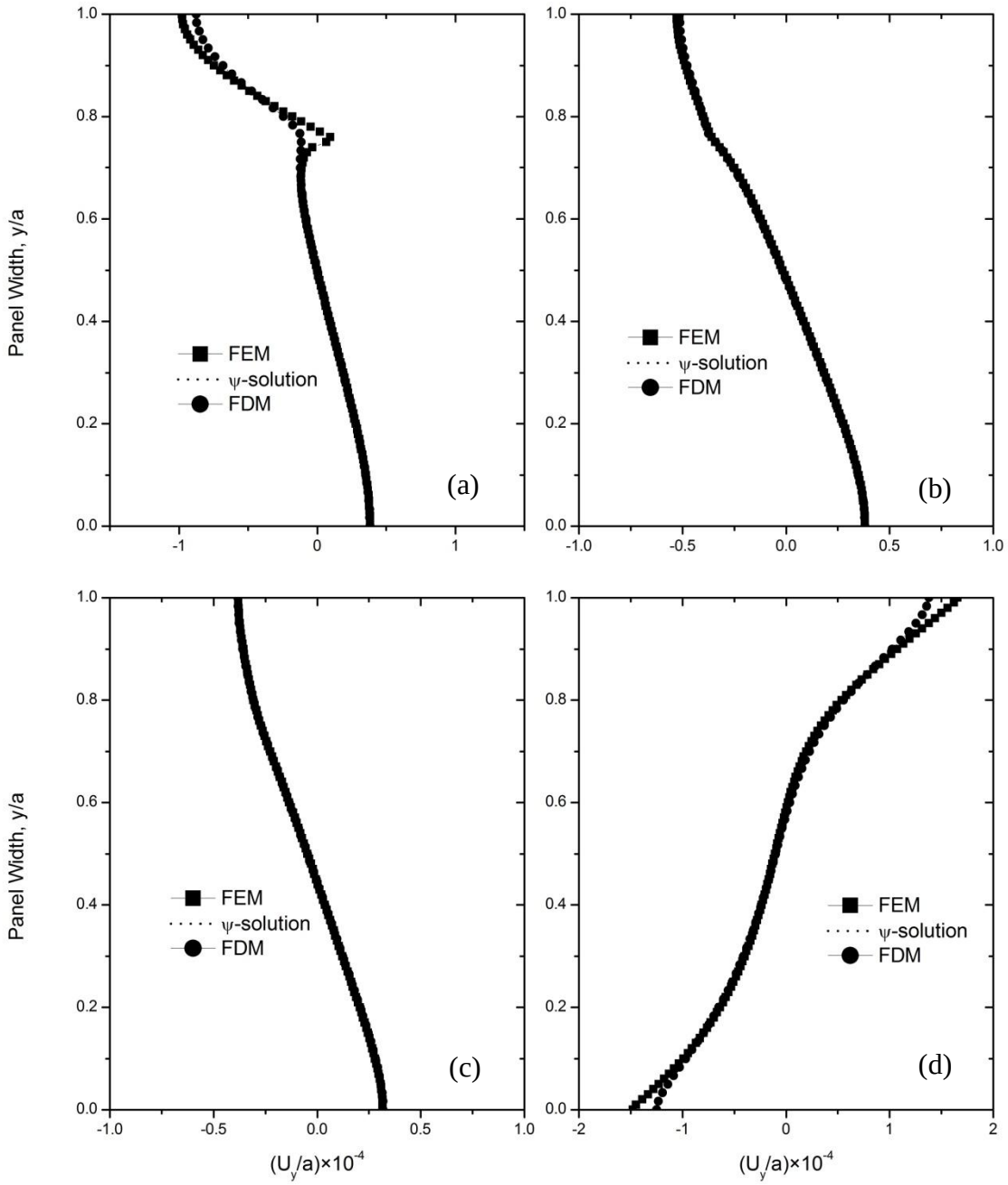

Fig. 7.20: Comparison of normalized lateral displacement at section (a) x/b = 0.0 (b) x/b = 0.1 (c) x/b = 0.5 and (d) x/b = 1.0 of the stiffener (axial) composite ($\theta = 0^o$) panel (b/a = 1, h/a = 0.25).

7.7 Cracked Composite Panel under Axial Stiffeners Subjected To Axial Tension

Fiber orientation $\theta = 90^o$ has been considered for the comparison in this section instead of the orientation $\theta = 0^o$. The parameters are same as the previous problem. The results of normalized stress components of all methods shown in Fig. 7.21, 7.22 and 7.23 are in good agreement with each other. But it can be observed that ψ-solution is not so much smooth at crack and loading end as found in the previous problem. As usual the deviation for FDM solution has also been found at crack surface and load termination end. The solution of normalized axial displacement as shown in Fig. 7.24 for all methods is exactly the same. But in case of normalized lateral displacement as shown in Fig. 7.25, ψ-solution and FDM solution coincides with each other, But FEM solution deviates from those. In general, the stress is higher in fiber direction while the displacement is lower in fiber direction. That's why, FEM solution has shown some deviation from reliable results that have found by ψ-solution.

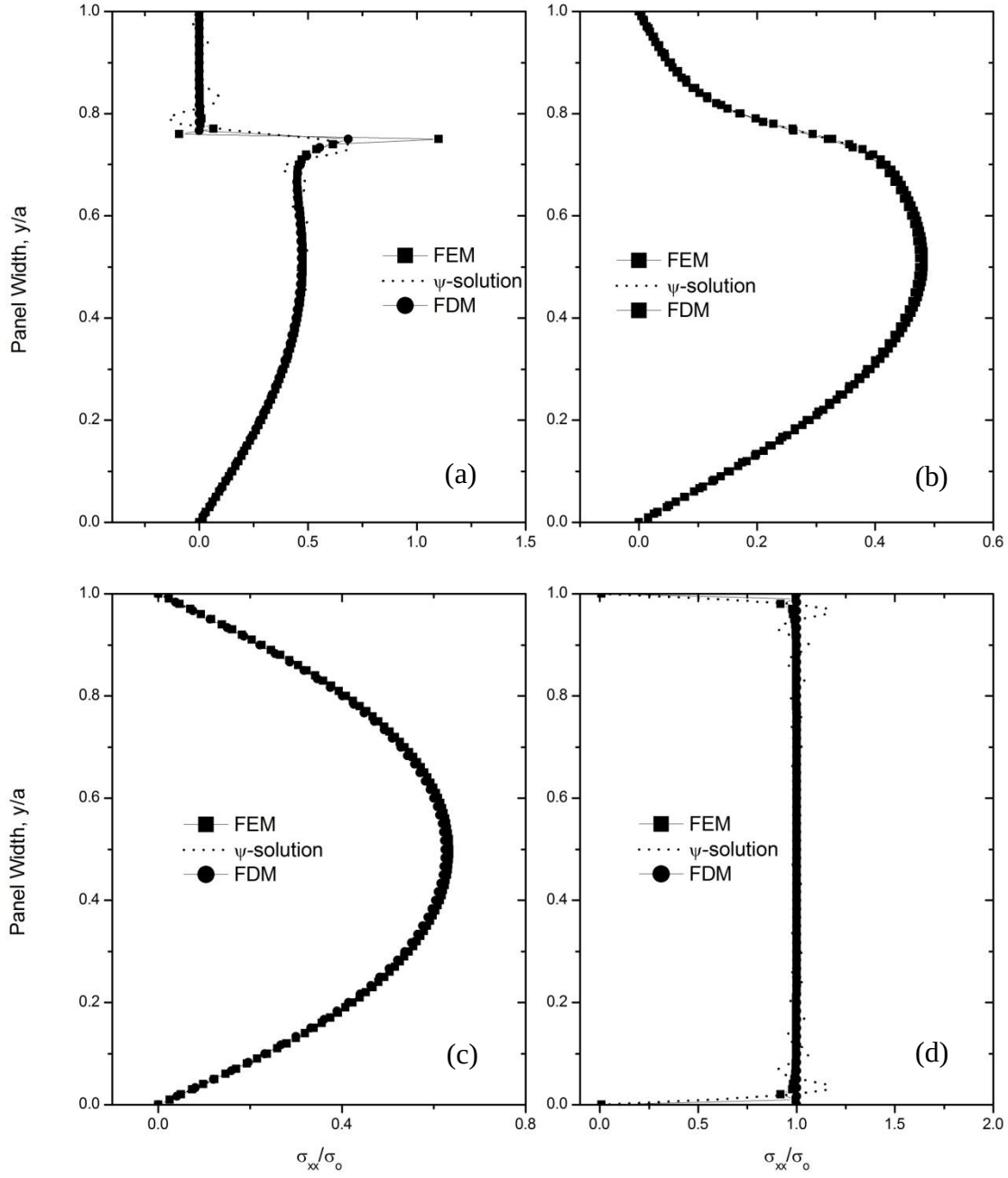

Fig. 7.21: Comparison of normalized axial stress at section (a) *x/b* = 0.0 (b) *x/b* = 0.1 (c) *x/b* = 0.5 and (d*) x/b* = 1.0 of the stiffener (axial) composite ($\theta = 90^o$) panel (*b/a* = 1, *h/a* = 0.25).

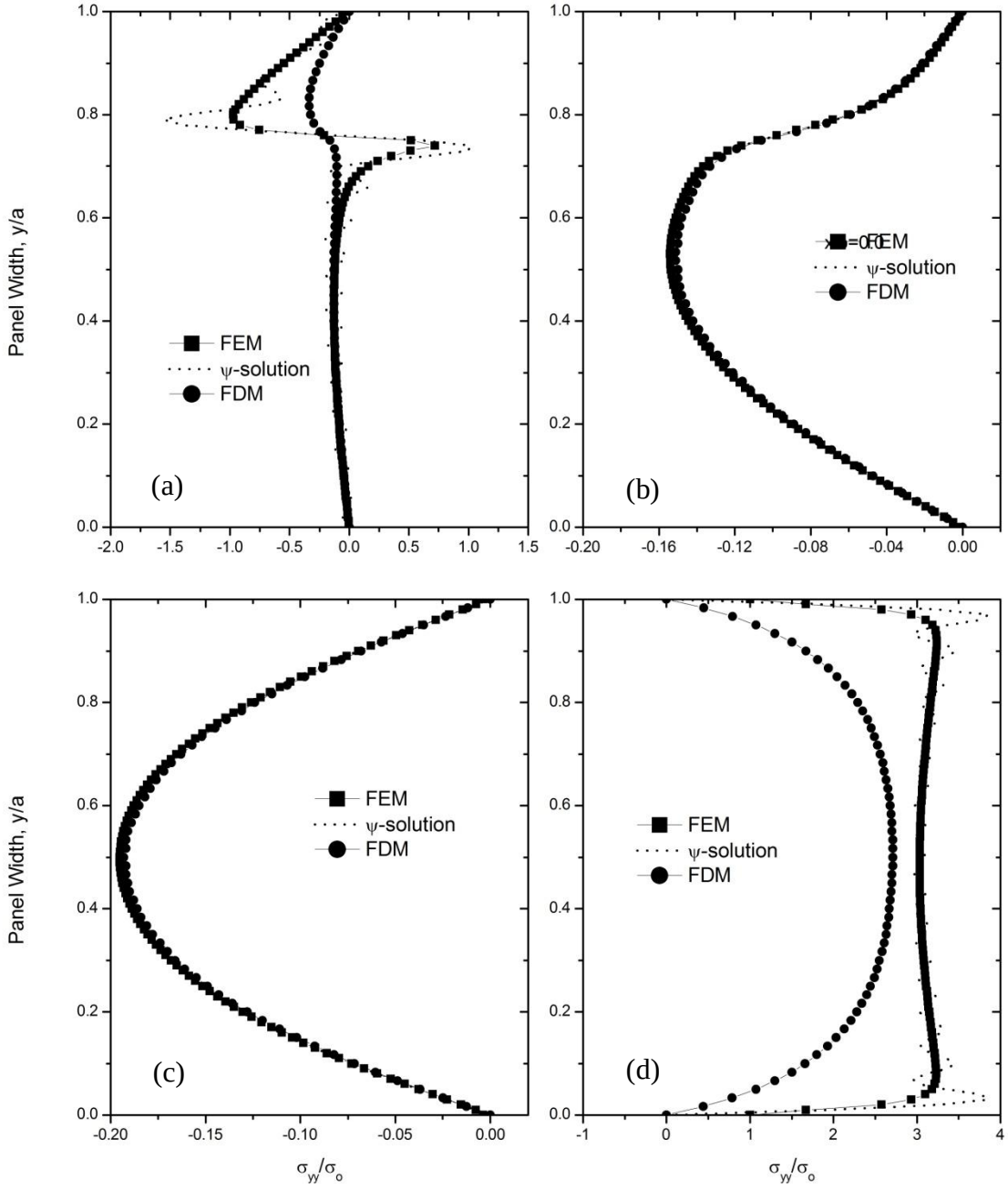

Fig. 7.22: Comparison of normalized lateral stress at section (a) *x/b* = 0.0 (b) *x/b* = 0.1 (c) *x/b* = 0.5 and (d) *x/b* = 1.0 of the stiffener (axial) composite ($\theta = 90^o$) panel (*b/a* = 1, *h/a* = 0.25).

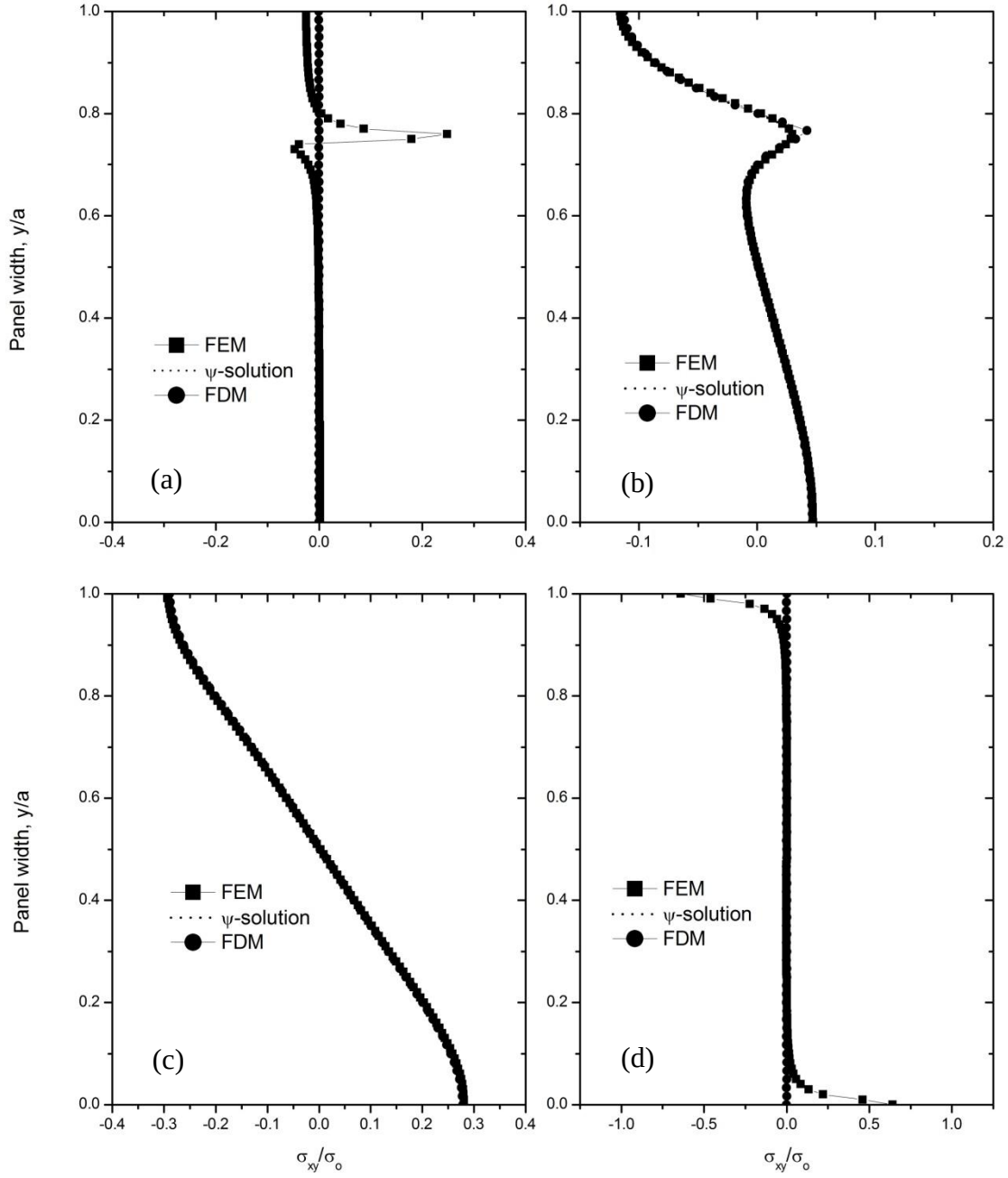

Fig. 7.23: Comparison of normalized shear stress at section (a) *x/b* = 0.0 (b) *x/b* = 0.1 (c) *x/b* = 0.5 and (d) *x/b* = 1.0 of the stiffener (axial) composite ($\theta = 90^o$) panel (*b/a* = 1, *h/a* = 0.25).

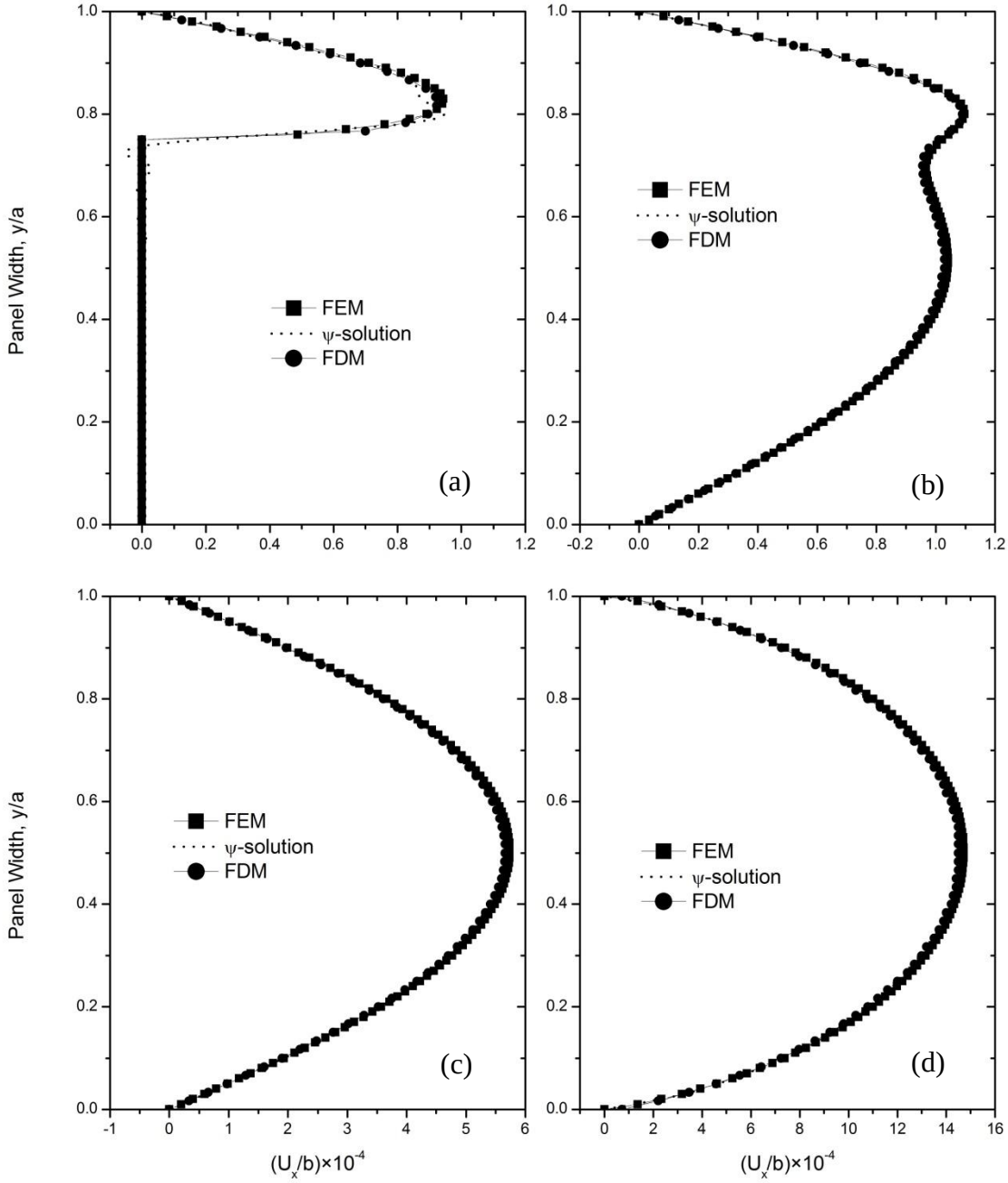

Fig. 7.24: Comparison of normalized axial displacement at section (a) x/b = 0.0 (b) x/b = 0.1 (c) x/b = 0.5 and (d) x/b = 1.0 of the stiffener (axial) composite ($\theta = 90^{o}$) panel (b/a = 1, h/a = 0.25).

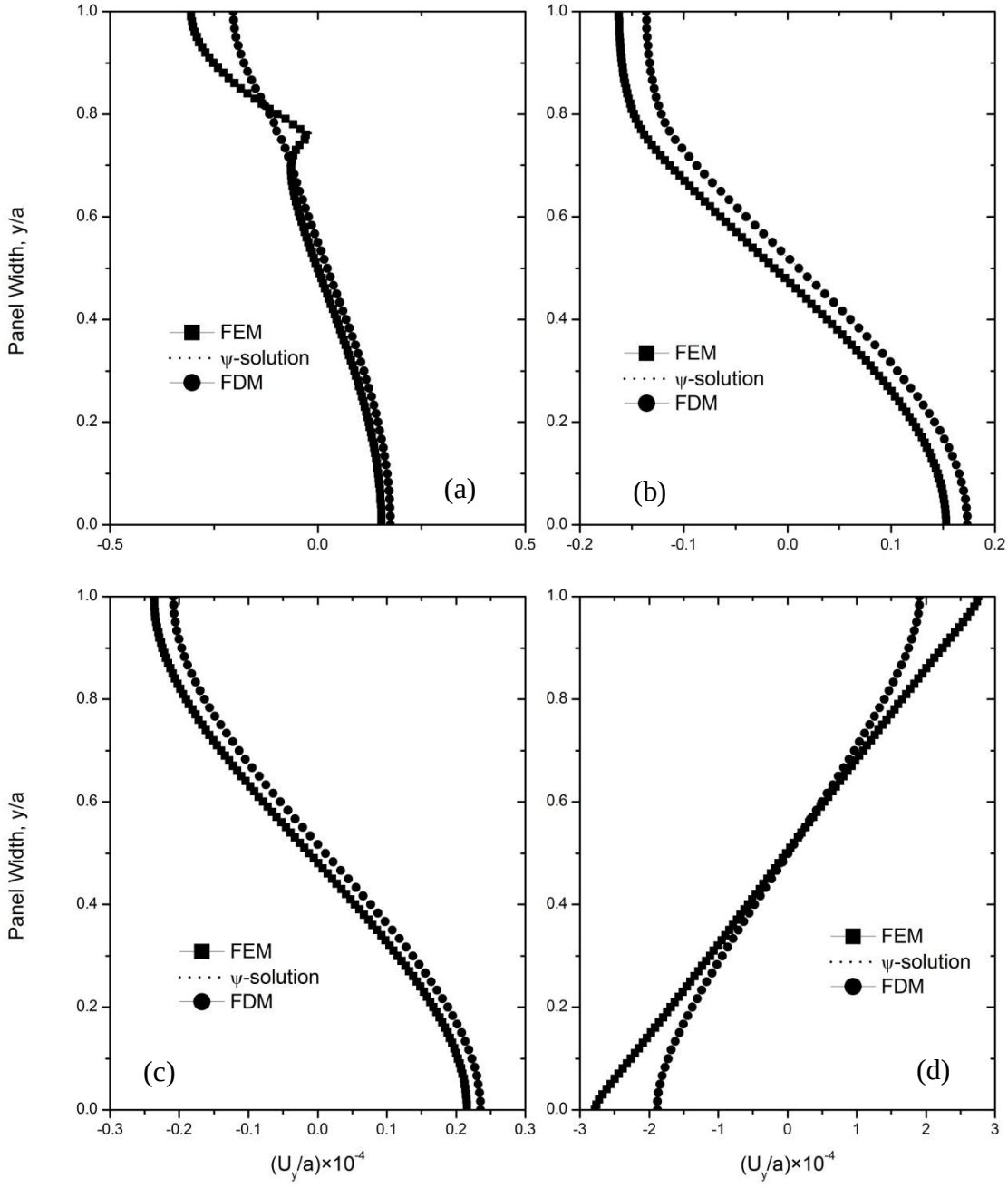

Fig. 7.25: Comparison of normalized lateral displacement at section (a) *x/b* = 0.0 (b) *x/b* = 0.1 (c) *x/b* = 0.5 and (d) *x/b* = 1.0 of the stiffener (axial) composite ($\theta = 90^{o}$) panel (*b/a* = 1, *h/a* = 0.25).

CHAPTER 8

CONCLUSIONS AND RECOMMENDATIONS

8.1 Conclusions

An analytical method usually provides exact solution whereas any numerical method gives approximate solution. Exact analytical solution is always preferable over any numerical solution of a particular problem. But the practical fact is that the analytical methods of solutions are usually limited to only very ideal cases. That is why the analytical methods of solution could not gain popularity in the field of stress analysis of actual structures. This limitation of the literature has been removed in the present research by developing a new analytical method for stress analysis of cracked stiffened panels.

The analytical solution for the elastic field of stiffened panels with an edge crack subjected to different kinds of loading has been successfully derived for both isotropic and orthotropic composite materials. Appropriate alternative expression for one of the boundary conditions at the crack surface has been derived from the numerical solution of the problem performed in terms of the same potential function. Having appropriate analytical expressions for all the necessary boundary conditions, an efficient and accurate analytical scheme has been developed in terms of a potential function defined in terms of displacement components for the analysis of elastic field of cracked stiffened panels. The analytical scheme developed is not only limited to the problems of isotropic materials, but also equally applicable to orthotropic composite materials with all possible mixed mode of boundary conditions whether they are prescribed in terms of displacements, strains or stresses or even any combination thereof. The superiority of the present modeling scheme over the existing approaches is that it reduces the solution of a plane problem to the determination of a single function satisfying a single differential equation of equilibrium. The capability of the method is demonstrated by solving a number of

problems of stiffened cracked panels of isotropic and composite materials with different types of stiffener subjected to different types of loading.

The main concluding remarks are summarized as follows

1) The overall analysis of the results of the cracked stiffened panels under different loading as well as different kinds of stiffeners reveals that the presence of material discontinuity, that is, the crack has significant influence on the overall elastic behavior of the panel. This conclusion has been made evident when the results of elastic field are analyzed in the perspective of crack length including those of un-cracked panel. Stress concentration is found to increase with the increase of crack length for all the panels investigated.
2) The influence of panel aspect ratio plays an important role in defining the state of displacement and stress in the panel. The intensity of stress is found to decrease with the increase of panel aspect ratio.
3) From the comparison of results of panels with two different types of stiffeners it is revealed that the panel supported by lateral stiffeners at the two opposing longitudinal edges is more critical in terms of stresses then the panel supported by axial stiffeners.
4) The results of fiber reinforced composite materials show that the orientation of fiber in the panel has quite a substantial influence on the state of stresses as well as displacements. The results of the present investigation show that the axial and shear stress components assume much higher value for the case of fibers oriented parallel to the direction of loading in comparison with the case of perpendicular fibers. The lateral stress component however shows dominating characteristics for the case of fibers oriented perpendicular to the direction of loading.
5) In order to check the reliability and accuracy of the present analytical scheme, solutions are compared with the corresponding solution of approximate numerical methods, namely, Finite Element Method and Finite Difference Method. This is because of the fact that no other reliable solution is available in the literature that can be compared with the present solutions. From

comparison of the results of different methods, it is observed that solutions are in good agreement with each other. More specifically, the present analytical solutions are found to be almost identical to those of the FEM with few exceptions only at the point of singularities. Finite Difference solutions also compare well with the present solutions, but slight discrepancies are observed for some sections, especially at the cracked section and the loaded boundary, which is probably because of the low mesh density used to model the panel by Finite Difference Method as well as the management procedure of singularity, is different in FDM compared to FEM.

8.2 Recommendations

This is completely a new analytical method to find out the stress and displacement filed of edge- crack stiffened panels.

1) This work can be further extended with opposing edges and internal cracks.
2) The method has been investigated and instituted as capable to deal isotropic and orthotropic stiffened panels effectively for axial and bending loads. It also requires to be investigated for a variety of loading configuration in order to have its wide range of adoptability and versatility.
3) The method can effectively and efficiently deal with the structures of unidirectional composite lamina. Further, even for a unidirectional lamina, the loading should be either in the direction of fibers or perpendicular to the fiber. Therefore, the method, at its present states, cannot be directly applied to laminated (multilayered) composites with fibers oriented in different directions. However, with minor modification in the formulations, the method can be made suitable for laminated composites without any limitation of the fiber direction.

REFERENCES

[1] Inglis, C. E., "Stresses in a plate due to the presence of cracks and sharp corners", Transactions of the Institution of Naval Architects, London, England, Vol. 60, pp. 219 (1913).

[2] Griffith, A. A., "The phenomena of rupture and flow in solids", Philosophical Transactions of the Royal Society of London, England, Vol. 221, pp. 163-198 (1921).

[3] Williams, M. L., "On the stress distribution at the base of a stationary crack", Journal of Applied Mechanics, Vol. 24, pp. 109–114 (1957).

[4] Irwin, G. R., Encyclopedia of Physics, Vol. 6, Springer, Berlin (1958).

[5] Irwin, G. R., "The crack extension force for a part through crack in a plate", Journal of Applied Mechanics, vol. 29, pp. 651–654 (1962).

[6] Timoshenko, S. P. and Goodier, J. N., "Theory of Elasticity". 3rd Edition, *McGraw Hill Book Company*, New York (1970)

[7] Sedov, L. I., A course in continuum mechanics, Vol. 4, Groningen, Volters-Noordhoff (1972)

[8] Bowie, O. L., and Neal, D. M., "Single edge crack in rectangular tensile sheet", Journal Applied Mechanics, 708, 708-710 (1965).

[9] Lhermet, G., Vessiere, G., and Bahuaud, J., "Determination of stress intensity factors from stress concentrations for v-notched beams", Engineering Fracture Mechanics, Vol. 28 (3), pp. 331-343 (1987).

[10] Ebrahimi, A., Behzad, M., and Meghdari, A., "A bending theory for beams with vertical edge crack", International Journal of Mechanical Sciences, Vol. 52, pp. 904-913 (2010).

[11] Tada, H., Paris, P. C., and Irvin, G. R., "The stress analysis of cracks handbook", 3rd Edition, Professional Engineering Publishing (2000).

[12] Shkarayev, S. V., and Moyer, E. T., "Edge cracks in stiffened panels", Engineering Fracture Mechanics, Vol. 27(2), pp. 127-134 (1987).

[13] Swift, T., "Development of the fail safe design features of the Dc-10. Damage tolerance in aircraft structures, ASTM STP, Vol. 486, pp. 164-213 (1971)

[14] Ratwami, M. M., and Wilhem, D. P., "Influence of bi-axial loading on analysis of cracked stiffened panels", Engineering Fracture Mechanics, Vol. 11, pp. 585-593 (1979).

[15] Salgado, N. K., and Aliabadi, M. H., "The application of the dual boundary element method to the analysis of cracked stiffened panels", Engineering Fracture Mechanics, Vol. 54 (1), pp. 91-105 (1996).

[16] Ahmed, S. R., Khan, M. R., Islam, K. M. S., and Uddin, M. W., "Investigation of stresses at the fixed end of deep cantilever beams, Computers & Structures", Vol. 69, pp. 329–338 (1998).

[17] Ahmed, S. R., Hossain, M. Z., and Uddin, M. W., "A general mathematical formulation for finite-difference solution of mixed-boundary-value problems of anisotropic materials", Computers & Structures, Vol. 83, pp. 35-51 (2005).

[18] Ahmed, S. R., Idris, A. B. M., and Uddin, M. W., "Numerical solution of both ends fixed deep beams," Computers & Structures 61(1),pp. 21–29 (1996).

[19] Ahmed S.R., Idris A.B.M. and Uddin M.W., "An alternative method for numerical Solution of mixed boundary value elastic problems". Journal of Wave-Material Interaction, vol.14, No.1-2, pp.12-25 (1999).

[20] Akanda, M. A. S., Ahmed, S. R. and Uddin, M. W., "Stress analysis of gear teeth using displacement potential function and finite differences," International Journal for Numerical Methods in Engineering, 53, pp. 1629–1640 (2002).

[21] Ahmed, S. R., Nath, S. K. D., and Uddin, M.W., "Optimum shapes of tire treads for avoiding lateral slippage between tires and roads," International Journal for Numerical Methods in Engineering, 64, pp. 729–750 (2005).

[22] Nath, S. K. D., Afsar, A. M., and Ahmed, S. R., "Displacement potential approach to solution of stiffened orthotropic composite panels under uniaxial tensile load," Journal of Aerospace Engineering, Part G, IMechE, 221(5),pp. 896–881 (2007).

[23] Airy, G.B., British Association for the Advancement of Science Report, 1862.

[24] Timoshenko, S.P. and Goodier, J. N., Theory of Elasticity, -3rd Ed., McGraw Hill Book Co., New York, 1970.

[25] Mukhopadhyay, M., "Mechanics of Composite Materials and Structures," Universities Press, Hydrabad, pp 46 (2004).

[26] Hardy, S. J. and Pipelzadeh, M. K., "Static analysis of short beams", Journal of strain Analysis, vol. 26, No. 1, pp.15-29 (1991).

[27] Haryadi, S. G., Kapania, R. K. and Haftka, R. T., " Global/ local analysis of composite plates with cracks", Composites Part B: Engineering, vol. 29, pp. 271-276 (1998).

[28] Tang, S., "A boundary layer theory – part 1: laminated composites in plane stress", Journal of composite materials, vol. 9, pp. 33-41 (1975).